FEDERAL UNIVERSITY OF MINAS GERAIS

PROGRAM OF GRADUATION IN MECHANICAL ENGINEERING

Dynamic Modeling of a Compressed Air Energy Storage System in a Grid Connected Photovoltaic Plant

Author: **Ahmad Arabkoohsar**

Supervisor: **Ricardo Nicolau Nassar Koury**

Co-Supervisor**: Luiz Machado**

Belo Horizonte, April 18, 2016

Ahmad Arabkoohsar

Dynamic Modeling of a Compressed Air Energy Storage System in a Grid Connected Photovoltaic Plant

This work is presented to the Program of Graduate Studies in Mechanical Engineering of Federal University of Minas Gerais for obtaining a PhD degree in Mechanical Engineering.

Concentration Area: Energy and Sustainability

Supervisor: Ricardo Nicolau Nassar Koury
Co-Supervisor: Luiz Machado
Federal University of Minas Gerais - UFMG

Belo Horizonte
Engineering School of UFMG
2016

Federal University of Minas Gerais
Program of Graduation in Mechanical Engineering

Av. Antônio Carlos, 6627 - Pampulha - 31.270-901 - Belo Horizonte – MG.
Tel.: +55 31 3499-5145 - Fax. +55 31 3443-3783
www.demec.ufmg.br - Email: cpgmec@demec.ufmg.br

Dynamic Modeling of a Compressed Air Energy Storage System in a Grid Connected Photovoltaic Plant

Ahmad Arabkoohsar

The dissertation is defended on April 18, 2016. The examiner bank selected by the board of Program of Graduation in Mecanical Engineering of Federal University of Minas Gerais (UFMG) for this qualification exam which is for defending the research proposal given for obtaining a PhD degree in the area of Energy and Sustainability includes:

PROF. RICARDO NICOLAU NASSAR KOURY
Supervisor–Doctor, Departament of Mechanical Engineering, UFMG.

PROF. LUIZ MACHADO
Co–Supervisor–Doctor, Departament of Mechanical Engineering, UFMG.

PROF. RALNEY NOGUEIRA DE FARIA
Examiner–Doctor, Centro Federal de Educação Tecnológica de Minas Gerais, CEFET-MG.

PROF. RAPHAEL NUNES DE OLIVEIRA
Examiner–Doctor, Centro Federal de Educação Tecnológica de Minas Gerais, CEFET-MG.

PROF. ANTONIO CARLOS LOPES DA COSTA
Examiner–Doctor, Centro de Desenvolvimento de Tecnoligia Nuclear de Minas Gerais-CDTN-MG.

"Life's battles don't always go to the stronger or faster man. But sooner or later, the man who wins is the man who thinks he can."

Vince Lombardi

Acknowledgement

First of all, I thank my compassionate and merciful God for letting me go successfully through all the difficulties and destining this beatiful fate for me to feel such wondeful. Thank you Lord.

I proudly dedicate this PhD thesis to the three angels of my life, i.e. my lovely and patient parents and my devoted wife who endowed themselves so that I could just concentrate on my research career and nothing else. Words cannot express how grateful I am to you all for all of the sacrifices that you have made. Undoubtedly, your prayer was what brought me thus up.

Next, I would like to express my special appreciation and thanks to my supervisor Prof. Ricardo N. N. Koury, my tremendous mentor, for encouraging me thorough my PhD study and for trusting me in one by one of my research project steps. I also thank my kind and helpful advisor, Prof. Luiz Machado, for all his kind supports. He was, surely, the best lecturer that I have ever seen. I do appreciate my former advisor, Prof. Farzaneh-Gord from Shahrood University of Technology of Iran, for his very beneficial advices on my dissertation and other our joint research projects over this 2.5 years. He has got a very big heart and has a unique character.

The last but not the least, I'm really thankful to all of my good friends for their valuable companionship and all their supports, especially, my very dear friend Ali Moallemi and his kind wife, Naier Mahdinejad, those very helpful Colombian guys in the Refrigeration laboratory of DEMEC and my super generous Brazilian friends and neighbors. God bless them all.

ABSTRACT

The main problem of renewable energy power plants is the intermittency of the source of energy. Therefore, instantaneous variations of power demand could not be properly recovered. For overcoming this problem, the best solution, by far, seems to be employing energy storage systems and reclaiming the stored energy by the time of demand. Among all possible energy storage systems, compressed air energy storage (CAES) system is the most efficient candidate due to its high efficiency, lower cost of capital and being environmentally friendly. In spite of huge numerical, theoretical and experimental works conducted on CAES technology, dynamic modelling of a CAES system in a renewable energy source power plant with actual fluctuations has never been studied. On the other hand, as Brazil lies among top countries of the world in terms of solar irradiation reception, and pay attention to the fact that not many solar power plants have been installed in the country yet, this thesis presents a dynamic modeling of a CAES system in a large scale grid connected photovoltaic (PV) plant in Brazil. For this power generation system, it is shown that a CAES system with 50 MW capacity for a PV farm with 100 MWp capacity and a power sales strategy of equal to 70% of its monthly-instantaneously averaged energy production can efficiently damp the power ramps of the power plant and minimize the financial fines that power plant can be exposed to due to its sharp ramps. However, it was also concluded that this power generation system can be enhanced in terms of energy and exergy performance if there is an extra source of energy parallel to the power plant output. As a result, the feasibility of utilizing the power output of a power productive natural gas pressure drop station, also known as city gate station (CGS), along with the first power generation system is studied. The results of simulations prove that not only the energy and exergy efficiencies of the power plant increase considerably, but also the CAES system capacity decreases and the power sales strategy of the power plant is modified considerably.

Keywords: Compressed Air Energy Storage System, Photovoltaic Farm, Power Ramp, Energy Storage, City Gate Station

Resumo

O principal problema de usinas de energia renováveis é a intermitência da fonte de energia. Portanto, as variações instantâneas da demanda de energia não poderia ser devidamente recuperado. Para resolver este problema, a melhor solução parece estar empregando sistemas de armazenamento de energia e recuperar a energia armazenada no momento da demanda. Entre todos os sistemas de armazenamento de energia possíveis, sistema de armazenamento de energia de ar comprimido (CAES) é o candidato mais eficiente, devido à sua alta eficiência, menor custo de capital e ser ambientalmente amigável. Apesar de enormes obras numéricos, teóricos e experimentais realizados em tecnologia CAES, modelagem dinâmica de um sistema CAES em uma usina com fonte de energia renovável com as flutuações reais nunca foi estudada. Por outro lado, o Brasil encontra-se entre os principais países do mundo em termos de recepção de irradiação solar, e prestar atenção ao fato que nao muitas usinas de energia solar nao foram instalados no país, no entanto, esta tese apresenta uma modelagem dinâmica de um sistema CAES em uma grade escala planta fotovoltaica (PV) conetado ao rede no Brasil. Para este sistema de geração de energia, mostra-se que um sistema CAES com capacidade de 50 MW para uma fazenda PV com capacidade de 100 MWp e uma estratégia de vendas de eletricidade igual a 70% da sua produção média instantaneamente-mensal pode eficientemente amortecer as rampas de energia de a usina de energia e minimizar as multas financeiras que usina podem ser expostos a devido à sua rampas acentuadas. No entanto, concluiu-se também que este sistema de geração de energia pode ser melhorada em termos de eficiencia de energia e exergia se tem uma fonte adicional de energia paralelo à produção dele. Como resultado, a possibilidade de utilizar a potência de saída de uma estação de reduzir de pressão de gás natural, também conhecida como a city gate station (CGS), juntamente com o primeiro sistema de geração de energia é estudada. Os resultados das simulações provar que não só as eficiências de energia e exergia da usina aumentar consideravelmente, mas também a capacidade do sistema CAES diminui ea estratégia de venda de energia da usina é modificado consideravelmente.

Palavras-chave: Sistema de Armazenamento de Ar Comprimido, Usina Fotovoltaica, Rampa de Poder, Armazenamento de Energia, City Gate Station

Content

FIGURES LIST

LIST OF TABLES

NOMENCLATURE

A	Heat transfer area	(m^2)
c	Specific thermal capacity	(kJ/kg.^oC)
c_p	Specific thermal capacity in constant pressure	(kJ/kg.^oC)
CAES	Compressor air energy storage system	
CGS	City gate station	
D and d	Diameter	(m)
D_h	Hydraulic diameter	(m)
e	Electron charge	(J/V)
E	Overall energy of control volume	(kJ)
$\overline{E}$	Heat exchanger effectiveness	
FF	Fill factor	
F’	Collector efficiency factor	
F_R	Collector removal factor	
G_{sc}	Solar Constant	(W/m^2)
h	Specific enthalpy	(kJ/kg)
$\bar{h}$	Convective heat transfer coefficient	($W/m^2.K$)
$\hat{h}$	Molar enthalpy	(kJ/kmol)
H	Enthalpy	(kJ)
I	Current	(Ohm)
I	Solar irradiation on a horizontal surface on the earth	($W/m^2.hr$)
I_b	Beam component of solar irradiation	($W/m^2.hr$)
I_d	Diffuse component of solar irradiation	($W/m^2.hr$)
I_o	Solar irradiation on a horizontal surface beyond the atmosphere	($W/m^2.hr$)
I_T	Solar irradiation on a slopped surface	($W/m^2.hr$)
$\dot{I}$	Irreversibility	(kW)
k	Thermal conductivity	(W/m.^oC)
K_T	Sky clearness index	
LHV	Lowering heating value	(kJ/kg)
m	Mass	(kg)
$\dot{m}$	Total air mass flow rate	(kg/s)

$\dot{n}$	Molar flow rate	(kmol/s)
N	Number	
NRSME	Normalized root square mean error	
P	Pressure	(kPa)
P_E	Extra power available for the CAES system	(MW)
P_{E-G}	Energy shortage in the system	(MW)
Pr	Prandtl number	
PR	Performance ratio	
PV	Photovoltaic	
$\dot{Q}$	Heat transfer rate	(kW)
r	Radius	(m)
R	Heat resistance	(m^2.K/W)
RSME	Root mean square error	
Re	Reynolds number	
s	Specific entropy	(kJ/kg.K)
$\hat{s}$	Molar entropy	(kJ/kmol.K)
S	Entropy	(kJ/K)
S	Absorbed solar radiation	(W/m^2)
t	Time	(s)
T	Temperature	(ºC or K)
U	Overall heat transfer coefficient	(W/m^2.C)
V	Voltage	(V)
V	Volume	m^3
$\dot{V}$	Volume flow rate	(m^3/s)
w	Specific work	(kJ/kg)
W	Work	(kJ)
$\dot{W}$	Work rate	(kW)
Y	Yield	
Z	Compressibility factor	

Greek Symbols

φ	Latitude angle
δ	Declination angle

ω	Hourly angle
β	Slop Angle and Compression ratio
β'	Expansion ratio
ρ_g	Reflection solar irradiation coefficient
θ	Incident angle
θ_z	Zenith angle
γ	Surface azimuth angle
γ_s	Solar azimuth angle
η	Efficiency
λ	Time step
ξ	Overall energy efficiency
ε	Exergy efficiency
$\dot{\sigma}$	Exergy generation rate
ψ	Specific exergy
Ψ	Exergy
Γ	Uncertainty

Subscriptions

a	Air
am	Ambient
c	Collector
C	Compressor
ca	Cavern
che	Cooling heat exchanger
cm	Collector module
dah	Diesel air heater
e	External
f	Working fluid
ft	Fire tube
fu	Fuel
g	Generator
h	Heater
hyd	Hydrate forming

hst	Hot storage tank
i	Internal
NG	Natural gas
o	Dead state
OC	Open circuit
PM	Parallel module
rev	Reversible
SC	Short circuit
she	Solar heat exchanger
SM	Series modules
SS	Solar set
sst	Solar storage tank
sth	Hot storage tank
T	Turbine

1. Introduction

Nowadays, most of the required energy all over the world is provided by fossil fuels. There are two main problems that prohibit using such sources of energy. The first problem is that the fossil fuels are getting more expensive everyday as the underground reservoirs of such fuels are getting discharged and as a result, these sources of energy are becoming increasingly rare. The next problem is that burning fossil fuels for providing the required heat has serious negative impacts on the environment. This is why employing renewable and sustainable sources of energy in both industrial and domestic applications has been the concern of corresponding experts over the recent decades (Farzaneh-Gord *et al.*, 2011). One of the main sections that these sources of energy are widely used nowadays is power generation in both standalone and grid connected forms.

However, the main problem of renewable energy power plants is that the source of energy is inherently intermittent like wind and solar energies that are unstable and erratic dramatically. Therefore, instantaneous variations of electricity demand of the consumer, which could be either an individual consumer or a national electricity distribution grid, may not be accurately responded (Botterud, 2014). For overcoming this problem in a renewable energy source power plant, firstly, unpredictable and steep ramps in the electricity demand of the consumer, and secondly, the ramps in the source of energy should be taken into account. Therefore, accurate forecast would eliminate these problems entirely (Diagne *et al.*, 2014).

As accurate prediction of these two parameters is not achievable practically by far; the best solution seems to be employing an energy storage system and reclaiming the stored energy by the time of demand in such power plants (Pavković *et al.*, 2014). Various energy storage systems have already been proposed in the literature. Battery, flywheel, capacitor, pumped hydroelectric energy storage (PHES), super conducting magnetic energy storage (SMES), cryogenic energy storage (CES) and compressed air energy storage (CAES) are the most efficient systems proposed ever (Gadhamshetty *et al.*, 2014). For large scale storage capacities, PHES and CAES are the most promising systems, though PHES has certain adverse environmental effects (Rodrigues *et al.*, 2014). Comparing to all the aforementioned storage technologies, the CAES has a lower capital and maintenance cost and is also totally environmentally friendly. This is why the CAES system has attracted more

attention in the recent years (Breeze, 2014). Figure 1.1 shows the schematic diagram of a CAES system. According to the figure, in a CAES system, the extra power for being stored is used to run a compressor that intakes ambient air. The compressed air, which is also hot now, after passing through a heat exchanger, is stored within an air storage reservoir. The compressed air could be reclaimed to pass through a turbine and produce work when required. In order to meet the desired temperature before the expansion process, the air stream is warmed up by an auxiliary diesel air heater.

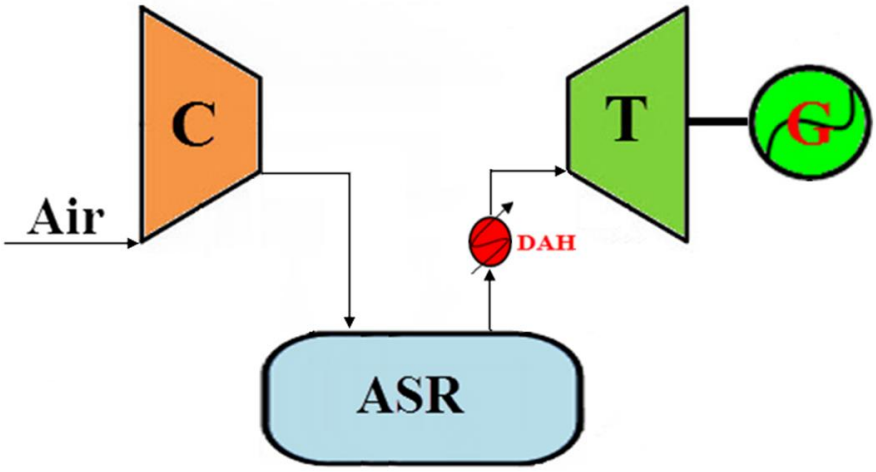

FIGURE 1.1 – The schematic of a conventional CAES system: C: compressor, T: turbine, G: generator, ASR: air storage reservoir, DAH: diesel air heater

The primary question about a CAES system is about its performance in a renewable energy source power plant under real operational circumstances. In fact, although the CAES technology has been well studied and progressed over the last years, no professional and specific work on dynamic modeling of a CAES system has been addressed in the literature yet. Therefore, the main goal of this dissertation is accomplishing a comprehensive energy and exergy analysis on a CAES system dynamically while operating in a renewable energy source power plant. For the sake of having a more accurate and precise simulation, in the first step of this project, a renewable energy source power plant with real transient operational conditions in Brazil is considered and the CAES performance in this power plant is simulated for a whole year.

But, what type of power plant is going to be opted for this investigation? Undoubtedly, among all renewable energy sources, the sun is the most plentiful and available. The radiated energy from the sun is 3.8×10^{23} kW, of which, almost 1.8×10^{14} kW is received

by the earth. This amount of energy is almost well above 7500 times the world's total annual energy demand (Midilli *et al*., 2007).

Solar energy technologies include solar heating, cooling, photovoltaics and agriculture and this wide range of application caused it to play an important role to solve some of basic energy problems of the world. Solar technologies are generally known as passive and active solar techniques depending on the matter they harness and convey solar energy. Active solar techniques consist of using photovoltaic panels or solar thermal collectors to profit the energy of the sun. Passive solar techniques, on the other hand, are those in which the energy of the sun is utilized without any special instrument to be employed; for example, orienting a building toward the sun to harvest the sun light and heat (Farzaneh-Gord *et al.*, 2014).

A lot of studies have already been done to propose new active solar systems or improve the already proposed ones in both terms of electricity production and solar heat. For solar heating objectives, the variety of proposed systems is much wider. In fact, in a solar heating system, the solar collector is the most important part of system. Kalogirou (2004) has introduced various kinds of solar thermal collectors and their respective applications. According to this reference, there are three main types of solar collectors namely flat plate collectors, evacuated tube collectors and concentrator collectors. In all cases, the device receives the solar heat and transfers it to a working fluid (usually water or the mixture of water and glycol) to be employed for various applications (Ghali *et al.*, 2011). Generally, the flat plate solar collectors are appropriate to be used in low temperature heat application as they can only provide heat up to only 80 ^{o}C and in moderate temperatures (80-200 ^{o}C) and high temperatures (200-2000 ^{o}C) applications evacuated tube and concentrator collectors are used, respectively (Kalogirou, 2004). Figure 1.2 shows the schematic diagram of all the three solar collector types.

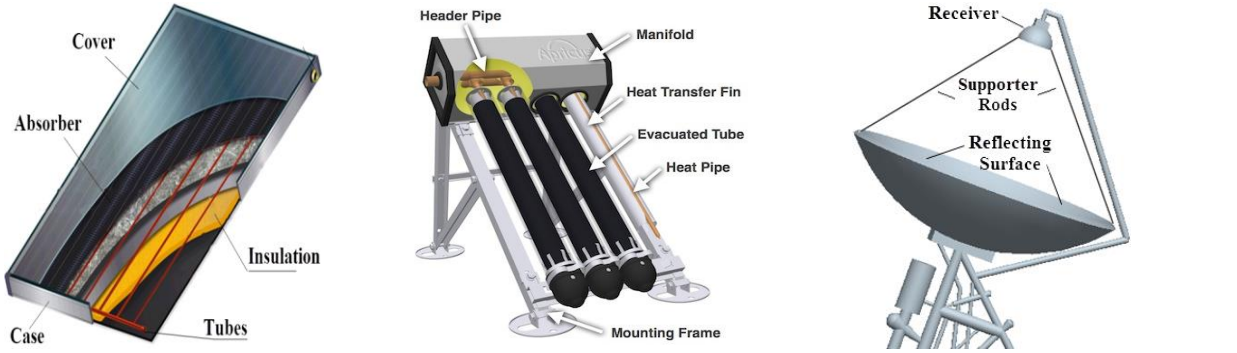

a) Flat Plate Collector **b) Evacuated Collector** **c) Concentrator Collector**

FIGURE 1.2 – The schematic of various types of solar collectors

Thirugnanasambandam et al. (2010) presented various types of solar thermal technologies such as solar water heaters, solar cookers, solar driers, solar ponds, solar architecture, solar air-conditioning and solar chimneys. Norton (1999) presented the most common applications of industrial process heat presenting the solar industrials and agricultural applications background and samples. Sharma et al. (2009) reviewed solar energy drying systems consisting of passive and active solar dryers. Bal et al. (2009) presented a review of solar dryers with thermal energy storage facilities employed in agricultural industry. Muthusivagami et al. (2010) thoroughly reviewed solar cookers with and without thermal storage equipment. Muneer et al. (2006) have studied the prospects of solar water heating for textile industry in Pakistan. Benz et al. (1998) presented the planning of two solar thermal systems generating process heat for a brewery and a dairy in Germany. In another work, Benz et al. (1999) presented a study for utilizing non-concentrating collectors for food industry in Germany. The aforementioned works are only a few out of thousands of studies accomplished on the solar heating systems and many others could also be referred in the literature.

In terms of solar power generation, also, many studies have been done over the last decades. Overall, there are two different types of solar electricity generations as direct and indirect power production methods. In the indirect solar power production method, the solar heat provided by thousands of reflector surfaces called heliostats equipped with tracking systems is used as the source of heat in the conventional power plants (Poghosyan and Hassan, 2015). Figure 1.3 shows the schematic diagram of a concentrating solar power plant.

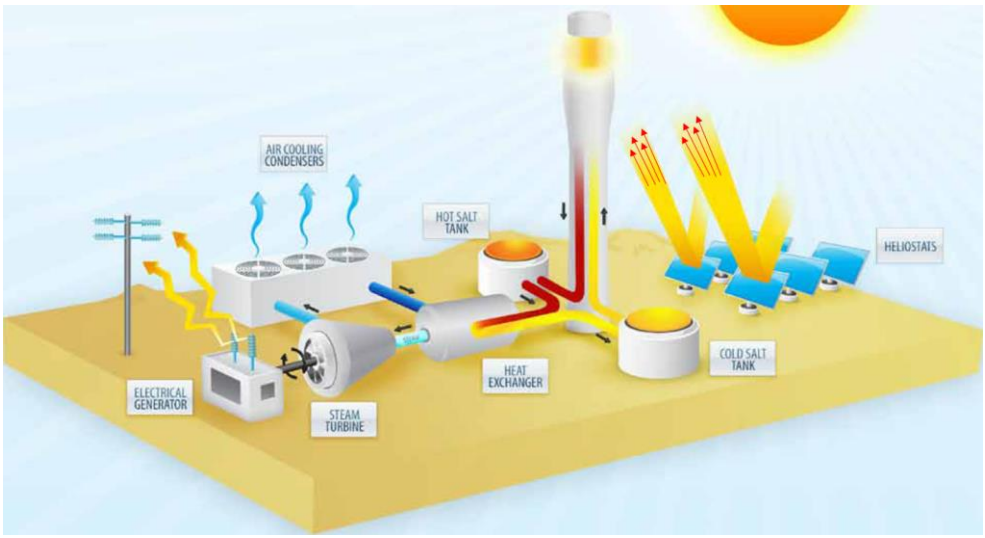

FIGURE 1.3 – The schematic diagram of a concentrating solar power plant

On the other hand, in direct solar power generation method photovoltaics (PV) cells are used to convert directly sunlight into electricity using the photovoltaic effect. PV technology has been widely used to provide power in both large and small scales. In a PV system, sunlight is directly converted into electricity by striking PV panels (Khadidjaa *et al.*, 2014). In small scale, standalone PV systems (not connected to the grid) are used for producing power where there is no access to electricity distribution grid or even for reducing electricity bills in grid connected places. In large scale, on the other hand, large PV farms can be built to provide the required electricity of cities, big factories and so on (Thanaraka and Sae-Erib, 2012). Figure 1.4 shows the schematic of a PV farm.

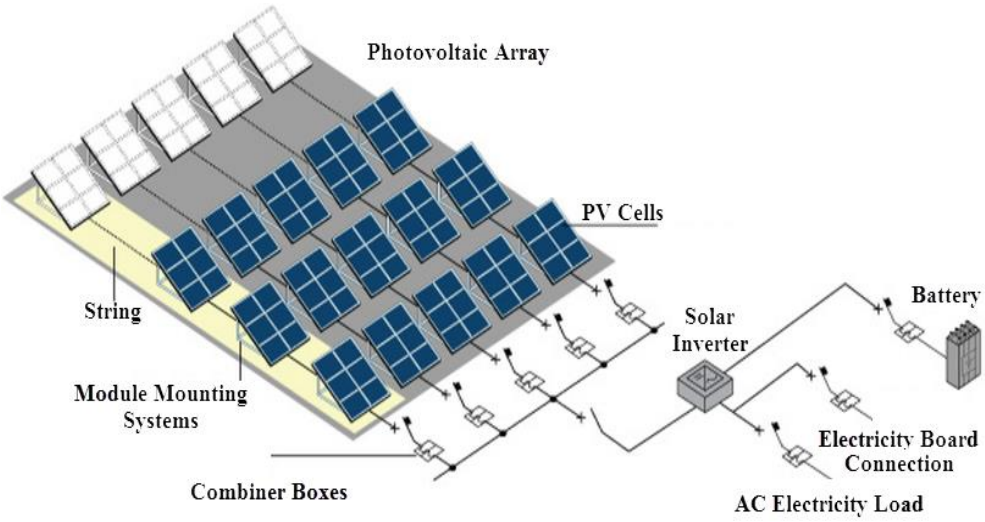

FIGURE 1.4 – The schematic diagram of a PV farm

According to the introduction given for solar energy and considering this fact that Brazil is among top countries worldwide in terms of solar irradiation, a PV farm has been chosen to host a CAES system for this study. In this regards, in this dissertation, first of all, a comprehensive introductions and backgrounds about the PV and the CAES technologies are presented and detailed formulation and mathematical model related to both of these technologies are given. The proposed configuration is presented and comprehensive exergy and energy analysis formulation related to this system is also given. As the power plant is supposed to be in Brazil, the best location in terms of the most available solar irradiation all over the country is selected.

One problem that all renewable energy source plants have is determining the most economically efficient pattern based on which the power plant sells power to the grid. In fact, the amount of power that each power plant should supply for the grid is defined in advance based on mutual agreement between the grid and the power plant and there will be huge penalties for the plant in case of any power ramp comparing to the agreed value. There are mainly two different types of power sale pattern as daily constant power strategy and time dependent power strategy. Overall, as accurate prediction of the intensity of renewable energy sources is not possible, even in presence of an energy storage system, the power plant could not guarantee how much power can exactly supply to the grid in every moment. Pay attention to the fact that, the more power is sold to the grid, the higher revenue is earned by the plant, one should find a solution by which not only the power plant maximizes the total annual amount of power sold to the grid, but also minimizes the total annual financial fines. Therefore, the most efficient power sales strategy of the PV plant is found in the next step.

As the amount of storable power by the storage unit of the power plant has direct effects on both the revenue and the financial fines of the power plant, therefore, the CAES system sizing and the power sales strategy selection are accomplished simultaneously. For this objective, the authentic economic assessment method of net present value (NPV) is used. After sizing the CAES system capacity, the CAES system belongings and equipment, such as compressors, expanders and etc., are sized component by component. Finally, a thorough energy and exergy analysis simulation on the system is carried out to observe the dynamic performance of the CAES system in this PV plant and demonstrate its effects on the power plant operation.

After simulating this power plant, a second proposal is given to improve the performance of the first configuration proposed. In fact, this proposal aims at enhancing the stability of the power produced and increasing the revenue of the previous PV plant. This system adds a large scale natural gas pressure drop station, which is called city gate station (CGS) to the previous PV plant configuration. After introducing CGSs and calculating the producible power by such a system, the proposed hybrid configuration is illustrated and detailed mathematical model about it is given. The best power sales strategy along with determining the most optimal CAES size for this hybrid system are chosen and comprehensive exergy and energy simulation on the optimized configuration of the power plant while working under real circumstances for a whole year is accomplished.

In the end, the authentic economic method of internal rate of return (IRR) which is a very reliable method for comparing different systems economically is used to prove the effect of adding the CGS power output to the PV plant as a kind of stabilizer source.

2. Compressed Air Energy Storage System

As the main goal of this work is simulating and dynamic moddeling of the performance of a CAES system in a PV farm, therefore, the CAES technology should be first introduced. This chapter present a detailed background, information and mathematical moddeling of the CAES technology.

2.1 CAES Background

Substantiated by issues of energy security, climate change and rising fossil fuels prices, many countries around the world lead an energy policy focusing on energy efficiency and increasing the share of renewable energy sources (International Energy Agency and Organization for Economic Co-operation and Development, 2015). In some countries and regions, these policies also involve increasing the share of combined heat and power (CHP) (European Commission, 2002 and 2008). Such energy policies lead to the challenge of balancing electricity supply and demand (Andersen and Lund, 2007). Various technological options have been analyzed and several measures have been implemented including changes in the regulation of distributed CHP plants (Eriksen, 2001). The different technological options in question include electric boilers and heat pumps (Blarke and Lund, 2007), flexible demands (Meibom *et al.*, 2007), electricity for transportation (Mathiesen *et al.*, 2008), re-organization of energy conversion in relation to waste treatment (Münster, 2007) and various energy storage options (Mathiesen and Lund, 2009).

For energy storage purpose, various systems have already been proposed in the literature. Battery, flywheel, capacitor, pumped hydroelectric energy storage (PHES), super conducting magnetic energy storage (SMES), cryogenic energy storage (CES) and compressed air energy storage (CAES) are the most efficient systems proposed ever (Gadhamshetty *et al.*, 2014). For large scale storage capacities, PHES and CAES are the most promising systems, though PHES has certain adverse environmental effects (Rodrigues *et al.*, 2014). Comparing with all the aforementioned storage technologies, CAES has a lower capital and maintenance cost and is also totally environmentally friendly. That is why CAES system has attracted more attention in the recent times (Breeze, 2014). In fact, on a utility scale, compressed air energy storage (CAES) is one of the technologies with the highest economic feasibility which may contribute to creating a flexible energy system with a better utilization of fluctuating renewable energy sources [Linden and Bulk, 2006].

The CAES is a modification of the basic gas turbine technology, in which low-cost electricity or extra electricity available is employed to actuate some compressors and produce compressed air and store this compressed air in an underground reservoir. This is could be reclaimed for producing power when required. Thus, the air should be heated and expanded in a gas turbine in order to produce electricity during peak demand hours. As it derives from gas turbine technology, the CAES is readily available and reliable (Kondoh *et al.*, 2000).

The first CAES plant was commissioned in Huntorf, Germany in 1978 to provide peak power for a gas turbine plant. The Huntorf plant, which is still in operation, stores up to 310,000 m^3 of compressed air at a pressure range of 44–70 bar in two salt caverns and can produce up to 290 MW of electricity at full capacity for 4h at an air discharge flow rate of 417 kg/s (Raju and Khaitan, 2012). The second utility scale CAES plant was also commissioned in 1991 in McIntosh, capable to generate 110 MW of electricity at full capacity for 26h with an air discharge rate of 154 kg/s. It stores up to 540,000 m^3 of compressed air at a pressure range of 45-74 bars in a salt cavern (Powersouth, 2013).

Despite the successful operation of these two CAES plants, a series of events caused the development of CAES technology to slow down during the late 1980s and the 1990s. These events included the loss of momentum in the nuclear industry, the development of efficient and low capital intensive single and combined cycle gas turbines, a drop in natural gas prices, and an overbuilt generation capacity. However, the desire for higher penetration of clean but intermittent wind and solar energy sources into the electric grid has renewed interest in CAES as a method to overcome their intermittency and thus lower the GHG emissions from electricity generation. In this regards, announced in January of 2007, the Iowa Stored Energy Park (ISEP) is partnership between the Iowa Association of Municipal Utilities and the Department of Energy. They plan to integrate a 75-150 MW wind farm with underground CAES, 3000 ft. below the surface. The ISEP is currently in design phase with anticipated generation starting in 2015. The schematic of the proposed layout can be seen in figure 2.1.

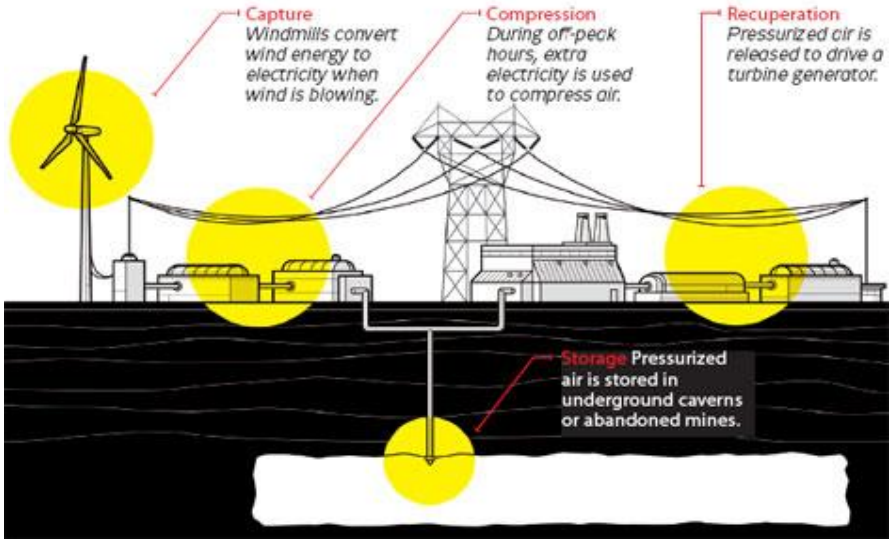

FIGURE 2.1 − Iowa wind-CAES power plant

The CAES technology was extensively investigated in the 1970s to provide load following services and to gain a high capacity factor for base load power plants (especially nuclear) by storing off-peak electricity (Najjar and Zaamout, 1998). Given the limited pumped hydro energy storage potential of CAES, early literature focused on the technical description of CAES plant designs for load leveling and fuel saving applications in combination with coal and nuclear base load power plants (Sharma *et al.*, 1979). With the development of renewable energy, the CAES has increasingly been analyzed as a method of improving the integration of fluctuating wind power into the electricity supply (Giramonti *et al.*, 1978). Bullough et al. (2004) analyzed the technical development and economic feasibility of an advanced adiabatic CAES (AA-CAES) system in various European countries with the EU target of 20% renewable energy by 2020 as a basis. Denholm (2006) suggests a fully renewable base load power plant using a combination of wind power, the CAES, and biofuels. A hybrid wind-CAES system was also proposed by Cavallo (2007) as a compensation for the intermittency of wind power. Greenblatt et al. (2007) compared the marginal production cost of a base load wind-CAES to coal and wind/gas turbine systems and conclude that the CAES can be highly economically competitive, especially if externality costs of GHG emissions are included. The GHG perspective is also presented in Denholm et al. (2004), where the CAES is compared to other electricity storage options seen from a life cycle perspective in relation to greenhouse gas emissions. The literature described focuses on specific CAES plant applications (both alone and in combination with another technology such as coal or wind). This ignores the system perspective in which combined technologies

interact with each other. Salgi and Lund (2008) performed a technical system analysis with an increased wind power penetration in Denmark. The mentioned study, however, does not take into account the economic feasibility of a CAES plant. Swider (2007) presented a stochastic model for analyzing the economic competitiveness of CAES in a system with growing wind power penetration. The study concludes that the CAES can be economically competitive with other technologies in a system characterized by the phasing out of nuclear power. While stressing the importance of flexible technologies, the study does not compare CAES to other such available technologies.

2.2 CAES System Configuration

The first configuration proposed as a CAES system was the simplest configuration proposed for this objective ever. This proposal was given by 1940 (Kousksou *et al.*, 2014).

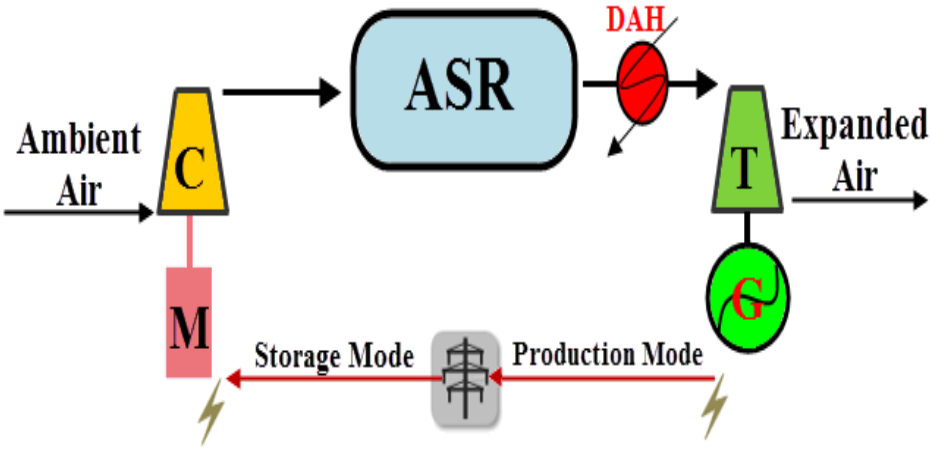

FIGURE 2.2 − The first configuration proposed for the CAES; M: motor, C: compressor, ASR: air storage reservoir, DAH: diesel air heater, T: turbine, G: generator

Figure 2.2 depicts the schematic diagram of this simple CAES system. According to the figure, the CAES system is employed while there is extra power available. The power is used to actuate a motor that is coupled with an air compressor. The compressor sucks ambient air and produces compressed air. The air flow rate through the compression process depends on the amount of extra electricity available. The compressed air is stored in an air storage reservoir which is usually an underground cavern. When there is need for an auxiliary source of energy, the compressed air is reclaimed to be used for producing power. For this objective, after being heated up to the desired temperature through an auxiliary air heater, the compressed air has to pass through a turbine to be expanded. Therefore, the air stream rotates

a turbine shaft which is coupled with an electricity generator rotor. This process causes the generator to produce the required power. Note that the expanding air mass flow rate depends on the amount of power required in every moment.

Although the idea given by this system was a novel and innovative proposal, the net efficiency of such a system was not that much satisfactory that made too expensive the power produced by this system. A variety of newer CAES designs have been proposed in the past few decades to improve the storage efficiency of conventional CAES plants. The Energy Storage and Power Corporation in the 1990s proposed the first modified version of the conventional configuration of CAES system based on pairing CAES plants with conventional gas turbines. The main idea of this approach is eliminating the air heater in the CAES facility and utilizing the exhaust stream from the gas turbine instead of the combustor to heat the compressed air and thus improving the overall efficiency. Figure 2.3 shows the schematic diagram of the CAES system accompanying with a gas turbine plant.

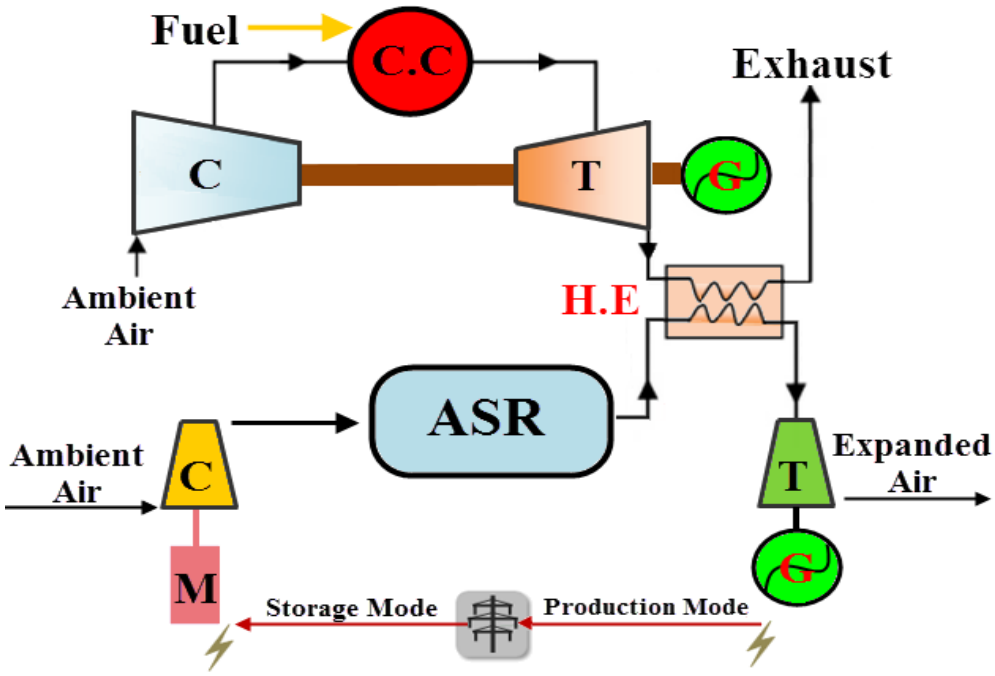

FIGURE 2.3 − The schematic diagram of a CAES system accompanying with a gas turbine plant; C.C: combustion chamber, H.E: heat exchanger

As can be seen, in the CAES configuration, the auxiliary heater (combustor) has been removed and the heat along with combustion production outgoing from the gas turbine is used to preheat expanding air stream in the CAES system instead.

In contrast to this approach which focuses on waste heat recovery during the discharging process, Adiabatic CAES (A-CAES) design is based on storing the heat generated in the air stream through the compression process in a thermal energy storage facility. This stored heat then would be utilized to heat the compressed air during the generation (expansion) process and thus lower (or even eliminate) the fuel consumption of the CAES plant. This concept was introduced in the 1980s and the interest in this concept is recently renewed both in Europe and the United States (Porto *et al.*, 2013). Figure 2.4 illustrates the schematic diagrams of a simple design A-CAES system.

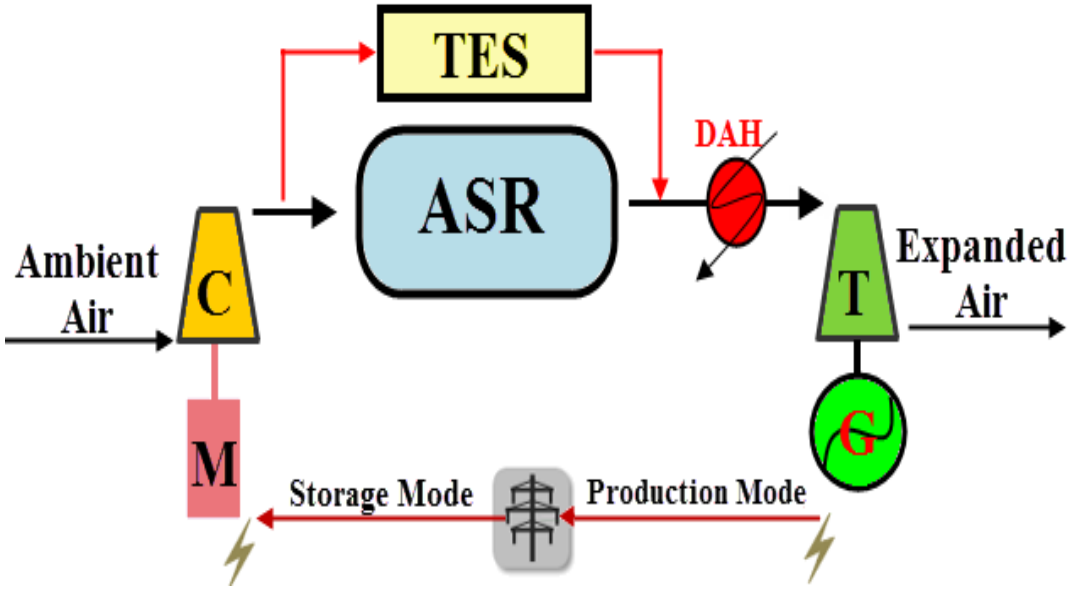

FIGURE 2.4 − The schematic diagram of the first A-CAES system design; TES: thermal energy storage

According to the figure, the thermal energy storage system is added to the first configuration proposed for CAES system. In this way, one could collect the heat generated in the air stream while being compressed. This is usually done by some heat exchangers in which water or industrial oils act as the working fluid. The heated working fluid is then stored in the TES and at the time of power production, this heat is transferred to the expanding air stream. This procedure also takes place in another heat exchanger. After this heat exchanger, in case the air has not met the desired temperature, the auxiliary air heater provides the extra heat required.

As A-CAES system is still in the research and development phase, its development is challenged by few major technical issues including design of high pressure, high temperature, large scale and economically attractive TES systems, high pressure and

high temperature compressors, and high pressure expanders. For example, in the above system, using only one TES could not be so effective because a high gradient inside the tank is needed to reach two completely different boundary conditions inside the tank: high temperature when it goes to the turbine (top side of the tank) and low temperature when enters the storage tank (bottom side). For solving this problem, as another step of modification on the CAES system configuration, it was proposed to use two separate TESs (cold and hot). Figure 2.5 shows the schematic diagram of an A-CAES system with two separate cold and hot TESs.

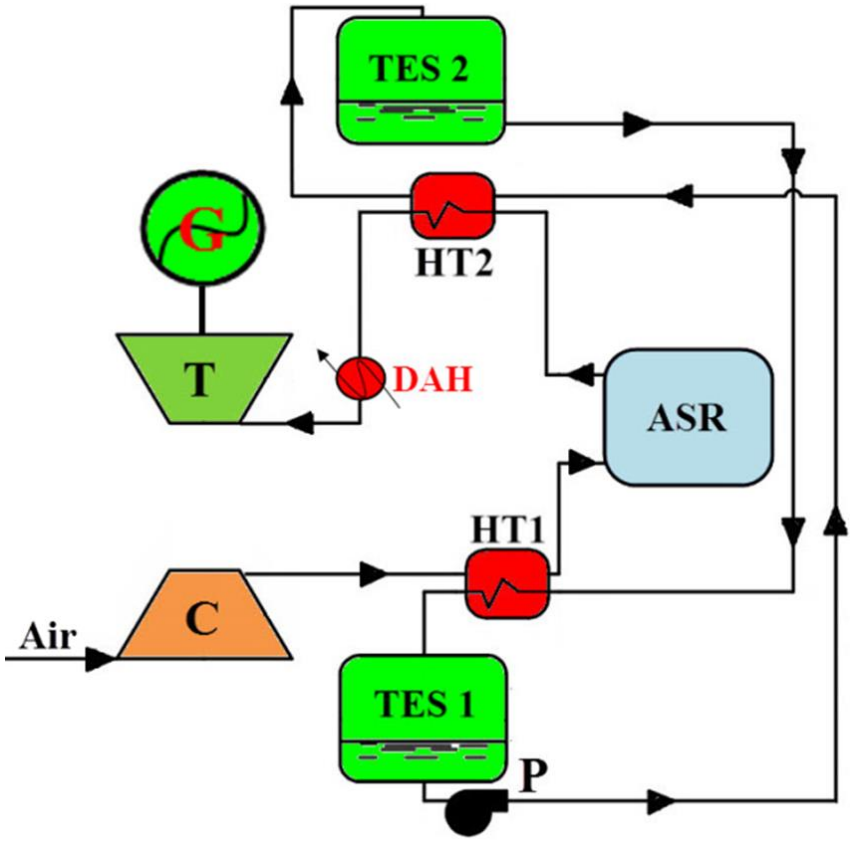

FIGURE 2.5 − The schematic diagram of two-TES A-CAES system

According to the figure, in this system, the working fluid receives heat from the compressed air through the first heat exchanger (HT1) and the heated working fluid enters the first TES 1 (Hot). The cold compressed air, then, enters the air storage reservoir. When the cold compressed air is reclaimed for producing power, the hot working fluid from TES 1, heats the cold compressed air stream through the second heat exchanger (HT2) and then enters the TES 2 (Cold). Again, in compression process, the cold working fluid stored in TES 2, flows through HT1 and receives heat from the compressed air and enters the hot TES 1.

Although the system shown in figure 2.5 has a reasonable efficiency comparing to the previous configurations, it was not the most efficient system proposed ever. In the next proposal, employing multistage compressors and expanders by which the adiabatic processes in the compressor and expanders approached isothermal processes was proposed. Therefore, train mode of exchanging heat in both giving and getting heat could increase the efficiency to more values up to almost 80% by reducing the compressor inlet temperature and increasing the turbine outlet temperature. This configuration is illustrated in figure 2.6.

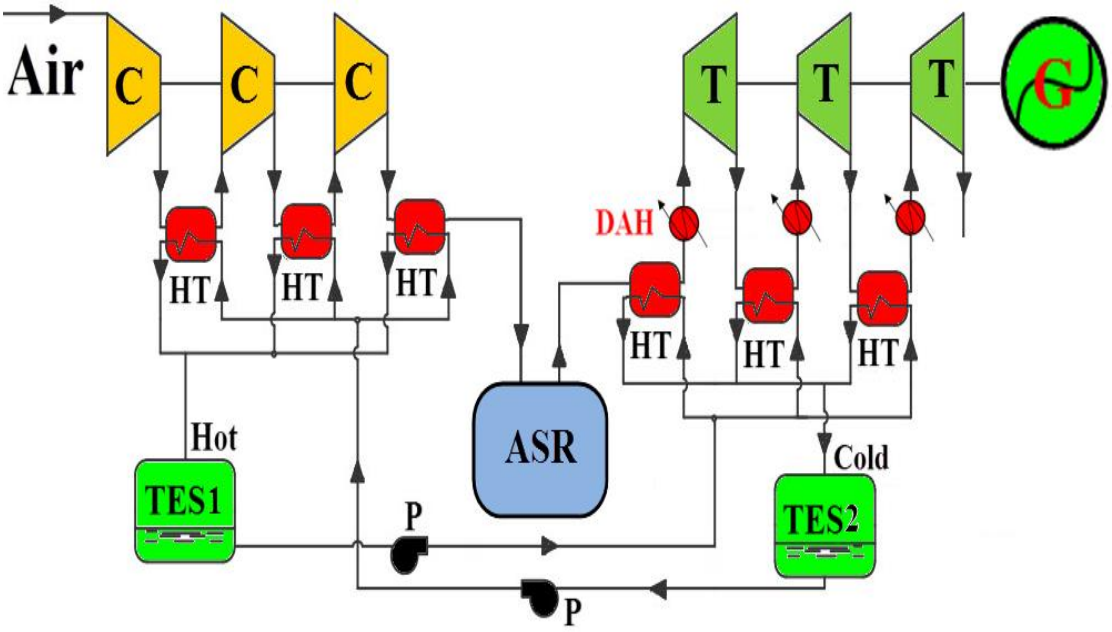

FIGURE 2.6 − A-CAES system with multiple stage compressor and turbine

According to the figure, by this proposal, the heat exchangers act as intercoolers for the compressors and inter-heaters for the expanders. Therefore, the air temperature at compressor inlet is kept as low as possible. Clearly, the lower inlet temperature for a compressor, the higher efficiencies are achievable by that compressor. Also, for the turbines, the inlet temperature is recovered and remains as much as possible. Naturally, this makes the expanders to work with as high efficiency as possible. Figure 2.7 shows how employing a multiple compressor leads to reaching higher efficiencies by decreasing the amount of required work for producing the same amount of air at the same pressure (Farzaneh-Gord *et al.*, 2014).

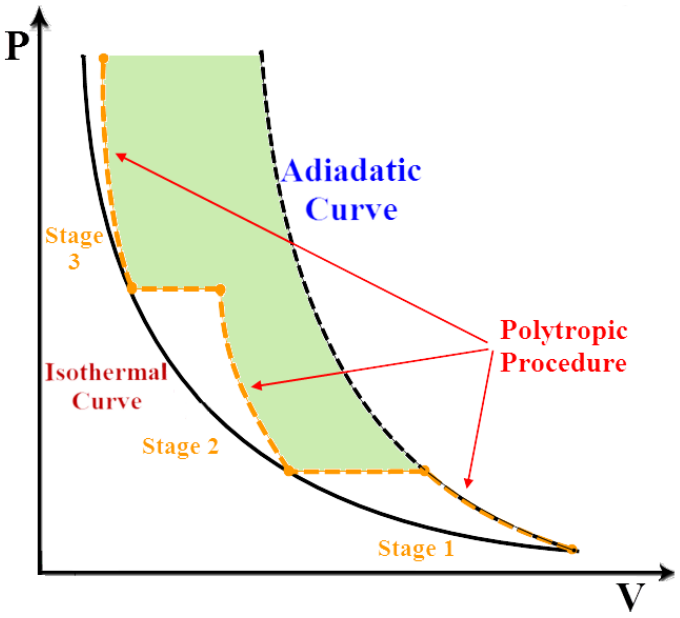

FIGURE 2.7 − The effect of employing multiple stage compressors on the amount of required work

According to the figure, the least amount of required work is for an isothermal process. In a sharp contrast, the maximum amount of work required for the compressor is when the process is adiabatic. Having a compressor which works in an isothermal process is impossible practically. However, one could approach this state by employing multiple stage compressors. In such case, the work of each compressor is adiabatic; however, by using intercoolers one could reduce the next stage compressor significantly and as a result, the work required in the next stage reduces remarkably. The work implemented by the whole compressor unit is called a polytropic process. The green area represents the amount of work reduction caused by employing multiple stage compressors comparing to the amount of work required for a single stage compressor. Note that, by the same approach, the effect of employing multiple turbines on increasing the expansion process efficiency could be explained as well.

Finally, in a newer configuration, as an improvement on the previous configuration of the A-CAES system, employing a solar energy heating system in order to provide all or at least a significant portion of the extra heat for the expanding air in the expansion process (which was provided by an auxiliary diesel air heater) was proposed. Figure 2.8 shows the schematic diagram of this configuration which is the most efficient configuration of A-CAES system proposed ever.

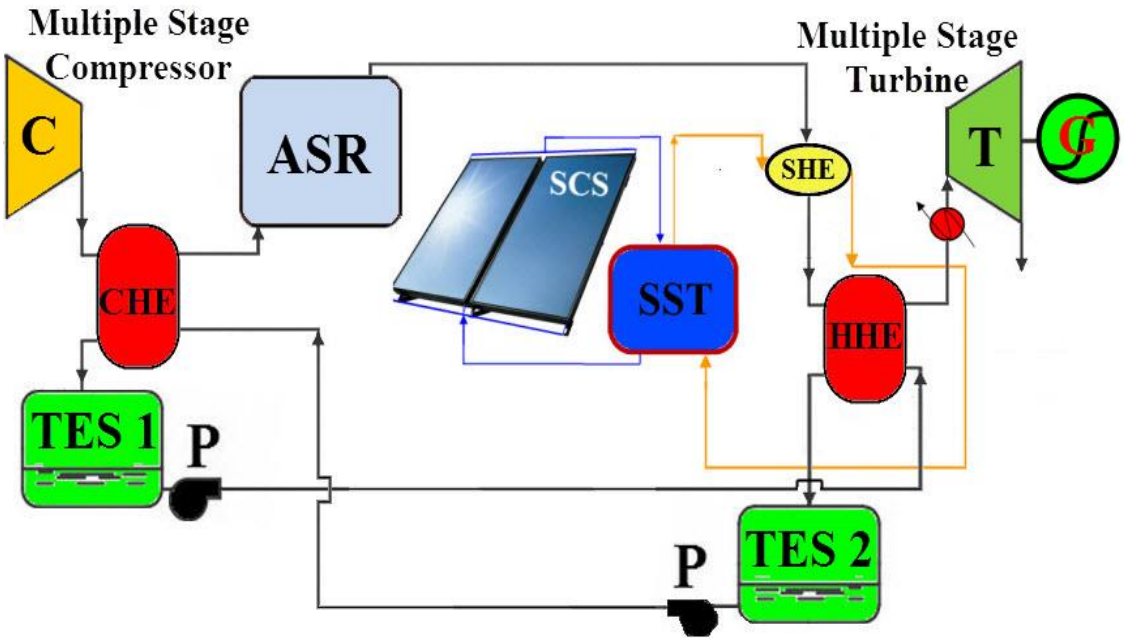

FIGURE 2.8 − Schematic of the A-CAES system equipped with a solar heating system; SST: solar storage tank, SCS: solar collector series, SHE: solar heat exchanger

As the figure shows, in expansion process, firstly, the air steam should pass through the solar heat exchangers to be warmed up to possible temperatures. Then, the hot heat exchangers are employed to heat the air stream. In final stage, if still required, the auxiliary heater could also be used. Note that, the solar heat exchanger is supported by hot water produced by solar heating unit including a flat plate collector module and a solar storage tank. In fact, the solar collectors, during the day, collect solar heat and produce hot water. This hot water is then stored in a storage tank and is used in production mode.

Another possible system related to CAES systems is D-CAES concept which is based on improving the economics of the conventional CAES facilities through the use of the heat generated in compression process for space and water heating demands. Waste heat recovery from industrial compressors is a mature technology and therefore introduces less technical complexity compared to the A-CAES design which requires heat recovery and storage at high pressures and temperatures (Safaei *et al.*, 2013). On the other hand, the D-CAES design requires a pipeline between the compression site (region with high density of heat load) and the storage site (e.g. cavern). In the admittedly unrealistic case where the heat load and the CASE storage facility are co-located, then D-CASE would always be preferred to the CASE since it provides heat for free. The tradeoff between the increased capital cost of the D-CAES system compared to conventional CAES (mainly due to the air pipeline) and

savings on fuel (used for heating purposes) can make the D-CAES system cheaper compared to the conventional CAES in certain situations. The intensity and fluctuations of the heat load, size and fluctuations of the electric load, distance between the heat load and storage facility, and the fuel and construction costs are the major players in this tradeoff. This configuration is, however, helpful only when there is a conventional CAES system and another system with heating demand. Therefore, this system is out of this work scope.

2.3 A-CAES System Formulation

As it was claimed before, the configuration shown in figure 2.8 is the most efficient system among all CAES systems. Therefore, this configuration is the target CAES system which is used in this work and the mathematical model of this configuration is presented in this section.

Before continuing the discussion, there is an important issue that should be taken into account. The problem is that whether or not the working fluid (air) can be considered as an ideal gas?

In this regard, one should calculate the compressibility factor of air entering and exiting the compressors by calculating the compressibility factor of the air at each stage (Wark and Richards, 1999).

$$Z = 1 + \frac{B}{\upsilon'_r} + \frac{C}{\upsilon'^2_r} + \frac{D}{\upsilon'^5_r} + \frac{c_4}{T_r^3 \upsilon'^2_r} + \left(\lambda + \frac{\xi}{\upsilon'^2_r}\right) \exp\left(-\frac{\xi}{\upsilon'^2_r}\right) \tag{2.1}$$

In which, B, C, D, v_r and T_r can be given by the following equations.

$$B = b_1 - \frac{b_2}{T_r} - \frac{b_3}{T_r^2} - \frac{b_4}{T3}; \quad C = c_1 - \frac{c_2}{T_r} + \frac{c_3}{T_r^3}; \quad D = d_1 + \frac{d_2}{T_r}; \quad T_r = \frac{T}{T_c}; \quad \upsilon'_r = \frac{\upsilon}{RT_c / P_c} \tag{2.2}$$

Where, v, T_c and P_c are specific volume, critical temperature and critical pressure of the working fluid (specifically air here), respectively. Also, the other parameters in the above equations, which are all constant, can be found in the following table (Wark and Richards, 1999).

TABLE 2.1 − Compressibility formulation constant coefficients values

Constant	Value	Constant	Value
b_1	0.1181193	c_3	0
b_2	0.265728	c_4	0.042724
b_3	0.154790	d_1	0.0000155488
b_4	0.030323	d_2	0.0000623689
c_1	0.0236744	λ	0.65392
c_2	0.0186984	ζ	0.060167

Employing the above formulation, if the value of compressibility factor is obtained equal to 1, the gas can be considered as an ideal gas; otherwise, it should be considered as a real gas and appropriate formulation should be adopted.

Note that in mathematical modelling of the system, overall, the following assumptions are taken:

a. The effect of ambient air humidity on the CAES system performance is neglected as the CAES systems always take advantage of dehumidifiers.

b. The air throughout the compression and expansion process in the CAES system is considered as ideal gas. Considering the maximum pressure and the temperature of air in the system, this assumption is totally reasonable.

c. The compressors, expanders and heat exchangers in the CAES system could react to the instantaneous fluctuation of depending parameters very fast and the variations of kinetic and potential energies through them are assumed to be negligible.

d. The processes of compressors and expanders are considered as isentropic procedures.

e. The heat exchangers and storage tanks in the CAES system are assumed to be totally insulated.

f. The temperature of compressed air within the air reservoir is assumed to be equal to the ambient temperature. This assumption is also totally reasonable as not only the heat exchangers between the compressors cool the compressed air stream down to points much close to the ambient temperature, but also the air within the reservoir, which is not

isolated, has usually enough time to approach the ambient temperature when the expansion unit is in standby state.

In the target configuration, for the sake of simulating the system, five separate control volumes could be defined including the compression unit, the air storage reservoir (cavern), the solar heating unit, the expansion unit and the auxiliary air heater.

2.3.1 Energy Performance Investigation

The general format of the first law of thermodynamics or energy conservation law for a control volume is (Wark and Richards, 1999):

$$\frac{dE_{C.V}}{dt} = \dot{Q}_{C.V} + \dot{W}_{C.V} + \sum \dot{m}_i \left(h_i + \frac{Ve_i^2}{2} + gz_i \right) - \sum \dot{m}_e \left(h_e + \frac{Ve_e^2}{2} + gz_e \right) \tag{2.3}$$

Where, $\dot{Q}$ and $\dot{W}$ refer to the amount of heat and work exchanged between the control volume and the environment respectively. $\dot{m}$, h, Ve and z also represent the mass flow rate, enthalpy, velocity and potential term of the flows incoming or outgoing into/from the control volume. $E_{C.V}$ also refers to the total energy of the control volume including internal energy (U), kinetic energy (KE) and potential energy (PE). Note that the above equation subscripts i and e represent the inlet and outlet conditions respectively. In addition, the mass conservation law for the control volume (if applicable) can be written as:

$$m^{\lambda+1} = \left(\sum \dot{m}_i - \sum \dot{m}_e \right)^{\lambda} \Delta t + m^{\lambda} \tag{2.4}$$

Where, m is the total mass of the control volume and the superscript λ counts the operational time steps of the control volume.

The first law efficiency, based on the definition, shows what portion of the inlet energy in the system has been effectively employed to produce power output by the control volume. Thus:

$$\xi = \frac{\text{Useful energy output}}{\text{Energy input}} \tag{2.5}$$

After presenting the fundamentals of the first law of thermodynamics, one could analyze all the system components individually. In the first control volume i.e. the

compression unit, based on the conception, the compressor set total work ($\dot{W}_C$) is equal to the extra produced electricity (P_E) multiplied by the compressor set overall efficiency (η_C).

$$\dot{W}_C = P_E \, \eta_C \tag{2.6}$$

Due to the high mass flow rate and pressure required in the CAES system, centrifugal compressors are selected to be used in this work for which isentropic efficiency is considered to be equal 85% (Li, 2013).

Knowing the compressor efficiency and employing simple thermodynamic correlations, one could easily calculate the specific isentropic work ($w_{C,is}$) and subsequently actual work ($w_{C,act}$) of compressors and, subsequently, the compressor actual outlet temperature ($T_{C\text{-}e}$):

$$T_{C\text{-}e} = \frac{w_{C,act} + c_{p-i} T_{C\text{-}i}}{c_{p-e}} \tag{2.7}$$

Where, $T_{C\text{-}i}$ is compressor inlet air temperature and $c_{p\text{-}i}$ and $c_{p\text{-}e}$ are air specific heat capacity at compressor entrance and exit respectively. As c_p value depends on the temperature, therefore, iterative solution is required here.

Calculating the specific works of all compressors, one can obtain the total air mass flow rate ($\dot{m}_{C,t}$) intake into the compressor set as:

$$\dot{m}_{C,t} W_{C,t} = \dot{W}_{C,t} = \sum \dot{m}_c w_c \tag{2.8}$$

The first compressor inlet air temperature is known (ambient temperature) and energy analysis on the cold heat exchanger series could reveal the value of inlet air temperature for the other compressors.

The rate of heat transferred from the air to the working fluid (which will be industrial oil) in each heat exchanger (cooling heat exchanger series) is given by:

$$q_{che} = U_{che} A_{che} \Delta T_{lm} \tag{2.9}$$

In this equation, A_{che} is the heat transfer area. U_{che} and ΔT_{lm} are respectively the overall heat transfer coefficient and logarithmic temperature difference and could be

calculated as:

$$\frac{1}{U_{che}} = \left(\frac{1}{\bar{h}_f} + \frac{\Delta r}{k}\left(\frac{A_o}{A_{lm}}\right) + \frac{1}{\bar{h}_a}\left(\frac{A_o}{A_i}\right)\right) \tag{2.10}$$

$$\Delta T_{lm} = \frac{(T_{i-a} - T_{i-f}) - (T_{e-a} - T_{e-f})}{Ln\left(\frac{(T_{i-a} - T_{i-f})}{(T_{e-a} - T_{e-f})}\right)} \tag{2.11}$$

Where, A_o, A_i are respectively the internal and external areas of the tube, A_{lm} the log mean of these values and Δr is difference between the internal and external radiuses of tube. Also, $\bar{h}_a$, $\bar{h}_f$, and k are convective heat transfer coefficients for the air and working fluid streams and the conductivity coefficient of the tube, respectively. T_{i-a}, T_{i-f}, T_{e-a} and T_{e-f} are respectively the temperature of air and working fluid entering the heat exchangers and the temperature of air and working fluid outgoing from the heat exchangers.

One should note that the flow regime for the working fluid is laminar due to the high viscosity of the industrial oil while for the air clearly a turbulent regime is expected. Thus, for calculating the value of convective heat transfer coefficients, the following equations are used (Incropera and DeWitt, 2002).

$$\bar{h}_a = \frac{0.023\, Re_a^{0.8}\, Pr_a^{0.4}\, k_a}{D_i} \tag{2.12}$$

$$\bar{h}_f = \frac{4.36\ k_f}{D_h} \tag{2-13}$$

In which, Re_a, Pr_a, k_a, k_f, D_i and D_h are Reynolds and Prandtl numbers for the air stream, the thermal conductivity of air and working fluid, the internal diameter for the inner tube and hydraulic diameter for the outer tube, respectively.

Employing the above formulation, the air temperature outgoing from each heat exchanger (T_{e-a}) and the outlet working fluid temperature (T_{e-f}) are calculated by:

$$T_{e-a} = T_{i-a}\left(1 - \bar{E}_{che}\right) + \bar{E}_{che}\, T_{i-f} \tag{2.14}$$

$$T_{e-f} = \frac{\overline{E}_{che}\ \dot{m}_a\ c_{p-a}\left(T_{i-a} - T_{i-f}\right)}{\dot{m}_f\ c_f} + T_{i-f} \tag{2.15}$$

Where, $\overline{E}_{che}$ is the heat exchanger effectiveness given by:

$$\overline{E}_{che} = \frac{UA/C_{min}}{1 + UA/C_{min}}; \quad C_{min} = \dot{m}_a\ c_{p-a} \tag{2.16}$$

In the above formulation, compressor inlet temperatures are required for calculating the specific work of each compressor. On the other hand, for calculating the compressors inlet temperatures the value of heat exchanger effectiveness is needed. As a result, this formulation will only be calculable with iterative solution.

Finally, by implementing the mass conservation law and the first law of thermodynamics for the hot storage tank (TES 1), one has:

$$m_{hst}^{\lambda+1} = m_{hst}^{\lambda} + \left(\sum \dot{m}_i - \sum \dot{m}_e\right)^{\lambda} \Delta t \tag{2.17}$$

$$T_{hst}^{\lambda+1} = \frac{\left(\sum \dot{m}_i\ c_f\ T_i - \sum \dot{m}_e\ c_f\ T_e\right)^{\lambda} \Delta t + m_{hst}^{\lambda}\ c_f\ T_{hst}^{\lambda}}{m_{hst}^{\lambda+1} \cdot c_f} \tag{2.18}$$

Where, c_f, m_{hst} and T_{hst} are the specific heat, mass and temperature of working fluid in the cold storage tank respectively. The superscriptions λ and $\lambda+1$ also count the system operational time steps.

For the second control volume (the cavern), from the mass conservation law, one has:

$$m_{ca}^{\lambda+1} = m_{ca}^{\lambda} + \left(\sum \dot{m}_i - \sum \dot{m}_e\right)_{ca}^{\lambda} \Delta t \tag{2.19}$$

In which, m_{ca} is the mass of air encapsulated in the cavern. Also, considering air as an ideal gas (if possible), the cavern pressure (P_{ca}) could be obtained as:

$$P_{ca} = \frac{m_{ca} R\, T_{ca}}{V_{ca}} \tag{2.20}$$

In this equation, T_{ca} is the cavern temperature and is always considered to be equal to the ambient temperature.

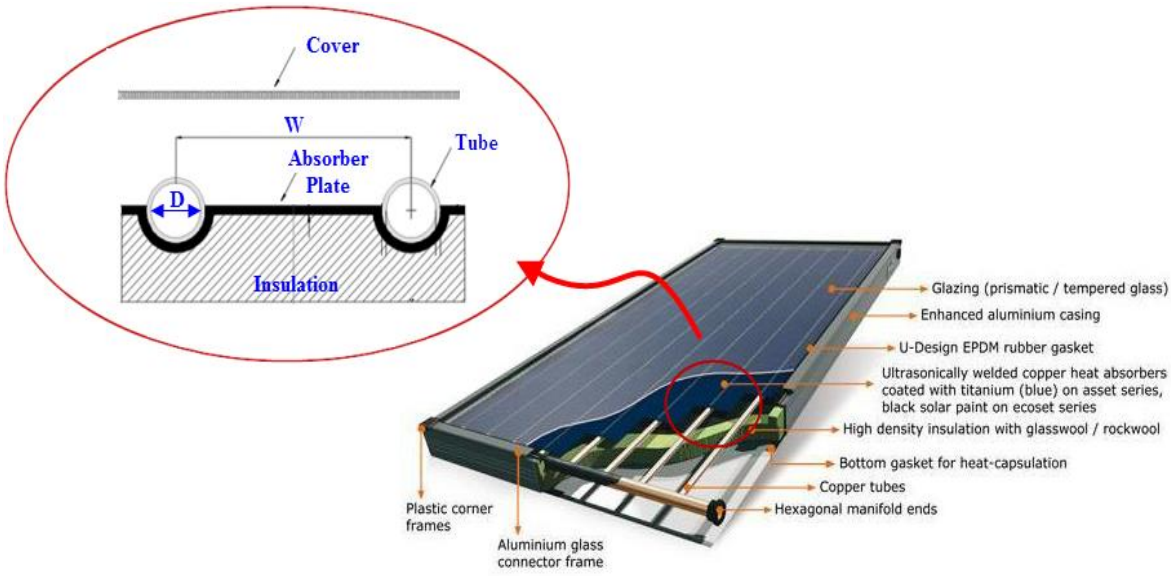

FIGURE 2.9 − The schematic diagram of a simple flat plate solar collector with cross sectional of a single tube

The third control volume is the solar heating system which is hired to provide a portion of the required heat for preheating the air stream before the expansion process. Note that in both cases of employing either flat plate evacuated tube or simple flat plate collectors; similar formulation with minor differences applies for the collectors. Figure 2.9 and figure 2.10 illustrates the schematic diagram of these two collectors with the required dimensions for modelling them.

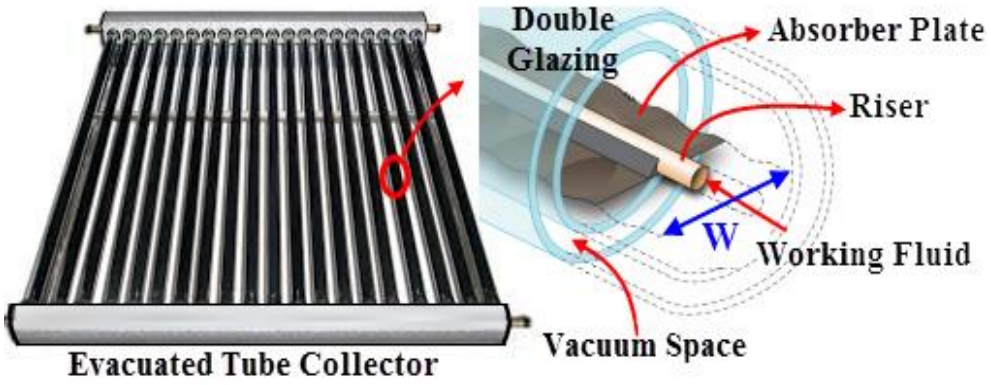

FIGURE 2.10 − The schematic diagram of a flat plate evacuated solar collector with cross sectional of a single tube

The obtainable energy by the working fluid through such solar collectors ($\dot{Q}_u$) could be computed as follow (Duffie and Beckman, 1980):

$$\dot{Q}_u = A_c F_R \{ S - U_l (T_{fi} - T_{am}) \} \tag{2.21}$$

Where, A_c, S, U_l, T_{fi} and T_{am} are respectively the collector absorber surface area, the absorbed solar flux, the overall loss coefficient of collector, the inlet working fluid temperature and ambient temperature. F_R is also the removal factor of collector which is given by:

$$F_R = \frac{\dot{m}_f c_f}{A_c U_l} \left[1 - \exp\left(\frac{-A_c U_l F'}{\dot{m}_f c_f} \right) \right] \tag{2.22}$$

In which $\dot{m}_f$ and c_f are the working fluid mass flow rate and specific heat respectively. Also, F′ is the efficiency factor of collector and could be calculated by:

$$F' = \left(W U_l \left[\frac{1}{\left(\frac{1}{U_l (W - D_{ot}) \varphi} + \frac{\delta_p}{k_p D_{ot}} \right)^{-1} + U_l D_{ot}} \right] + \frac{1}{\pi D_{it} \bar{h}_{fi}} \right)^{-1} \tag{2.23}$$

Where, W, δ_a, D_{ot}, D_{it}, k_p and h_{fi} are the gap between the tubes of collector, the absorber plate thickness, the inner and outer diameters of collector tubes, the thermal conductivity factor of absorber plate and the convective heat transfer coefficient of working fluid through the collector tubes, respectively.

Also, U_l in equation 2.21 is the overall loss coefficient of collector which is the origin of difference between the two collector types. For a simple flat plate collector it is the summation of three loss coefficients U_t, U_b and U_e which are respectively the loss coefficients from top, from back and from edge of the collector (Duffie and Beckman, 1980).

$$U_l = U_t + U_b + U_e \tag{2.24}$$

Where, U_t could be calculated by:

$$U_t = \left\{ \frac{N}{\frac{C}{T_{pm}}\left(\frac{T_{pm}-T_{am}}{N+f}\right)^e} + \frac{1}{\bar{h}_{wind}} \right\}^{-1} + \cdots \cdots \frac{\sigma\left(T_{pm}+T_o\right)\left(T_{pm}^2+T_o^2\right)}{\left(\bar{\varepsilon}_p+0.00591N\bar{h}_{wind}\right)^{-1}+\frac{2N+f-1+0.133\bar{\varepsilon}_p}{\bar{\varepsilon}_g}-N} \tag{2.25}$$

Where, $\bar{\varepsilon}_p$, $\bar{\varepsilon}_g$, T_{pm}, T_o and N are the plate and the cover emittance, the absorber plate average and ambient temperature and the number of glass layers. The other parameters could be calculated by the following equations:

$$f = \left(1+0.089\bar{h}_{wind}-0.1166\bar{h}_{wind}\bar{\varepsilon}_p\right)\left(1+0.07866N\right) \tag{2.26}$$

$$C = 520\left(1+0.000051\beta^2\right) \tag{2.27}$$

$$e = 0.43\left(1-\frac{100}{T_{pm}}\right) \tag{2.28}$$

In which, $\bar{h}_{wind}$ is wind convective heat transfer coefficient from the upside of the collector which could be calculated by:

$$\bar{h}_{wind} = 9.4\sqrt{Ve_m} \tag{2.29}$$

The losses coefficient through the back of the collector could be obtained as:

$$U_b \cong \frac{k\,A}{d} \tag{2.30}$$

Where, k is thermal conduction factor, A is the collector back area, and d is the collector insulator thickness. For the loss coefficient through the edge of the collector also, one has:

$$U_e \cong \frac{(U\,A)_e}{A_c}; \quad \text{where}: (U\,A)_e = \frac{P\,d_c\,k_e}{d_e} \tag{2.31}$$

In which, A_c, P, d_c, d_e and k_e are the absorber plate area, the collector perimeter, the collector thickness and the edges insulator thickness and the thermal conductivity factor from the edges. The value of T_{pm} could also be given by:

$$T_{pm} = T_{fi} + \frac{\dot{Q}_u / A_c}{F_R U_l}(1 - F_R) \tag{2.32}$$

On the other hand, the overall loss coefficient for a flat plate evacuated tube collector is similar to that for normal flat plate collectors by ignoring the conduction and convection heat transfer from the absorber plate to the glass tube since high vacuum normally exists inside the glass tube. Therefore, the overall heat loss coefficient from the collector is calculated by:

$$\frac{1}{U_l} = R_{r,p-g} + \frac{1}{\frac{1}{R_{cv,g-a}} + \frac{1}{R_{r,g-a}}} \tag{2.33}$$

According to the equation, the overall heat resistance from the collector includes radiative resistance from the absorber plate to the glass tube ($R_{r,p-g}$), radiative resistance from the glass tube to the environment ($R_{r,g-a}$) and convective resistance from the glass to the environment ($R_{cv,g-a}$).

Calculating the overall heat transfer coefficient of collector and the other unknown parameters in the above formulation, the obtainable heat from each collector is computed and subsequently, multiplying the number of collector modules by this value, one could calculate the total heat supplied to the system by the solar heating unit. Having the amount of absorbable solar energy by the collector set and obtainable energy by the working fluid, by implementing the first law of thermodynamic on the solar storage tank, one has:

$$m_{sst}\, c_f \frac{dT_{sst}}{dt} = n\dot{Q}_u - \dot{Q}_l \tag{2.34}$$

Where, n, m_{sst} and T_{sst} are the the number of collecto modules, the mass and temperature of working fluid in the solar storage tank, respectively. Also, $\dot{Q}_l$ is the amount of energy given to the solar heat exchangers to preheat the air stream and could be given by:

$$\dot{Q}_l = \dot{m}_{hf}\ c_f\ \left(T_{sst} - T_{fe}\right) \tag{2.35}$$

Where, $\dot{m}_{hf}$ and T_{fe} are the mass flow rate of hot working fluid injected into the solar heat exchanger and the temperature of working fluid outgoing from this heat exchanger, respectively. Finally, the temperature of working fluid in the solar storage tank over time could be given by:

$$T_{sst}^{\lambda+1} = \frac{\left(\dot{Q}_u - \dot{Q}_l\right)^{\lambda}}{m_{sst}\, c_f} + T_{sst}^{\lambda} \tag{2.36}$$

Note that the last three equations consider the storage tank as a lumped control volume. However, as warmer layers of working fluid lie in upper levels of the storage tank and vice versa; therefore, in order to have an accurate simulation, the storage tank could also be considered as a multi-node tank instead of being simply assumed as a lumped control volume. The number of nodes in a solar storage tank is recommended to be opted equal to 3 (Farzaneh-Gord *et al.*, 2013). Figure 2.11 illustrates the schematic of a three-node storage tank for which the energy balance on each node should be written as:

$$\begin{aligned} m_i \frac{dT_{s,i}}{dt} = {} & \left(\frac{UA}{c_p}\right)_i \left(T_a - T_{s,i}\right) + F_i^c \dot{m}_c \left(T_{co} - T_{s,i}\right) + \cdots \\ & \cdots \dot{Q}_{st} + \begin{cases} \dot{m}_{m,i}\left(T_{s,i-1} - T_{s,i}\right) & \text{if} \quad \dot{m}_{m,i} > 0 \\ \dot{m}_{m,i+1}\left(T_{s,i} - T_{s,i+1}\right) & \text{if} \quad \dot{m}_{m,i+1} < 0 \end{cases} \end{aligned} \tag{2.37}$$

Where, T_{co}, $\dot{m}_c$, T_L, T_o, and $\dot{m}_L$ are the temperature and mass flow rate of water entering the storage tank from the collectors side, the temperature of water outgoing toward the solar heat exchanger and the collectors and the mass flow rate of water coming back from the solar heat exchanger.

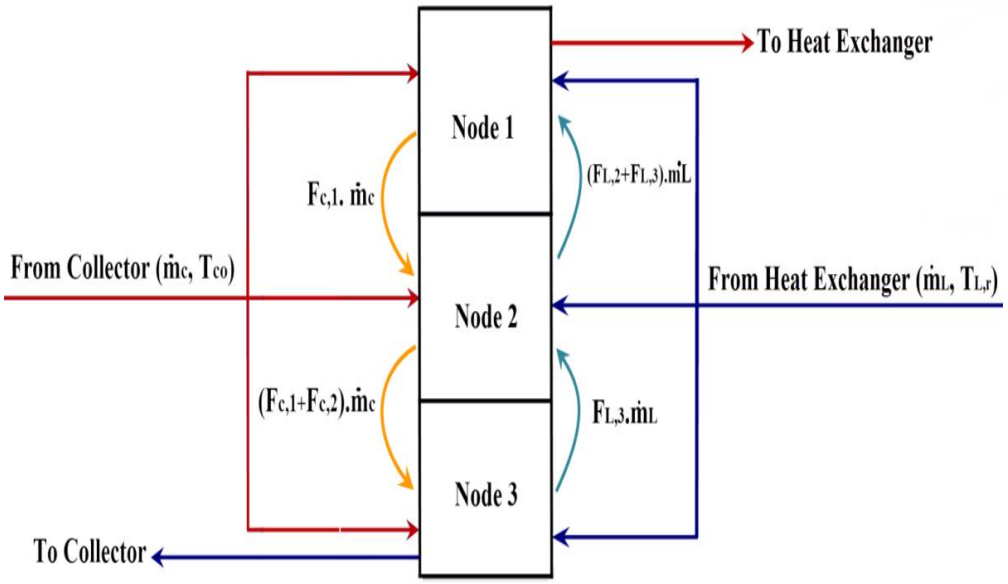

FIGURE 2.11 − The schematic of a three-node storage tank

Also, the function F_i^c in this equation specifies which node receives the hot water incoming from the collector modules side.

$$F_i^c = \begin{cases} 1 & \text{if} \quad i = 1 \ \text{and} \ T_{co} > T_{s,i} \\ 1 & \text{if} \quad T_{s,i-1} \geq T_{co} > T_{s,i} \\ 0 & \text{if} \quad i = 0 \ \text{or if} \ i = N+1 \\ 0 & \text{Otherwise} \end{cases} \tag{2.38}$$

In which, $T_{s,i}$ is the temperature of node i. Also, the function F_i^L determines which node receives the water coming back from the solar heat exchanger.

$$F_i^L = \begin{cases} 1 & \text{if} \quad i = 1 \ \text{and} \ T_{L,r} > T_{s,i} \\ 1 & \text{if} \quad T_{s,i-1} \geq T_{L,r} > T_{s,i} \\ 0 & \text{if} \quad i = 0 \ \text{or if} \ i = N+1 \\ 0 & \text{Otherwise} \end{cases} \tag{2.39}$$

Also, the water net mass flow rate between nodes i-1 and i can be given by:

$$\begin{cases} \dot{m}_{m,1} = 0 \\ \dot{m}_{m,i} = \dot{m}_c \sum_{j=1}^{i-1} F_j^c - \dot{m}_L \sum_{j=i+1}^{N} F_j^L \\ \dot{m}_{m,N+1} = 0 \end{cases} \quad (2.40)$$

Finally, $\dot{Q}_{st}$ in energy balance equation on the storage tank is the rate of energy flow from the storage tank into the heat exchanger can be calculated by:

$$\dot{Q}_{st} = F_i^L \dot{m}_L \left(T_{L,r} - T_{s,i}\right) \quad (2.41)$$

Note that for the solar heat exchangers the same formulation as hot heat exchangers could be used.

The fourth control volume is the expansion unit. Naturally, the electricity shortage in the PV farm could be offset by the turbo-generator set. Thus, the expander set total work ($\dot{W}_T$) could be given by:

$$\dot{W}_T = \frac{P_{E-G}}{\eta_{T-G}} \quad (2.42)$$

Where, P_{E-G} and η_{T-G} are the amount of auxiliary electricity required and the turbo-generator set overall efficiency, respectively. Taking the value of isentropic efficiency of expanders ($\eta_{T,is}$) into account, the isentropic outlet temperature and isentropic work of each turbine could be calculated. The actual work of each expander ($w_{T,act}$) and actual outlet temperature (T_{T-e}), then, could be given by:

$$w_{T,act} = w_{T,is}\,\eta_{T,is}\,; \quad T_{T-e} = \frac{w_{T,act} + c_{p-i} T_{T-i}}{c_{p-e}} \quad (2.43)$$

Just the same as the first control volume, iterative solution is required for calculating the accurate value of T_{T-e}. The total air mass flow rate through the turbine set ($\dot{m}_{T,t}$) can be given by:

$$\dot{m}_{T,t} W_{T,t} = \dot{W}_{T,t} = \sum \dot{m}_t w_t \quad (2.44)$$

Note that the heating heat exchanger series and the solar heat exchanger set are also related to this control volume for which the same formulation as the first control volume could be employed. Also, the formulation presented for the hot storage tank could be used for the cold storage tank. In this stage also, iterative solution is required to obtain the values of different parameters such as the turbine set total mass flow rate, turbines inlet and outlet temperatures, the work done by each expander, the temperature of water outgoing from each stage of solar heat exchanger as well as the temperature of working fluid outgoing from the hot heat exchangers.

For the auxiliary diesel air heater, as the fifth control volume in the target configuration, the amount of fuel ($\dot{V}_{fu}$) required for providing the required extra heat at each stage of expansion ($\dot{Q}_{dah}$) could be given by:

$$\dot{V}_{fu} = \frac{\dot{Q}_{dah}}{LHV\,\eta_h} \tag{2.45}$$

Where, LHV and η_h are respectively lower heating value of the fuel and the heater thermal efficiency (Arabkoohsar *et al.*, 2014). It should be noted that the air heater is supposed to burn natural gas as its main fuel for which the LHV is 37.8 MJ/Sm^3 (mega joule per standard cubic meter) with an efficiency of 50%. Note that $\dot{Q}^{j}_{dah}$ in each stage could also be calculated by:

$$\dot{Q}^{j}_{dah} = \dot{m}^{j}_{a} c^{j}_{p\text{-}a} \left(T_{dah\text{-}e} - T_{dah\text{-}i}\right)^{j} \tag{2.46}$$

In which, $T_{dah\text{-}e}$ and $T_{dah\text{-}i}$ are the required temperature before expansion and the auxiliary air heater inlet air temperature, respectively. The superscription j also refers to the number of stage.

It should be mentioned that during compression process, the equations related to the first and second control volume should be solved simultaneously while during the expansion process, the formulas associated with the second, the third, the fourth and the fifth control volumes must be solved at the same time.

In the end, regarding the formulation presented above, the overall daily fist law efficiency of the CAES system (ξ_{CAES}) could be defined as:

$$\xi_{CAES} = \frac{SPS}{\sum_{t=6}^{24}\left(I_{T,cm} + P_E + P_{fu}\right)} \tag{2.47}$$

In which, SPS is the total daily power produced by the CAES system, $I_{T,cm}$ is the total solar energy harvested by the collector modules, P_E is the extra power used by the compression unit to compress air and P_{fu} is total daily energy entered the system by consuming fuel (calculable by multiplication of the fuel mass flow rate by the fuel LHV). The variable t also refers to hourly time steps from 6 am to 12 pm.

2.3.2 Exergy Performance Investigation

In this section, the formulation related to the exergy analysis of the system is presented. Based on the second law of thermodynamic, the entropy balance for a control volume could be written as (Kargaran *et al.*, 2013):

$$T_o \frac{dS_{C.V}}{dt} - T_o \sum \dot{m}_i s_i + T_o \sum \dot{m}_e s_e - T_o \sum_{j=1}^{m} \frac{\dot{Q}_j}{T_j} - T_o \dot{\sigma}_{C.V} = 0 \tag{2.48}$$

Where, S, $\dot{m}$, $\dot{Q}_j$ and $\dot{\sigma}_{C.V}$ are the entropy, the mass flow rate, the rate of heat transfer and entropy generation in the control volume, respectively.

The exergy of a fluid stream (Ψ) is defined as the maximum work output that can be obtained from the stream as the fluid state changes reversibly from the given state to dead state. The dead state is a state of system when it is in thermodynamic equilibrium with its environment. Normally, the dead state is taken to be our environment and for many cases it is taken as 298 K and 101.325 kPa where the velocity and elevation relative to the environment are zero. Indicating the dead state with the subscript o, Ψ is defined as:

$$\Psi = \dot{m}\psi = \dot{m}\left[\left(h - h_o\right) - T_o\left(s - s_o\right) + \frac{Ve^2}{2} + gz\right] \tag{2.49}$$

Also, the irreversibility in the control volume is defined as the difference between the amount of maximum producible work in a reversible process and the amount of actual work.

$$\dot{I}_{C.V} = \dot{W}_{rev,u} - \dot{W}_{act} \tag{2.50}$$

As it was explained before, the first law efficiency shows what portion of the inlet energy in the system has been effectively employed to produce power by the control volume. Clearly, in many cases this definition, by itself, cannot be a strong criterion to judge the system performance. In such cases, the second law efficiency can be helpful to evaluate the system performance more accurately. In fact, the first law efficiency shows how well energy is used comparing with an ideal process and the second law efficiency (ε) indicates how well availability is used [26].

$$\varepsilon = \frac{\text{useful availabili ty output}}{\text{availabili ty input}} = 1 - \frac{\text{availabili ty distruction and losses}}{\text{availabili ty input}} \tag{2.51}$$

After presenting this fundamentals on exergy analysis, one could assess the exergy performance of a CAES system. For the compressor set, considering the assumptions taken for the compressors, the entropy balance on each compressor could be written as:

$$\dot{\sigma}_C = \dot{m}_a \left(s_e - s_i\right)_C \tag{2.52}$$

Where, $\dot{\sigma}_C$ is the rate of entropy generation through the compressor. In addition, the amount of irreversibility in the compressor is also given by:

$$\dot{I}_C = T_o \left[\dot{m}_a \left(s_e - s_i\right)\right]_C \tag{2.53}$$

Finally, defining the second law efficiency for a compressor as the ratio of exergy increase in the fluid through the compressor to the actual work of compressor, the compressor second law efficiency could be calculated as:

$$\varepsilon_C = 1 - \frac{T_o\left(s_e - s_i\right)_C}{\left(h_e - h_i\right)_C} \tag{2.54}$$

For the heat exchangers, on the other hand, regarding the assumptions taken, from the second law of thermodynamic, one has:

$$\dot{\sigma}_{che} = \dot{m}_a \left(s_e - s_i\right)_{che,a} + \dot{m}_f \left(s_e - s_i\right)_{che,f} \tag{2.55}$$

Where, subscripts che,a and che,f refer to the air and working fluid streams through the cooling heat exchangers, respectively. Finally, the amount of irreversibility in each heat exchanger can be calculated by:

$$\dot{I}_{che} = -\dot{m}_a\left[(h_e - h_i) - T_o(s_e - s_i)\right]_{che,a} - \dot{m}_f\left[(h_e - h_i) - T_o(s_e - s_i)\right]_{che,f} \quad (2.56)$$

Defining the second law efficiency for a heat exchanger as the ratio of exergy increase in the cold fluid to exergy increase in the hot fluid, one has:

$$\varepsilon_{che} = \frac{\dot{m}_f\left[(h_e - h_i) - T_o(s_e - s_i)\right]_{che,f}}{\dot{m}_a\left[(h_i - h_e) - T_o(s_i - s_e)\right]_{che,a}} \quad (2.57)$$

Note that, in a heat exchanger, there are mainly two reasons for wasting availability. The first one is due to heat exchange across a finite difference temperature and the second one is due to fluid friction.

The third component in the compression unit is the hot storage tank. The entropy balance on the storage tank may be written as:

$$S_2 - S_1 = \left(\sum \dot{m}_i s_i - \sum \dot{m}_e s_e + \dot{\sigma}\right)_{hst} \Delta t \quad (2.58)$$

Irreversibility in a thermal energy storage system by doing an exergy balance on the storage tank is given by:

$$I_{hst} = \left(\sum \dot{m}_e\left[(h_e - h_o) - T_o(s_e - s_o)\right] - \sum \dot{m}_i\left[(h_e - h_o) - T_o(s_e - s_o)\right]\right)_{hst} \Delta t + (m_2 u_2 - m_1 u_1)_{hst} \quad (2.59)$$

The second law efficiency for the hot storage tank can only be defined for a period of performance including a full charging step as well as a complete discharging step and it is written as below (Arabkoohsar *et al.*, 2014):

$$\varepsilon_{hst} = \left(\frac{\Delta\Psi_{Discharging}}{\Delta\Psi_{Charging}}\right)_{hst} = \left(\frac{[\Delta H - T_o \Delta S]_{Discharging}}{[\Delta H - T_o \Delta S]_{Charging}}\right)_{hst} \quad (2.60)$$

In other words, the second law efficiency measures the energy quality degradation due to both the difference in charging and discharging temperatures and thermal losses. It is a measure of the conservation of exergy through the storage, i.e. the ability to generate the same amount of power from the hot storage tank as from the original energy used to charge the system.

For the the air storage reservoir, the entropy balance results to:

$$S_2 - S_1 = \left(\sum \dot{m}_i s_i - \sum \dot{m}_e s_e + \dot{\sigma} \right)_{ca} \Delta t \tag{2.61}$$

The irreversibility of the reservoir could be given by:

$$I_{ca} = \left(\dot{m}_e \left[(h_e - h_o) - T_o (s_e - s_o) \right] - \dot{m}_i \left[(h_i - h_o) - T_o (s_i - s_o) \right] \right)_{ca} + \left(m_2 u_2 - m_1 u_1 \right)_{ca} \tag{2.62}$$

The second law efficiency of the reservoir should also be defined for a period of performance including a full charging step as well as a complete discharging step.

$$\varepsilon_{ca} = \left(\frac{\Delta \Psi_{Discharging}}{\Delta \Psi_{Charging}} \right)_{ca} = \left(\frac{\left[\Delta H - T_o \Delta S \right]_{Discharging}}{\left[\Delta H - T_o \Delta S \right]_{Charging}} \right)_{ca} \tag{2.63}$$

The next control volume is the solar heating unit. In this control volume, for the solar collector module, the second law efficiency is defined as the ratio of the net exergy obtained from the collector by the working fluid (Ψ_f) to the received solar exergy by the collector (Ψ_{cm}) (Pathak *et al.*, 2014).

$$\varepsilon_{cm} = \frac{\Psi_f}{\Psi_{cm}} \tag{2.64}$$

The amount of solar exergy received by the solar collectors (either evacuated tube or simple flat plate collectors) could be calculated by (Arabkoohsar *et al.*, 2014):

$$\Psi_{cm} = \eta_o \cdot I_{T,cm} \cdot A_{cm} \cdot \left[1 - \left(\frac{T_{am}}{T_{sun}} \right) \right]; \quad \eta_o = \frac{S_{cm}}{I_{T,cm}} \tag{2.65}$$

Where, η_o is the optical efficiency of the collector. The rate of net exergy gained by water while passing through the collector could also be given by:

$$\Psi_f = \dot{m}_f \left[(h_e - h_i) - T_o (s_e - s_i) \right]_f \tag{2.66}$$

Finally, the irreversibility of the collector module is calculated by:

$$\dot{I}_{cm} = \Psi_{cm} - \Psi_f \tag{2.67}$$

For calculating the storage tank entropy balance, exergy efficiency and irreversibility, the same correlations as the formulation presented for the cold storage tank in the second control volume could be employed.

The next control volume in the CAES system is the expansion unit in which the first component to be analyzed is the expanders set. The entropy balance on each expander could be presented as:

$$\dot{\sigma}_T = \dot{m}_a \left(s_e - s_i \right)_T \tag{2.68}$$

The amount of irreversibility in each turbine stage is also obtained by:

$$\dot{I}_T = \dot{m}_a \, T_o \left(s_e - s_i \right)_T \tag{2.69}$$

The second law efficiency of each expander is defined as the ratio of the actual work of the turbine to the amount of decrease in the availability of air while passing through that:

$$\varepsilon_T = \frac{1}{1 + \dfrac{T_o (s_e - s_i)_T}{c_{p,ave} (T_i - T_e)_T}} \tag{2.70}$$

For exergy analysis on the other components in this control volume such as the solar heat exchangers, the heating heat exchangers and the cold storage tank the same formulation as previous sections could be presented.

The last control volume is the auxiliary air heater for which the second law of thermodynamic could be written as:

$$\dot{\sigma}_{dah} = \dot{m}_a \left(s_e - s_i\right)_{dah} \tag{2.71}$$

Naturally, the heater inlet exergy ($\Psi_{h,i}$) is the summation of the inlet air exergy and the chemical exergy along with the fuel (Arabkoohsar *et al.*, 2014).

$$\Psi_{h,i} = \Psi_{fu} + \dot{m}_a \left[(h_i - h_o) - T_o (s_i - s_o)\right]_a \; ; \quad \Psi_{fu} = \dot{n}_{fu} \left[(\hat{h} - \hat{h}_o) - T_o (\hat{s} - \hat{s}_o) + \hat{\psi}^{ch}\right]_{fu} \tag{2.72}$$

Note that the fuel used by the heater is assumed to be pure methane. The heater outlet exergy ($\Psi_{h,e}$) is also the summation of exergy along with the outgoing combustion productions from the exhaust (Ψ_{ex}) and the heated air outgoing from the heater. Therefore:

$$\Psi_{h,e} = \Psi_{ex} + \dot{m}_a \left[(h_e - h_o) - T_o (s_e - s_o)\right]_a \tag{2.73}$$

It is worth mentioning the prior study of the authors shows the combustion procedure in such an air heater is usually done with approximately 300% theoretical air (Arabkoohsar *et al.*, 2014). As the fuel is natural gas which mainly could be considered as pure methane, therefore, the combustion production for one mole of the fuel is a mixture of different gases as:

$$CH_4 + 6\left(O_2 + 3.76N_2\right) \rightarrow \left(CO_2\right) + 2\left(H_2O\right)_g + 22.56\left(N_2\right) + 4\left(O_2\right) \tag{2.74}$$

Therefore, the combustion production exergy could be calculated by:

$$\Psi_{ex} = \sum \dot{n}_j \left[(\hat{h} - \hat{h}_o)_j - T_o (\hat{s} - \hat{s}_o)_j + \left(y_j \hat{\psi}^{ch} + \hat{R} \cdot T_o \cdot y_j \cdot Ln\left(y_j\right)\right)\right]_{ex} \tag{2.75}$$

In the last few equations, $\hat{\psi}^{ch}$, $\hat{R}$, $\dot{n}$ and y are the chemical exergy, universal constant of gases (8.314 kJ/kmol.K), the molar flow rate and fraction of the fuel and combustion productions, respectively. $\hat{h}$, $\hat{s}$, $\hat{h}_o$ and $\hat{s}_o$ are also the molar enthalpy and entropy of the combustion productions at exhaust and reference conditions, respectively. The EES software could be used to solve the values of all these parameters. The value of chemical

exergy and molar entropy and enthalpy in reference conditions related to the aforementioned elements are given in table 2.2.

TABLE 2.2 − The values of chemical exergy and molar enthalpy of different elements in reference conditions

Properties	**CH_4**	**CO_2**	**H_2O**	**N_2**	**O_2**
Chemical Exergy (MJ/kmol)	831	14.1	8.6	0.64	3.95
Molar Enthalpy in Reference Condition (MJ/kmol)	-74.87	-393.5	-241.8	0	0
Molar Entropy in Reference Condition (MJ/kmol)	0.186	0.213	0.188	0.191	0.205

Taking the results of the above formulation into account, one could calculate the amount of irreversibility in the heater by:

$$\dot{I}_h = \Psi_{h,i} - \Psi_{h,e} \tag{2.76}$$

The second law efficiency of the heater is also calculated as:

$$\varepsilon_h = \frac{\dot{m}_a \left[\left(h_e - h_i\right) - T_o \left(s_e - s_i\right) \right]_a}{\Psi_{h,i}} \tag{2.77}$$

Finally, the total daily second law efficiency of the CAES unit (ε_{CAES}) could be calculated by the following equation:

$$\varepsilon_{CAES} = \frac{SPS}{\sum_{t=6}^{24} \left(\Psi_{cm} + P_E + \Psi_{fu} \right)} \tag{2.78}$$

Where, Ψ_{cm} and Ψ_{fu} are the total daily exergies entered the system by the collector modules and consuming fuel, respectively. The other parameters have been already addressed in the previous section.

3. PV Technology

In this chapter, PV technology is discussed comprehensively and subsequently, after presenting the fundamentals of this technology, detailed energy and exergy modeling of a PV farm is presented. Also, this chapter includes a thorough uncertainty analysis description about PV farms. In order for being more coherent in giving the required information, this chapter is classified into six subsections.

3.1 Fundamentals of PV Technology

PV is the method of converting sunlight into direct current (DC) electricity. The main part of a PV system is the PV cell made by semiconducting materials exhibiting the PV effect and contains no moving part. PV cells have their origins from some of the most important scientific developments of the 20^{th} century. In the beginning of this century, Max Planck tried to explain the nature of light emitted by hot bodies such as the sun by making some assumptions about energy being restricted to discrete levels to match theory and observations. He postulated that light was made of small particles (photons) each of which has trifle energy depending on its color, so that, a blue photon has almost twice a red photon energy while an infrared photon has even less energy than a red photon. Einstein's radical suggestion led to the formulation and development of quantum mechanics and then wave equation (Stachel, 1998). By solving this equation for solid materials, Wilson explained the difference between metals as good conductors of electricity, insulators and semiconductors with their intermediate electrical properties (Green, 2000).

In metals, electrons which are the carriers of electrical charge are free to move around in metals, allowing electrical currents to flow easily. In insulators, electrons are locked into the bonds holding the atoms of the insulator together and need a jolt of energy to free them from these bonds. The same applies to semiconductors, but a smaller jolt is needed here. In fact, in semiconductors, even the red photons in sunlight have enough energy to free the electrons. The first silicon solar cell was discovered totally by accident when Ohl shone a flashlight on a subject that he thought it is a pure rod of silicon and he surprisingly observed a very large voltage (Riordan and Hoddeson, 2005).

Closer investigation showed that small concentrations of impurities were giving portions of the silicon properties dubbed negative (n-type) existing due to a surplus of mobile

electrons with their negative charge. Other regions had positive (p-type) properties due to a deficiency of electrons, causing an effect similar to a surplus of positive charge (something close to a physical demonstration of the mathematical adage that two negatives make a positive). Shockley designed the first transistor by studying the theory of the devices formed from p-n junctions (Riordan and Hoddeson, 2005). The studies on semiconductors followed and finally the first efficient solar cell was made in 1954 and the first commercial use of the new solar cells was on spacecrafts in 1958. Thereafter, solar cells were employed in many other systems while more studies in this area would result in producing more efficient PV cells every day.

In the PV cell there are two or more thin layers of semiconducting material, most commonly silicon. When the silicon exposed to light, electrical charges are generated and this can be conducted away by metal contacts as direct current. In fact, a PV cell is composed of a P-type and an N-type semiconductor. Solar irradiation hitting the cell produces two types of electrons, negatively and positively charged electrons in the semiconductors. Negatively charged electrons gather around the N-type semiconductor while positively charged electrons gather around the P-type semiconductor. Upon connecting loads, electric current flows between the two electrodes (Manor and Katz, 2012). Figure 3.1 shows how a PV cell produces electricity current.

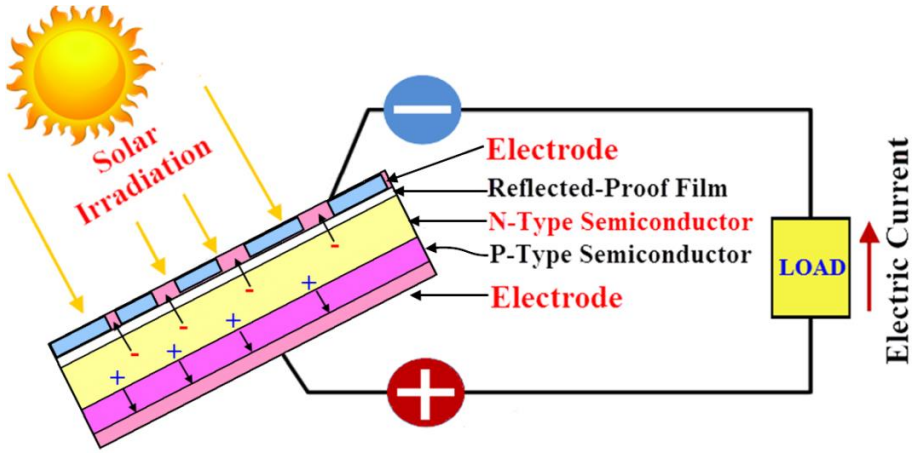

FIGURE 3.1 − The schematic diagram of a PV cell

It is noteworthy that depending on the power capacity required, any number of panels can be added to an existing system. Clearly, the higher capacities are required, the more numbers of PV cells should be employed and connected. Normally, a PV power generation unit is rated in peak kilowatts (kWp) referring to the maximum amount of power

that the system is expected to produce (naturally, when the sun is directly overhead on a clear day). Generally, PV systems may be built in various configurations as grid connected configuration equipped with an energy storage system (mainly battery), off-grid (standalone) configuration without any energy storage system and off-grid with energy storage and AC converter. A PV system in each of the aforementioned configurations could also be a residential or utility system, a distributed or centralized system, a system with tracking planes or only fixed planes and so on.

3.2 PV Technology Background

In recent years, extensive experimental and simulation studies are being carried out on the application of PV systems as distributed energy sources to harness power from the non-conventional energy sources with low environmental impacts. Mendez et al. have studied the applicability of autonomous PV systems in supplying power to remote isolated villages in Morocco (Mendez *et al.*, 2013). Wies et al. have carried out the economic analysis and environmental impact assessment of integrating a PV array into diesel electric power systems for remote villages (Wies *et al.*, 2013). Simulation or analytical studies mainly involve development of robust mathematical models for PV arrays which can be further utilized for the analysis of hybrid power systems. Russell has presented the accurate flexible PV array and inverter models to analyze the performance of PV system, and has addressed the issues, which are important to designers and manufacturers (Russell, 1994). King et al. (1996) have developed a Microsoft Windows based electrical simulation model for PV cell, modules and arrays that can be used to analyze individual cells, to analyze the effects of cell mismatch or reverse bias heating in modules, and to analyze the performance of large arrays of modules including bypass and blocking diodes. Gow and Manning have reported the development of an effective system to characterize polycrystalline PV cells and generated the device dependent data that provides a link between the environmental variables such as irradiance and temperature, and the electrical characteristics of the device (Gow and Manning, 1996). A computer simulation model able to demonstrate the cell's output features in terms of irradiance and temperature environmental changes have been given by Chenni et al. They have also tested the model to simulate three popular type of photovoltaic panels constructed with different materials like copper indium diselenide thin film, multi-crystalline silicon and mono-crystalline silicon (Chenni *et al.*, 2006).

Many studies also have been done on the PV systems connected to grid. In fact, a PV grid connected system provides power for a large independent grid which in most cases is the public electricity distribution grid. The grid connected PV systems could vary in size from a few kWp (mainly for residential purposes) up to tens of GWp. Experience curves methodology, which is used to predict the required levels of cumulative PV shipments for reaching the computed break-even costs of PV systems, was employed by Poponi to evaluate the prospects of PV technology diffusion for power generation in grid connected systems (Poponi, 2003). Rehman et al. used a database including the monthly-daily averaged solar irradiation and sunshine duration to study Saudi Arabia in terms of solar energy receiving potential. They also evaluated the feasibility of power production by a 5 MW grid connected PV plant (Rehman *et al.*, 2007). Al-Hassan et al. studied the electricity demand pattern improvement in Kuwait using grid connected PV systems. During the performance evaluation, they found out that the peak electricity demand is equal to the maximum solar irradiation in Kuwait. This, actually, would emphasize that firstly, how effective could be the PV station in minimizing the electrical load demand and secondly, the peak load could significantly decrease with grid connected PV systems (Al-Hasan *et al.*, 2004). Ito et al. (2003) proposed installing a 100 MW PV plant in the Gobi desert. They evaluated this PV plant economically (by calculating the probable payback period) and environmentally (by computing the life-cycle CO_2 emission rate). Muneer et al. studied the long term prospects of PV power generation in large scales in arid and semi-arid areas (Muneer *et al.*, 2003). Another work that shows the great advancement in large scale PV power generation was done by Cunow et al. who explained the PV plant at the new Munich Trade Fair Centre in terms of the employed system technology, operational control and costs (Cunow and Giesler, 2001). Kivaisi (2000) proposed the installation of a PV plant with 3 kWp capacity in Zanzibar, Tanzania aimed at providing the required power of a school, health center, school staff quarters, and mosques.

A PV power production system could be used to generate electricity along with another power production unit. This type of generation is called hybrid power generation. Actually, a hybrid power generation system combines a renewable energy source system (specifically, a PV system) with other forms of power generation. The accompanying power generation system could be either a conventional or another renewable energy source power generator system. Numerous works and simulations have also been done in this area. In this regards, Barton et al. described a novel method of modeling an energy store used to match the

power output of a power production unit, including a wind turbine and a PV array, to a variable electrical load (John and David, 2006). Deshmukh et al. (2008) thoroughly explained the methodologies of modeling of hybrid renewable energy system designs. They showed induced that the hybrid PV/wind energy systems are getting popular fast. They also comprehensively discussed the issues related to penetration of such system in the power distribution grids as it provides prospects of incorporating in power generation capacity to improve power quality, due to the dispersed generation. El-Shatter et al. (2002) designed a hybrid PV/fuel cell generation system employing an electrolyzer for hydrogen generation and applied a fuzzy regression model (FRM) for maximum power point tracking to extract maximum available solar power from PV arrays under variable insulation conditions. They then proposed an energy system comprising three energy sources, namely PV, wind and fuel cells each of which is controlled so as to deliver energy at optimum efficiency employing fuzzy logic control to achieve maximum power tracking for both PV and wind energies and to deliver the maximum power to a fixed dc voltage bus (El-Shatter *et al.*, 2006). Maclay et al. (2006) developed a model of a solar–hydrogen powered residence, in both stand-alone and grid-parallel configuration using Matlab/Simulink that assesses the viability of employing a regenerative fuel cell (RFC) as an energy storage device to be used with photovoltaic (PV) electrical generation and investigated the design requirements of RFC sizing, battery sizing, charge/discharge rates, and state of charge limitations. Zervas et al. (2008) studied a hybrid power generation system consisting of the following main components: Photovoltaic Array (PV), Electrolyzer, Metal Hydride Tanks, and Proton Exchange Membrane Fuel Cells (PEMFC) that can efficiently store solar energy by transforming it to hydrogen, which is the fuel supplied to the fuel cell. Nelson et al. (2006) presented unit sizing and an economical evaluation of a hybrid wind/PV/fuel cell (FC) generation system and a cost comparison with a wind/PV/battery system for a typical home in the US Pacific Northwest and the current cost figures as well as the break-even line distance comparison showed a clear economic advantage of the traditional wind/PV/battery system over the wind/PV/FC/electrolyzer system, indicating a need for research and technological advances in the FC/electrolyzer area. Shahid et al. (2008) analyzed long-term solar radiation data of Dhahran to assess the techno-economic feasibility of utilizing hybrid PV–diesel–battery power systems to meet the load of a typical residential building and exhibited that for a given hybrid PV–diesel configuration, the number of operational hours of diesel generators decreases with increase in PV capacity and the decrease in diesel run time is further enhanced by inclusion of battery storage.

The abovementioned works are only a few out of thousands of studies carried out in the field of solar PV technology that caused such a considerable advancement in this field. Overall, according to all of the various studies accomplished on the PV systems, one could conclude that:

a) The geographical location has a strong impact on the level of reliability obtained by utilizing the PV system and the economic benefits from the fuel offsets.

b) The effect of local climate conditions on the temperature of module is significant and hence, affects the electrical energy generation.

c) The size of the incentive, cost of residential solar PV, electrical energy price, and solar irradiation intensity decide the strength of the solar renewable energy credit policy.

d) It is important to model the solar photovoltaic system to optimize system design, to improve reliability of projected outputs to ensure favorable project financing and to facilitate proper operation and maintenance.

e) Precise near-term forecasting of system production for use in grid-integration, and for smart and micro grid development can be made using Regression analysis.

f) Regression modeling can also be used for prediction of PV system health, and thus to identify cell and module failures in a system.

3.3 PV System Components

A PV system consists of various components such as the PV cells, mechanical and electrical connections and mountings and the electrical output regulators and modifiers. Figure 3.2 shows the main components of a PV power generation system.

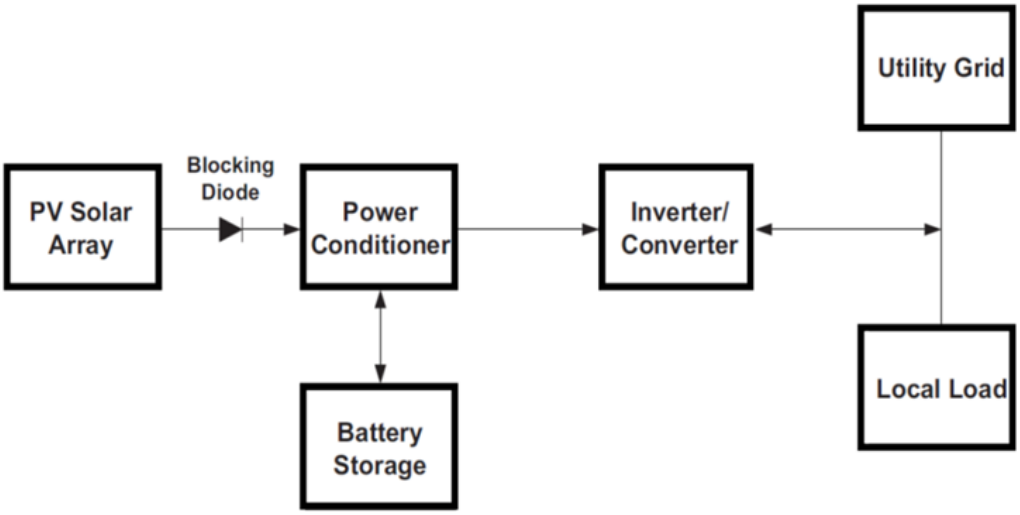

FIGURE 3.2 − The PV power production components

According to the figure, the PV array converts the solar energy to DC power and the blocking diode facilitates this power to flow only towards the power conditioner. Without a blocking diode, the battery would discharge back through the solar array during low solar irradiations. Power conditioner contains a maximum power point tracker (MPPT), a battery charge and a discharge controller. The MPPT ensures that the maximum power generated by the PV cells is extracted at all instants while the charge discharge controller is responsible for preventing overcharging or over discharging of the battery bank required to store electricity generated by the solar energy during sunless time. In simple PV systems, where PV module voltage is matched to the battery voltage, use of MPPT electronics is generally considered unnecessary, since the battery voltage is stable enough to provide near-maximum power collection from PV module. A standalone system does not have a connection to the grid (Cunow and Giesler, 2001).

3.3.1 PV Array

As it was mentioned before, the main part of a PV system is the PV cell. Many types of PV cells are available today. The plates employed in the PV systems over the last years could mainly be divided into four categories. The first one is monocrystalline silicon cell which is made of pure monocrystalline silicone. In this cell, the silicone has a single continuous crystal lattice structure with almost no defects or impurities. The main advantage of monocrystalline cells is their high efficiency, which is typically more than 15%. The advantage of these cells is that a complicated manufacturing process is required to produce

monocrystalline silicon, which results in slightly higher costs than the other technologies (Liu *et al.*, 2014).

The second PV cell type is multicrystalline silicon cell. Multicrystalline cells are produced using numerous grains of monocrystalline silicon. In the manufacturing process, molten polycrystalline silicon is cast into ingots, which are subsequently cut into very thin wafers and assembled into complete cells. Multicrystalline cells are cheaper to produce than monocrystalline ones because of the simpler manufacturing process required. They are, however, slightly less efficient with average efficiencies being around 12% (Liu *et al.*, 2014).

The third group of PV cells is made of amorphous silicon. Generally, the main difference between these cells and the previous ones is that, instead of the crystalline structure, amorphous silicon cells are composed of silicon atoms in a thin homogenous layer. Additionally, amorphous silicon absorbs light more effectively than crystalline silicon, which leads to thinner cells, also known as a thin film PV technology. The greatest advantage of these cells is that amorphous silicon can be deposited on a wide range of substrates, both rigid and flexible. Their disadvantage is the low efficiency, which is on the order of 6%. Nowadays, the panels made of amorphous silicon solar cells come in a variety of shapes, such as roof tiles, which can replace normal brick tiles in a solar roof (Zhang *et al.*, 2014).

Finally, the fourth group of solar cells is thermo-photovoltaics. These are PV devices that use the infrared region of radiation instead of sunlight. In fact, these devices use the thermal solar irradiation. A complete thermo-photovoltaics system includes a fuel, a burner, a radiator, a long wave photon recovery mechanism, a PV cell and a waste heat recuperation system. Such devices convert radiation using exactly the same principles as PV devices, however, the key difference between them and PV conversion are the temperatures of the radiators and the system geometries. In a solar cell, the radiation is received from the sun (with a temperature of about 6000 K and a distance of 150×10^6 km) while a complete thermo-photovoltaics device receives radiation in either the broad or narrow band, from a surface at a much lower temperature of about 1300-1800 K and a distance of only a few centimeters. Although a blackbody power radiated by a surface varies at the fourth power of the absolute temperature, the inverse square law dependence of the power received by the detectors dominates. Therefore, although the power received by a non-concentrator solar cell is on the order of 0.1 W/cm^2, that received by a complete thermo-photovoltaics converter is likely to be

5-30 W/cm^2, depending on the radiator temperature. Consequently the power density output of such converter is expected to be significantly greater than that from a non-concentrator PV converter (Griffin *et al.*, 1998).

In addition to the aforementioned types, a number of other promising materials such as a cadmium telluride and copper indium diselenide are used today for PV cells. The main trends today concern the use of polymer and organic solar cells. The attraction of these technologies is that they potentially offer fast production at low cost in comparison to crystalline silicon technologies, yet they typically have lower efficiencies (about 4%), and despite the demonstration of operational lifetime and dark stabilities under inert conditions for thousands of hours, they suffer from stability and degradation problems. Organic materials are attractive; primarily due to the prospect of high output manufacture using reel-thin, flexible devices, which may be integrated into appliances or building materials and tuning of color through the chemical structure (Jhong-Ciao *et al.*, 2015).

In addition to the PV cell material; there are two other important parameters that should be taken into account about the PV array in a PV power generation system as the tracking mode and the mode of connection of the PV cells (parallel or series).

Table 3.1 details the most common types of PV cells in the market with their expected efficiencies.

TABLE 3.1 − Details of various PV cells available in the market

Cluster	Type	Expected Efficiency (%)
Silicon Semiconductor	Monocrystalline	15-20
	Multicrystalline	10-14
	Amorphous	7-9
Compound Semiconductor	Gallium Arsenide	19-22
Organic Semiconductor	Dye-Sensitized	6-8

A solar tracker is a device that orients the PV array toward the sun so that the PV array angle relative to the solar rays is always adjusted and as a result, the amount of incident solar irradiation on the panels increase significantly. There are various methods of tracking the sun to maximize the amount of solar irradiation receivable during the day. In fact, in addition to a horizontal surface on the floor, seven more different cases are possible to improve the amount of solar irradiation receivable by a plane.

The first way to improve the obtainable solar irradiation by a surface is employing slopped surfaces. The angle of declination is recommended to be opted equal to the local latitude plus a value between 10 and 15 (Farzaneh-Gord *et al.*, 2012). This approach will improve the solar irradiation collection slightly; however, the advantage of such system is that no cost is added to the initial cost required.

The second tracking mode is a slopped plane rotating around a vertical axis. The third option is employing east-west axis rotator tracker system with single daily adjustment. The fourth option is employing the previous type of tracker with continuous adjustment instead of daily adjustment. Naturally, such a tracker is better than the single daily adjustment tracker, however, the cost of this system may be higher than the previous one due to the more complicated technology required in manufacturing process. North-south axis rotator tracker with continuous adjustment and a plane rotated about the north-south axis parallel to the earth's axis with continuous adjustment are the other two possible methods of solar tracking (Chin *et al.*, 2011).

In addition to the above mentioned tracking modes which are all single axis tracking systems, the last possible system to be employed is a dual axis tracker which is clearly more efficient than others as the incident angle of solar rays to the PV panel is always zero. This system, however, is the most expensive and costly one among all the tracking mode candidates and one should trade off energy-economically to choose the best option for being employed in a PV system (Barker *et al.*, 2013). Detailed formulation about all of the above tracking modes will be presented in the next sections.

In terms of PV cells arrangement, the cells are normally grouped into modules which are encapsulated with various materials in order to protect the cells and the electrical connectors from the environment. PV cell modules consist of N_{PM} parallel branches and each branch has N_{SM} solar cells in series. The values of N_{SM} and N_{PM} depend on the values of required current and voltage. Figure 3.3 shows the schematic diagram of PV cells arrangement in a PV power generation system.

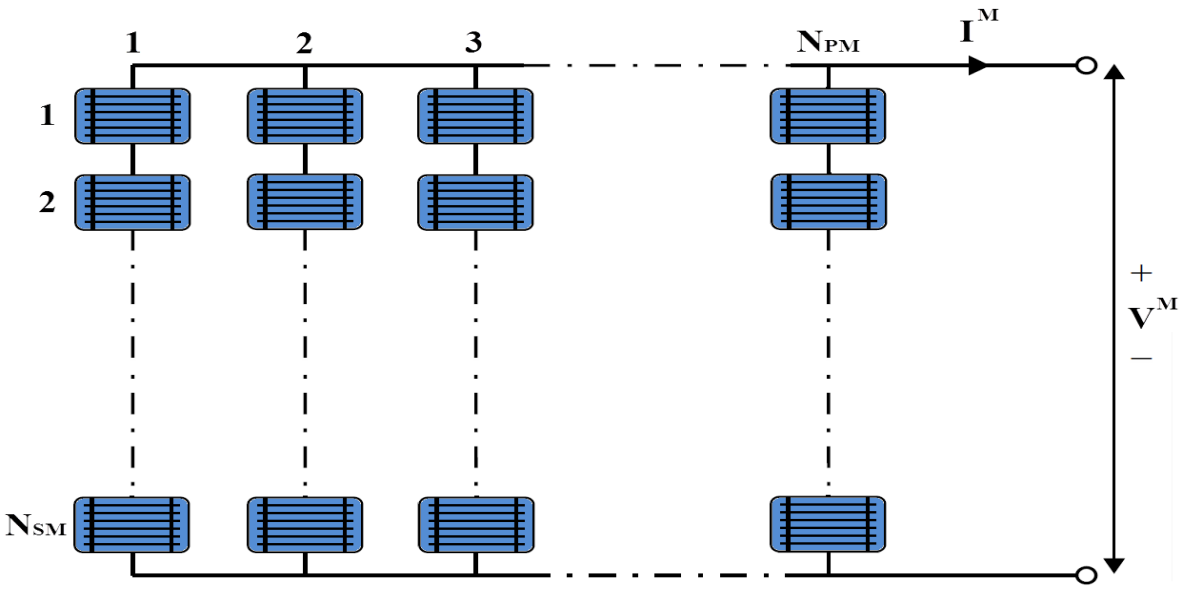

FIGURE 3.3 − Schematic diagram of a PV module consisting of N_{PM} branches each with N_{SM} cells in series

The formulation about this issue is also presented in the next sections.

3.3.2 Battery

Batteries (energy storage systems) are required in many PV systems to supply power at night or when the PV system cannot meet the demand. The selection of battery type and size depends mainly on the load and availability requirements. When batteries are used, they must be located in an area without extreme temperatures, and the space where the batteries are located must be adequately ventilated. The main types of batteries available today include lead-acid, nickel cadmium, nickel hydride and lithium. Deep cycle lead-acid batteries are the most commonly used. These can be flooded or valve-regulated batteries and are commercially available in a variety of sizes. Flooded or wet batteries require greater maintenance but, with proper care, can last longer, whereas valve regulated batteries require less maintenance (Reference Module in Chemistry, 2014).

The principal requirements of batteries for PV system are that they must be able to accept repeated deep charging and discharging without damage. Although PV batteries have an appearance similar to car batteries, but latter are most designed for repeated deep discharges and should not be used. For more capacity, batteries can be arranged in parallel. Batteries are used mainly in standalone PV systems to store the electrical energy produced during the hours when the PV system covers the load completely and there is excess or when there is sunshine but no load is required. During the night or during periods of low solar

irradiation, the battery can supply the energy to the load. Additionally, batteries are required in such a system because of the fluctuating nature of the PV system output. Batteries are classified by their nominal capacity, which is the number of ampere hours (Ah) that can be maximally extracted from the battery under predetermined discharge conditions. The efficiency of a battery is the ratio of the charge extracted during discharge divided by the amount of charge needed to restore the initial state of charge. Therefore, the efficiency depends on the state of charge and the charging and discharging current. The state of charge is the ratio between the present capacity of the battery and the nominal capacity. According to the definition, the value of the state of charge should be from 0 to 1 (Unterrieder et al., 2015).

The other parameters related to batteries are the charge or discharge regime and lifetime of the battery. The charge regime is the parameter that reflects the relationship between the nominal capacity of a battery and the current at which it is charged (or discharged). The lifetime of a battery is also the number of charge-discharge cycles the battery can sustain before losing 20% of its nominal capacity (Dufo-López *et al.*, 2014).

It should be mentioned here that in grid connected and large scale PV power generation systems, batteries cannot be the best choice due to the very large size of batteries required, limited capacity and some technical problems such as internal self-discharge. For these reasons, other methods of energy storage are preferred which will be discussed in the next chapter.

3.3.3 Inverter

An inverter is used to convert the DC type electricity into AC electricity. The output of the inverter can be single or three phase. Inverters are rated by the total power capacity ranged from hundreds of watts to mega watts. Some inverters have good surge capacity for starting motors and others have limited surge capacity. The designer should specify that both the type and size of the load the inverter is intended to service. The inverter is characterized by a power-dependent efficiency. Besides changing the DC into AC, the main function of the inverter is to keep a constant voltage on the AC side and convert the input power into the output power with the highest possible efficiency. Naturally this efficiency is defined as the ratio of power output to the power input. Numerous types of inverters are available, but not all are suitable for use when feeding power back into the main supply (Ozdemir *et al.*, 2014).

3.3.4 Charge Controller

Controllers regulate the power from PV modules to prevent the batteries from overcharging. The controller can be shunt type or series type and also function as a low battery voltage disconnect to prevent the battery from over discharging. The controller is chosen for the correct capacity and desired features (Müller *et al.*, 2014). Normally, controllers allow the battery voltage to determine the operating voltage of a PV system. However, the battery voltage may not be the optimum PV operating voltage. Some controllers can optimize the operating voltage so that the PV operates at its maximum power point. Any power system includes a controller and a control strategy which describes the interactions between its components. In PV systems, the use of Batteries as a storage medium implies the use of a charge controller. This is used to manage the flow of energy from PV system to batteries and load by using the battery voltage and its acceptable maximum and minimum values. Most controllers have two main modes of operations as normal operating condition (where the battery voltage varies between the acceptable maximum and minimum values) and overcharge or over discharge condition (which occurs when the battery voltage reaches a critical value). The second mode of operation is obtained by using a switch with a hysteresis cycle such as electromechanical or solid state devices.

3.3.5 Power Peak Tracker

PV cells have a single operating point where the values of the current (I) and voltage (V) of the cell result in a maximum power output. These values correspond to a particular resistance, which is equal to V/I, as specified by Ohm's law. A PV cell has an exponential relationship between current and voltage, and there is only one optimum operating point, also called a maximum power point (MPP), on the power-voltage (or current) curve, as shown in figure 3.4.

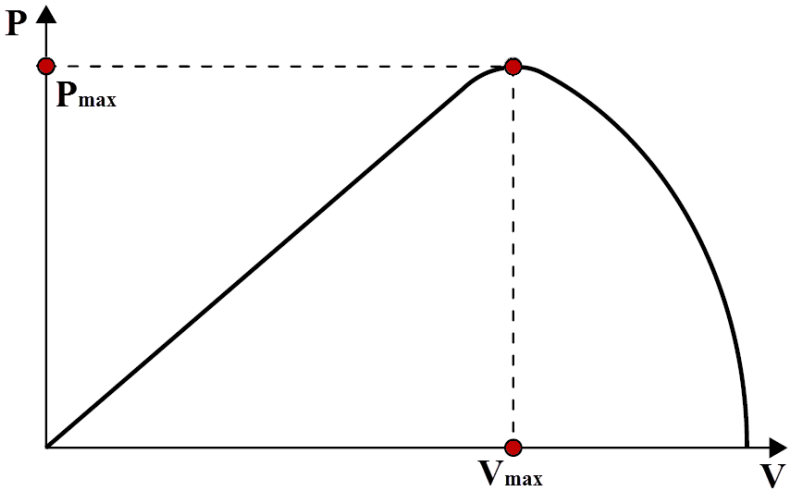

FIGURE 3.4 − Representative power-voltage curve for a PV cell

MPP also changes according to the radiation intensity and the cell temperature as shown in figure 3.5. Maximum power point trackers (MPPTs) utilize some type of control circuit or logic to search for this point and thus allow the converter circuit to extract the maximum power available from a cell. In fact, peak-power trackers optimize the operating voltage of a PV system to maximize the current. Typically, the PV system voltage is charged automatically. Simple peak-power trackers may have fixed operator-selected set points. The MPPT is a method to let the controller operate at the optimum operating point. A maximum power point tracker is a specific kind of charge controller that utilizes the solar panel to its maximum potential. The MPPT compensates for the changing voltage against current characteristic of a solar cell. The MPPT monitors the output voltage and current from the solar panel and determines the operating point that will deliver that maximum amount of power available to the batteries or load.

A maximum power point tracker is a high efficiency DC to DC converter that functions as an optimal electrical load for a solar panel or array and converts the power to a voltage or current level that is more suitable to whatever load the system is designed to drive. MPPT charge controllers are desirable for off-grid power systems to make the best use of all the energy generated by the panels. The benefits of MPPT regulators are greatest during cold weather on cloudy or hazy days or when the battery is deeply discharged (Kalogirou, 2009).

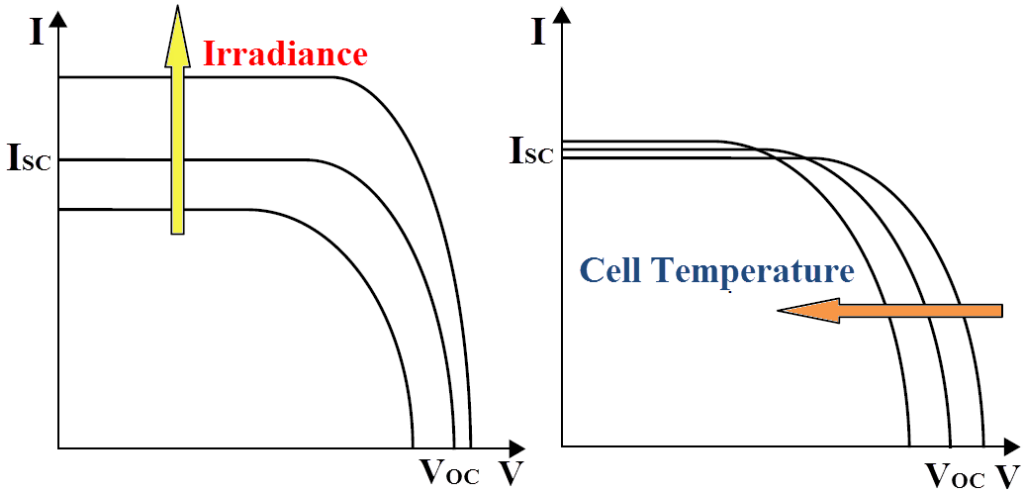

FIGURE 3.5 − Influence of irradiation and temperature on PV cell characteristics

3.4 PV System Energy Analysis

3.4.1 Solar Irradiation General Formulation

In formulating a solar system, either a power generation or a heating unit, the most important factor is the amount of solar energy which could be received locally. For this objective, first of all, the value of incident solar irradiation beyond the atmosphere should be calculated. The total hourly solar radiation on a horizontal surface beyond the atmosphere (I_o), based on the clear sky model, can be calculated employing by (Duffie and Beckman, 1980):

$$I_o = \frac{12\times 3600}{\pi}\times G_{sc}\left(1+0.033\cos\frac{360\,n}{365}\right)\left[\cos\varphi\cos\delta\,(\sin\omega_2-\sin\omega_1)+\frac{\pi(\omega_2-\omega_1)}{180}\times\sin\varphi\sin\delta\right] \quad (3.1)$$

Where, the angle φ is the latitude of the place. δ is the declination angle of the sun relative to the earth. This angle can be given by the following equation.

$$\delta = 23.45\sin\left(360\left(\frac{284+n}{365}\right)\right) \quad (3.2)$$

In which, n shows the number of the day in the year so that in January 1st n=1 and in December 31st n=365. The angle ω is also the hourly angle and could be given by the following equation.

$$\omega = (\text{Time} - 12)\,15^{\,o} \quad (3.3)$$

Note that ω_1 and ω_2 represent the hourly angle related to the beginning and end of

the hourly period. Also, G_{sc} in the first equation is the solar constant with the value of 1367 W/m^2. Employing the above formulation, the total hourly solar radiation received by a horizontal surface beyond the atmosphere can be calculated. For calculating the hourly available solar irradiation on the earth by a horizontal surface (I), the local sky clearness index (K_T) should be taken into consideration as (Duffie and Beckman, 1980):

$$I = I_o K_T \tag{3.4}$$

Where, the sky clearness index depends on two different parameters. Firstly, it is as a functional of the local atmosphere density (which is constant influence) and secondly, it depends on the effect of clouds (which is variable). For calculation of K_T, Angstrom correlation could be employed as below:

$$K_T = \left(a + b \frac{S}{S_o} \right) \tag{3.5}$$

In which, the constants a and b are Angstrom coefficients with values between 0 and 1. These coefficients for various locations all over the world have already been calculated by different scientists and are available in the literature. The term S/S_o also shows what portion of each hour the sky has been totally clear and without any cloud.

It should be mentioned that the solar irradiation comprises the beam and diffuse components. For calculating the portion of diffuse irradiation out of the entire solar radiation, the following equation could be employed (Duffie and Beckman, 1980):

$$\frac{I_d}{I} = \begin{cases} 1 - 0.09 K_T & \text{if} \quad K_T < 0.22 \\ 0.9511 - 0.1604 K_T + 4.388 K_T^2 - 16.638 K_T^3 + 12.336 K_T^4 & \text{if} \quad 0.22 \le K_T < 0.8 \\ 0.165 & \text{if} \quad K_T \ge 0.8 \end{cases} \tag{3.6}$$

As can be seen, the portion of diffuse solar irradiation depends on the value of sky clearness index. Naturally, by calculating this parameter, the beam component of solar radiation could be computed as:

$$I_b = I - I_d \tag{3.7}$$

3.4.2 Available Solar Irradiation by Various Tracking Modes

The formulation presented in the previous section was for calculating the solar irradiation on a horizontal plane on the earth. There are many approaches by which the amount of receivable solar irradiation by a surface could be improved. Using fixed titled planes and even employing various the sun tracker systems are the measures that could be taken of this objective. All these systems try to maximize the amount of solar irradiation received by changing their position and angle relative to horizon. Therefore, they are non-horizontal planes for which the amount of incident solar irradiation could be calculated by:

$$I_T = I_b R_b + I_d\left(\frac{1+\cos\beta}{2}\right) + I\rho_g\left(\frac{1-\cos\beta}{2}\right) \tag{3.8}$$

Where, the first, the second and the third parts on the right side of the equation are respectively associated with the direct, the diffuse and the reflected components of solar irradiation. Also, β and ρ_g are the slop angle and reflection coefficient respectively. The slop angle is the title of the plane relative to a horizontal surface. R_b is also given as below:

$$R_b = \frac{\cos\theta}{\cos\theta_z} \tag{3.9}$$

Where, θ and θ_z are incident angle and zenith angle respectively. The zenith angle could be calculated by (Duffie and Beckman, 1980):

$$\theta_z = \cos^{-1}\left[\left(\cos\delta\cos\varphi\cos\omega\right) + \left(\sin\delta\sin\varphi\right)\right] \tag{3.10}$$

Overall, 8 different methods are possible to be used for improving the amount of solar irradiation received by a plane. For all these cases, the value of receivable solar energy could be obtained by employing equation 3.8 where the incident and slop angles are different in each case.

The first approach is employing a fixed slopped angle. Although this approach will improve the solar irradiation collection slightly, the advantage of such system is that no cost is added to the initial cost required. The incident angle for a fixed slopped surface is calculated by:

$$\theta = \cos^{-1}\left[\begin{array}{r}(\sin\delta\sin\varphi\cos\beta)-(\sin\delta\cos\varphi\sin\beta\cos\gamma)+(\cos\delta\cos\varphi\cos\beta\cos\gamma)\\ +(\cos\delta\sin\varphi\sin\beta\cos\gamma\sin\omega)+(\cos\delta\sin\beta\sin\gamma\sin\omega)\end{array}\right] \quad (3.11)$$

In which, γ is the surface azimuth angle which shows the deviation of projection on a horizontal plane of the normal to the surface from the local meridian with zero to the south, east negative and west positive. The value of this angle is between -180^o to +180 ^{o}. Also, for such a plane, the angle of declination is recommended to be opted equal to the local latitude plus a value between 10 and 15 (Farzaneh-Gord *et al.*, 2012). However, for the sake of more accuracy, experimental investigation could reveal the exact value of this angle.

All the seven other systems in this regards are the sun tacking systems. Among the sun tracking modes, the simplest method is employing a slopped surface with fixed declination angle which rotates around a vertical axis. Naturally, for such a plane also the slopped angle is constant again. The incident angle, however, is different and could be given by:

$$\theta = \cos^{-1}\left(\cos\theta_z\cos\beta+\sin\theta_z\sin\beta\right) \quad (3.12)$$

The second tracking mode is employing an east-west axis rotator plane with single daily adjustment. For this case, the value of instantaneous incident and slop angles are given by the following two equations respectively:

$$\theta = \cos^{-1}\left(\sin^2\delta\right)+\cos^2\delta\cos\omega \quad (3.13)$$

$$\beta = \left|\varphi-\delta\right| \quad (3.14)$$

The next option is employing the previous type of tracker but with continuous adjustment instead of daily adjustment. Here, the instantaneous incident and slop angles are calculated as:

$$\theta = \cos^{-1}\left(\sqrt{1-\cos^2\delta\sin^2\omega}\right) \quad (3.15)$$

$$\beta = \tan^{-1}\left(\tan\theta_z\left|\cos\gamma_s\right|\right) \quad (3.16)$$

Where, γ_s is solar azimuth angle and can have values in the range of 180^o to -180^o. For north or south latitudes between 23.45^o and 66.45^o, γ_s will be between 90^o and -90^o for

days less than 12 hours long; for days more than 12 hours between sunrise and sunset, γ_s will be greater than 90^o or less than -90^o early and late in the day when the sun is north of the east-west line in the northern hemisphere or south of the east-west line in the southern hemisphere. For tropical latitudes, γ_s can have any value when (δ-φ) is positive in the northern hemisphere or negative in the southern. Thus, for calculating γ_s, one must know in which quadrant the sun will be. This is determined by the relationship of the hour angle ω to the hour angle ω_{ew}, when the sun is due west (or east). A general formulation for γ_s is conveniently written in terms of γ'_s a pseudo solar azimuth angle in the first or fourth quadrant (Duffie and Beckman, 1980):

$$\gamma_s = C_1\ C_2\ \gamma'_s + C_3\left(\frac{1 - C_1 \cdot C_2}{2}\right)180 \tag{3.17}$$

Where,

$$\gamma'_s = \sin^{-1}\left(\frac{\sin\omega\cos\delta}{\sin\theta_z}\right) \tag{3.18}$$

$$C_1 = \begin{cases} 1 & \text{if } |\omega| < \omega_{ew} \\ -1 & \text{if } |\omega| \geq \omega_{ew} \end{cases};\quad C_2 = \begin{cases} 1 & \text{if } \varphi(\varphi - \delta) \geq 0 \\ -1 & \text{if } \varphi(\varphi - \delta) < 0 \end{cases};\quad C_3 = \begin{cases} 1 & \text{if } \omega \geq 0 \\ -1 & \text{if } \omega < 0 \end{cases} \tag{3.19}$$

$$\omega_{ew} = \cos^{-1}\left(\frac{\tan\delta}{\tan\varphi}\right) \tag{3.20}$$

North-south axis rotator tracker with continuous adjustment is the fourth tracker system that can be employed. For this system, the incident and slop angles in each moment are given by (Duffie and Beckman, 1980):

$$\theta = \cos^{-1}\left(\sqrt{\cos^2\theta_z + \cos^2\delta\sin^2\omega}\right) \tag{3.21}$$

$$\beta = \tan^{-1}\left(\tan\theta_z\,|\cos(\gamma - \gamma_s)|\right) \tag{3.22}$$

The next tracking system is a plane rotating about the north-south axis parallel to the earth's axis with continuous adjustment. In this case, the two important angles could be calculated by:

$$\theta = \delta \tag{3.23}$$

$$\beta = \tan^{-1}\left(\frac{\tan\varphi}{\cos\gamma}\right) \tag{3.24}$$

Finally, the last possible system to be employed is a dual axis tracker which clearly is more efficient than others as the incident angle is always zero. The slop angle for this system is given by (Duffie and Beckman, 1980):

$$\beta = \tan^{-1}\left(\frac{\tan\alpha}{\cos\left(\gamma_s - \gamma\right)}\right) \tag{3.25}$$

Where,

$$\alpha = \sin^{-1}\left(\cos\varphi\cos\delta\cos\omega + \sin\varphi\sin\delta\right) \tag{3.26}$$

With the above formulation, one could calculate the amount of solar irradiation received by a plane (I_T). For calculation of the amount of solar energy absorbed by the plane, the following equation could be used.

$$S = I_b R_b (\tau\alpha)_b + I_d (\tau\alpha)_d \left(\frac{1+\cos\beta}{2}\right) + I(\tau\alpha)_g \left(\frac{1-\cos\beta}{2}\right) \tag{3.27}$$

Where, the parameter ($\tau\alpha$) represents the emittance of the plane cover (mainly glass) and the absorption of the plane as:

$$(\tau\alpha) = 1.01\,\tau_c\,\alpha_p \tag{3.28}$$

In which, τ_c is the PV cell cover emittance factor and α_p is the absorption coefficient of the plate. The emittance factor of the PV cell cover, itself, is calculated by:

$$\tau_c = \tau_a\,\tau_r \tag{3.29}$$

Where,

$$\tau_a = \frac{KL}{\cos\theta_2}; \quad \tau_r = 0.5\left\{\frac{1-r_{II}}{1+r_{II}} + \frac{1-r_{\infty}}{1+r_{\infty}}\right\} \tag{3.30}$$

In which, K and L are the extinction coefficient and thickness of the cover. Also,

θ_2, r_{II} and r_∞ are respectively the fraction angle of the cover, the fraction coefficient of the cover relative to the parallel rays and the fraction coefficient of the cover relative to the normal rays. These items could respectively be obtained by:

$$\theta_2 = \sin^{-1}\left(\frac{\sin\theta}{1.536}\right) \tag{3.31}$$

$$r_{II} = \frac{\tan^2(\theta_2 - \theta)}{\tan^2(\theta_2 + \theta)} \tag{3.32}$$

$$r_\infty = \frac{\sin^2(\theta_2 - \theta)}{\sin^2(\theta_2 + \theta)} \tag{3.33}$$

Also, the absorption coefficient of plane could be calculated by:

$$\alpha_p = \alpha_n \cdot \left[1 + (2.0345\times10^{-3}\theta) - (1.99\times10^{-4}\theta^2) + (5.324\times10^{-6}\theta^3) - (4.799\times10^{-8}\theta^4)\right] \tag{3.34}$$

In which, α_n is the absorption coefficient of the plate for the normal solar rays with a constant value.

It should be noted that the emittance-absorption coefficient of the plane for direct, diffuse and reflected components of irradiation has different values. The same formulation as 3.28 to 3.34 could be employed for calculating these items where the incident angles for the reflected and diffuse components are respectively calculated by:

$$\theta_g = 90 - (0.5788\beta) + (0.002693\beta^2) \tag{3.35}$$

$$\theta_g = 59.7 - (0.1388\beta) + (0.001497\beta^2) \tag{3.36}$$

3.4.3 PV Cell Formulation

When solar energy hits the solar cell, electrons are knocked loose from the atoms in the semiconductor material, creating electron-hole pairs. If electrical conductors are attached to the positive and negative sides, forming an electrical circuit, the electrons are captured in the form of electric current, called photocurrent (I_{ph}). As can be understood from

this description, during darkness the solar cell is not active and works as a diode (a p-n junction that does not produce any electricity). If it is connected to an external voltage supply, it generates a current called dark current (I_D). A solar cell is usually represented by an electrical equivalent one-diode model, shown in figure 3.6. This circuit can be used for an individual cell, a module consisting of a number of cells, or an array consisting of several modules. According to the figure, the model contains a current source (I_{ph}), one diode, and a series resistance (R_S), which represents the resistance inside each cell. The diode has also an internal shunt resistance. The net current is the difference between I_{ph} and I_D as (Kalogirou, 2009):

$$I = I_{ph} - I_D = I_{ph} - I_o \left\{ \exp\left[\frac{e(V + I R_S)}{k T_C} \right] - 1 \right\} - \frac{V + I R_S}{R_{SH}} \tag{3.37}$$

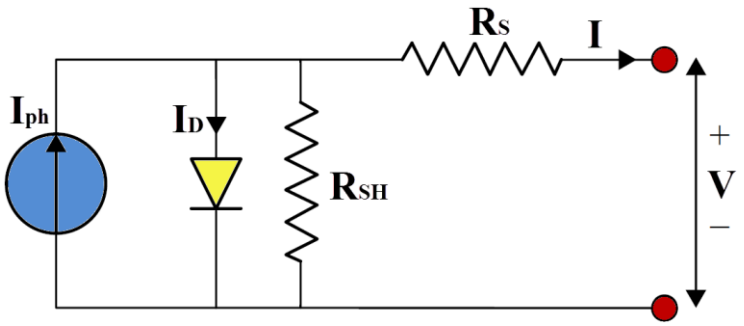

FIGURE 3.6 − single solar cell model

It should be noted that RSH is usually much bigger than a load resistance, whereas the series resistance is much smaller than a load resistance, so that less power is dissipated internally within the cell. Therefore, by ignoring these two resistances, one has:

$$I = I_{ph} - I_D = I_{ph} - I_o \left\{ \exp\left[\frac{e V}{k T_C} \right] - 1 \right\} \tag{3.38}$$

In which, k, T_C, e, V and Io are respectively Boltzmann's gas constant (1.381×10^{-23} J/K), absolute temperature of the cell (K), electronic charge (1.602×10^{-19} J/V), voltage imposed across the cell (V) and dark saturation current which depends strongly on temperature (A).

Figure 3.7 shows the I-V characteristic curve of a solar cell for a certain irradiation (I_T) at a fixed cell temperature (T_C). The current from a PV cell depends on the

external voltage applied and the amount of sunlight on the cell. When the cell is short-circuited, the current is at maximum (short-circuit current (I_{SC})), and the voltage across the cell is 0. When the PV cell circuit is open, with the leads not making a circuit, the voltage is at its maximum (open-circuit voltage (V_{OC})), and the current is 0. In either case, at open circuit or short circuit, the power (current × voltage) is 0. Between open circuit and short circuit, the power output is greater than 0. The typical current voltage curve shown in figure 3.7 presents the range of combinations of current and voltage. In this representation, a sign convention is used, which takes as positive the current generated by the cell when the sun is shining and a positive voltage is applied on the cell's terminals.

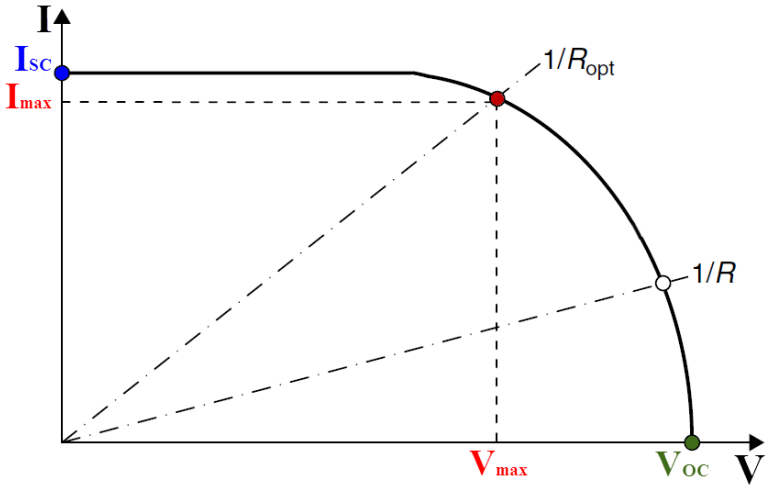

FIGURE 3.7 − Representative current-voltage curve for a PV cell

The maximum power passes from a maximum power point at which the load resistance is optimum (R_{opt}) and the power dissipated in the resistive load is maximum and given by (Kalogirou, 2009):

$$P_{max} = I_{max} V_{max} \tag{3.39}$$

Calculating P_{max}, one could calculate the fill factor (FF) which is a measure of the real I-V characteristic:

$$FF = \frac{P_{max}}{I_{SC} V_{OC}} \tag{3.40}$$

For good cells, FF has a value greater than 0.7. The FF decreases as the cell temperature increases. Thus, by eliminating and loading a PV cell so that the voltage equals the PV cell's V_{max}, the output power is maximized.

It is worth mentioning that I_{SC} is the higher value of the current generated by the cell and is obtained under short-circuit condition (when V=0) and is equal to I_{ph}. Also, the open-circuit voltage (V_{OC}) corresponds to the voltage drop across the diode when it is traversed by the I_{ph} which is equal to I_D when the generated current is 0. This is the voltage of cell during nighttime and could be obtained by:

$$V_{OC} = \frac{k\,T_C}{e}\,\mathrm{Ln}\left(\frac{I_{SC}}{I_o}+1\right) \tag{3.41}$$

Overall, the output power of a PV cell could be given by:

$$P = I\,V = I\,R^2 = \left\{I_{SC} - I_o\left[\exp\left(\frac{e\,V}{k\,T_C}\right)-1\right]\right\}V \tag{3.42}$$

The current load which maximizes the output power is also given by:

$$I_{max} = \frac{e\,V_{max}}{k\,T_C + e\,V_{max}}\left(I_{SC} + I_o\right) \tag{3.43}$$

As a result, the maximum power output could be calculated as:

$$P_{max} = \frac{e\,V^2{}_{max}}{k\,T_C + e\,V_{max}}\left(I_{SC} + I_o\right) \tag{3.44}$$

Efficiency is another measure of PV cells that is sometimes reported. Efficiency is defined as the maximum electrical power output divided by the incident light power. Efficiency is commonly reported for a PV cell temperature of 25 ^{o}C and incident light at an irradiance 1000 W/m^2 with a spectrum close to that of sunlight at solar noon. Another parameter of interest is the maximum efficiency which is the ratio between the maximum power and the incident light power, given by:

$$\eta_{max} = \frac{P_{max}}{P_{in}} = \frac{I_{max}\,V_{max}}{A_c\,I_T} \tag{3.45}$$

In which, A_c is the area of the cell. As it was discussed in previous sections, there are various types of PV cells available in the market each of which has different efficiency.

Table 3.1 details information about different types of PV cell and their corresponding maximum efficiencies.

Calculating the current, voltage and power obtainable from a PV cell under sunlight, one could analyze the performance of a module of solar cells. The total current of PV module shown in figure 3.4, under arbitrary operating condition could be calculated by:

$$I^{M} = I_{SC}^{M}\left[1-\exp\left(\frac{V^{M}-V_{OC}^{M}+R_{S}^{M}I^{M}}{N_{SM}V_{t}^{C}}\right)\right] \tag{3.46}$$

Where,

$$I_{SC}^{M} = N_{PM}I_{SC}^{C};\quad V_{OC}^{M} = N_{PM}V_{OC}^{C};\quad R_{S}^{M} = \frac{N_{SM}}{N_{PM}}R_{S}^{C};\quad V_{t}^{C} = \frac{kT^{C}}{e} \tag{3.47}$$

Note that in the above formulas, the superscript M and C refer to the PV module and the cell, the subscripts PM and SM respectively refer to the parallel branch of PV module and PV series in each branch and N shows the number of PV cells in each branch.

In the end, overall, according to the definition presented for energy efficiency in chapter 3, the energy efficiency of a PV system (a PV farm specifically here) could be defined as the ratio of the produced power (P_{PV}) to the incident solar irradiation on the PV cell modules ($I_{T,PV}$). Therefore:

$$\xi_{PV} = \frac{P_{PV}}{I_{T,PV}} \tag{3.48}$$

3.5 PV System Exergy Analysis

Similar to the energy analysis section and considering the definition given for the second law efficiency, the second law efficiency for a PV farm is defined as the ratio of the amount of useful exergy gained, i.e. the net power produced (P_{PV}), to the solar exergy received by the PV cells (Ψ_{PV}).

$$\varepsilon_{PV} = \frac{P_{PV}}{\Psi_{PV}} \tag{3.49}$$

The amount of solar exergy received by 1 m^2 area of a PV cell, on the other hand, could be calculated as:

$$\Psi_c = I_{T,c} \cdot \left[1 - \frac{4}{3}\left(\frac{T_o}{T_{sun}} \right) + \frac{1}{3}\left(\frac{T_o}{T_{sun}} \right)^4 \right] \tag{3.50}$$

In which, T_{sun} is the effective temperature of the sun (4350 K). Naturally, for calculating the total exergy of the whole PV system, the total area of the PV cells should be multiplied by the value given by the above equation. The irreversibility of the PV system could then be calculated by:

$$\dot{I}_{PV} = \Psi_{PV} - P_{PV} \tag{3.51}$$

3.6 Loss Sources and Uncertainty of a PV System

One of the most important issues in assessing or designing a PV system is taking all the possible losses and uncertainties of the PV system into account. The term uncertainty refers to the root mean square error (RMSE) related to the estimation of a value given by the following equation (Farzaneh-Gord *et al*., 2015):

$$RMSE = \sqrt{\frac{1}{n}\sum_{n=1}^{n}\left(\bar{\tau}_i - \tau_i\right)^2} \tag{3.52}$$

In which, $\bar{\tau}_i$ and τ_i are respectively the estimated and the actual values of the corresponding parameter. The normalized RMSE (NRMSE) for a database with n samples could be calculated as:

$$NRMSE = \frac{RMSE}{\bar{\tau}_i}; \quad Where: \tau_i = \frac{1}{n}\sum_{1}^{n}\tau_i \tag{3.53}$$

For systems with multiple sources of uncertainty assuming independent variables, the combined uncertainty (Γ_c) for a given function f(x,y) is calculated as:

$$\Gamma_c = \sqrt{\left(\frac{\partial f}{\partial x}\right)^2 \cdot \Gamma_x^2 + \left(\frac{\partial f}{\partial y}\right)^2 \cdot \Gamma_y^2} \tag{3.54}$$

Generally, for the proposed system, the uncertainties could be classified into two groups as solar energy monitoring uncertainties and PV modelling uncertainties. Figure 3.8 shows energy flow diagram in a grid connected PV plant.

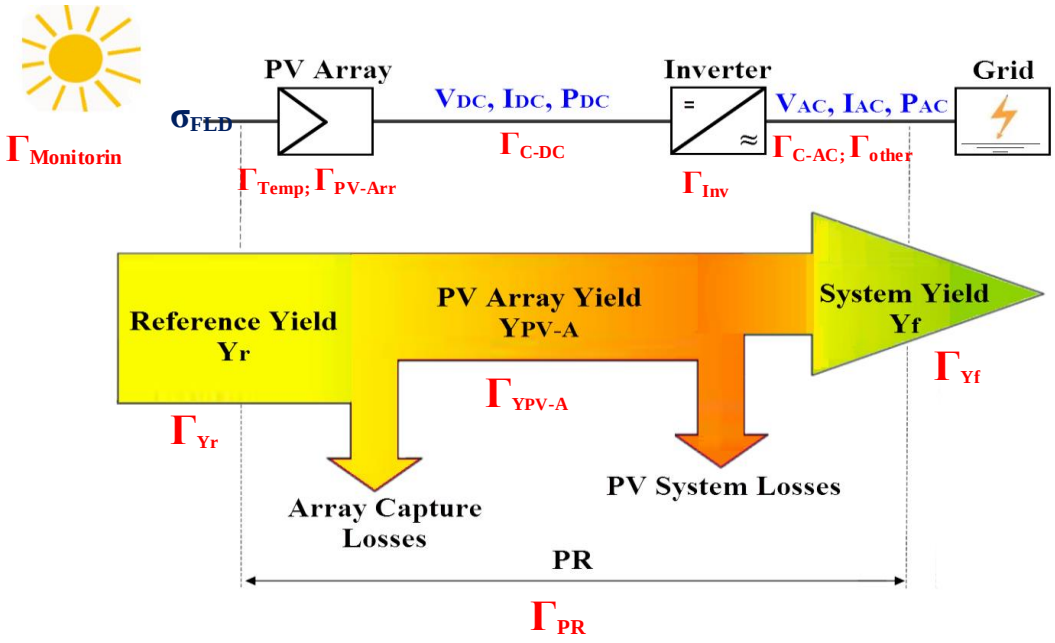

FIGURE 3.8 − Energy flow diagram of a PV plant

In this figure, Y_r, $Y_{PV\text{-}A}$ and Y_f are respectively the solar yield, the PV array yield and the final power delivered to the grid. Therefore, the performance ratio (PR) of the PV plant could be defined as:

$$PR = \frac{Y_f}{Y_r} \tag{3.55}$$

According to figure 3.8, after estimating the individual uncertainties in each category, one should calculate the combined uncertainty of each category and subsequently, the value of combined uncertainty for the PV plant. The combined uncertainty of the PV plant is then calculated by:

$$\Gamma_{PR} = \sqrt{\left(\frac{1}{Y_r}\Gamma_{Y_f}\right)^2 + \left(\frac{Y_f}{Y_r^2}\Gamma_{Yr}\right)^2} \tag{3.56}$$

Uncertainties related to solar energy monitoring could be due to various factors. The first factor is the deviation in the estimation of the global horizontal solar irradiation value that can be affected by some factors like pollution, climate change and etc. The other

source of uncertainty in this category is the possible deviations in the values of solar irradiations recorded over the sample year. As the performance of a solar irradiation measurement device can be suffered from various parameters such as calibration uncertainty, drift over time, offset originated by thermal radiation, offset originated by the temperature change, non-linearity tilt response and etc., the measured value may deviate from the actual value if the operational conditions differ significantly from calibration conditions. The other uncertainty in this category is related to the deviations in solar irradiation intensity forecast which depends on different parameters such as the forecast horizon, spatial and temporal resolutions and etc. For the proposed system which takes advantage of the CAES system as an energy storage unit with fast reaction capability, the common forecast methods using the sky imagers in the range of 10 to 25 minutes could be suitable. Finally, the other uncertainty in this category is due to the variation of solar irradiation over the years comparing to the values recorded in the sample year as the database of the simulations. In lifetime simulation methods, the uncertainty due to the changes in the amount of annual solar irradiation has a relatively small effect as years with less irradiation are generally compensated by other years with more irradiation.

The second uncertainty category is the uncertainties in PV modelling. In fact, different performance models are used in the industry to predict the amount of energy that a PV system can produce. These models can differ significantly in their mathematical formulations, approach and in the amount of data required for the simulation. Moreover, the large amount of input parameters as irradiation, temperature, array orientation and module and inverter performance have inherent uncertainties and have to be properly taken into account. These parameters could also be classified in four groups as the uncertainties related to PV module temperature model, PV array model, PV inverter model and other possible losses. Also, the other uncertainties in a PV system could be the other possible losses in the PV cell array and the energy storage unit due to some factors such as the effects of soiling and birds. An uncertainty of losses for long term and short term efficiency degradation of the PV panels should also be considered. Finally, an uncertainty for other factors, such as mismatch caused by row to row shading, deviation in tracking system, module tolerance, reflection, cabling losses, should also be taken into account.

4. City Gate Station

4.1 Pressure Reduction in Natural Gas Transmission Pipeline

Natural gas extracted and refined in refineries is transmitted by transmission pipelines to consuming points. Considering the long distance that the natural gas has to pass from the refinery to the consuming points, it must overcome friction losses along the path. This is why, firstly, the natural gas stream is pumped into the pipeline at much higher pressure than consumption values and secondly, numerous attenuator and booster pressure stations work out along this way. Near the consumption points, the first step of pressure regulation is carried out through a City gate station (CGS). Through a CGS, the natural gas stream pressure is dropped from nearly 70 barg to almost 17 barg (Farzaneh-Gord *et al.*, 2011). There are also two further pressure reduction steps. The second step is carried out at Town Border Station (TBS) in which the natural gas pressure decreases from 17 barg to 4 barg and the last step is done by a small regulator at consumption points which converts the natural gas pressure from 4 barg to almost 0.02 barg (Farzaneh-Gord *et al.*, 2012).

4.2 Conventional Configuration of a CGS

In a conventional CGS, the pressure reduction mission is mainly done by some expansion values through a throttling process. Due to the positive Joule-Thompson coefficient, the pressure reduction process leads to considerable temperature drop in the natural gas stream. If the amount of temperature drop exceeds the maximum allowable value, it could result in hydrate forming in the stream. In fact, hydration point is a temperature in which suspended water droplets in the natural gas stream start to freeze, obstructing the transmission pipeline (Arabkoohsar *et al.*, 2014). Hydration point range varies for different natural gas mixtures because it is a direct functional of the natural gas compositions. In order to not approach the hyrate forming temperature at CGSs, the natural gas stream is preheated before the pressure reduction process. Line heaters, which usually burn a remarkable portion of the passing natural gas, are mostly used for this objective (Arabkoohsar *et al.*, 2015). In fact, line heaters are some indirect water bath gas heaters as shown schematically in figure 4.1.

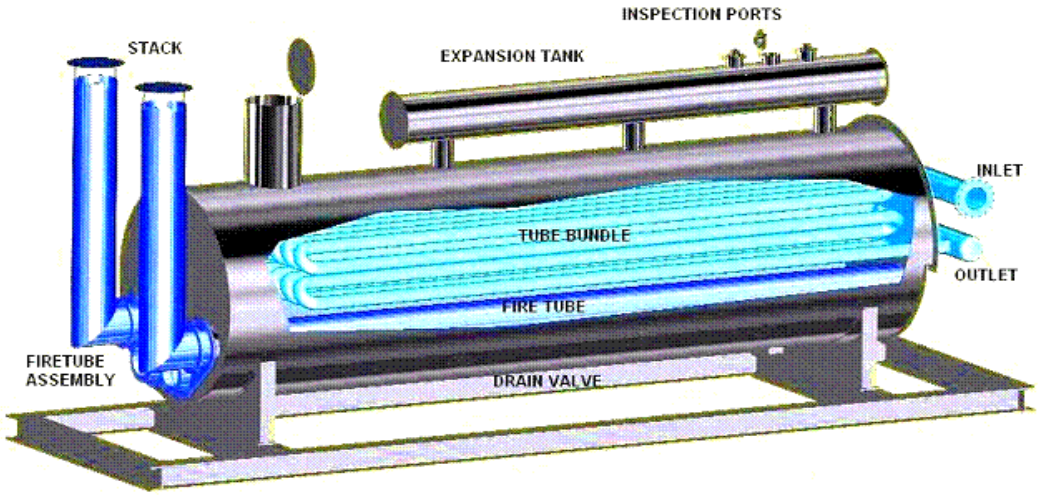

FIGURE 4.1 – The schematic diagram of a line heater employed in a CGS for preheating the natural gas stream

According to the figure, the heaters are comprised of four basic components, the heater shell, fire tubes, gas coils and a water expansion section. The heater shell surrounds the fire tube, gas coil and water bath. The fire tube (which burns natural gas) provides heat to water which acts as intermarry fluid. The water, then, transfers heat safely to natural gas flowing through a coil immersed in the water bath. As the water bath is heated, the bath expands and the expanded heat media flows into the expansion section. As shown, the fire tube is located in the bottom of the water bath and transfers heat indirectly to the natural gas as flows through the coil. Due to location of the fire tube, the maximum temperature within the water bath may not be encountered at highest water level. This explains why the coil exits at middle of the shell. Also, figure 4.2 illustrates the detailed configuration of a conventional CGS.

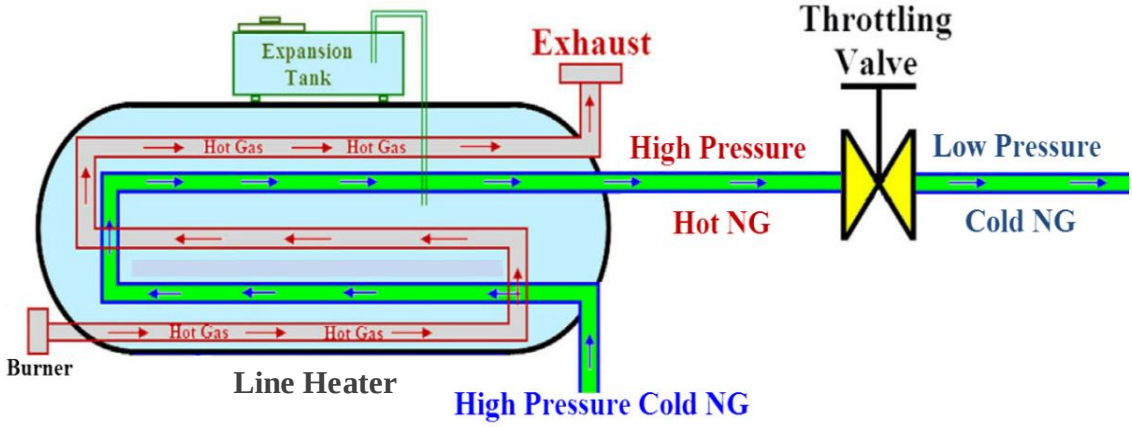

FIGURE 4.2 − The conventional configuration of a CGS

As can be seen, as the natural gas stream enters the CGS, it passess the line heater to be heated up the desired temperature before being expanded. Then, it enters the throttling valve to be expanded as much as required. The expanded gas then flows toward the consumption points.

4.3 The Modified Configuration

The first problem of a CGS with a conventional configuration is that the line heaters low thermal efficiency which causes them to burn too much fuel. The current thermal efficiency of conventional heaters have been reported to be in range of 0.35 to 0.5 (Arabkoohsar *et al.*, 2014). In order to overcome this problem many proposals have already been presented previously. These proposals mainly include employing renewable energy source heating systems to support the line heater at the CGS and reduce its heating duty. In one of the first efforts in this regards, employing a direct solar heat system for a typical CGS station in Iran was proponed (Farzaneh-Gord *et al.*, 2011). As the previous proposed system considered an ideal instantaneaously controllable line heater, in contrats with the real common available heaters in the market, the authors modified their previous work by considering an actual heater and adding a solar storage tank to store the collectoed solar heat and using it at nightly hours during which the heating demand of CGS is naturally higher than daily hours (Farzaneh-Gord *et al.*, 2012). In another work, by the same token, employing a smart solar heating system equipped with a solar storage tank along with a controllable line heater in CGSs was proposed and a thorough exergy and energy analysis on such a CGS was carried out (Arabkoohsar *et al.*, 2014). In another work, employing geothermal system in CGSs was evaluted and this system was economically compared to the previous systems proposed for the same objective (Farzaneh-Gord *et al.*, 2015).

On the other hand, due to the high mass flow rate and pressure of natural gas stream passing through a CGS, it clearly has a very high exergy value that could be utilized. Therefore, the second blindspot of CGSs in conventional configuration is that this exergy is totally wasted by the throttling valves. A few proposals have been already given in order for overcoming this problem as well. In fact, evaluating natural gas stream exergy through the transmission pipeline has been of interest for many years. The first study related to this issue is employing a mechanical air compressor to utilize the exergy of natural gas flow in the transmission pipeline (Bisio, 1995). In another work, the feasibility of using turbo expanders

in exothermic chemical mixing procedures has been carried out, leading to considerable energy providence in the processes (Greeff *et al.*, 2004). Another study introduced a method to calculate the existing exergy in multi-component liquid flows like natural gas streams in pipelines (Hinderink *et al.*, 2005). Another research also studied the feasibility of employing turbo expanders in CGSs using HYSIS software and assessed the effects of the isentropic efficiency of these turbines on temperature and pressure drop of the natural gas as well as electricity generation (Pozivili, 2004). In another work, the amount of exergy destruction in Iran's CGSs was investigated and it found out that the total of 4200 MW electricity could be generated in these stations (Farzaneh-Gord and Magrebi, 2009). The authors of this work also studied the methods of utilizing the existing pressure exergy in the CGS of Bandar Abbas refinery and implemented a comprehensive research on enhancing the output energy of CGSs by employing turbo expanders and presented some useful suggestions (Farzaneh-Gord *et al.*, 2008).

In one of last efforst in modifying CGSs pattern, simultaneaous application of a solar heating system equipped with a bulky enough storage tank and a turbo-expander set that takes advantage of the natural gas stream exergy to produce power by a generator was proposed and was investigated in terms of energy, exergy and economic performance (Arabkoohsar et al., 2015). This configuration is most likely the best pattern proposed for a CGS ever. Figure 4.3 represents this configuration schematically.

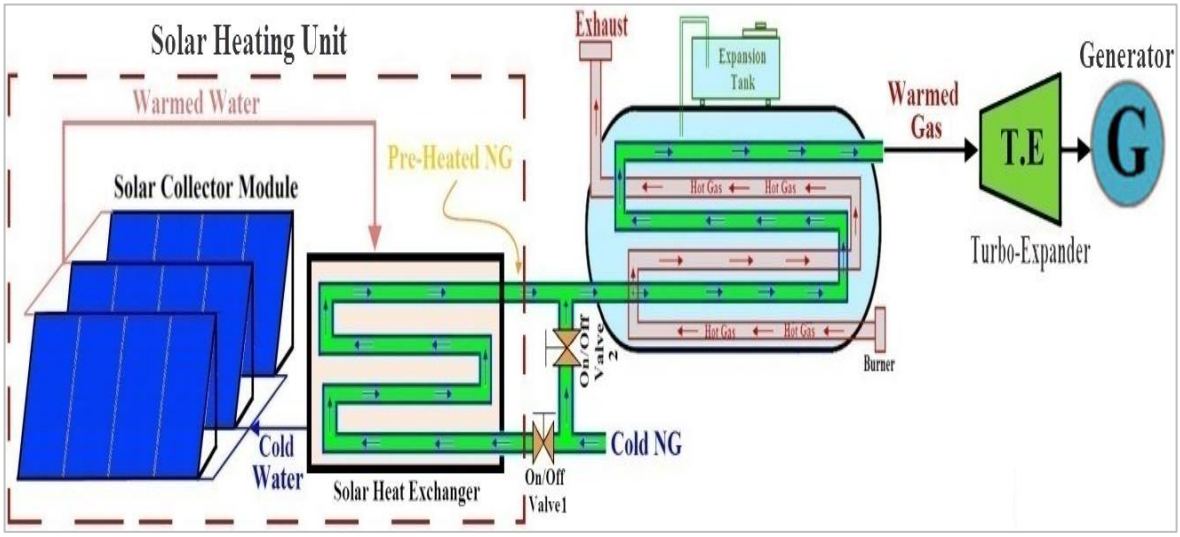

FIGURE 4.3 − The modified configuration of CGS

According to the figure, the first stage of heating is carried out by solar heating system and the second stage is a line heater. Note that as CGS station works continuously and heating demand is always at high levels, there is no need for a solar storage tank here and the collected heat by the solar collector modules in from of a hot working fluid could be directly used to preheat the natural gas stream through a bath type heat exchanger. Note that the number of collector modules and the size of the solar heat exchanger in the system are chosen based on thermo-economic considerations. The line heater is then responsible to heat the natural gas stream up to the desired temperature. Note that as line heaters are limited in capacity, therefore, multiple line heaters may be used in large scale CGSs, if appropriate.

4.4 Mathematical Modelling of Modified CGS

4.4.1 Energy Analysis

Considering the above presented information about CGSs, the optimum temperature which the natural stream has to reach before the expansion process (T_{NG-3}) could be calculated as:

$$T_{NG-e} = T_{hyd} + 5\,^{o}C + \Delta T_{d-v} \tag{4.1}$$

In which, T_{hyd} and ΔT_{d-v} refer to the hydrate forming temperature and the temperature drop in the natural gas stream through the turbo expander, respectively. ΔT_{d-v} is normally recorded at the station place for all days of the year and ΔT_{d-v} is a functional of the natural gas compisitions and turbo-expander inlet and outlet pressures. Also, the value of 5 ^{o}C is also taken as a confidence factor. Overall, the prior study in this respects demonstrates that the required temperature before the turbo expander is 85 ^{o}C (Farzaneh-Gord *et al.*, 2008). The total amount of energy that natural gas stream has to gain ($\dot{Q}_{NG}$) to meet this temperature is calculated by:

$$\dot{Q}_{NG} = \dot{m}_{NG}\, c_{P-NG} \left(T_{NG-e} - T_{NG-i}\right) = \dot{Q}_{SS} + \dot{Q}_{h} \tag{4.2}$$

In which, $\dot{m}_{NG}$, $c_{p\text{-}NG}$, $\dot{Q}_{SS}$ and $\dot{Q}_{h}$ are the mass flow rate and heating capacity of natural gas, the total heat provided by the solar heating unit and the line heater heating duty, respectively. Also, $T_{NG\text{-}i}$ is the CGS inlet natural gas temperature and could be considered as a functional of ambient temperature as (Najafi-mod *et al.*, 2008):

$$T_{NG-i} = 0.0084T_{am}^2 + 0.318T_{am} + 11.40 \quad (4.3)$$

In fact, the above equation calculates the temperature of soil at the depth of 1.5 m where the natural gas transmission pipeline is placed. As the maximum temperature required after the preheating process in presence of a turbo-expander is uniforemly 85 ^{o}C, therefore, in order to be able to provide middle range temperatures as continuously as possible, evacuated tube solar collectors are again chosen to be employed in CGS solar heating unit as well. As detailed mathemtical modelling on evacuated tube solar collectors has been presented in chapter 2, the formulation about the obtainable heat from solar collector modules is skipped here. Also, having the amount of producible heat by each evacuated solar collector ($\dot{Q}_u$) and assuming the solar heat exchanger as a well mixed reservoir, based on the first law of thermodynamics, the hourly variations of working fluid temperature within the solar heat exchanger could be written as:

$$T_{f,she}^{\lambda+1} = \frac{\left(n\overbrace{\dot{m}_f\, c_{pf}\left(T_{f\text{-}i} - T_{f\text{-}e}\right)}^{\dot{Q}_u} - \overbrace{\dot{m}_{NG}\, c_{p-NG}\left(T_{NG\text{-}e} - T_{NG\text{-}i}\right)}^{\dot{Q}_{SS}} \right)}{m_{f,she}\, c_f} - T_{f,she}^{\lambda} \quad (4.4)$$

While considering the natural gas coils in the solar heat exchanger as constant temperature surface tubes, the relation between the fluid bath temperature and solar heat exchanger inlet and outlet natural gas temperatures in a specific time step could be written as below (Incropera and DeWitt, 2002):

$$\frac{T_f - T_{NG-e}}{T_f - T_{NG-i}} = e^{Y}, \quad Y = \frac{-\pi\, D_{oc}\, L_c\, U_c}{\dot{m}_{NG} \cdot c_{p-NG}} \quad (4.5)$$

Having the last two equations, one could calculate the solar heat exchanger outlet natural gas temperature as well as the heat exchanger content temperature in each time step. It is noteworthy here that the parameters n, $\dot{m}_f$, c_{pf}, $m_{f,she}$, $T_{f,she}$ and $T_{NG\text{-}o}$ in equation 4.4 are the number of the number of collector modules, the working fluid mass flow rate through a single collector, the working fluid specific heat, the mass and temperature of working fluid within the heat exchanger and the natural gas temperature at the solar heat exchanger outlet,

respectively. Also, the superscripts λ and λ +1 in this equation count the instantaneous operational time steps of the system.

In addition, in equation 4.5, D_{oc} and L_c are the outer diameter and the length of natural gas coils, respectively. Also, U_c is the overall heat transfer coefficient between the coils and the hot fluid within the heat exchanger which could be calculated by:

$$\frac{1}{U_c} = \frac{D_{oc}}{D_{ic}\bar{h}_{ic}} + R_{ic} + \frac{\frac{D_{oc}}{2}\ln\frac{D_{oc}}{D_{ic}}}{k_c} + R_{oc} + \frac{1}{\bar{h}_{oc}} \tag{4.6}$$

In which, k_c, D_{ic}, R_{oc}, R_{ic}, $\bar{h}_{oc}$ and $\bar{h}_{ic}$ represent the conductivity heat transfer coefficient, the inner diameter, the outer and inner thermal resistances of sediments and the outer and inner convective heat transfer coefficients of the coils, respectively. Previous studies show that, for natural gas coils in a hot fluid bath, the overall heat transfer coefficient of 100 Btu/hr.ft^2.F (586 W/m^2.K) is expected (Ken *et al*., 1999).

Calculating the natural gas temperature at the solar heat exchanger outlet, and subsequently the amount of heat that natural gas obtained through the this heat exchanger, one could easily calculate the line heater heating duty in every moment. Note that, as it was explained before, line heaters are also water bath heat exchangers; therefore, the last two correlations could be considered to formulate them as well. Therefore, the line heater heating duty at the CGS in presence of the solar heating unit could be calculated as follow:

$$\dot{Q}_h = \dot{Q}_{NG} + m_f\, c_{p\text{-}w} \cdot (T_w^{\lambda+1} - T_w^{\lambda}) - \dot{Q}_{SS} \tag{4.7}$$

Where, m_w, T_w and $c_{p\text{-}w}$ are the mass and temperature of water within the line heater and the specific heat capacity of water respectively. Finally, the mass flow rate of fuel required to be burnt for providing this amount of heat by the line heater ($\dot{m}_{fu}$) could be computed by:

$$\dot{m}_{fu} = \frac{\dot{Q}_h}{LHV_{fu}\,\eta_h} \tag{4.8}$$

In the next step, one should calculate how much power is going to be produced by the tutrbo-expander and electricity generator set at the CGS. Based on the first law of thermodynamics, the actual producible work by the expander could be calculated as:

$$\dot{W}_{E,a} = \eta_{E,is}\dot{W}_{E,is} = \eta_{E,is}\left[\dot{m}_{NG}\, c_{p-NG}\left(T_i - T_{e,is}\right)\right] \tag{4.9}$$

Where, the subscripts a and is refer to actual and isecntropic procedures and E represents the turbo-expander. Naturally, having the expander inlet condition and its outlet pressure, one could easily calculate the outlet isentropic temperature of natural gas and compute the isentropic work of the expander in every moment. Subsequently, by having the value of isentropic efficiency of the turbo-expander ($\eta_{E,is}$), one could finally calculate its actual producible work. It should be mentioned that this parameter has been considered equal to 85% in this study (Arabkoohsar *et al.*, 2015). In the end, knowing the electricity generator efficiency (η_g, considered as 90%), one can compute the net producible power at the CGS place as follow:

$$P_{CGS} = \eta_g\, \dot{W}_{E,a} \tag{4.10}$$

Finally, the first law efficiency for the CGS could be calculated by:

$$\xi_{CGS} = \frac{P_{CGS}}{P_{fu} + I_{T,cm}} \tag{4.11}$$

Where, P_{fu} and $I_{T,cm}$ are the amount of energy entered the whole CGS control volume by consuming fuel of the line heater and solar energy received by the evacuated tube solar collector modules, respectively.

4.4.2 Exergy Analysis

Taking the information and details presented for CGS in previous section into account and considering its modified configuration, one could present its exergy performance mathematical model. Evidently, two different approaches for analyzing the exergy performance of a given system could be taken. The first approach is developing the exergy balance of system which was employed in exergy analysis of CAES systems in chapter 2. The other possible measure that can be taken for this objective is calculating the rate of exergy

destruction in the system. This approach is going to be used for analyzing the performance of a power productive CGS equipped with a solar heating unit exergetically. Before formulating the target system, one should know that rate of exergy destruction through a control volume could is calculated as follow (Kargaran *et al*., 2013):

$$\dot{\Psi}_d = \sum_k \left(1 - \frac{T_o}{T_k}\right)\dot{Q}_k - \dot{W}_{C.V} + \sum_i \dot{m}\left(\psi_i - \psi_e\right) \tag{4.12}$$

Where, $\dot{\Psi}_d, \dot{W}_{C.V}, \dot{Q}_k$ and T_o are the rate of exergy destruction, the rate of work done, the rate of heat transfer from the control volume and the ambient temperature, respectively. Also, ψ refers to the summation of physical, chemical, potential and kinetic exergies of the control volume. As the kinetic and potential terms of exergy in all stages of exergy analysis of a CGS could be neglected, physical and chemical exergies are only considered terms in this study. Note that chemical exergy has the same definition as thermo mechanical (physical) exergy with this difference that thermo mechanical exergy does not consider chemical composition.

Figure 4.4 illustrates the required detailes of the control volume associated with the modified configuration of a CGS.

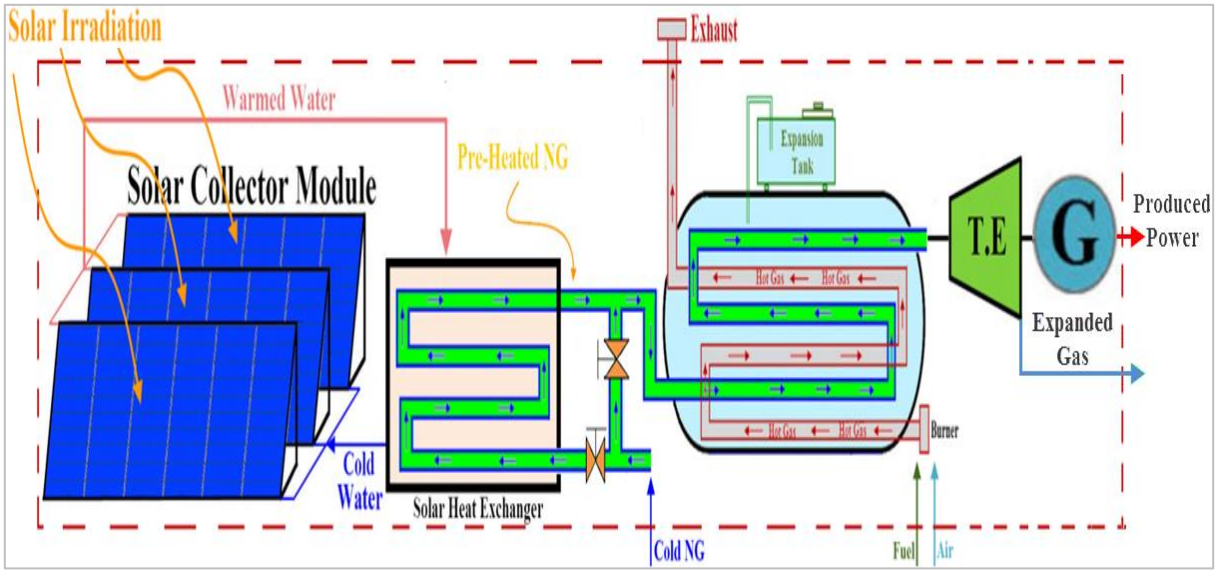

FIGURE 4.4 − The control volume selected for exergy analysis of a CGS

The exergy balance correlation for the control volume in steady state could be written as follow:

$$\dot{\Psi}_{d} = \Delta\dot{\Psi}_{ft} + \dot{\Psi}_{SS} - \Delta\dot{\Psi}_{NG} - \dot{W}_{E,a} \tag{4.13}$$

Where, $\dot{\Psi}_{d}$, $\Delta\dot{\Psi}_{ft}$, $\dot{\Psi}_{SS}$, $\Delta\dot{\Psi}_{NG}$ and $\dot{W}_{E,a}$ are the rate exergy destruction rate, the variation of exergy through the fire tubes of the line heater , the rate of solar exergy entered the control volume, the variation of exergy of natural gas stream through the whole CGS and the rate of producible work by the turbo-generator set, respectively.

The exergy balance of the fire tubes could be written as:

$$\Delta\dot{\Psi}_{ft} = \dot{\Psi}_{fu} + \dot{\Psi}_{a} - \dot{\Psi}_{ex} \tag{4.14}$$

In which, the subscripts fuel, air and exh refer to the burned fuel, the inlet air to the fire tubes and the heater exhaust, respectively. The principal correlation for the calculation of fuel exergy is:

$$\dot{\Psi}_{fu} = \dot{n}_{fu}\left[(\hat{h} - \hat{h}_{o}) - T_{o}(\hat{s} - \hat{s}_{o}) + \hat{\psi}^{ch}\right] \tag{4.15}$$

Where, $\hat{\psi}^{ch}$ is the chemical exergy of each component in the consuming fuel and $(\hat{s} - \hat{s}_{o})$ and $(\hat{h} - \hat{h}_{o})$ are the molar entropy difference and the molar enthalpy difference compared to the dead state conditions both of which can be considered to be zero as the fuel enters the fire tube in reference condition. Also, in this equation, $\dot{n}_{fu}$ refers to the molar flow rate of fuel which can be determined as:

$$\dot{n}_{fu} = \frac{\dot{m}_{fu}}{M_{fu}} \quad \& \quad \dot{m}_{fu} = \frac{\dot{Q}_{h}}{LHV_{fu}\,\eta_{h}} \tag{4.16}$$

In which, $\dot{m}$ and M refer to the fuel mass flow rate and molecular weight, respectively. Note that as natural gas is mainly comprised of Methane (even up to 99% in many cases), the fuel could be considered as pure methane without any significant deviation in the results.

On the other hand, as the inlet air enters fire tube in the reference conditions, the middle item in the right side of equaiton 4.13 is also equal to zero while for calculating the exergy of combustion products at the heater exhaust, the following equation could be used:

$$\dot{\Psi}_{ex} = \sum_i \dot{n}_i \left[\left(y_i \, \hat{\psi}_i^{ch} + \bar{R} T_o \, y_i \, Ln(y_i) \right) - T_o \left(\hat{s}_i - \hat{s}_o \right) + \left(\hat{h}_i - \hat{h}_o \right) \right] \quad (4.17)$$

Where, y_i and $\dot{n}_i$ are the molar ratio and the number of moles for each component in the combustion products, respectively. For calculation of these two items, the following combustion reaction should be completed. It is worth mentioning that the combustion reaction is completed based on this assumption that the combustion procedure of a line heater is usually done with approximately 300% theoretical air (Arabkoohsar et al., 2014).

$$CH_4 + 6(O_2 + 3.76N_2) \rightarrow (CO_2) + 2(H_2O)_g + 22.56(N_2) + 4(O_2) \quad (4.18)$$

Also, $\hat{s}_i, \hat{h}_i$ in equation 4.16 are the molar entropy and enthalpy of each combustion production component in exhaust temperature, respectively. For computing the exhaust temperature, the first law of thermodynamics should be written for the control volume as follow:

$$\frac{\dot{Q}_{NG}}{\dot{n}_{fu}} + \hat{h}^o_{CH_4} = \left(\hat{h}^o_{CO_2} + \Delta\hat{h}_{CO_2} \right) + 2 \left(\hat{h}^o_{H_2O(g)} + \Delta\hat{h}_{H_2O(g)} \right) + 22.56 \left(\Delta\hat{h}_{N_2} \right) + 4 \left(\Delta\hat{h}_{O_2} \right) \quad (4.19)$$

In the next step, the rate of solar exergy which enters the control volume through the solar collector modules must be calculated for which the same formulation as that presented in chapter 2 is used.

In the end, the natural gas stream exergy variation through the CGS could be calculated as follow:

$$\Delta\dot{\Psi}_{NG} = \dot{m}_{NG} \left(\psi_{NG-i} - \psi_{NG-e} \right) = \dot{m}_{NG} \left[\left(h_i - h_e \right) - T_o \left(s_i - s_e \right) \right]_{NG} \quad (4.20)$$

Where, h_i, h_e, s_i and s_e are the enthalpies and entropies of inlet and outlet natural gas into/from the control volume, respectively. Extracting the required values from the thermodynamics tables as well as using the known parameters in the above equation, the exhaust temperature and subsequently the exhaust exergy could be calculated.

Now that all the rate of fire tube exergy variations, natural gas exergy changes and solar exergy support are calculated, and taking the value of producible power by the turbo-generator set at the CGS given by the energy analysis section, one could calculate the rate of

exergy destruction in the CGS. Finally, exergy efficiency of the modified configuration of CGS is defined as:

$$\varepsilon_{CGS} = \frac{\text{The Effective Exergy}}{\text{The Supplied Exergy}} = \frac{P_{CGS}}{\dot{\Psi}_{fu} + \dot{\Psi}_{SS} + \dot{\Psi}_{NG}} \tag{4.21}$$

5. Proposed Power Generation Systems

As it was explained in introduction chapter and also claimed in the qualification exam associated with this dissertation, the main goal of this thesis is dynamic modeling of the performance of a CAES system in a renewable source power plant (for example, a PV farm), which has been the concern of experts and scientists over the last decades. As the having such a power plant while working under real circumstances is inevitable for simulating the dynamic performance of CAES, a large scale grid connected PV farm equipped with a CAES system is proposed to contribute in Brazil's national electricity distribution grid, in the first step. After simulating and investigating this system comprehensively, a further configuration consisting of the previous grid connected PV farm with its CAES system accompanied with a power productive CGS station, is proposed to enhance the power plant power output stability, revenue and overall performance. The details of each system are presented in a specific section in this chapter.

5.1 PV Farm Equipped with a CAES System

The first proposed power plant configuration in this thesis is a PV farm which is going to be equipped with a CAES system. As it was explained before, the necessity of using CAES systems instead of conventional batteries is due to the very large size of batteries required for large scale power plants, limited capacity and some technical problems such as internal self-discharging of batteries. Figure 5.1 illustrates the schematic of the first proposed configuration for this objective. According to the figure, an A-CAES system equipped with a solar heating system works alongside a PV plant. The PV plant is connected to the grid and supports it during its normal operation as much as required. Naturally, the amount of power that is sold to the grid should be specified in advance based on a mutual agreement between the grid and the power plant. In case of any extra power production than agreed values, the extra power is used to run the multiple stage compressor set to produce high pressure compressed air.

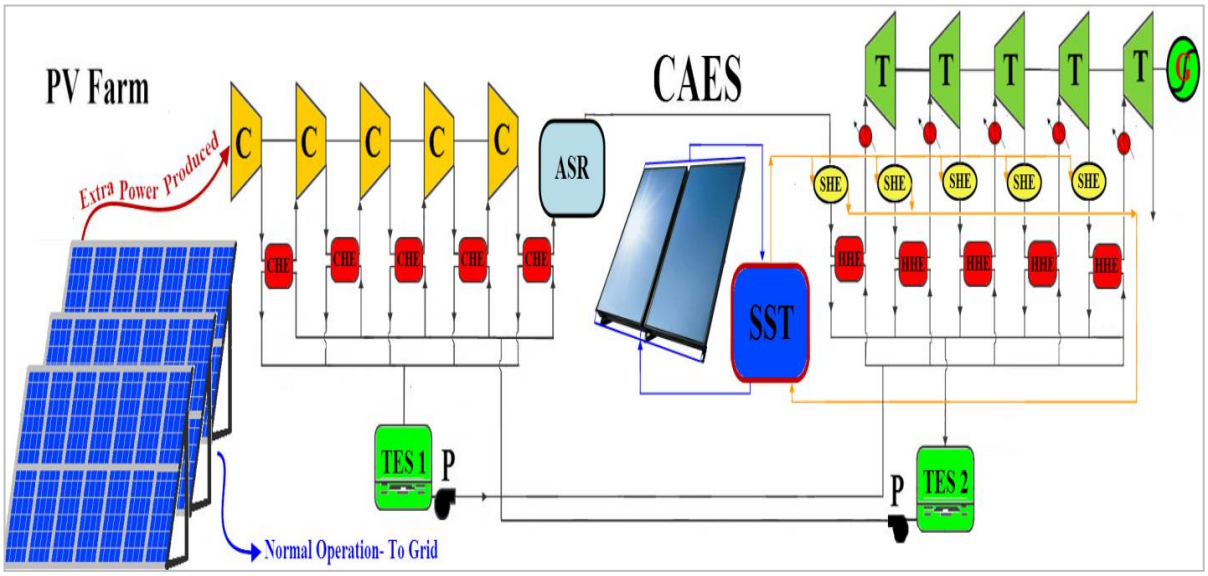

FIGURE 5.1 − The schematic of the proposed configuration

As can be seen, there are some cooling heat exchangers between the compressors to collect the heat generated in the air stream through the compression process. In fact, the heat exchangers are some shell and tube heat exchangers through which the air gives its heat to a working fluid. The heated working fluid is then stored in a thermal energy storage tank. As the figure shows, the cooling heat exchangers inlets are parallel and it means the working fluid temperature is the same at the heat exchangers inlets, though the outlet temperatures could be different as the compressors may work in different conditions. Note that the cold inlet working fluid comes from the other thermal energy storage tank existed in the system. The compressed air is finally kept in an air storage reservoir that can be an underground cavern.

Parallel with the compression unit which naturally should be working in sunny hours, the solar heating system also produces hot working fluid to be employed for heating purposes of the project. In this configuration, like the latest proposed CAES configuration, flat plate solar collectors are employed in the system. As flat plate collectors are only able to produce temperatures up to 85 ^{o}C, therefore, water can be used as the working fluid of the solar heating unit here. Therefore, water enters the flat plate solar collector modules and receives the heat absorbed in their absorber plates. The warmed water then enters the filled solar storage tank with the same fluid. Clearly, the collector module inlet water also origins from the bottom of the solar storage tank. Therefore, this cycle is repeated so that water could be warmed by the collectors up to higher temperatures.

The other possible operational condition is when the solar energy ramps make the PV farm to not be able to cover the grid demand. For this case, the stored compressed air is reclaimed to be used for generating power by passing through the multiple stage expander set. Naturally, the air should be preheated before being expanded. This is why the heating process in three phases is proposed to be accomplished before each stage of expansion. The first stage of preheating is done with solar heat exchangers supported by the solar heating system. In fact, the hot working fluid stored in the storage tank flows through the shell and tube solar heat exchangers and warms up the air stream up to possible temperatures. In the next step of preheating, the heat stored in the thermal energy storage tank 1 is employed for heating the air stream. These heat exchangers are also shell and tube type. Finally, if still air needs to be heated to higher temperatures, the auxiliary diesel air heaters could be used. After being heated, the air passes through the expanders and runs the turbines. The turbine shaft is synchronized by an electricity generator device and it produces power as much as required. It should be noted that the system is so designed that the air mass flow rate is regulated according to the amount of power shortage in the PV farm. It is also noteworthy that the working fluid outgoing from the solar heat exchangers comes back to the solar storage tank and the working fluid outgoing from the heating heat exchangers goes into the other thermal energy storage tank (No. 2).

Clearly, some different states are possible in the proposed system. The first case is that the PV plant produces exactly the same amount of power as required, which rarely happens due to the sharp fluctuations of solar irradiation. In this case, neither the compression unit nor the expansion unit of the CAES system is working. The second possible state is when the PV plant produces extra power during which the compression unit is in operation condition and as a result, the cavern is charged by compressed air. In this state, the solar heating system is also in operation to produce hot water and the expansion unit is in standby condition. The last operational condition is when the PV plant is not able to cover the grid demand and the expansion unit has this mission to offset the energy shortage of the PV farm. Naturally, in this case, the compression unit is again in standby state and the solar heating system and expansion unit work simultaneously. The solar heating unit may operate in both sides (producing hot oil by the collectors if there is solar irradiation available and supporting the solar heat exchangers by providing hot oil) in such state. In this condition also there can be two possibilities as: a) the CAES system could completely offset the energy shortage, b)

the CAES system is not able to offset all or even no energy shortage and as a result, depending on the amount of energy that could not be offset, there will be financial fines for the PV plant. Such penalties are usually defined for the ramps higher than 10% of the agreed values. Evidently, the less the CAES system offsets energy shortage, the more the power plant will be charged financially.

It is noteworthy that in this PV plant the design target is so that if there is still extra compressed air in the air reservoir at the end of the day, specific amount of air remains in the reservoir to offset the possible PV farm power slumps during the early daily hours of the next day (5 bar, if possible) and the remaining portion is used to produce power at peak power consumption hours (from 8 pm to 12 pm).

Note that, for designing the first proposed system shown in figure 5.1, some important parameters should be taken into account. In fact, there are some main questions related to the proposed power plant and the corresponding answer of each of these questions must be given first. These questions could be categorized into two separate classifications as the issues related to the PV farm and the problems associated with the CAES system.

5.1.1 PV Farm

The primary important question related to the PV farm is that where this power plant is supposed to be built (the PV plant location). Clearly, the best place for constructing a solar power plant is the point that receives the maximum amount of solar irradiation and has the least cloudy and rainy hours over the year. For this objective, as the PV farm is supposed to be in Brazil, solar irradiation intensity map throughout the country can be helpful. Figure 4.2 shows this map related to 2014 (CPC, 2014). According to the figure, the west and middle area of Rio Grande do Norte state is the best point for construction a PV farm. Therefore, this area can be opted as one of the most suitable places to host a solar power plant. The closest weather forecast station to this area is located in Natal city which is one of the biggest cities in the north-east of Brazil with latitude and longitude angles of 5.78° S, 35.20° W, respectively. Therefore, the weather data related to this station is used for simulating the proponed power plant.

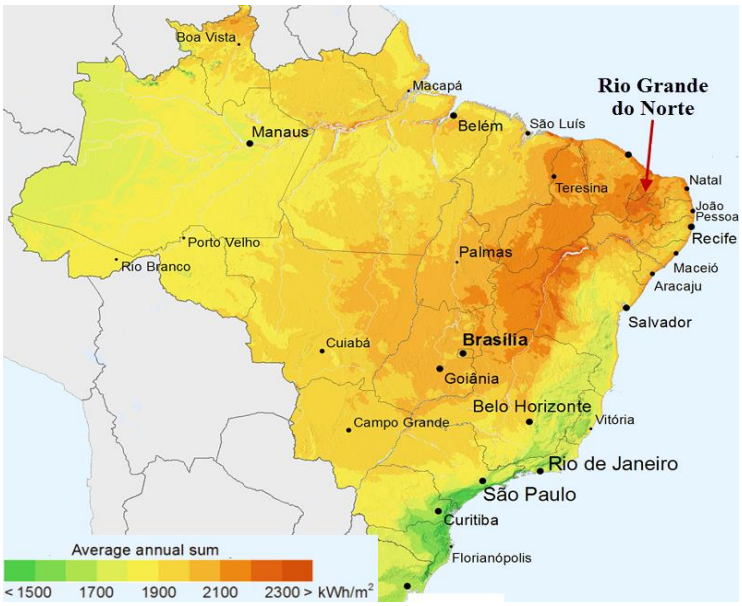

FIGURE 5.2 − Brazil's normal solar irradiation intensity map in 2014

The next parameter that must be determined is the capacity of the PV farm which is undoubtedly a functional of the investor budget, investment plans and the total local electricity demand. As Rio Grande do Norte population exceeds 3.4 million, there is no restriction for the amount of required electricity. In addition, as the power plant is only an assumptive station, there is no limitation in energy budget as well. Therefore, just as a sample case, a PV plant with 100 MWp capacity in Natal city is considered to be simulated.

In the next stage, the PV cell type that is supposed to be used for collecting solar irradiation should be selected. In this regards, both energy efficiency and the price of the PV cell are the key points and effective parameters in making decision. As it was thoroughly explained in chapter 3, there are various types of PV cells available in the market. However, it is highly recommended to employ monocrystalline silicone PV cells in PV plants according to their expected efficiency and price. Table 5.1 details the characteristics of the employed PV cell in the simulations of this work (Tensolar, 2015).

TABLE 5.1 − Details of various PV cells and tracker mode utilized in this work

Characteristics	Information
Type	Monocrystalline silicone
Dimensions	156mm × 156mm ± 0.5mm
Diagonal	200mm ± 1mm
Thickness	180µm ± 30µm / 200µm ± 30µm (Wafer thickness)
Front	Silver bus bars; blue/purple/brown, silicon nitride antireflection coating
Back	Silver bus bars; Full-surface aluminum BSF
Average Conversion Efficiency (%)	19.3
Rated Power (W_p)	4.59-4.64
Max. Power Current, I_{mp} (A)	8.52
Max. Power Voltage, V_{mp} (V)	0.540
Short Circuit Current, I_{sc} (A)	9.04
Open Circuit Voltage, V_{oc} (V)	0.638

It bears mentioning that the average energy conversion efficiency of the ground mounted PV arrays is normally different than the expected efficiency of an individual cell. In fact, there are many sources of losses and uncertainties for ground mounted PV arrays such as the effects of wind, humidity, dust and birds, losses in cabling, inverters and etc. According to (Fthenakis *et al.*, 2011), in this work, the average energy conversion of the ground mounted PV array is considered to be 90% of the average efficiency of an individual PV cell while operating in optimal conditions (19.3%). Therefore, the PV farm average energy conversion efficiency is calculated to be 17.4%.

The type of employed tracker technology is the next important factor to be chosen in the next step, considering energy-economic aspects of the project. Among all the tracking modes described in chapter 3, the plane rotating around north-south axis parallel to the earth's axis with continuous adjustment finally chosen to be employed in this work. The details of this selection will be given in results chapter. Figure 5.3 shows what exactly means this type of tacking.

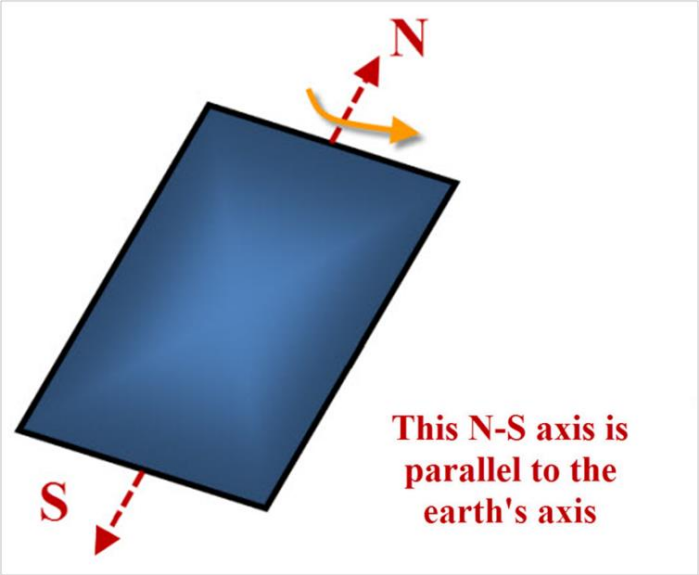

FIGURE 5.3 − Plane rotating around north-south axis parallel to the earth's axis with continuous adjustment

The investigations show that a maximum of 1220 W/m^2 solar irradiation could be absorbed by such a tracking cell in Natal city. Taking the average energy conversion of the ground mounted PV farm equal to 17.4%, therefore, for having a PV farm with 100 MWp capacity, one could easily calculate that a total absorbing PV cell area of 470,000 m^2 is required.

Also, as one of the most important parameters that need to be defined for the PV farm, one must specify how much electricity it sells to the grid over the year which is called power plant power sales strategy. In fact, the power sales strategy of the PV plant specifies based on what basis and pattern the PV farm pledges to support the grid in every moment over the year. Naturally, the more electricity is sold to the grid, the higher values of revenue are gained. However, on the other hand, there will be financial penalties for the plant if it cannot meet the grid demand (based on the mutual agreement between the grid authorities and the power plant). As it was mentioned before, usually, the ramps above 10% of the value indicated in the contract result in financial fines for the power producers. This is why the power sales strategy should be so specified that not only it maximizes the power plant revenue, but also minimizes the total annual fines. Mainly, two different strategies are possible to follow for selling power to the grid. The first strategy is selling a constant amount of power to the grid during the day. The second schema is selling power to the grid as a functional of daily time. Figures 5.4-a and 5.4-b show these strategies for a sample operating day, respectively.

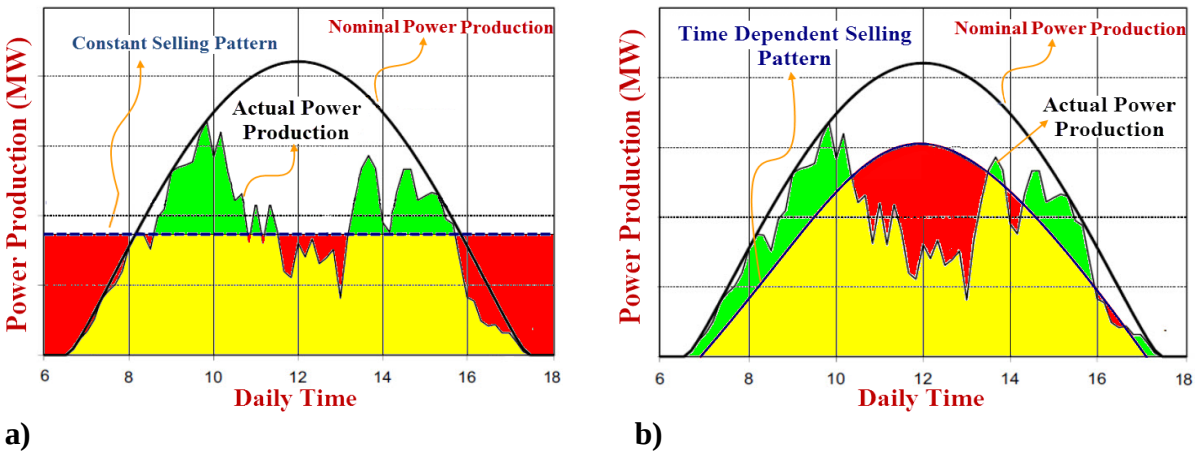

FIGURE 5.4 − Various power selling strategies during the day; a) constant power; b) time dependent power

In the figures above, the yellow areas represent the time in which the power plant supplies power for the grid. The red areas are the times during which the PV farm is not able to generate enough power for the grid. In such cases, the storage unit of the plant should offset this power shortage; otherwise, there will be penalties for the power plant. The green areas, finally, represent the time when the PV farm generates extra electricity and the storage system uses this power to produce compressed air. In both of these strategies, the values could be defined as a portion of the maximum or the average capacity of the PV farm. For choosing the best pattern for selling power, the normal and peak period consumption electricity prices as well as the penalty rates should be taken into account. In Brazil, the daily and nightly (peak consumption time) electricity prices are 0.153 USD/kWh and 0.2 USD/kWh respectively. The penalty rate is also considered equal to 750 USD/MWh (COSERN, 2015). It is also noteworthy that selecting the most appropriate power sales strategy strongly depends on the size of the energy storage system of the power plant, which is supposed to be a CAES system, and its components. This issue is discussed in the following section. As it will be comprehensively discussed and explained in the results chapter, the best power sales strategy of this power plant is selling power to the grid based on 70% of instantaneously-monthly averaged actual producible power by the PV farm.

5.1.2 CAES System

In CAES system design also, there are some important questions that should be answered. The first question is the maximum capacity of CAES system in the power plant i.e. the capacity of the compressors and expanders. This is a thorough thermo-economic matter and should be determined very carefully as accurate selection of CAES capacity could lead to the

best energy storage efficiency in the lowest possible capital cost. It is also important to mention that CAES system sizing should be carried out simultaneously with the power sales strategy selection because as the CAES system size changes the amount of recoverable power ramps and financial fines change and as a result, the revenue of the power plant changes significantly. Finally, the CAES optimum size associated with the understudy configuration is found to be equal to 60% of the maximum extra power produced by the PV farm relative to the power sales pattern determined. As with this pattern of selling power to the grid the maximum extra power produced by the PV farm over the year is 84 MW, therefore, the CAES system maximum capacity should be about 50 MW.

The other question is about the maximum pressure of the system. For answering this question it could be said that the system can produce power with any pressure, however, for the same capacities of the CAES system, the lower pressures requires the bigger volumes of cavern which is costly. On the other hand, for having a system with higher maximum pressures the cost of system could also increase due to the more advanced and more complex facilities required in the system. Therefore, one should tradeoff energetically and economically to choose the best maximum pressure of the CAES. Normally, the pressures from 60 bar up to 150 bar could be good choices for a CAES system in large scales (Grazzini and Milazzo, 2008). Also, the cavern volume is recommended to be chosen equal to 1% of total daily extra electricity available to be used by the CAES system (Grazzini and Milazzo, 2008). In this work, the volume of cavern is so selected that maximum pressure in cavern does not exceed 120 bar.

The next issue to decide is the number of stages in the compression and expansion units. This issue is also related to both energy efficiency and economic considerations. Clearly, when the number of stages increases, both the compression and expansion efficiencies and the system capital cost come up. Therefore, one should tradeoff for finding the best number of stages for the compressors and expanders. As figure 5.1 shows, the proposed system takes advantage of a five stage compressor and a five stage expander which is selected based on the advice given in a previous study specifically accomplished for this objective (Grazzini and Milazzo, 2008).

The compression and expansion ratios of the compressors and expanders are the other parameters that should be defined in design stage. Similar to the previous questions, the

compression and expansion ratios in the system depend on energy and economic considerations. There are air compressors and expanders with various ranges of compression/expansion ratios from slightly more than 1 up to even 5. The previous specific study on CAES details has an answer for this question as well. They proposed both of the compression ratio ($\beta'=P_e/P_i$) in each stage of the compressor set and the expansion ratio of the expanders ($\beta''= P_i/P_e$) to be equal to 2.88 (Grazzini and Milazzo, 2008).

Having the most efficient configuration of the compressors and the expanders such as their number of stages and the compression/expansion ratios, one should proceed to find out how to change the arrangement of compressors and expanders depending on the cavern pressure. It is clear that the compressors and the expanders should work in different arrangements (parallel or series) in different cavern pressures. Naturally, in lower pressures of the cavern, the compressors work in parallel to provide more flow rates of air in lower pressures. Because, even if they produce compressed air with higher pressures, the air will be expanded in the cavern and its pressure will decrease again. In higher cavern pressures, on the other hand, the compressors arrangement turns to series as the compressor set should provide compressed air with higher pressures than the cavern pressure to increase the cavern air mass and pressure. Obviously, if the pressure of air outgoing from the compressor is less than the cavern pressure the air cannot get into the cavern. This arrangement also applies for the expanders, though a reverse arrangement change versus the cavern pressure variations is required here. Table 5.2 shows how the arrangement of the expanders and compressors change as a functional of the cavern pressure.

TABLE 5.2 − Compressors and expanders arrangements in different operational conditions

Pressure Range (bar)	Compressors Arrangement	Turbines Arrangement
$P_{ca}<2.9$	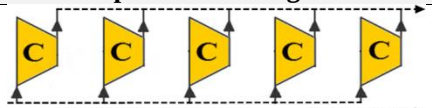	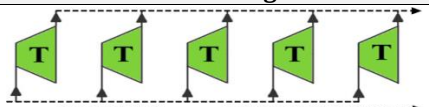
$2.9<P_{ca}<8.3$	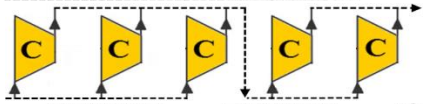	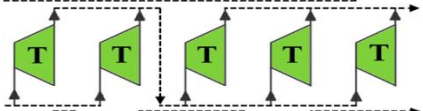
$8.3<P_{ca}<24$	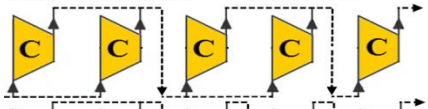	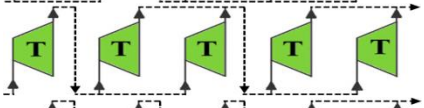
$24<P_{ca}<69$	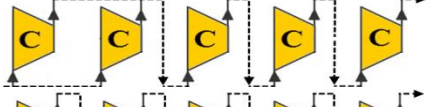	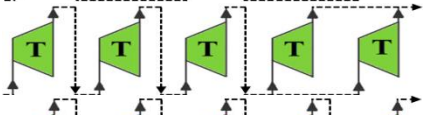
$P_{ca}>69$	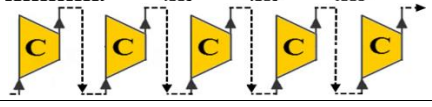	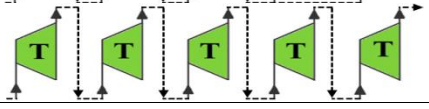

In the next step, the capacity of the solar heating unit including the number and the type of solar collector modules and the capacity of the solar storage tank needs to be determined. This depend on the amount of heat required in the expansion process and the efficiency of the collectors utilized in the system. As it was explained before, evacuated tube solar collectors are supposed to be employed in the system. Table 5.3 details the characteristics of the widely available flat plate solar collectors in the market.

TABLE 5.3 − Properties of employed solar collectors

Characteristic	Information
Collector Length	200 cm
Collector Wide	95 cm
Collector Thickness	9.5 cm
Cover Matter	Glass
Cover Thickness	4 mm
Absorber Plate Thickness	0.5 mm
Tubes Inner Diameter	10 mm
Tubes outer Diameter	12 mm
Tubes Space	150 mm
Plate Area	1.51 m^2
Plate Matter	Copper

Also, according to the table, for such solar collectors, it is recommended to have a storage tank with 100 l per collector. The number of collectors in the CAES system should be calculated based on the maximum amount of extra heat required in an individual day over a whole year of simulating system. The number of required collectors in the solar heating system is found to be 2500 collector modules and subsequently, the storage tank capacity should be 250 m^3.

The capacity of the thermal energy storage units need to be also specified. Obviously, both of them have the same capacity as they should exchange working fluid with each other. The size of the thermal energy storage systems depends on the maximum daily amount of the working fluid required in the system over a whole year which itself is a functional of the working mass flow rate in the cooling and heating heat exchangers. Normally, the working mass flow rate is a submultiple of the air mass flow rate. The results of simulations over a whole year show that the thermal energy storage units must be at least 5500 m^3 in volume.

Finally, in the CAES system, the capacity of the auxiliary air heaters must be defined. Clearly, as these devices are only for emergency cases, there is no certain rule based on which the air heaters capacities could be defined. Therefore, in this work, the air heaters

are so sized that they can make a 10 ^{o}C temperature increase in the maximum mass flow rate of air over the year. For this objective, the air heaters capacities should be 1.05 MW.

Note that in CAES system sizing, the maximum extra generated power, the maximum ramps that the system should offset during the year and the capital cost of the CAES systems with different capacities should be taken into account. It is recommended to estimate the CAES system cost of capital up to 900 USD/kW (Espcine, 2015). For the solar heating system in the CAES system, the cost of capital is estimated equal to 380 USD per each collector (Transsen, 2015).

Table 5.4 details the characteristics specified as the optimal characteristics for the proposed PV plant configuration through the comprehensive dynamic energetic and economic simulation accomplished for it.

TABLE 5.4 − The characteristics of the sample PV plant

Characteristics	Information
PV Cell Type	Monocrystalline Silicon
Individual PV Cells Average Energy Conversion Efficiency	19.3 %
Tracking Mode	North-South Axis Parallel to the Earth's Axis Rotation
PV Farm Average Energy Conversion Efficiency	17.4 %
Total PV Cell Area	470000 m^{2}
Power Plant Power Sales Strategy	70% of the Instantaneous-Monthly Averaged PV Farm Production
CAES Power Production Capacity	50 MW (60% of Maximum Extra Power Available)
Air Reservoir Volume	20000 m^{3}
Air Reservoir Maximum Pressure	120 barg
Thermal Storage Tanks Volume	5500 m^{3}
The Heat Exchangers Working Fluid	Industrial Oil
Number of Compression/Expansion Stages	5
Compression/Expansion Pressure Ratios	2.88
Number of Collectors in the Solar Heating Unit	2500
Absorber Plate Area of each Collector	1.51 m^{2}
Collector Set Slop Angle	12^{o}
Solar Storage Tank Volume	250 m^{3}
Solar Heating Unit Working Fluid	Ethylene Glycol
Auxiliary Air Heater Capacity	1050 kW
Auxiliary Air Heater Fuel Type	Natural Gas

5.2. PV Farm Equipped with a CAES System and Accompanied with a CGS

According to what was claimed before, the second power plant configuration proposed in this thesis, which aims at enhancing the power output stability and reliability, decreasing its CAES size, modifying the power sales strategy and increasng the total net revenue of the previous configuration, is a hybrid power production station including a PV farm equipped with a CAES system plus a power productive CGS station. Figure 5.5 illustrates the schematic diagram of this innovatibe hybrid power plant.

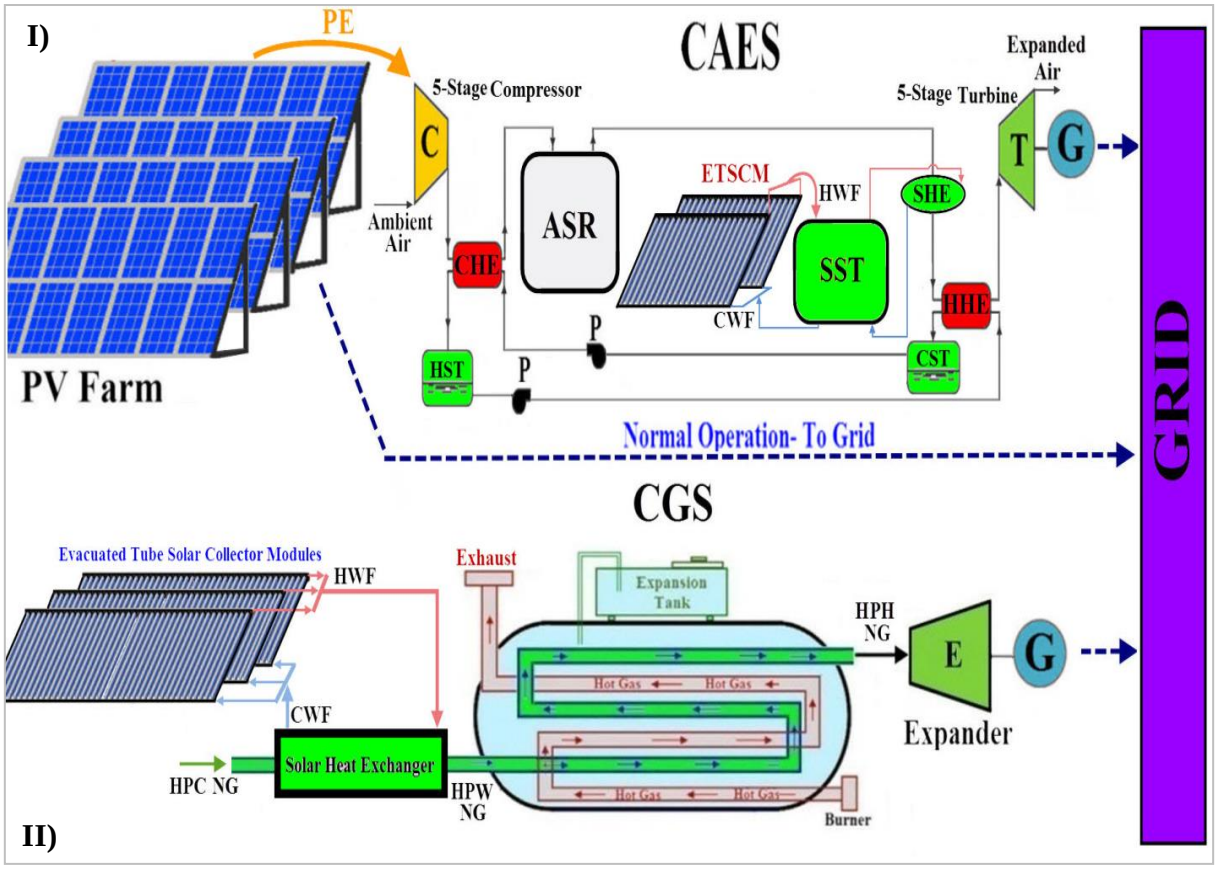

FIGURE 5.5 − The schematic of the proposed system; HPC PE: extra power produced; C: compressor set, CHE: cooling heat exchanger set, HST: hot storage tank, ASR: air storage reservoir, T: turbine set, HHE: cooling heat exchanger set, CST: cold storage tank; NG: high pressure cold natural gas; HPW NG: high pressure warmed natural gas; HPH NG: high pressure hot natural gas; CWF: cold working fluid; HWF: hot working fluid; E: expander; G: generator

According to the figure, the whole system includes two main parts, namely the CGS power productive station and the PV plant thoroughly discussed in the prior section. Based on the design strategy, the PV farm is again supposed to produce electricity employing solar irradiation directly. Depending on the power sales atrategy of the power plant, there may

be again either extra produced electricity or lack of electricity in the system. In case of producing extra power by the PV farm, this extra electricity is used by the CAES system for producing compressed air; otherwise, the compressed air in the cavern is employed to produce extra electricity to support the PV farm for poviding the grid demand. In the second part of the proposed configuration (the power productive CGS), on the other hand, the power produced by the CGS is either sold directly to the grid by the time there is electricity shortage in the PV farm output relative to the grid demand to improve the maximum level of power sales pattern or it is used by the CAES system to produced compressed air when the power output of the PV farm exceeds the local grid electricity demand. Clearly, not only the electricity that is produced in the CGS station could be used to improve the strategy of power sales of the power plant, but it also can increase the flexibility of the plant in offsetting its power output ramps occurred due to solar irradiation intensity fluctuations.

One important point here is that in this configuration of the PV plant the design target changes so that, even in case of existing extra compressed air in the caver at the end of the day, there is no need to have any air in the reservoir to offset the PV farm power fluctuations of the early daily hours of the upcoming day as the power supplied by the CGS could easily afford this issue by itself. Also, this time the extra remaining compressed air is used to produce power from 6 pm to 12 pm to increase the revenue of the power plant as much as possible. Another difference is that the type of collectors used in the solar thermal unit of the CAES system change to evacuated tube collectors in order to improve efficiency and increase acheivable temperature of the air stream after the solar heat exchangers.

5.2.1 Power Productive CGS

Naturally, as the PV farm is supposed to be located in Natal city, one of the CGS stations of this city should be employed to design the target configuration. It is worth mentioning that as there is no information about none of CGSs of Natal city, a sample CGS which supplies the natural gas demand of a part of this city has been considered in the simulations. The configuration and characteristics considered for this CGS and all the facilities are exactly in accordance with typical CGSs all around the world. Figure 5.6 illustrates the arrangement of facilities in this assumptive CGS.

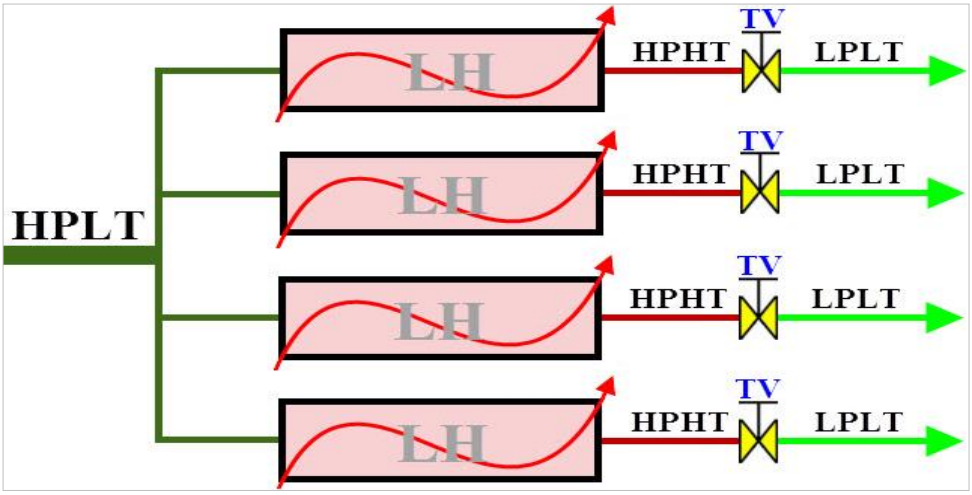

FIGURE 5.6 – The arrangement of facilities in the CGS; LH: line heater, TV: throttling valve, HPLT: high pressure-low temperature gas, HPHT: high pressure-high temperature gas, LPLT: low pressure-low temperature gas

Also, table 5.5 details the technical information about this CGS. It should be mentioned that the mass flow rate of natural gas passing through this station has been considered to be constant. As Natal is an industrial city and consequently a major portion of the passing natural gas is to supply the factories and industrial parts of the city continuously over the year, this assumption can be somehow reasonable.

TABLE 5.5 – The considered CGS technical information

Characteristics	Information
Total Capacity of Station (Sm^3/h)	400,000
Number of Line Heaters	4
Individual Heater Maximum Capacity (Sm^3/h)	100,000
Hydrate Temperature (^oC)	5 ^oC
Nominal Inlet Pressure (kPa)	7100
Nominal Outlet Pressure (kPa)	1700
Relative Density (kg/Sm^3)	0.63

Also, table 5.6 gives information about the compositions of the natural gas passing through this station which are equal to the compositions of current natural gas in Brazil (Gasmig, 2014).

TABLE 5.6 – The natural gas compositions

Component	C1	C2	C3	C4	CO2	N2
Proportion (%)	89.96	5.80	1.78	0.68	1.79	0.47

Evidently, this CGS with the current configuration could not be helpful for the considered objective. Therefore, the first step is changing this configuration into a power

productive CGS based on the pattern introduced as the most recent and optimal CGS in prior chapter. Figure 5.7 represents the modified configuration of understudy CGS.

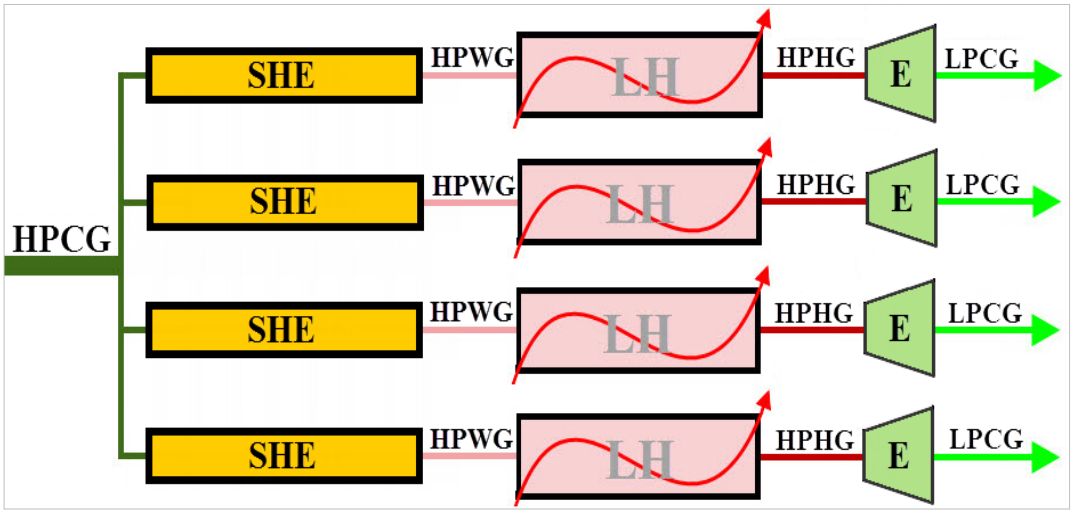

FIGURE 5.7 – The arrangement of facilities in the improved configuration of assumptive CGS in Natal city; SHE: solar heat exchanger; LH: line heater, E: expander, HPCG: high pressure-cold gas, HTWG: high pressure-warmed gas; HPHG: high pressure-hot gas, LPCG: low pressure-cold gas

According to this figure, one solar heat exchanger, which is supported by evacuated tube solar collectors, is placed before each line heater and all the throttling valves in the system have been replaced by some turbo expanders. Table 5.7 gives information about the evacuated tube solar collectors employed in simulating the CGS.

TABLE 5.7 – The characteristics of employed evacuated solar collectors

Characteristics	Information
Number of Tubes	18
Inner Diameter of Tubes (mm)	20
Outer Diameter of Tubes (mm)	22
Absorber Plate Width (mm)	5
Absorber Plate Length (mm)	1780
Absorber Plate Thickness (mm)	0.5
Absorber Plate Material	Copper
Coating Material	Borosilicate Glass 3.3
Glass Tube Diameter (mm)	58
Interval of Tubes (mm)	75
Storage Tank Capacity (liter per Collector)	100

The number of solar collectors are so selected that the maximum desirable temperature of the system (85 ^{o}C) is provided by the solar heat exchangers by the time the maximum solar irradiation is received by each individual solar collector and the rest of natural gas heating demand is provided by the line heater. In this case, no extra investment has been

put on the system as hiring more solar collectors equals to increasing the solar system capital cost. For achieving this goal a total number of 5200 evacuated solar collectors is required. Also, each of the turbo-generators should have a maximum power production capacity of 2.75 MW.

5.2.2 PV Farm

Naturally, the PV farm location and capacity, tracking mode, PV cell type and total PV cell absorbing area does not change relative to the previous configuration. However, what is directly affected by adding this extra source of power production to the power plant is its power sales strategy. As it will be shown in results chapter, the power sales strategy of the power plant improves considerably from only 70% to 90% of the instantaneously-monthly averaged actual producible power by the PV farm.

5.2.3 CAES System

Clearly, contemporary with the power sales strategy of the power plant, the CAES size and consequently all the dependent characteristics vary significantly. In this system, the CAES capacity decreases from 50 MW to 30 MW which means how the power output of the PV farm along with the CGS is stable and also equals to the reduction of CAES capital cost. The cavern volume and the air heater capacity in this case are found to be 12500 m^3 and 1.25 MW, respectively. Also, the number of collector modules in the CAES system should be 1800 and the storage tank volume is 180 m^3 while the thermal storage tanks volumes must be 3300 m^3 each. It is noteworthy that the compressors and expanders stage numbers, arrangement change pattern, compression/expansion ratios as well as the cavern maximum pressur as the certain parameters of the CAES system in the power plant configurations with and without a power productive CGS do not differ.

It is finally re-mentioned that the details of calculating and selecting the values given in this chapter as well as the explanation of the economic evaluation method used for this objective will be presented in chapter 6.

6. Results and Discussion

In this chapter, the results of the dynamic analysis carried out on both of the proposed configurations for the PV plant are presented. First of all, the common parameters of both of the proposed configurations of this dissertation, such as the PV farm performance, available solar energy and etc., are investigated and the corresponding results are given. The primary key information that is needed for doing the simulation is the ambient temperature and the total sunny hours that can be expected in the chosen location for implementing the simulations. It should be mentioned here that in order to do a thorough simulation, the data related to an entire sample year (the most recent data released by the corresponding station, 2012) is used in this work.

Figure 6.1 shows the monthly maximum, minimum and mean averaged ambient temperature as well as the total monthly sunny hours in Natal in 2012.

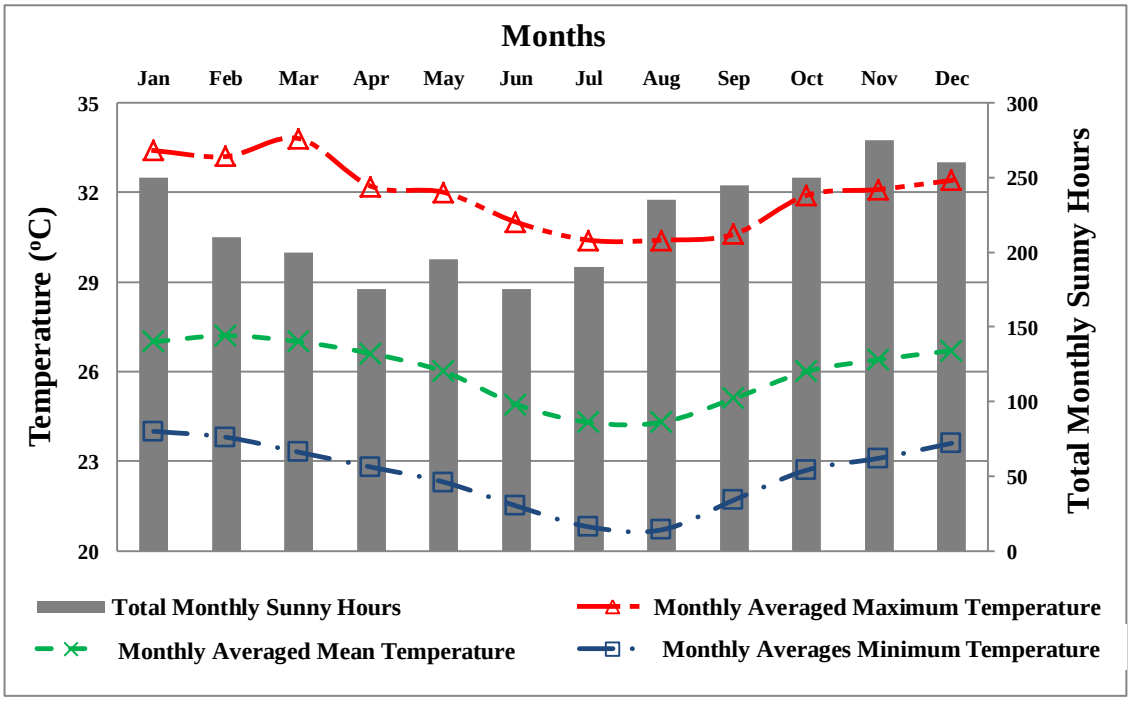

FIGURE 6.1 – Maximum, minimum and mean averaged ambient temperature in Natal in 2012

Expectedly, as Brazil is located in the south hemisphere, January and February are the warmest months of the year while the coldest period of the year occurs from July to August. The maximum monthly averaged temperature is around 32 ^{o}C and the minimum monthly averaged temperature is almost 21 ^{o}C. It is noticeable that the single point maximum

and minimum temperatures observed over the year are different than these values where the maximum temperature over the whole year is 38 ^{o}C in January and the least temperature recorded is 17 ^{o}C in August. In this work, the monthly averaged temperatures are used through the simulation process. Also, the sunniest month over the year is November by almost 280 hours whereas April and June are the least sunny months by about 175 hours.

The next figures are going to present the amount of solar irradiation expected to be received by a solar collector in Natal over the year in case the sky is totally clear (theoretically available solar irradiation based on the clear sky model). However, showing a single graph for all days of the year is not reasonable as it needs much space to present. The total daily format is another option for showing the theoretically available solar irradiation, but this method is not illustrative enough as showing the variation of solar energy intensity over a whole year is important in the simulation process. Therefore, the best form of data presentation for such cases is hourly-monthly averaged format. In fact, the hourly-monthly averaged means that there are 24 values (24 hours of the day) for each month of the year. For more clarification, imagine that the variation of ambient temperature in January is supposed to be presented. Based on the hourly-monthly averaged format, the graph should comprise 24 values each of which is the mean value of 31 temperatures (31 days of January). For example, the ambient temperature at 7 pm in all the 31 days of January is averaged and the result is given as the hourly-monthly averaged value of ambient temperature in January at 7 pm.

Figure 6.2 shows the hourly-monthly averaged solar irradiation intensity that can be expected to shine on a horizontal surface with 1 m^2 area in Natal. As can be seen, in February, at noon, up to 1150 W/m^2 on a horizontal surface could be expected. In a sharp contrast, by changing the season, in June, 900 W/m^2 is at most receivable by a horizontal surface. What is clear is that in summer months the solar irradiation intensity is much more than colder months of the year and this change occurs little by little by changing the months.

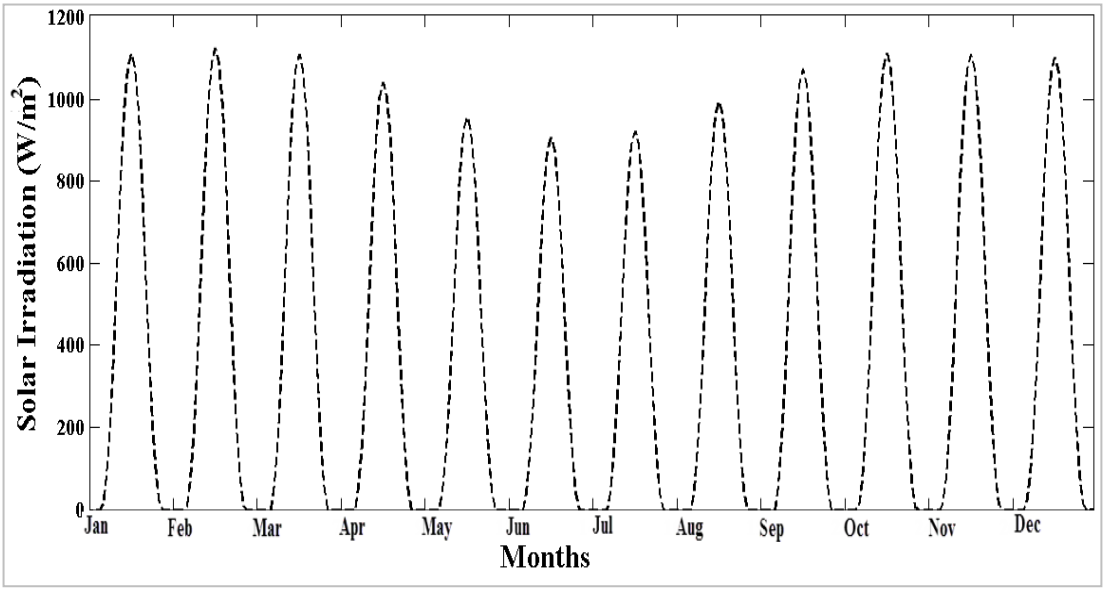

FIGURE 6.2 − Hourly-monthly averaged solar irradiation on a horizontal surface with 1 m^2 area in Natal

The data given by the above figure does not include the effect of clouds and for starting the simulation process, one should have the actual solar irradiation receivable in Natal over the whole year. This parameter is also measured in Natal weather forecast station in minutely gaps. Figure 6.3 illustrates the actual solar energy intensity on a horizontal surface with 1 m^2 area in Natal for all days of the year in 2012.

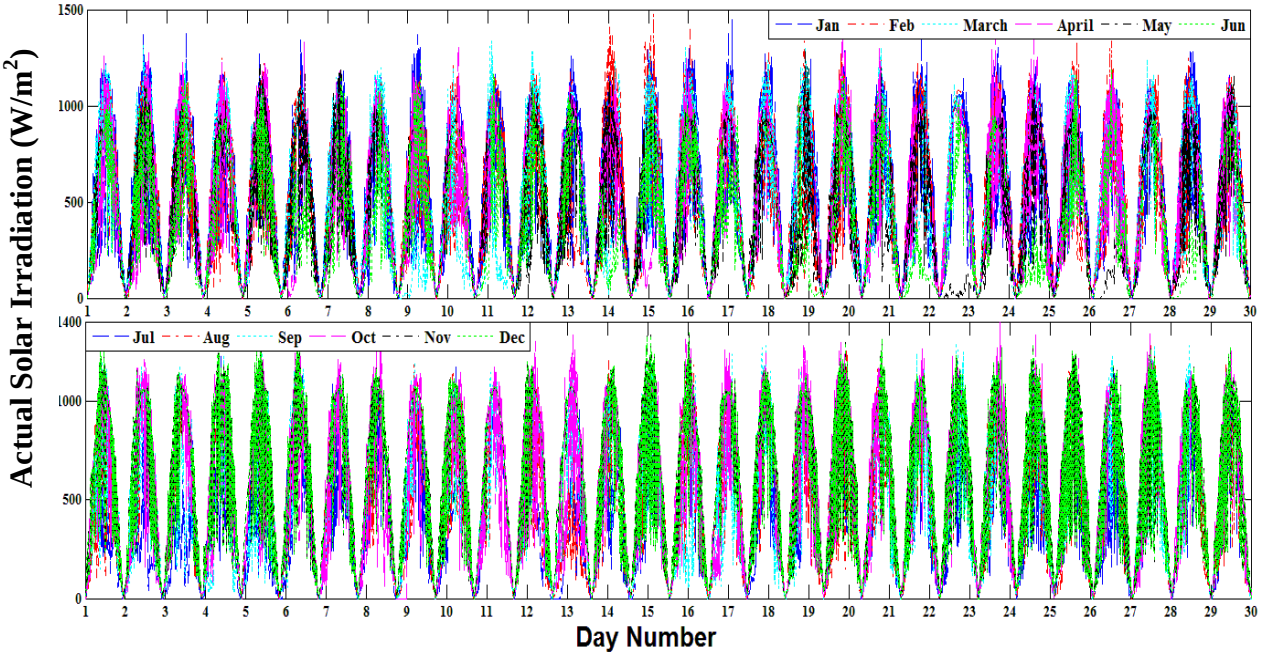

FIGURE 6.3 − Actual solar irradiation on a horizontal surface with 1 m^2 area in Natal in 2012

According to the figure, solar irradiation sometimes exceeds the maximum hourly-monthly values given by the previous figure at noon. This is actually because of two main reasons, firstly, the values given by figure 6.2 are mean values and as a result, their values are surely a little lower than the maximum single values over a month, secondly, the clear sky model (detailed in chapter 3) underestimates the available solar irradiations.

By the above figures, one could identify how susceptible Natal is in terms of solar energy reception and how clouds affect the amount of solar energy reception in this city during the year. In the next step, we should decide about the type of tracker that is going to be used in the PV farm. For this objective, all the tracking modes introduced in chapter 3 should be assessed and finally the best candidate by taking energy efficiency and economic considerations into account could be selected. As employing fixed sloped cells in the PV farm is also a possible option, therefore, first of all, one should find the most optimal slop angle for flat plate collectors in Natal. Generally, it is recommended to opt the slop angle of the collectors equal to the local latitude plus a value between 10^o to 15^o, however, in this work, the most optimum slop angle of the flat plate collectors in Natal has been calculated by computing the maximum annual receivable solar irradiation by a solar collector with 1 m^2 area with different slop angles. Figure 6.4 shows the results of this assessment. According to the figure, the best slop angle on which the most solar irradiation could be received by a sloped flat plate solar cell is 12^o. In this case, almost 11.045 GJ/m^2-year solar energy could be received.

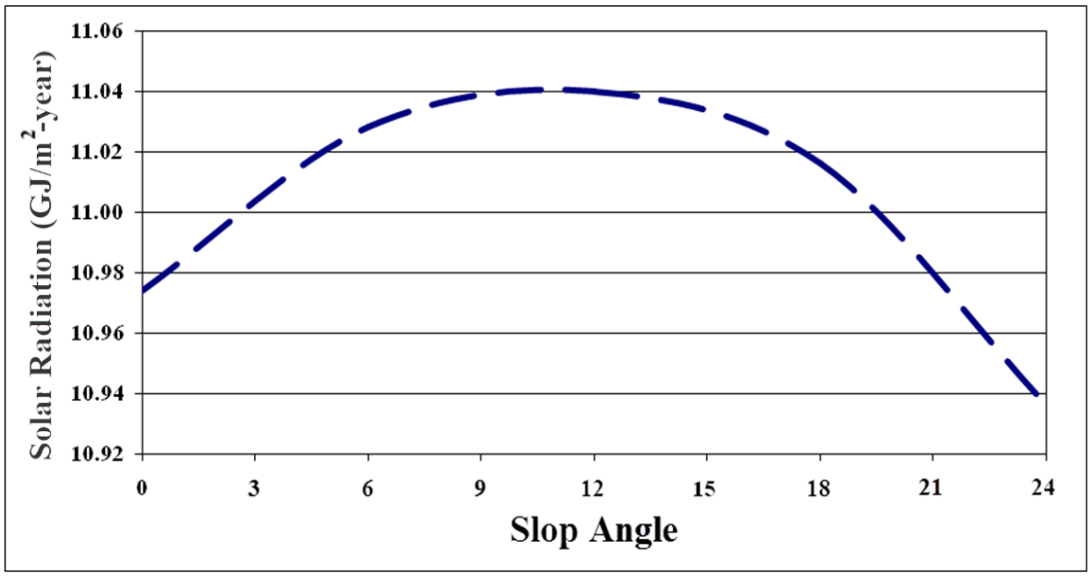

FIGURE 6.4 − Selecting the best slop angle for a flat plate collector in Natal

In the next step, figure 6.5 compares the hourly-annual averaged solar irradiation theoretically receivable by various types of surfaces including a horizontal surface, a fixed slopped surface and the possible trackers, all with 1 m^2 in area.

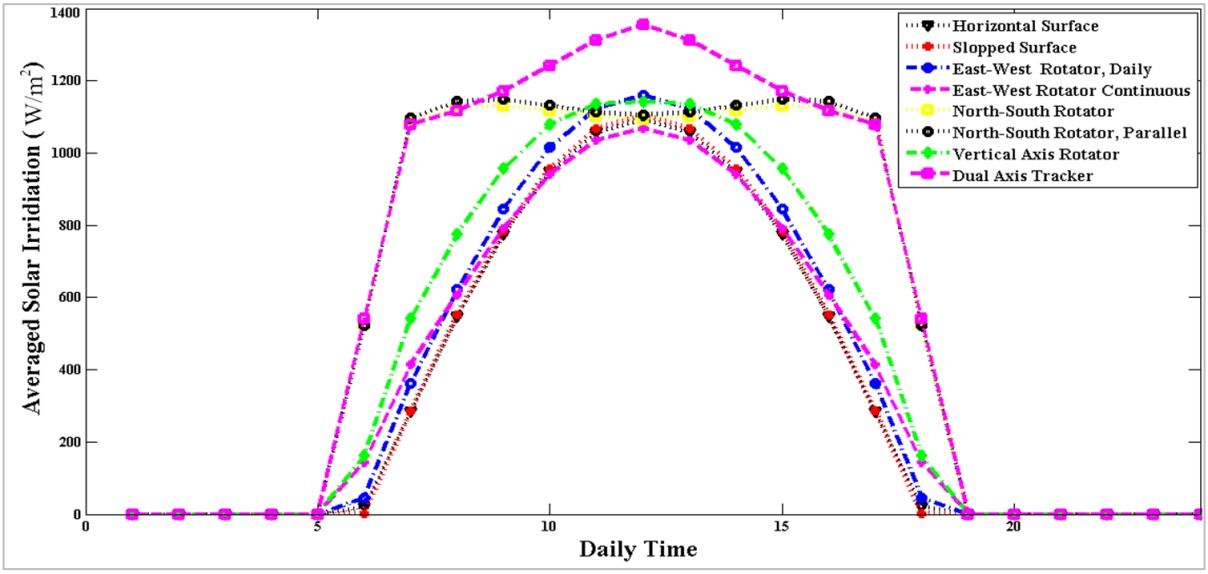

FIGURE 6.5 − Hourly-annual averaged irradiation theoretically receivable by various tracking modes in Natal

As the figure shows, clearly, the dual axis tracker surface receives much more solar irradiation than others. In a sharp contrast, the horizontal surface is under the least solar energy intensity and the fixed slopped surface is the second worst case. Among single axis trackers, the plane rotating around north-south axis parallel to the earth's axis with slightly superiority relative to the surface rotating around north-south axis with continuous adjustment shows the best performance in terms of the amount of solar energy reception over the whole year. This issue can be proved by comparing the total annual solar irradiation received by these planes as figure 6.6 represents. Confirming the results of the previous figure, as can be seen, the dual axis tracker receives much more solar energy over a whole year. The second best case is a plane rotating around the north-south axis parallel to the earth's axis with a trifle priority comparing to the plane rotating about the north-south axis with daily adjustment. As dual axis tracker is much more costly than single trackers due to the difficulties and complications in manufacturing and operation, usually the best single tracking mode is recommended to be employed. Therefore, PV cells tracking the sun by rotating around the north-south axis parallel to the earth's axis are supposed to be installed in the PV farm of this project. By the presented formulation related to this type of tracker in chapter 3, one could calculate how much solar energy will be received by this surface over the year.

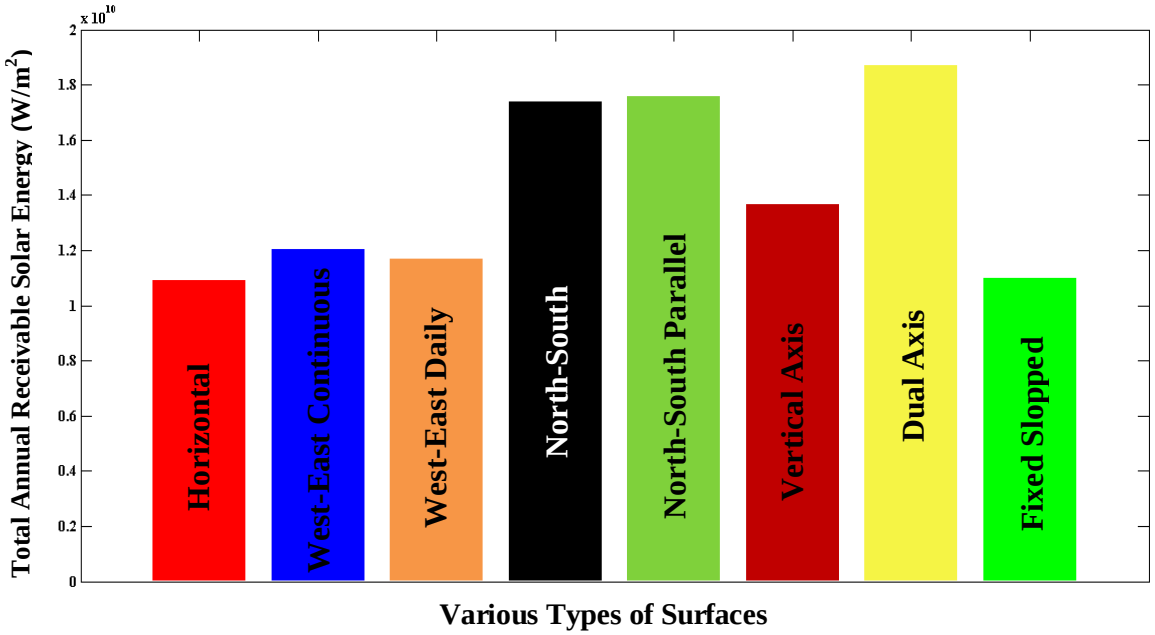

FIGURE 6.6 − Total annual solar irradiation on various surfaces with 1 m^2 area in Natal

Having the actual and theoretical available solar energy on a horizontal surface, and calculating the theoretically available solar irradiation by the tracking plane, one could calculate how much solar energy is going to be received actually by the tracker plane in Natal during the year. Also, as it was claimed before, flat plate evacuated tube collectors are supposed to be hired in the CAES and CGS systems as well. Therefore, figure 6.7 compares the amount of minutely-monthly averaged solar energy received theoretically and actually by the selected tracking surface and a flat plate collector with 1 m^2 area each in different months of the year in Natal. As the figure shows, in the theoretical version, the amount of receivable solar irradiation by the tracker cell at noon is less than the times around noon. This is mainly because of the type of tracker chosen. In fact, in this tracking mode, the plane so rotates around the north-south axis that is perfectly normal toward the solar irradiations at the times before and after noon and this perfect angle could not be preserved at noon and as a result, the solar irradiation receivable at noon decreases. Overall, in March and October the maximum and in June the minimum solar energy is radiated. Also, according to the figure, for a flat plate collector the same results are expected and the least amount of solar energy is received in June while the maximum levels of energy are received by the collector in October. Note that for flat plate collector, the highest level of solar energy is radiated on the collector surface exactly at noon.

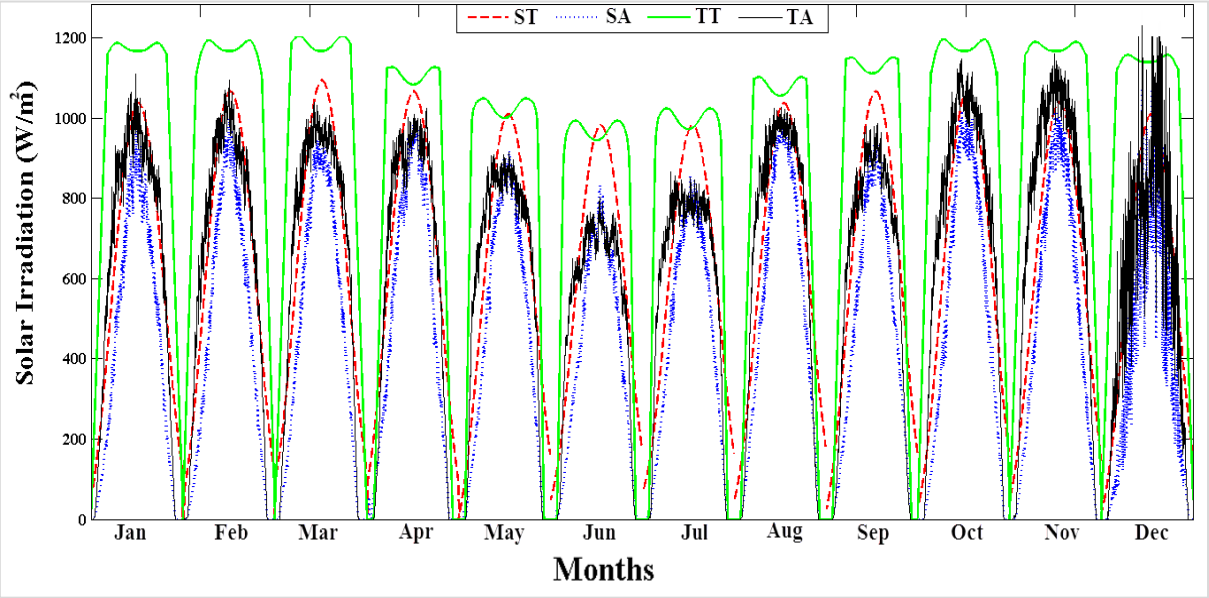

FIGURE 6.7 − Minutely-monthly averaged actual/theoretical solar energy on the tracking surface with 1 m^2 area in Natal; ST: sloped-theoretical; SA: sloped-actual; TT: tracking-theoretical; TA: tracking-actual

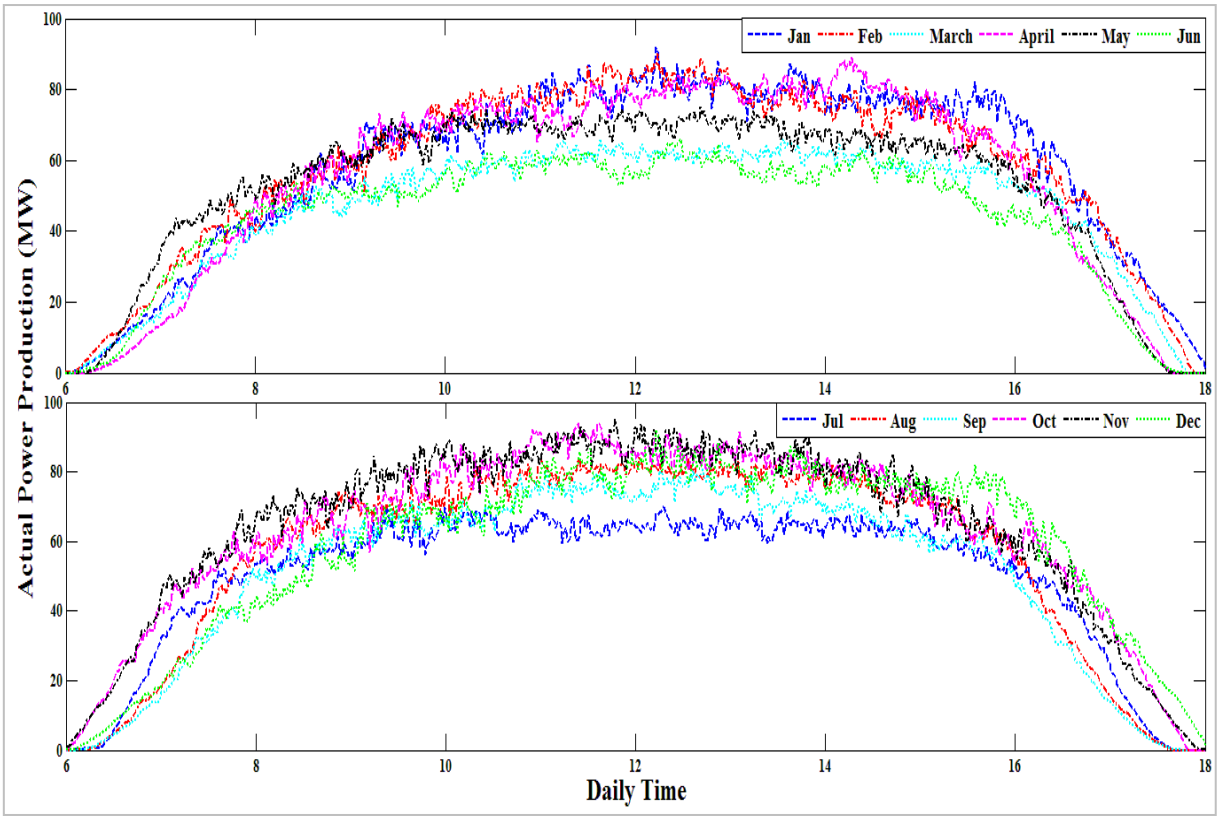

FIGURE 6.8 − Instantaneously-monthly averaged actual producible power of the PV farm

As it was explained before, the capacity of the PV farm is to be 100 MWp. Evaluation of actual available solar energy on a PV cell throughout the year, one could notice that a maximum of 1220 W/m^2 could be received by a tracking cell which occurs in March.

Therefore, taking this value into account and considering the utilized PV cells efficiency (19.3%) and the ground mounted PV farm average efficiency (17.4%), a total PV cell area of 470,000 m^2 is required for the PV farm. Figure 6.8 illustrates the instantaneously-monthly averaged power output of the PV farm for the first and second six months of the year in Natal city in 2012, respectively. As the figure shows, confirming the results of the previous graph, the least electricity is produced in June while October and March are responsible to produce the maximum amount of electricity.

The other noticeable point in this figure is that the amount of producible power during mornings, especially in the first six months of the year, is less than what is producible in the afternoon which means the sky in Natal is cloudier in the morning than in the afternoons.

Note that for accomplishing the desired simulation on the PV farm, all the uncertainty parameters and possible losses discussed in chapter 3 have been taken into account. For the first category, i.e. the uncertainties related to monitoring, comparing all the databases available all around the world, it is proved that for the locations geographically similar to the selected location of this project (Natal city, it will be discussed later), standard deviation values below ±4% for uncertainties in solar irradiation monitoring due to the effects of some external factors like air pollution, could be observed. Also, for the recorded values of received solar energy due to the bad operation of measurement devices, for the device used in Natal station (secondary standard pyranometer) the measurement uncertainty of ±2% is recommended to be considered. For the uncertainties related to the deviations of short term forecast approach, the accuracy is not high and an uncertainty value as low as ±2% could be a fair estimation.

In the second category of uncertainties, overall, for the PV systems erecting nowadays, it is recommended to consider a PV array model uncertainty of ±3%, an irradiation model uncertainty of ±2% and an inverter uncertainty of ±1%. The uncertainty due to losses caused by soiling and birds for a city with precipitation at the level of Natal is proposed to be considered equal to ±2.5%. The uncertainty due to the long term and short term efficiency degradation of the PV panels employed in this work is recommended to be considered equal to ±2%. Finally, the uncertainty caused by other factors such as module tolerance, cabling losses and etc. are recommended to be considered equal to ±2%.

Considering the advices given by the references associated with each type of these uncertainties and losses, overall, in monitoring category, the combined monitoring uncertainty could have a value between ±2% and ±3%. The combined uncertainty in PV modelling category varies between ±6% and ±8%. Also, the uncertainty of faults and losses in the storage system (CAES system here) is considered equal to ±3%. The whole proposed system combined uncertainty is then considered to be in the order of ±7% to ±10%. In this work, in order to have a conservative economic assessment, the maximum possible total uncertainty, i.e. ±10%, is taken into account.

As for finding the best power sales strategy of the PV plants, monthly constant and time dependent producible powers by the PV farm are required, therefore, these items should be calculated first. For the monthly averaged format, averaging over the whole day gives a mean value for the producible power in each month. Table 6.1 details the actual monthly averaged producible power during the daily hours of each month.

TABLE 6.1 – The monthly average actual producible power during the daily hours of each month (MW)

	Jan	Feb	Mar	Apr	May	Jun	Jul	Aug	Sep	Oct	Nov
Average Power (MW)	58.21	58.08	46.32	55.23	53.02	43.98	49.89	56.36	50.88	63.10	64.54

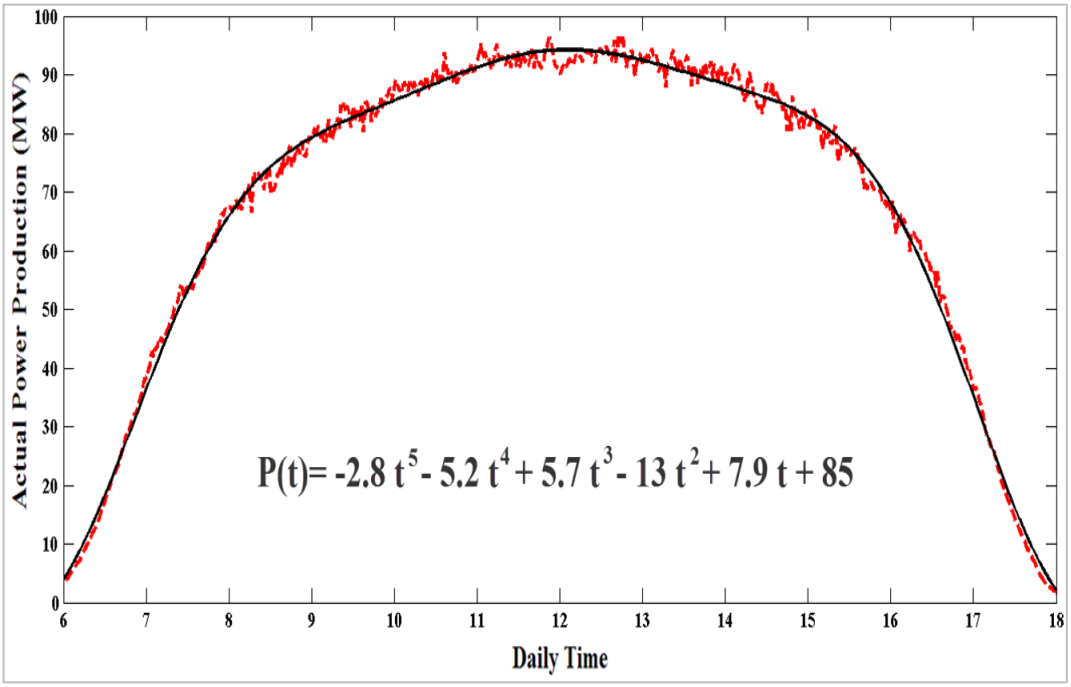

FIGURE 6.9 – Curve fitting on a graph presenting a time dependent function for instantaneously-monthly producible power of the PV farm

On the other hand, for time dependent power selling pattern, by curve fitting on the graphs related to each month in figure 6.8, a time dependent function is resulted by which the monthly-instantaneously averaged producible electricity for the corresponding month could be estimated. Figure 6.10 shows how curve fitting is applied for a sample graph to define the producible power as a functionalof daily time.

The other parameter that should be discussed in this stage is the method by which the best power sales strategy is going to be chosen for the power plants. For both of the strategies, i.e. the constant value pattern and the time dependent schema, various percentages (from 50% up to 110% with 10% gaps, seven states for each case and 14 cases altogether) of the given values by table 6.1 and by the functions extracted from the graphs associated with each month are considered to be sold by the PV plant to the grid over the year. Here also, various portions (from 50% up to 110% with 10% gaps, seven cases) of the values given by the fitted curves could be considered to be sold. Note that for each of these 14 cases various sizes of CAES system are applicable. For this objective, the maximum extra power produced and the maximum ramps occurred are considered and various portions of the maximum extra power produced over the year (from 20% up to 100% with 10% gaps, nine cases) are considered as the nominal power of the CAES system. Therefore, overall, 126 different possible cases are considered in this assessment. In the end, by employing an authentic economic assesment method, the payback period of the system for all these 126 cases is calculated and the most efficient option among all is selected. The economic approach used in this work for analyzing and sizing the system is the NPV method. The value of NPV for a project could be calculated by:

$$\mathrm{NPV} = \sum_{n=0}^{N} \frac{C_n}{(1+r)^n} \tag{6.1}$$

Where, n, C_n and r refer to the number of year, cash flow of the project in the corresponding year and inflation rate, respectively. C_n, in practice, is the summation of cost of capital (which is negative, because it is spent); annual O&M costs of the system as a portion of cost of capital of each system (negative) and the annual revenue resulting from the application of the proposed system (positive). The number of the year in which the NPV value gets positive indicates the payback period of the system (Arabkoohsar *et al.*, 2014).

Also, after simulating both of the proposed configurations, the IRR method is used to compare the systems economically to prove the effects the second proposal on the first configurations proposed. The IRR approach is an authentic comparison method for industrial projects effectiveness economically. The IRR of a project is the rate of return that makes the NPV of all cash flows from a particular investment equal to zero. Clearly, the project with higher value of IRR is more desirable to be selected comparing other candidates (Farzaneh-Gord *et al*. 2015). The critical parameter for calculating the IRR of a project is the number of year in which the NPV should be equal to zero. This totally depends on the investor of the project; however, for such industrial projects the duration of 8 years seems to be a reasonable choice.

Note that there are numbers of important parameters for doing the economic analysis of such a power plant such as electricity price and fine rates and etc. Table 6.2 gives the values considered for these parameters to evaluate both of the systems economically. These values are exactly in accordance with Brazilian electricity market.

TABLE 6.2 − Economical information required for doing the economical aspect of the project

Item	Value
Daily Electricity Rate	0.153 USD/kWh
Peak Consumption Electricity Rate	0.200 USD/kWh
Fine Rate	0.750 USD/kWh
CAES Capital Cost	900 USD/kW
PV Farm Capital Cost	1430 USD/kW
Turbo-Generator Capital Cost	1200 USD/kW

About the PV farm cost, it is noteworthy that, in Brazil market, a large scale PV farm with fixed PV cells and without energy storage unit will cost almost 1100 USD/kWp of which, normally, 52% is related to PV modules, 23% is for inverters, 17% is associated with balance of system (cables, etc.) and 8% is for installation. Naturally, a tracking system requires more maintenance and must be just as stable as a rigid system, so that it can withstand a storm. It must be noted that installation and operating costs for these facilities can be up to 30 percent higher than for rigidly-installed systems. Therefore, a large scale PV plant with tracking cells will cost about 1430 USD/kWp (Lacchini *et al*., 2013). As a result, the final cost of the PV farm in this work will be $ 143 million.

6.1 The Results of Simulation on the First PV Plant Configuration

Having the results and discussions presented by far, one could simulate the first configuration proposed (the grid connected PV farm equipped with a CAES system) performance comprehensively. In the first step, the results of power sales strategy selection should be presented. As it was explained, the CAES sizing and power sales strategy selection are two coupled and dependent items. Therefore, figure 6.9 shows the payback periods corresponding with different cases through this economic assessment. Note that the results that are not included in this figure, such as CAES system with 90% and 100% of the maximum available extra electricity in the constant valuepattern, are not presented in the figure due to their too poor performances. In this figure, CV stands for daily constant value strategy and TD refers to time dependent pattern.

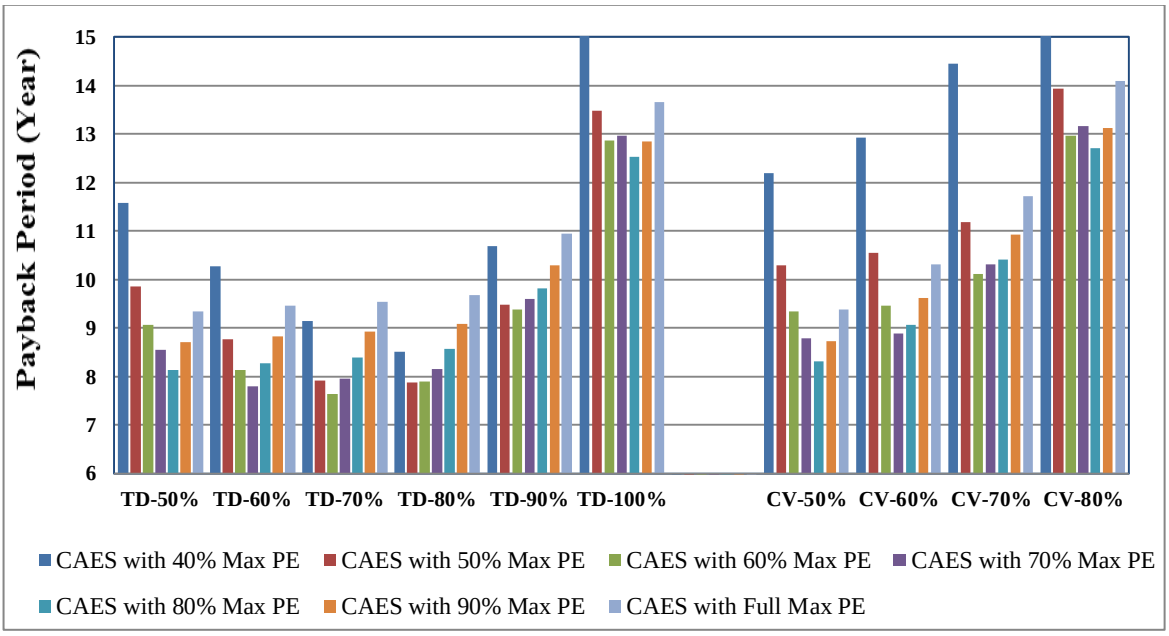

FIGURE 6.10 − Payback period of the system with different power sales strategies and CAES sizes (TD: time dependent; CV: constant)

As can be seen, generally, a time dependent pattern leads to much more satisfactory economic results, and among all possible cases in this state, the shortest payback period is obtainable if the PV farm sells power to the grid based on 70% of instantaneously-monthly averaged producible power and the CAES system capacity is selected 60% of the maximum extra power produced over the whole year. The maximum extra power produced by the plant in this case is almost 84 MW. Therefore, based on the results of this assessment, the CAES system maximum capacity should be about 50 MW.

Hereafter, the results of simulation accomplished on a PV plant with 100 MWp capacity, a CAES unit with 50 MW capacity, a time dependent power sales strategy with 70% of average producible power in each month are presented. Note that the simulation is done for all days of the year; however, for the sake of simplicity in showing the simulation results, the detailed results for only a few sample days of the year are presented. These days are so selected that one could observe the performance of the power plant in all possible cases from very cloudy sky (very poor performance of the plant) to very clear sky (very strong performance of the power plant).

Figure 6.11 shows the extra power produced by the PV farm that could be used by the CAES system in March 23rd, April 30th and May 24th. Clearly, March 23rd is one of the best; April 21st is a moderate and May 23rd is one of the worst days of the year in terms of available solar energy.

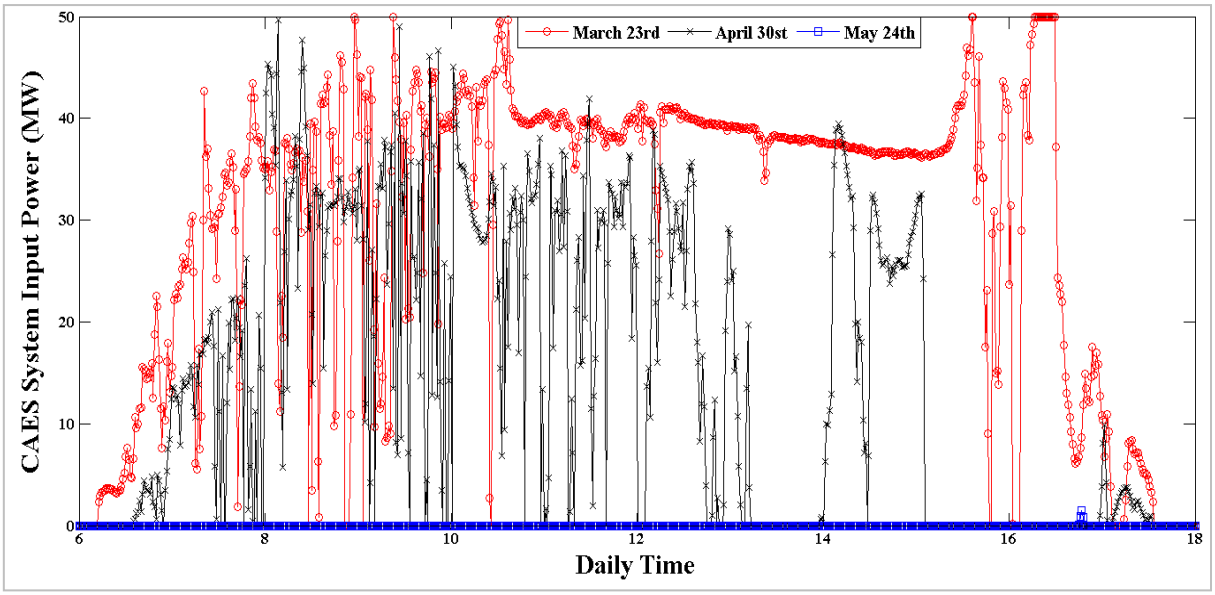

FIGURE 6.11 − The CAES system compressor set work for three sample days (MW)

According to the figure, the maximum extra power to be employed by the compressors is 50 MW. It should be noted that although there may be higher values of extra power available up to 84 MW in some points, the CAES system capacity is restricted to 50 MW because higher values of extra power produced are not worth to be harvested.

Figure 6.12 also shows the amount of power shortage in the power plant relative to the grid demand based on the chosen characteristics (the CAES unit capacity) and power sales strategy for the system during the three sample days. This energy shortage, in fact,

should be offset by the CAES system, if possible. Expectedly, the energy shortage in May 24th is so much so that even the CAES system may not be able to offset it. In a sharp contrast, the energy shortage during March 23rd is very trifle. The power shortage in April 30th is always in moderate levels.

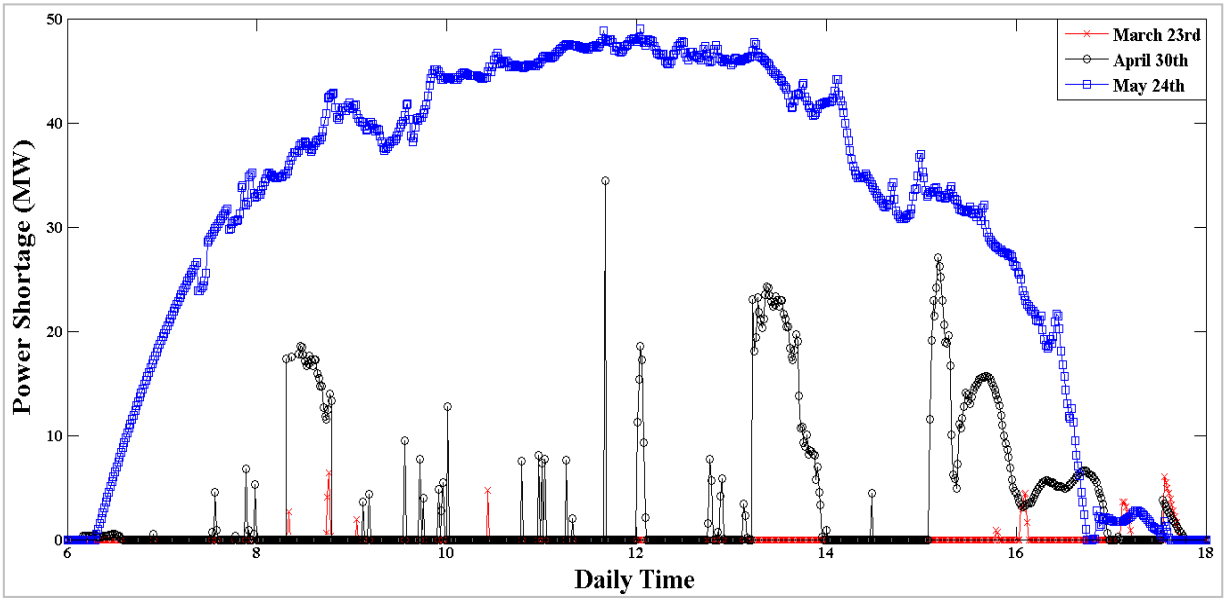

FIGURE 6.12 − Power shortage in the system that the CAES unit must offset during the sample days (MW)

Figure 6.13 shows the amount of power produced by the CAES system in each moment during the three sample days.

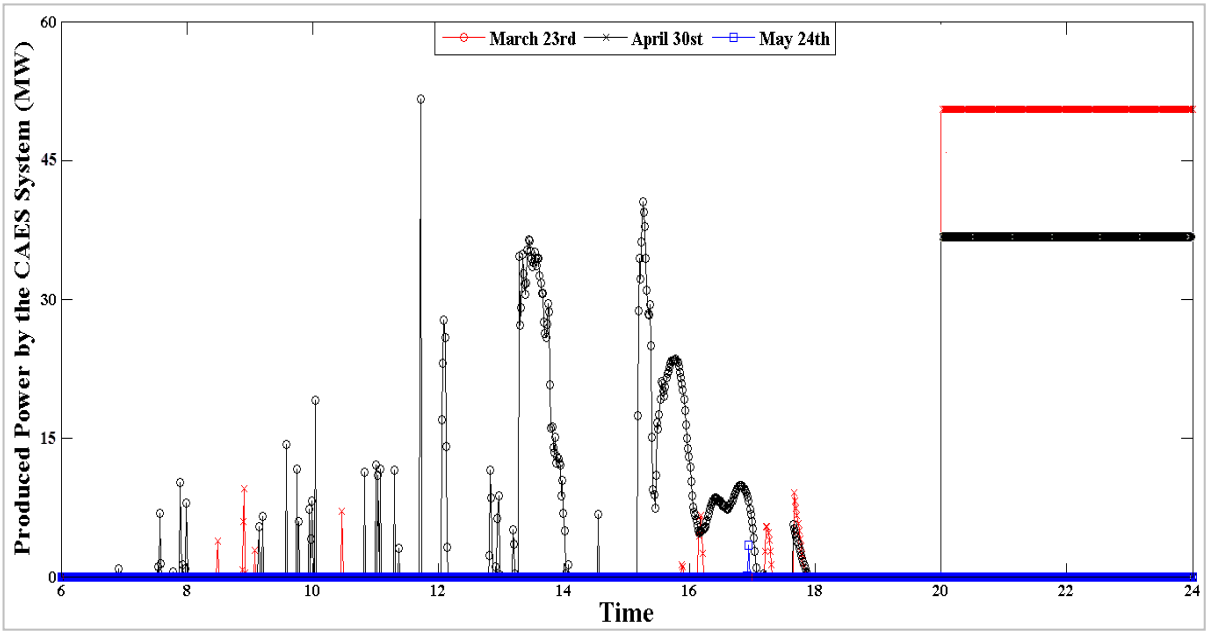

FIGURE 6.13 − Produced power by the CAES unit (MW)

As can be seen the maximum producible power is 50 MW which is produced during nightly hours in March 23rd. What is clear here is that the CAES system might produce higher amounts of power in this day as the PV farm provided more energy for being used to produce compressed air, however, the economic assessment carried out limited the CAES maximum capacity at 50 MW because it was proved that the higher values of extra power available are not worth to be harvested as higher capacities of the CAES system resulted to higher values of initial investment. The nightly produced power in April 30th and May 24th are also 35 MW and 0 MW, respectively. Note that these results are totally compatible with the information readable from the previous figure.

Figure 6.14 shows the variation of the air storage reservoir pressure during the three sample days (the reservoir volume is 20,000 m^3).

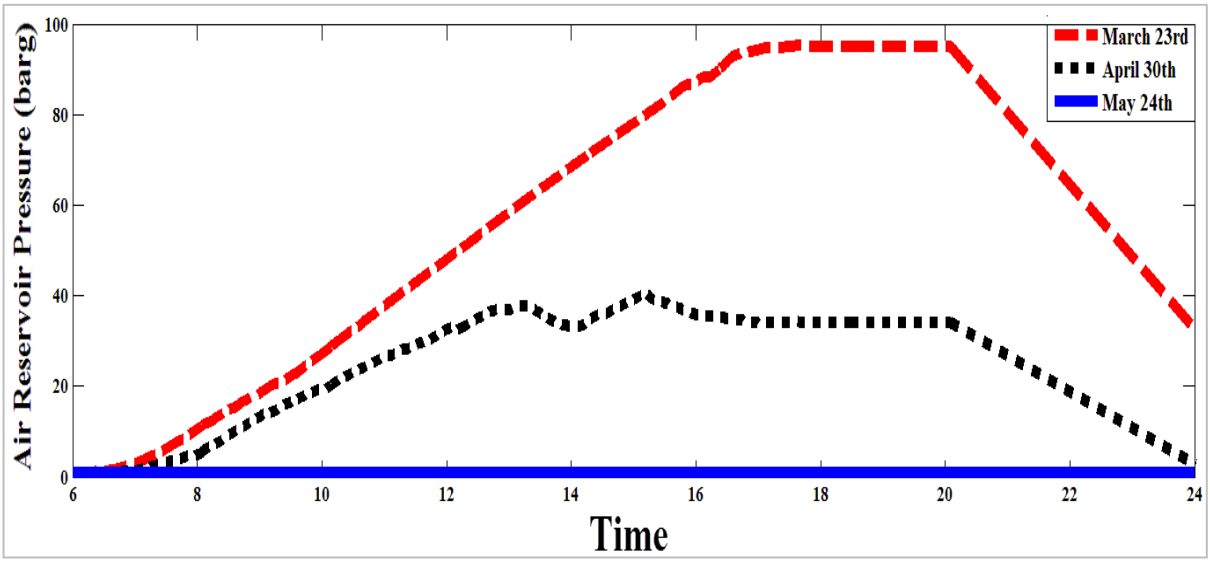

FIGURE 6.14 − Air reservoir pressure variation during the three sample days

As it was mentioned, if there is still compressed air in the cavern at the end of the day, it is used to produce power at peak consumption period for 4 hours (from 8 pm to 12 pm) so much so that the cavern pressure decreases to 5 bar. This amount of air remains in the cavern in order to offset the ramps during early daily hours of the upcoming day. According to the figure, in May 24th, the sky is so cloudy that the PV farm could not support the CAES system that much and as a result, not much compressed air is produced during the day. In a sharp contrast, in March 23rd, the PV farm produces much extra power and the CAES system could produce 20,000 m^3 compressed air with 120 bar at the end of the day. As solar ramps during the day had been trifle, this air is used to generate peak consumption period power. At

the end of the day, obviously, the cavern pressure in all cases reduces but not to zero while in May 24th the cavern pressure remains at 0 barg (gauge pressure) all day long.

Figure 6.15 shows the overall performance of the power plant including the amount of power directly sold to the grid, the amount of power ramp offset by the CAES system, the amount of power ramps that could not be offset during the day and the amount of nightly power sold to the grid.

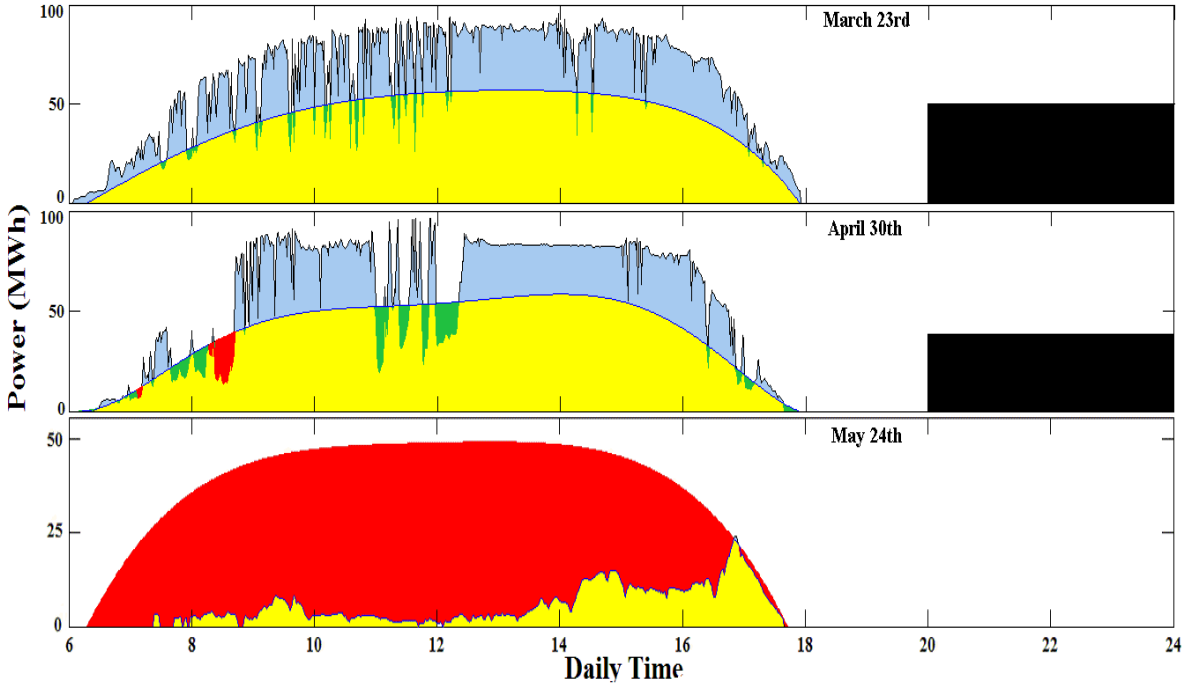

FIGURE 6.15 − Overall performance of the whole power plant in the three sample days

In this figure set, the yellow area shows the power delivered to the grid directly by the PV farm, the blue area shows the extra power produced by the PV farm to be used by the CAES system, the green area shows the power ramps compensated by the CAES unit when the solar energy fluctuations cause the PV farm to not be able to cover the grid demand, the red area represents the PV farm power production slumps that even the CAES system has not been able to offset and the power plant is financially penalized for them and finally, the black area shows the amount of nightly produced power by the CAES system. Overall, the summation of green and black areas show the power produced by the CAES system during the sample days and clearly, the amount of nightly produced power by the CAES system (black area) is more during the very sunny days while the power ramp compensation by the CAES system (green area) can be more during the days with moderate levels of sunshine.

Hereafter, the overall energy and exergy performances of the power plant for all days of the year are investigated. Figure 6.16 shows the total daily solar energy and exergy received by the PV farm. As it was explained before, taking all the losses and uncertainties in the system into account, with conservative considerations, the energy conversion efficiency of the PV farm is 17.4%; however, the exergy efficiency of the PV farm could be calculated by the correlations presented.

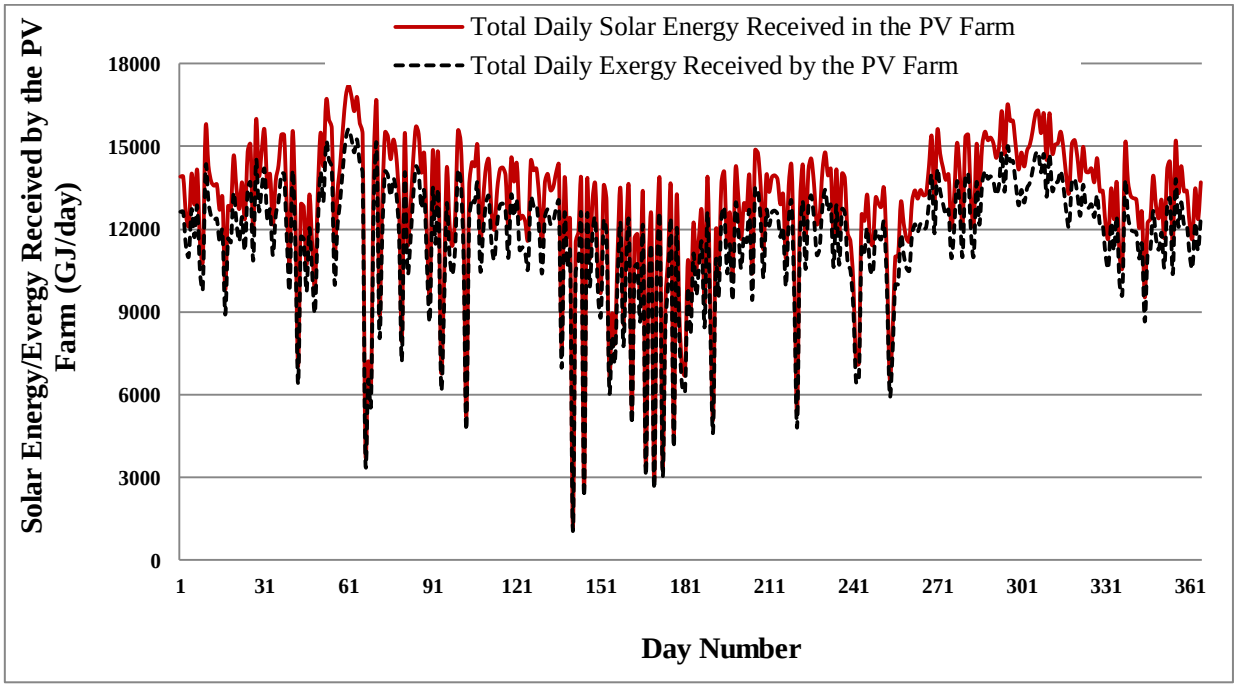

FIGURE 6.16 − Total daily solar exergy and energy received by the PV farm

Figure 6.17 gives information about the values of total daily exergy efficiency of the PV farm over the whole year. According to the figure, the daily exergy efficiency of the PV farm could rise up to 21% and fall down to 9% in different days. Also, the annual average exergy efficiency of the PV farm is calculated to be 13.8%.

The next important factor that should be specified in the sizing process of the CAES system is the volume of the storage tanks in which the working fluid is stored. For this objective, the working fluid volume flow rate required for cooling the air stream outgoing from the compressors should be calculated. The total daily volume of working fluid for all days over the year should also be calculated and the maximum value is chosen as the volume of the storage tank. Figure 6.18 shows the total daily volume of working fluid required to collect the heat generated in the air stream during compression process over the whole day.

According to the figure, the maximum total daily volume of working fluid required over the year is 5500 m^3.

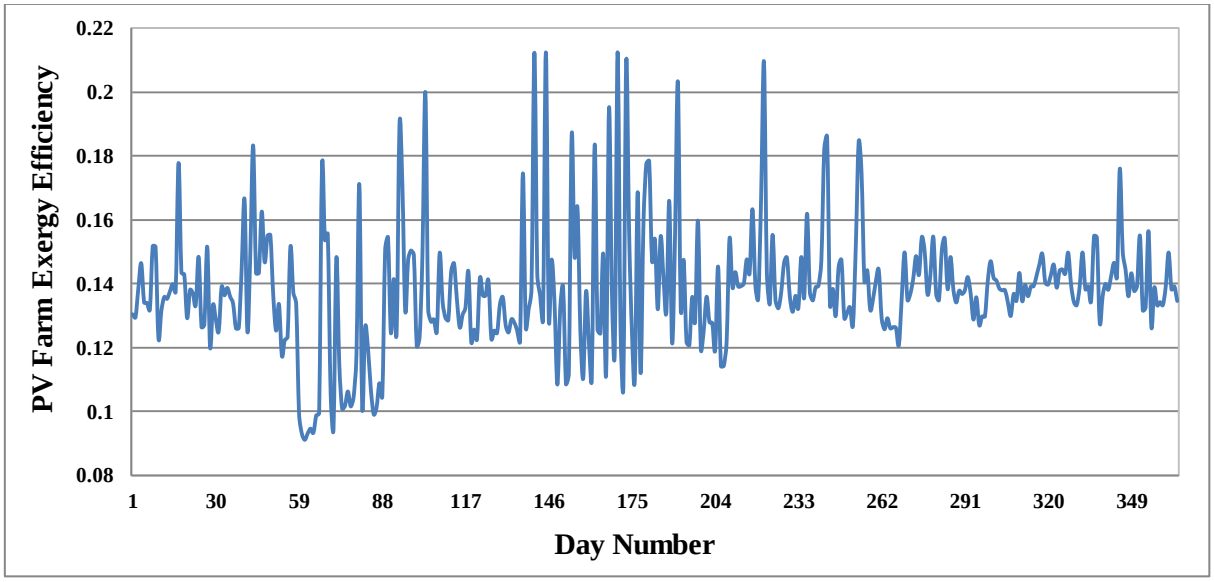

FIGURE 6.17 − Total daily exergy efficiency of the PV farm

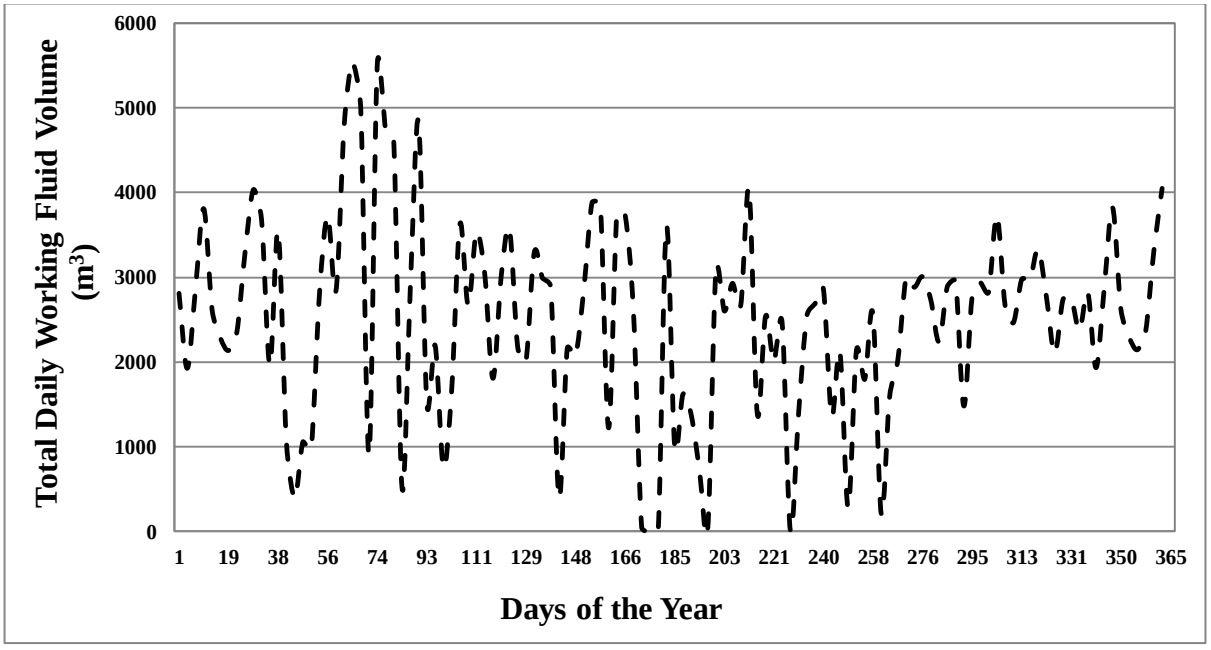

FIGURE 6.18 − The working fluid total daily volume required to collect the compressed air heat

The next step in the CAES system design is selecting the size of the solar heating unit. Note that due to the losses in heat transfer processes in both cooling and heating heat exchanger sets, the total heat generated in the air in compression process could not be given back to the air in expansion process. As a result, external sources of heat are required to provide the remaining portion of heating demand in the CAES system. The solar heating unit

along with the auxiliary heater is supposed to provide the required extra heat. In fact, the solar heating system should, first, preheat the air stream up to possible temperatures, then, the air stream passes through the heating heat exchanger set and finally, the auxiliary heater warms the air stream up to the target temperature, if required. Investigations show that the desired temperature for the expanding air before expansion process is 140 ^{o}C. As the solar heating system employes flat plate collectors, therefore, it can not provide as high temperatures as required. Therefore, the auxuliary air heater is considered in the system to support the air stream for reaching the favourable temperature. A maximum of 10 ^{o}C temperature increase in the air stream is considered for the heating duty of the auxiliary air heater in this work. Calculating the total heat required for expansion process, the amount of heat provided by the working fluid and the heating duty of the auxiliary heater, the heat that should be provided by the solar heating system could be obtained. In other words, the size of the solar system should be so opted that it is able to provide the maximum total daily heating demand of the CAES system in the presence of hot working fluid and the auxiliary heater. Figuer 6.19 shows the total daily heat required for preheating the air stream before expansion, the total daily heat provided by the working fluid, the total daily heating duty of the ancillary heater and the total daily heat that is supposed to be provided by the solar heating system.

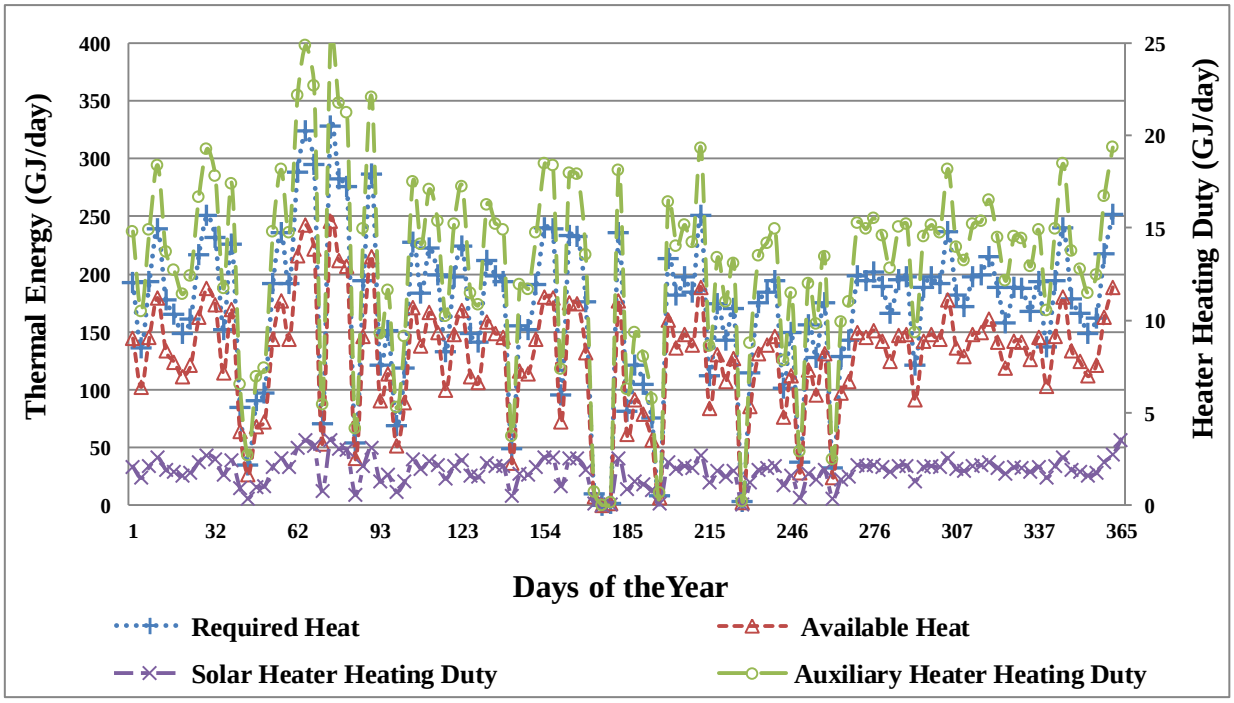

FIGURE 6.19 − Total daily available/required heat in the CAES system over the year

According to the figure, most of the required heat could be supplied by the hot

working fluid produced during compression process. The solar heating unit muxt provide considerable amount of heat during the day and the auxiliary heater is only responsible to provide a minor portion of the total daily required heat. As the figure shows, the maximum amount of heat that is supposed to be produced by the solar system during a day is 57.7 GJ in March 5th. By calculating the total heating duty of the solar heating system, one could proceed to calculate the size of this unit in the CAES system. For this objective, the performance of a single collector solar heating unit should be simulated in the given day. Figure 6.20 shows the performance of a single flat plate collector with its solar storage tank in a sample operating day (March 5th). This figure illustrates the variations of water temperature within the storage tank over time, the temperature of water outgoing from the collector and the instantaneous heat obtainable from the collector by the working fluid.

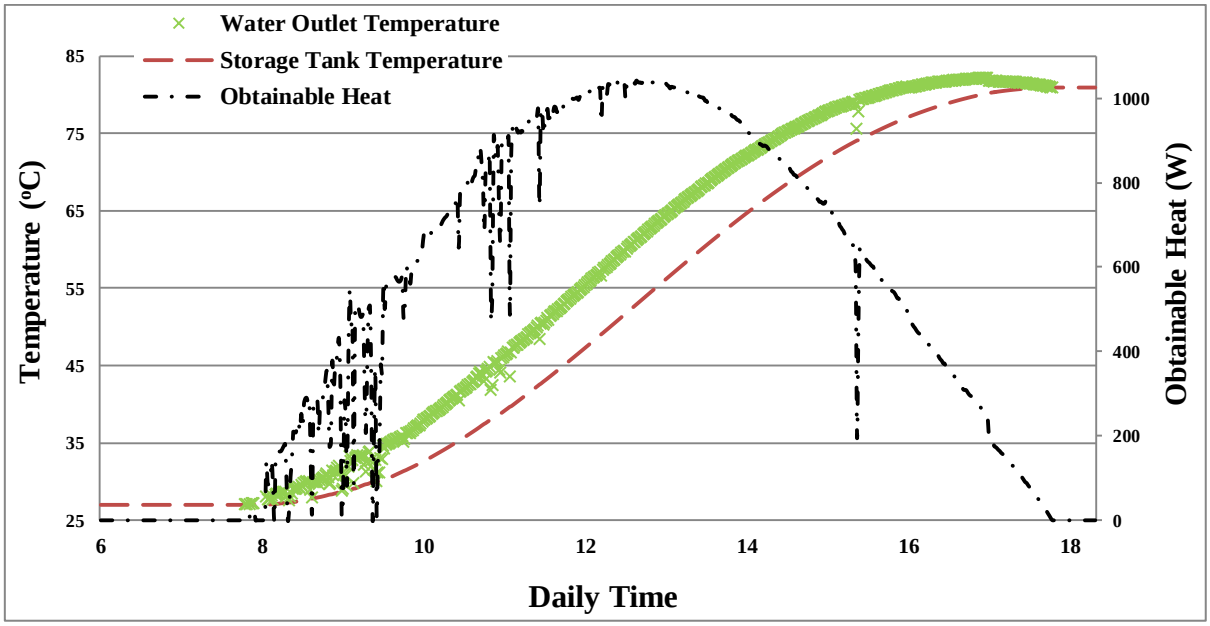

FIGURE 6.20 − The performance of a single collector solar heating system during March 5th in real condition

As can be seen, a single collector solar heating system produces 100 ltr hot water with the temperature of 82 ^{o}C in March 5th. Therefore, this system can provide 23.1 MJ energy in form of hot water. As a result, for providing 57.7 GJ energy in just the same conditions, almost 2500 collectors are required. According to the suitable storage tank volume for one collector (0.1 m^3), the volume of the storage tank should be 250 m^3.

Figure 6.21 shows the amount of solar exergy and energy received by the collector modules in the CAES system, including 2500 flat plate collectors with the slop angle of 12^{o}, and the useful obtained energy and exergy received by water as the working fluid of

the solar heating unit.

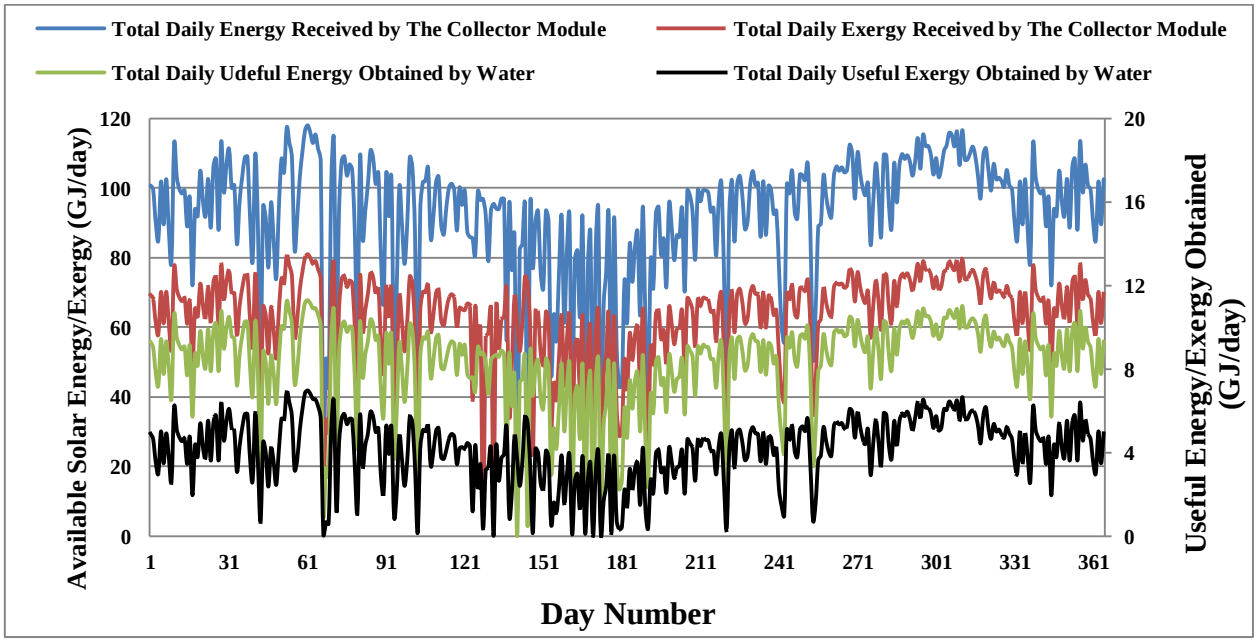

FIGURE 6.21 − Total daily exergy/energy received by the collectors and obtained by water in solar heating unit

Employing the data given in this figure, one could easily calculate the total daily exergy and energy efficiencies of the solar heating system. Figure 6.22 shows the values of these parameters for all days over the year.

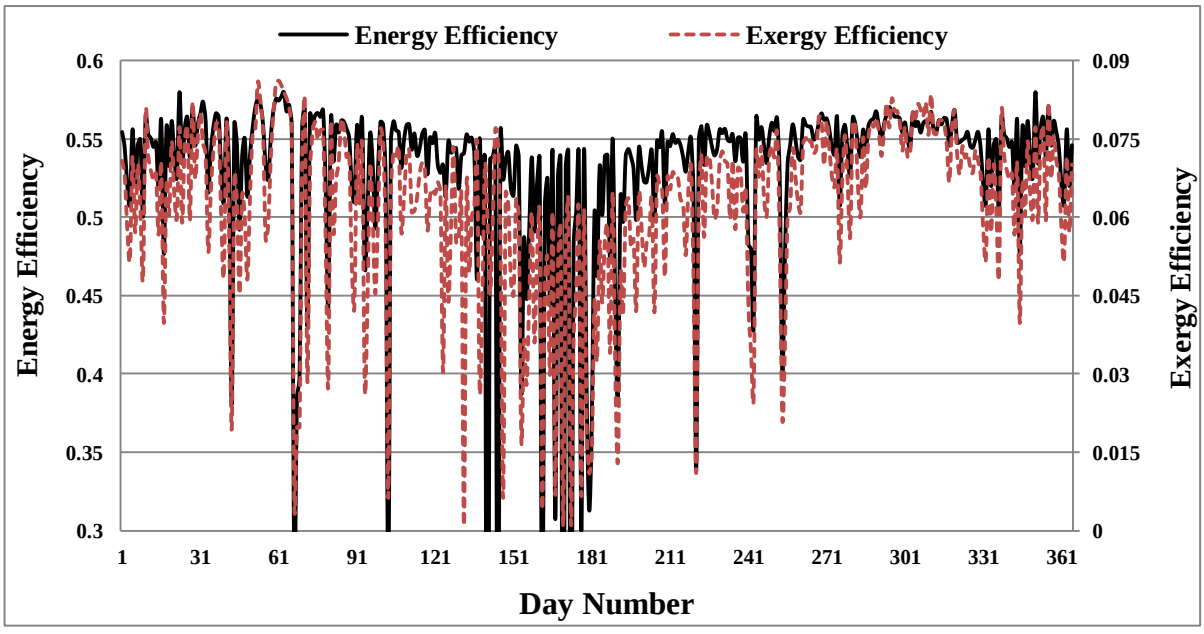

FIGURE 6.22 − Total daily exergy/energy efficiency of the solar heating unit

As can be seen, the value of exergy efficiency is extremely low and varies

between almost 0 up to only 9%. The total annual average exergy efficiency of the solar heating unit is also 6.2% which means the rate of exergy destruction in solar heating system is very high. On the other hand, the energy efficiency of the solar system is usually at a reasonable level and varies from 0.3 up to 0.6.

In addition, there is also an auxiliary air heater which burns natural gas to provide the extra heat required in air expansion process. By analyzing the energy and exergy performance of the air heater, one could, finally, calculate the overall exergy and energy efficiency of the CAES system. As explained before, in this system the airheater is supposed to increase the air temperature for 10 ^{o}C as flat plate collectors could not support high temperatures to the system. Figure 6.23 shows how much fuel (natural gas) is used in each day by the air heater. Evidently, by taking the values of natural gas LHV and the air heater thermal efficiency into account, one could calculate the total daily heating duty of the air heater, clearly resulting to the same trend as the above graph.

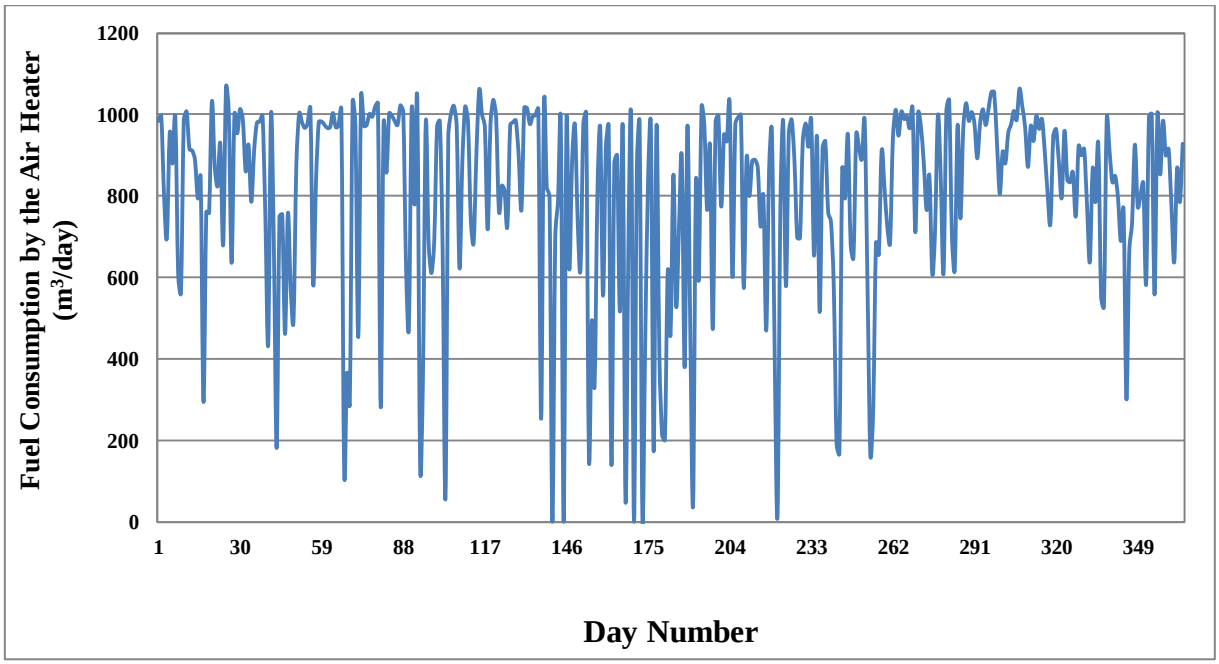

FIGURE 6.23 − Total daily fuel consumption of the air heater

Figure 6.24 also illustrates the total daily exergy received by the air through the air heater, the exergy exhausted from the air heater chimney and the exergy of fuel burnt during the whole day. Naturally, the total daily energy efficiency of the heater is 50% and considering the information given in previous figure, the total daily exergy efficiency of the heater is obtained to be equal to 42.2%.

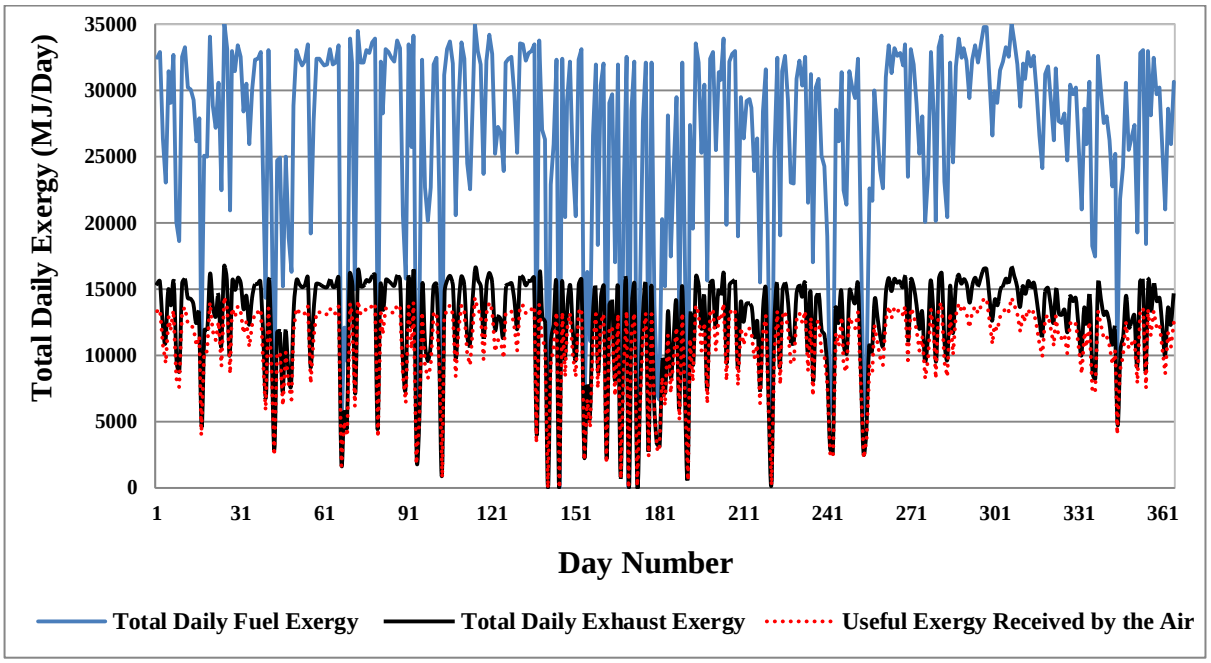

FIGURE 6.24 − Total daily fuel/exhaust and useful gained exergy through the air heater

Figure 6.25 gives information about total daily energy performance of the CAES system such as the total daily energy produced by the CAES system and the total daily power received by/available for the compressor set in the CAES system.

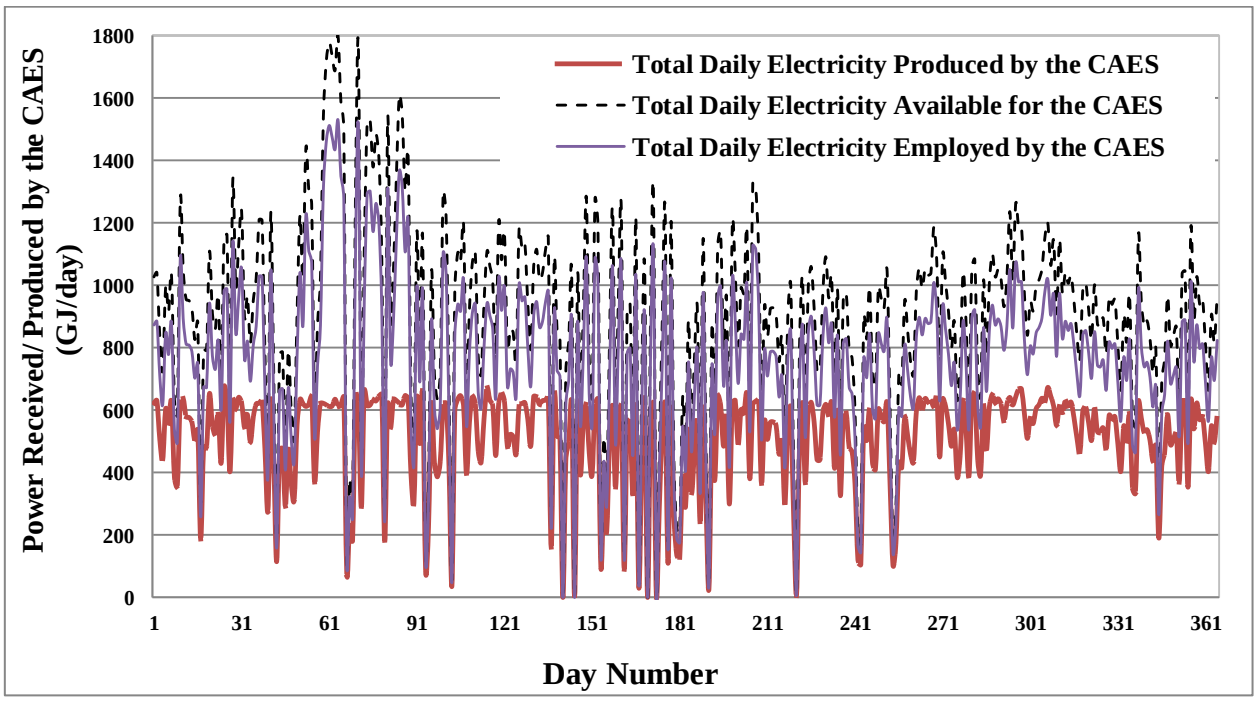

FIGURE 6.25 − Total daily energy performance of the CAES unit

As can be seen, the amount of power received by the CAES system is close to the

value of the available extra power and this means that selecting the capacity of the CAES system (60% of the maximum available extra power) has been so accurately selected that not only it maximizes the economic benefits of the plant, but also it minimizes the total annual power losses in the power plant. The total daily power produced by the CAES system varies from only 50 GJ/day (14 MWh) up to almost 650 GJ/day (181 MWh). Clearly, the more extra power is produced by the PV farm, the more the CAES system can produce power during the day and peak electricity consumption periods. This is why the graphs have the same trends. It is re-mentioned again that selecting higher capacities for the CAES unit would increase the amount of total daily power produced by the CAES unit considerably, however, the economic investigations showed that the higher capacities of the CAES system would not be as economically efficient as a CAES system with 50 MW capacity.

Figure 6.26 shows the total daily exergy and energy efficiency of the CAES system including the compression set, the expansion set, the air heater and the solar heating unit.

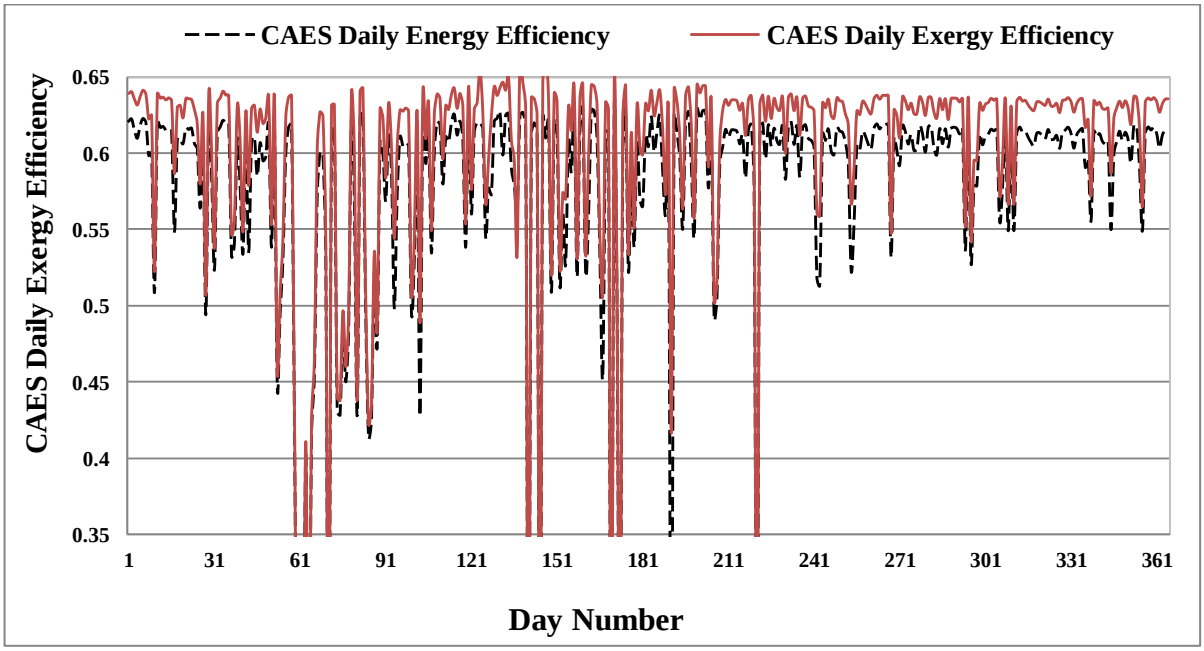

FIGURE 6.26 − Total daily exergy and energy efficiency of the CAES system

According to the figure, the values of energy and exergy efficiency of the CAES system are very close, with trifle superiority of exergy efficiency varying from 35% up to 65%. Note that the values of energy and exergy efficiencies would be higher if the CAES system actual energy input, which is limited to 50 MW, was considered in the calculations;

however, in order to present an accurate value for energy storage efficiency and the effect of restricting the CAES maximum capacity, the total extra power produced by the PV farm was taken into account as the CAES system energy input.

In the end, the performance of the whole power plant, including all of the above individually analyzed systems, is investigated. Figure 6.27 reveals how much power is totally sold by the power plant in each day, how much power ramps could (not) finally be offset and how much power is produced at peak consumption periods of each day. According to the figure, the amount of unrecoverable ramps in the power plant is always very small and there are only a few days in which the unrecoverable ramps rise sharply. Also, the graphs show that up to almost 400 MWh power ramp during a single day has been offset by the CAES system. The maximum nightly produced power should clearly be 200 MWh (50 MWh for 4 hours). As can be seen, this state is possible in many days during the year. During daily hours also, up to 720 MWh power could be given to the grid in the last months of the year while this value could fall down to only 100 MWh in a few cases in the middle days of the year.

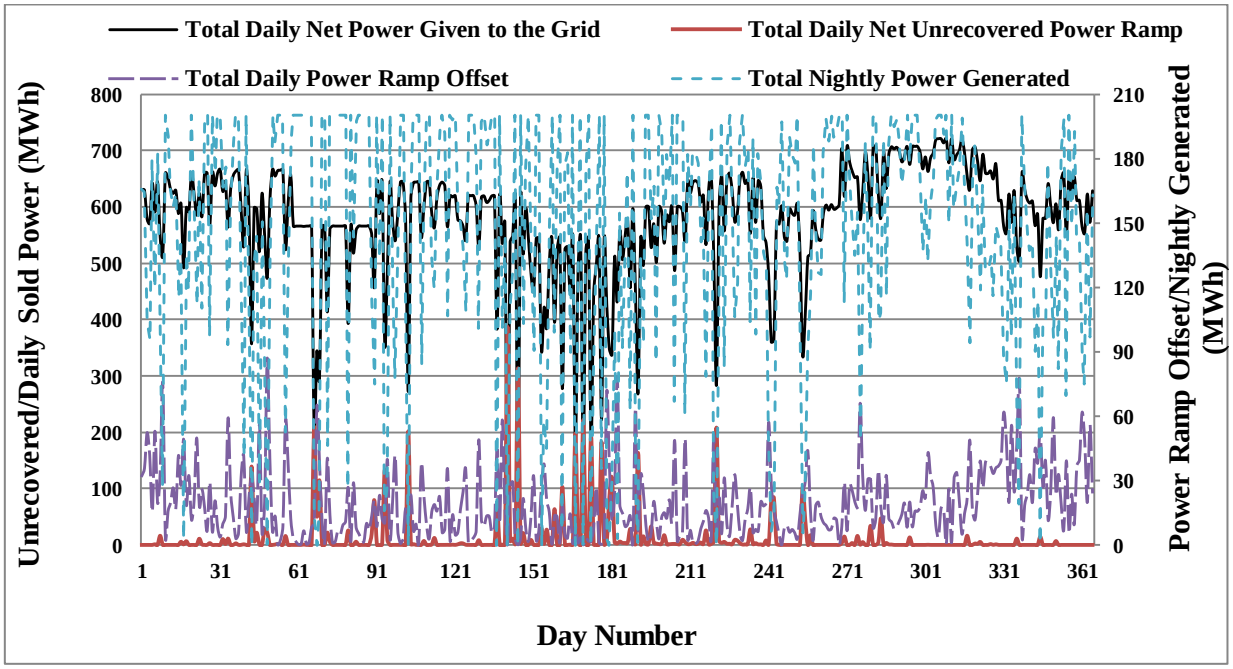

FIGURE 6.27 − Total daily power sold/offset/un-recovered and nightly produced in the power plant

Figure 6.28 shows the total daily energy and exergy efficiencies of the whole power plant.

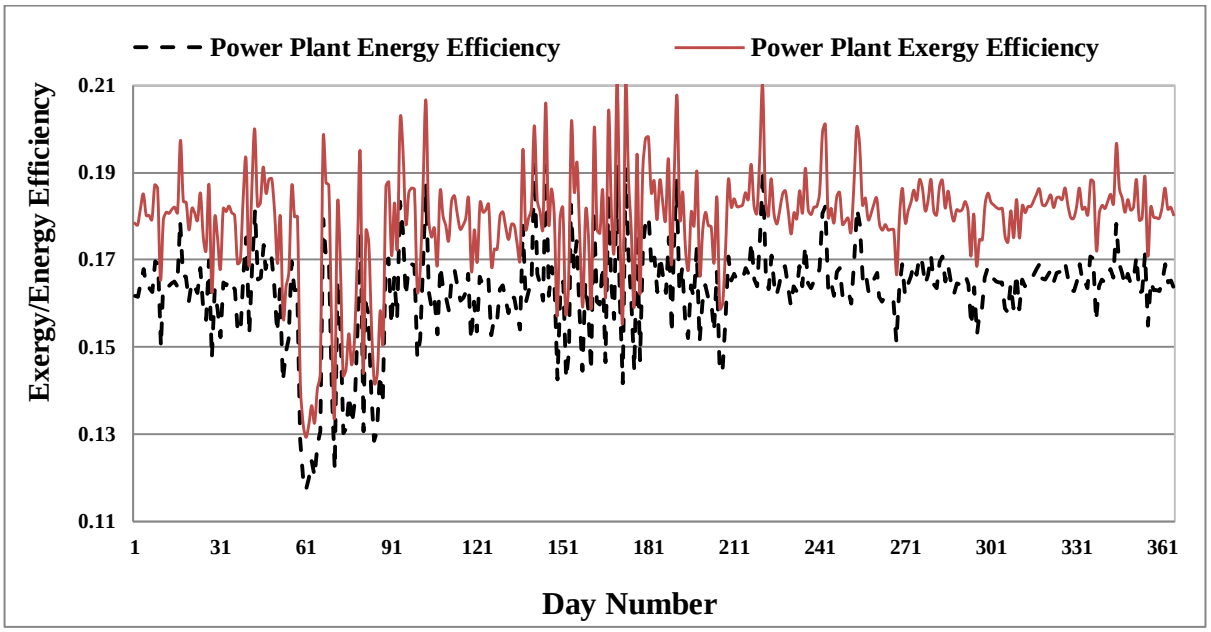

FIGURE 6.28 − Total daily energy and exergy efficiencies of the power plant

According to the figure, overall, the power plant exergy efficiency is more than its energy efficiency in all days of the year. The exergy efficiencies up to 21% are achievable in the plant while it does not fall below 13% in any day over the entire year. On the other hand, the energy efficiency of the plant varies from 12% in the first days of March to almost 19% in the middle days of May and June. The annual average exergy and energy efficiency of the power plant with all its peripheral equipment are 17.9% and 16.2%, respectively.

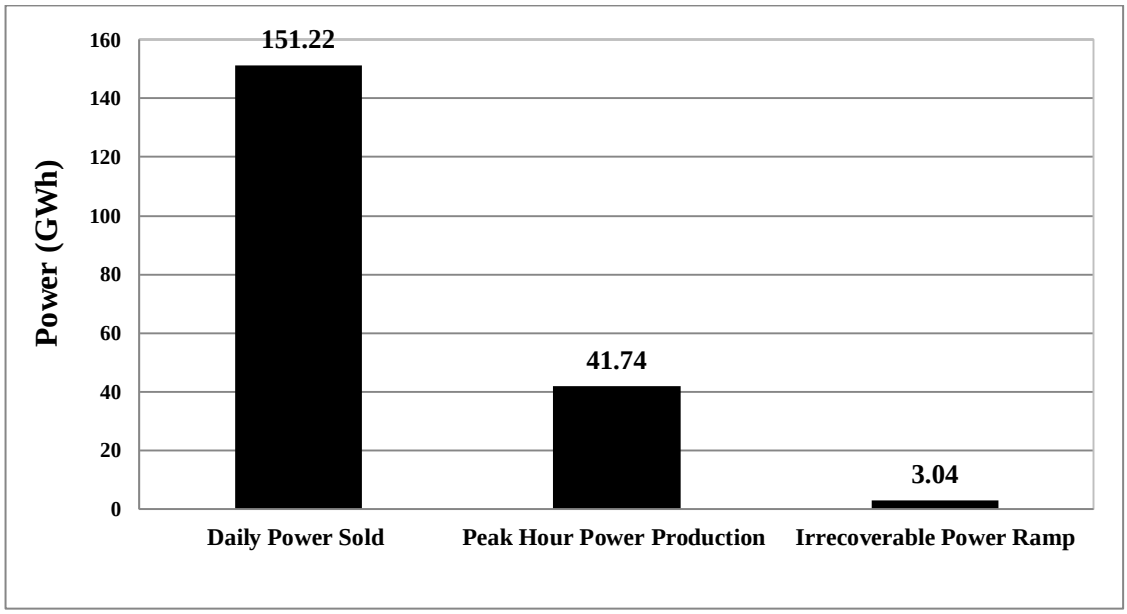

FIGURE 6.29 − Overall annual statistics of the power production and ramps of the power plant

In the end, the results of the economic analysis on the PV plant are presented. Figure 6.29 shows the total annual power sold by the power plant during daily hours, the power ramps offset by the CAES system and the power produced by the CAES system at nightly hours. According to the figure, the CAES sizing and power sales strategy has been so accurately selected that not only the amount of power sold to the grid is maximized, but also the irrecoverable power ramps of the PV farm are minimized over the year.

Taking the values reported in this figure into account, figure 6.30 shows the results of the NPV analysis on the power plant. With this data, the total annual income of the plant from selling power to the grid during the days is $ 23.13 million, the income due to nightly power production is $ 8.35 million and the penalty imposed to the plant is $ 2.28 million. On the other hand, considering the universal price of gasoil ($ 700/m^3), the annual operational cost of the air heater will be $ 92400, the annual O&M costs for the PV farm, the CAES system, the solar heating unit and the diesel air heater are also recommended to be considered equal to 3%, 5%, 3% and 4% of the corresponding cost of capital, respectively (Espicinc, 2015). It is re-mentioned that the total cost of capital of the plant is $189 million including $ 143 million for the PV farm, $ 45 million for the CAES system, $ 950000 for the solar heating unit and $ 50000 for the diesel air heater. Therefore, the net annual income of the plant is almost $ 30.5 million.

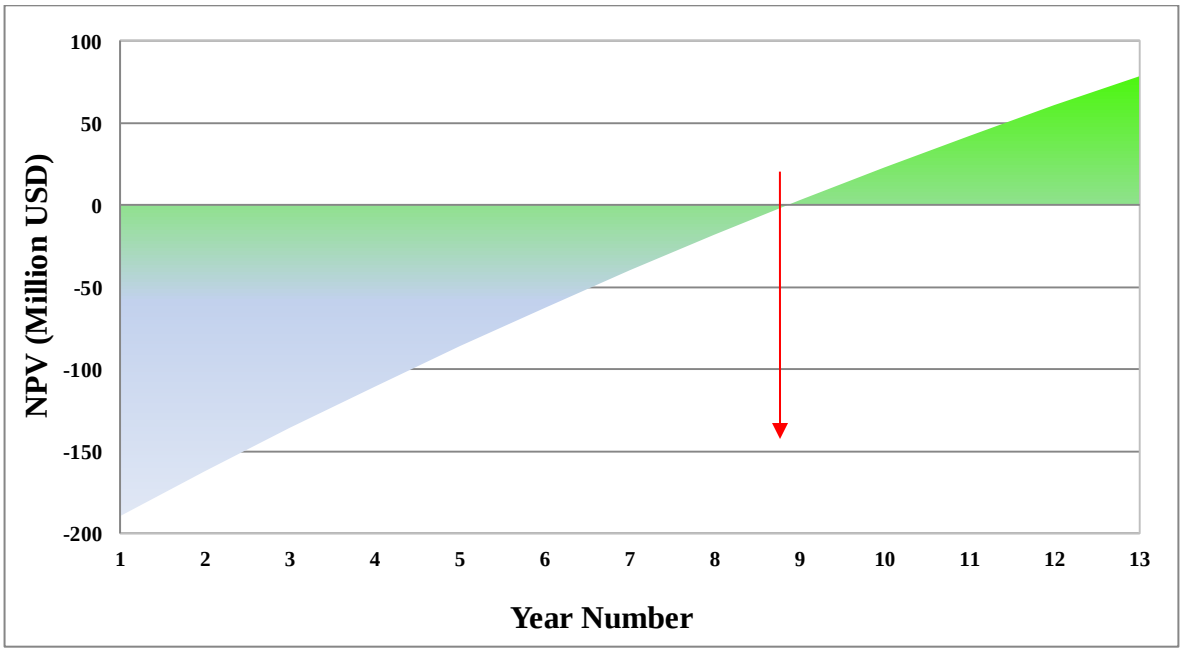

FIGURE 6.30 − The results of NPV analysis on the power plant

As the figure proves, the payback period of this power plant is less than 9 years. It is also noticeable that the inflation rate for dollar through the NPV analysis was considered to be equal to 4%.

6.2 The Results of Simulation on the Hybrid Power Plant

In this section the results derived from the simulation on the second configuration are presented. The first figure that is going to be presented is the total producible power in the system including the PV farm and the CGS. Naturally, presenting the monthly averaged data, in this step, cannot be illustrative enough as averaging process prohibits well showing the solar energy ramps effects on the PV farm output and the effect of utilizing the CGS power output as the stabilizer source of system. Therefore, the producible power of the whole system is presented for three sample days during the year in this step. Note that the sample days are so selected that one could observe the effects of the proposal in all possible cases i.e. a very sunny day, a very cloudy day and one temperate day. Figure 6.31 illustrates the total producible power of the whole system during these three sample days. According to the figure, March 4th is among top days of the year in terms of available solar irradiation as well as the least solar energy ramps while June 22nd is among the worst days of the year in this aspect and January 18th is a moderate level day.

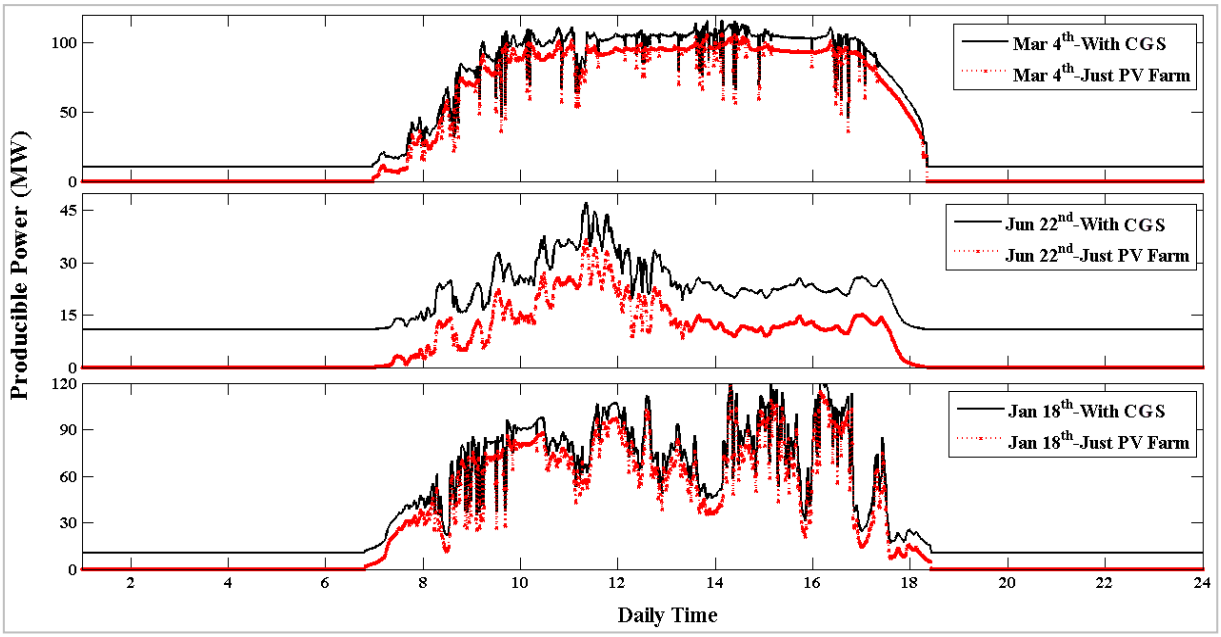

FIGURE 6.31 − Producible power in the PV farm in presence/absence of the CGS power production in three sample days

As can be seen, the power produced at the CGS increases the available power and can be used to stabilize the total power of the system. In addition, the previous study proved that early hours of the day, during which solar energy ramps are high, have significant impact to limit the power sales strategy as higher levels of power to sell cause remarkable values of penalty in these periods. Obviously from the figure, this problem can be totally solved by employing the power supplied to the system by the turbo-generator set in the CGS.

In the next step, the results of finding the best power sales strategy for the PV plant are presented. Like the previous configuration, the CAES sizing procedure and the power selling pattern selection should be carried out at the same time as these two factors are dependent to each other. Figure 6.32 presents the values of payback ratios for different CAES size and power sales patterns obtained from the energy-economic analysis accomplished one this configuration. Here also the results far away from the optimal value are not included in the figure.

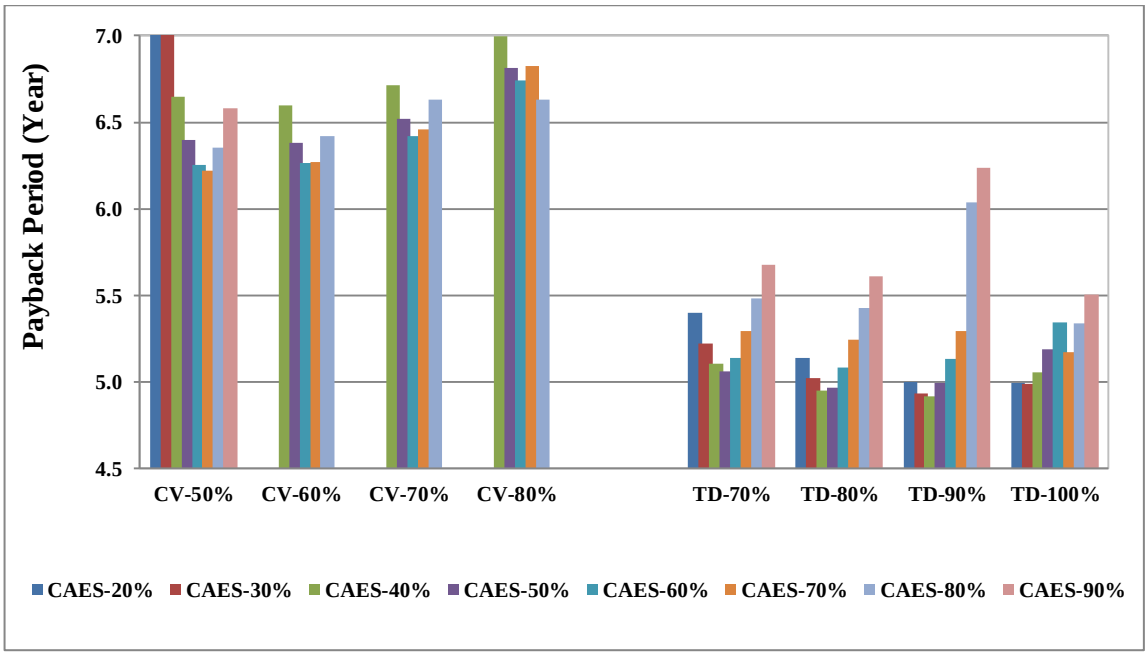

FIGURE 6.32 − Payback period of the power plant with different power sales strategies and CAES sizes (TD: time dependent; C: constant)

According to the figure, the time dependent category again shows better performance and among the considered cases in this category the best economic performance of the power plant will be observed if firstly, it sells power to the grid based on 90% of the minutely-monthly averaged producible power of the PV farm and secondly, the capacity of its CAES system is 40% of the maximum extra producible power by the PV farm during the year

(30 MW). Comparing the results of this assessment with the data related to the previous power plant, one notes that not only the directly vendible power of the grid increases significantly (from 70 to 90%), but also the capacity of energy storage system required decreases significantly (from 50 MW to 30 MW), which leads to lower cost of capital for the system. Clearly, this means how much the power supplied from the CGS is effective in stabilizing the producible power of the power plant. In this case, the required capacity of the CAES system is almost 30 MW. Note that, as this assessment only considers the daily performance of the power plant (from 6 am to 6 pm), half of the capital cost of the turbo-generator set in the CGS was taken into account in this stage.

Hereafter, the results of a simulation accomplished for a PV plant equipped with a CAES system with 30 MW capacity and with a time dependent power sales strategy equal to 90% of the minutely-monthly averaged producible power by its PV farm and accompanying with a power productive CGS station is presented. It is re-mentioned that, as averaged data could not show the variations and sudden ramps in the system clearly, the next few figures are presented and discussed for three selected sample days.

Figure 6.33 shows the variation of air pressure in the reservoir during these days. As can be seen, the cavern pressure increases up to almost 110 bar in March 4th as one of sunniest days of the year (not the suniest) while it could not exceed 5 bar at any point in June 22nd which is among worst days of the year in terms of solar irradiation. In January 18th, one the other hand, as a moderate day, the cavern pressure rises up to 55 bar.

It should be noted that the power sales strategy selected has significant impact on the reachable pressures in the cavern and if lower levels of power would be sold directly, the cavern pressure in all cases could increase up to higher levels. In addition, restricting the CAES maximum capacity caused the cavern pressure to not decrease down to zero. It is reminded that the cavern volume has been so selected that the maximum pressure in the system does not exceed 120 bar at any point. For this objective, in the current system, the cavern pressure should be 12500 m^3.

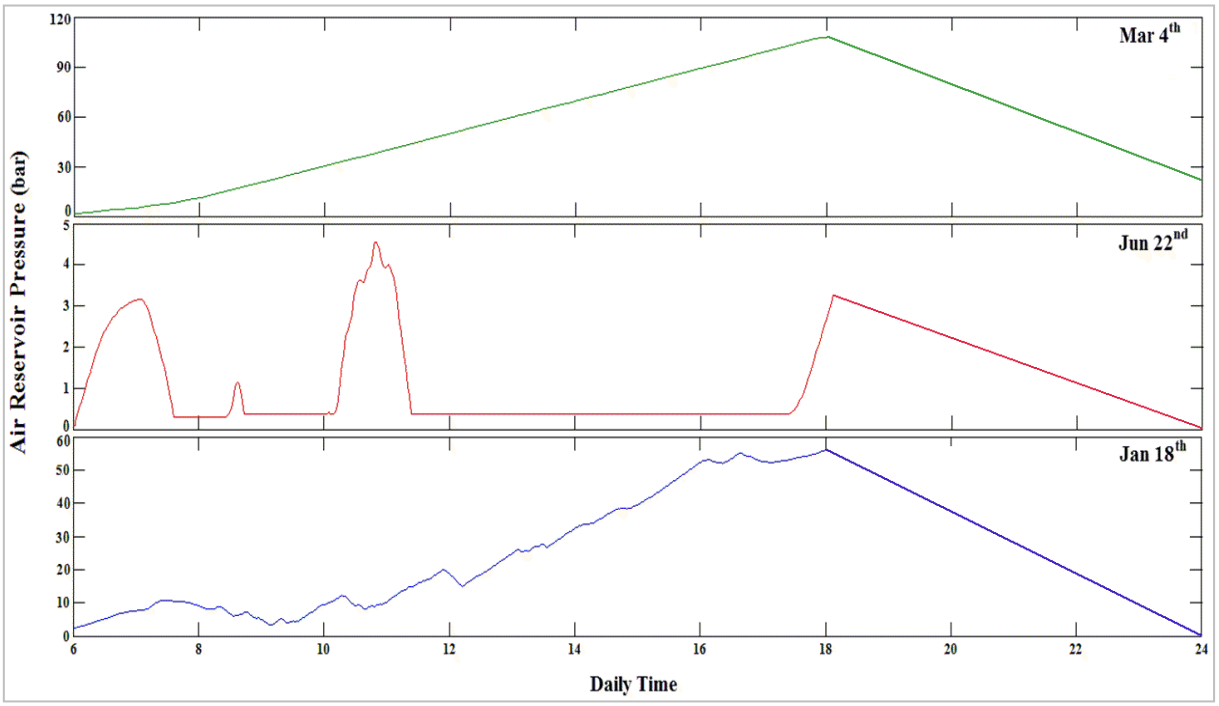

FIGURE 6.33 − Cavern pressure variation during the three sample days

Figure 6.34 shows the total turbine set and compressor set works in the same graphs. Evidently, the compressors work when there is extra power to be used by the CAES while turbines are in standby in this state and the situation is reverse when there is electricity shortage in the system.

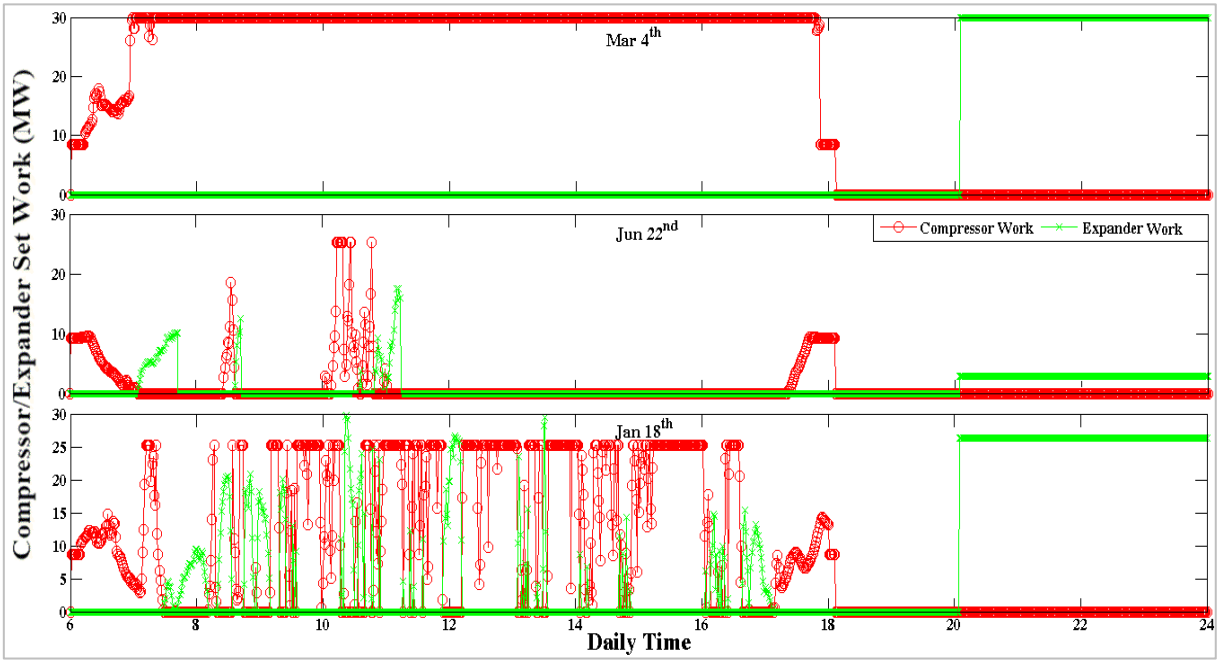

FIGURE 6.34 − Expander/Compressor set total work during the three sample days

Naturally, both of the maximum power output of turbine set and maximum inlet power of the compressor set should be 30 MW which occurs in March 4th as a very sunny day over the year. On the other hand, as can be seen, in June 22nd, sharp solar ramps cause the PV farm to not be able to cover the grid demand and as a result, the cavern is almost empty at the end of the day. That is why; the level of nightly producible power in this day is almost zero. Overall, the power plant seems to be subjected to heavy penalties in such days. The other noteworthy point in this figure is the duration of power production after sunshine hours which is 6 hours (from 6 pm to 12 pm). In the previous design, it was only 4 hours. This change was proposed for the system in order to utilize the extra compressed air in the cavern as much as possible.

By the same token, figure 6.35 shows the mass flow rate of compressing/expanding air during the three sample days.

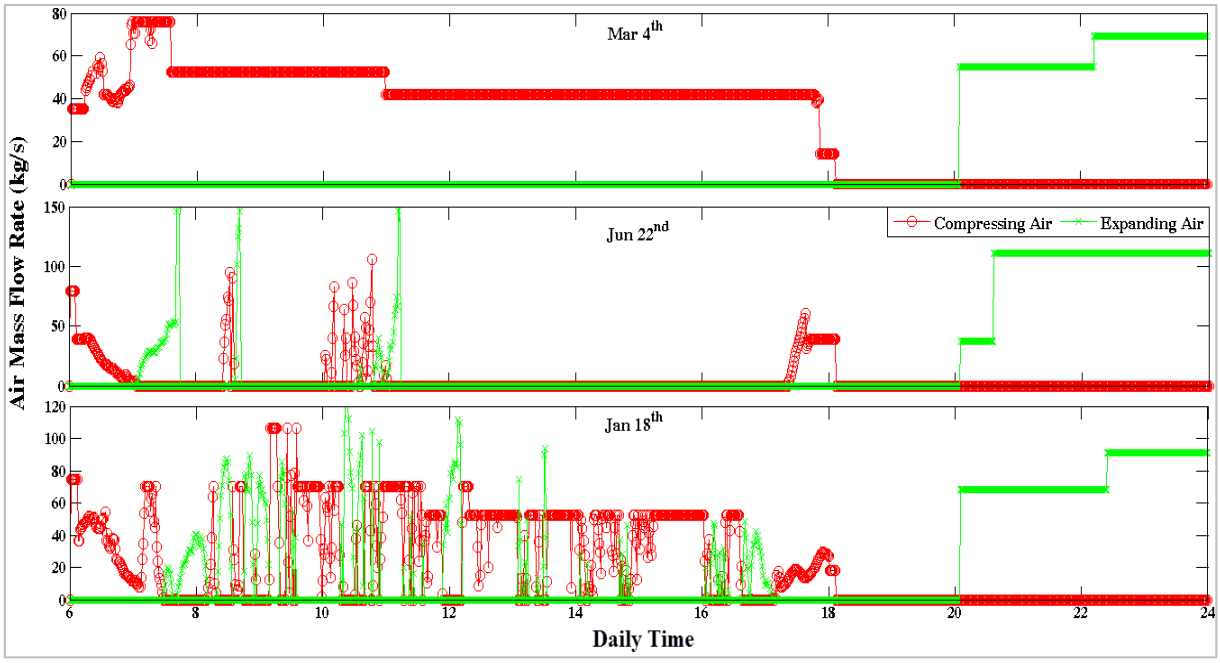

FIGURE 6.35 − Expanding/compressing air flow rates during the three sample days

According to the figure, Clearly, according to table 5.2, variation of cavern pressure may change the compressors and expanders arrangements. Therefore, even for a specific value of power, depending on the cavern pressure, different air mass flow rates may pass through the expanders and compressors. Overall, in lower cavern pressures, higher air mass flow rates are seen for both of the expanders and compressors. In contrast, air mass flow rate decreases for higher air reservoir pressures as both of the expander and compressor sets

tend to be in series instead of a parallel arrangement which is suitable for low cavern pressures.

In order to investigate the effect of the CAES system operation on the performance of the PV plant plus the CGS power production unit during the day (from 6 am to 6 pm), figure 6.36 is given for the three selected sample days. Note that this figure is presented to observe the level of power ramp offset by the CAES system, the level of power slumps that could not be recovered (fine levels) and the order of extra power production in the PV farm in each day. In this figure set, the brown area shows the amount of power that is sold to the grid directly by the PV farm. The red area also refers to the amount of power that is supplied to the system by the CAES system to offset the power ramps of the system. Also, the green area is the level of extra power that is produced by the PV farm and could be employed by the CAES system. Clearly, the value of this parameter is less than the total extra power that is produced by the PV farm as the CAES capacity is restricted to 30 MW. Finally, the blue zone is where the steep solar radiation slumps not only cause the PV farm to not be able to cover the grid demand, it cause the CAES system to fail in offsetting the power shortage in the system. Evidently, for such cases, financial fines are considered for the power plant.

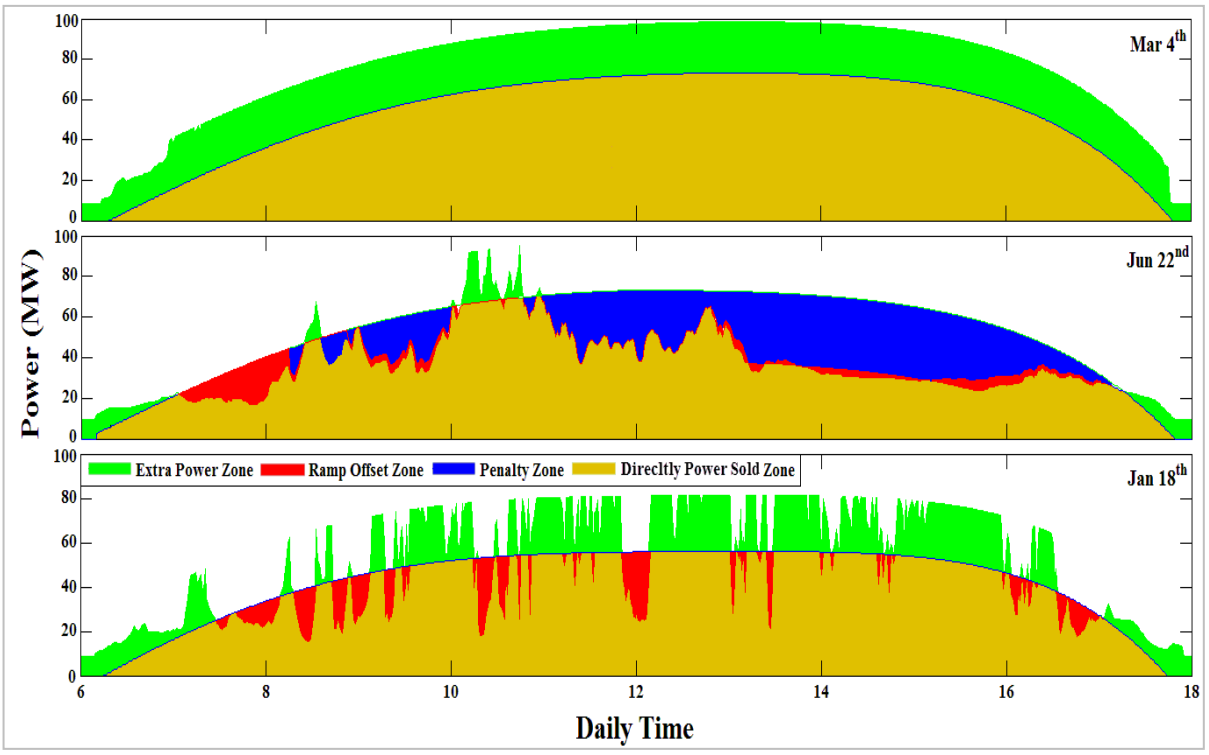

FIGURE 6.36 − Overall effect of the CAES system on the performance of the PV farm and the CGS power production station during the three sample days

According to the figure, in March 4th, the situation is very satisfactory and no sharp power ramp occurs during the day. In a sharp contrast, in June 22nd, the system is not able to cover the grid electricity demand and as a result, the power plant is subjected to huge financial penalties, though a portion of this shortage is offset by the CAES system. On the other hand, January 18th is a moderate day in which solar radiation slumps are recovered by the CAES system and there is no penalty for the power plant.

Hereafter, the overall energy and exergy performances of the power plant with all its belongings are evaluated for all days of the year. Naturally, as the PV farm of this configuration does not differ from the previous configuration, the same exergy and energy performances as the previous section are expected from the PV farm.

Based on the design objectives, in this power plant, evacuated tube collectors are supposed to be employed to remove the air heater necessity in the power plant. Actually, evacuated tube solar collectors are proposed to be hired this time as they can provide high temperatures up to 150 ^{o}C in the system. It should be noted that the air heater could not be eliminated practically from the CAES system configuration as it is surely required for emegency cases, however, its heading duty could be reduced down to zero theoretically. For this objective, the solar heating system capacity should be so selected that can provide all the extra heat required solely after the heating heat exchangers of the CAES system. Therefore, by calculating the total daily extra required heat in the system, and subtracting the given value from the heat supplied by the heating heat exchangers, one could size the solar heating unit.

Figure 6.37 shows the required heat in the system in presence of heating heat exchangers in a total daily format. According to the figure, the total daily extra required heat varies from almost 3 GJ/day up to over 45 GJ/day, which occurs in the 142nd day of the year, over year. Therefore, the number of solar collector modules and the size of solar storage tank in this system should be so selected that could provide this amount of heat in the given day.

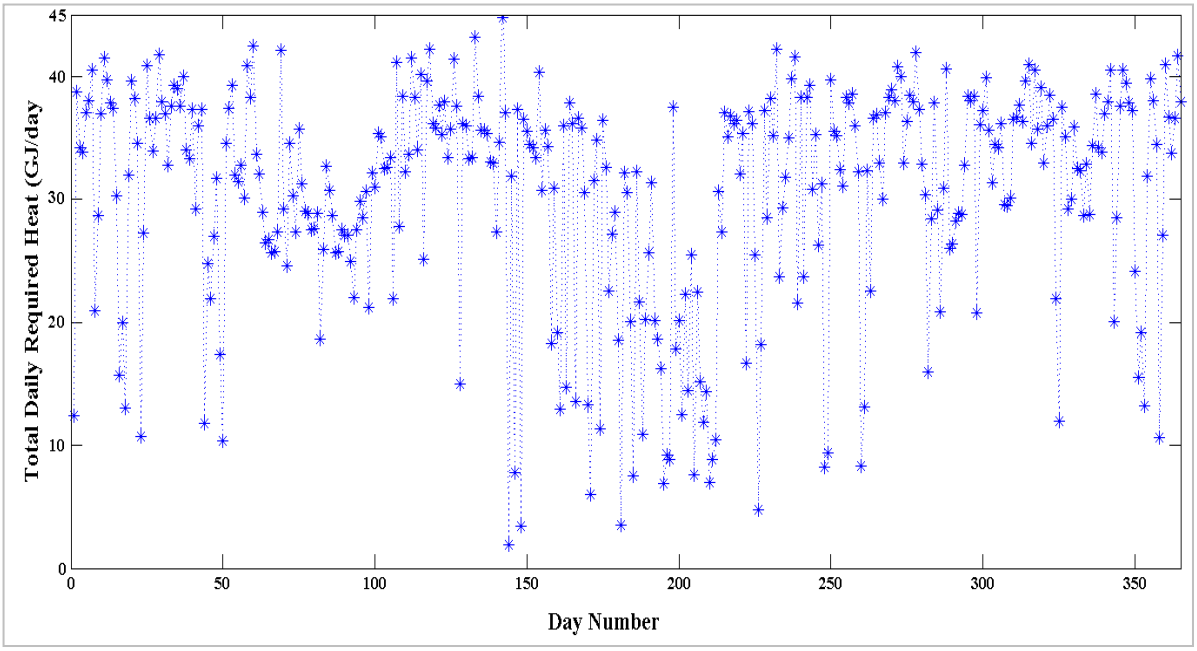

FIGURE 6.37 − Total daily heating duty of the air heater during the whole year

On the other hand, figure 6.38 illustrates the performance of a single collector evacuated tube solar collector system in the 142nd day of the year.

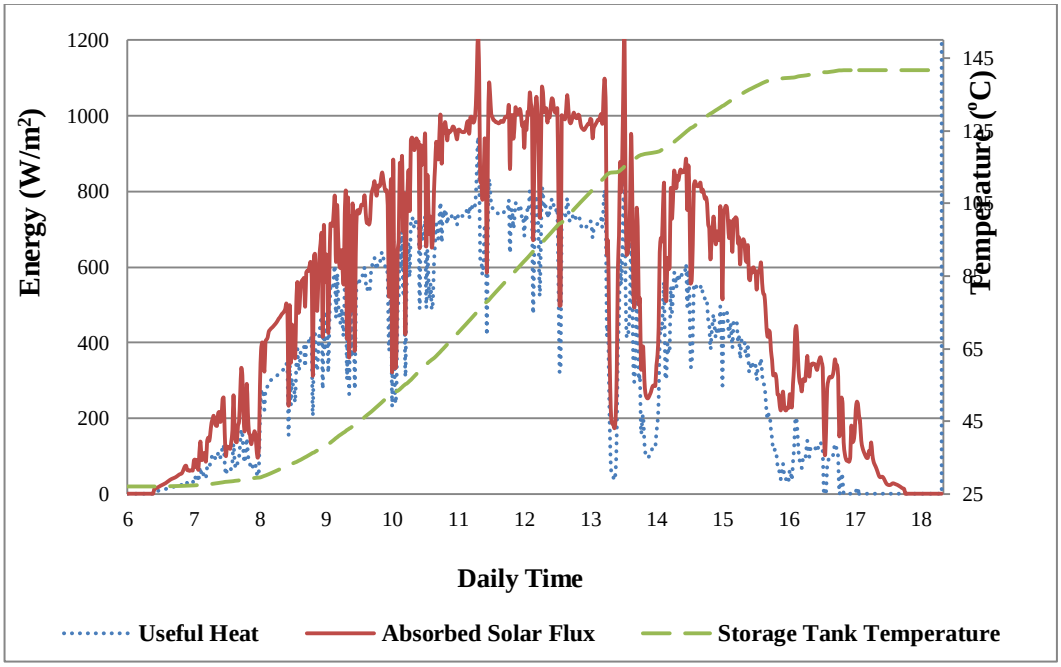

FIGURE 6.38 − A single collector solar heating unit performance in the 142nd day of the year in

As shown, the storage tank highest temperature could rise up to 140 ^{o}C in this day while there is no load. Naturally, the reachable temperature is restricted if there is any load for the solar heat exchangers. Overall, the total daily heat that could be provided by a single

collector is calculated to be 24.75 MJ/day in this day. Therefore, considering the total auxiliary heat required in the given day (45 GJ), one could conclude that the solar collector module should consist of almost 1800 collectors and as a result, a solar storage tank with 18 m^3 capacity.

Also, figure 6.39 illustrates the whole solar heating system performance in the CAES system through the considered day. This figure includes the working fluid temperature outgoing from the collector modules, the storage tank temperature and the increase achieved in the air stream through the solar heat exchangers.

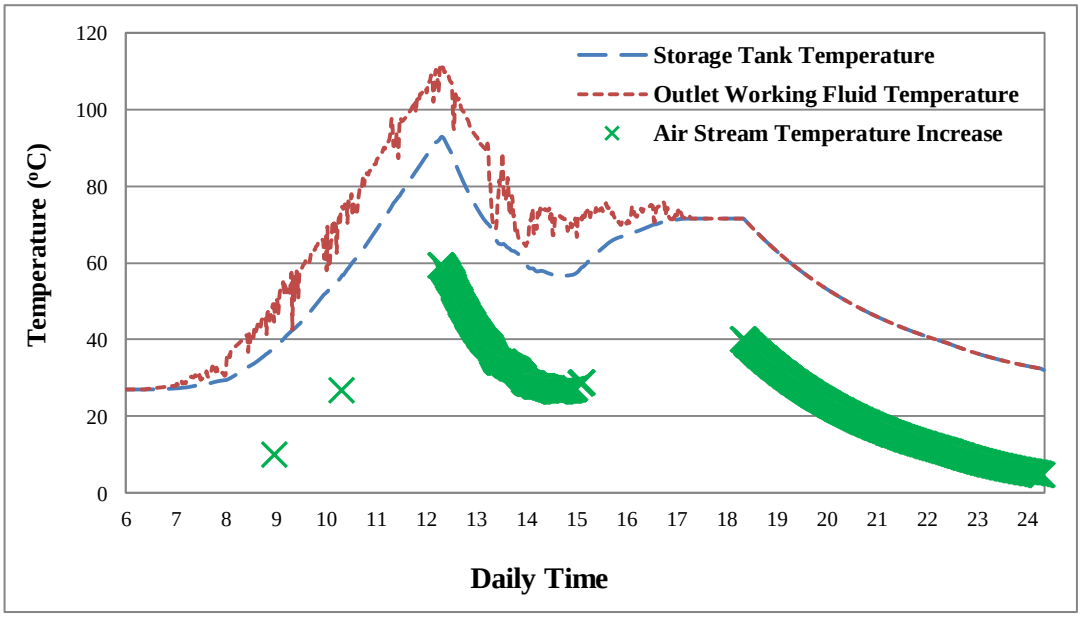

FIGURE 6.39 − The solar heating unit performance effect on the CAES system in the 142nd day of the year

As can be seen, while the solar system is coupled with the solar heating heat exchangers, the storage temperature could not increase that much as the air stream is heated by the collected heat through these heat exchangers. Also, evidently, there are some periods during which the figure does not give any information about the air stream temperature increase as expanding air mass flow rate is zero during these periods. In addition, evidently, at the end of the day, the storage tank temperature has not decreased to the ambient temperature level that means there is 18 m^3 hot working fluid in the storage tank which could used for other auxiliary applications at the power plant place. The working fluid of this solar system is glycol/water mixture.

After sizing and designing the solar thermal system and presenting its performance details, figure 6.40 gives information about the total monthly fuel consumption reduction occurred in the system relative to the previous power plant in which auxiliary air heaters are employed for this objective.

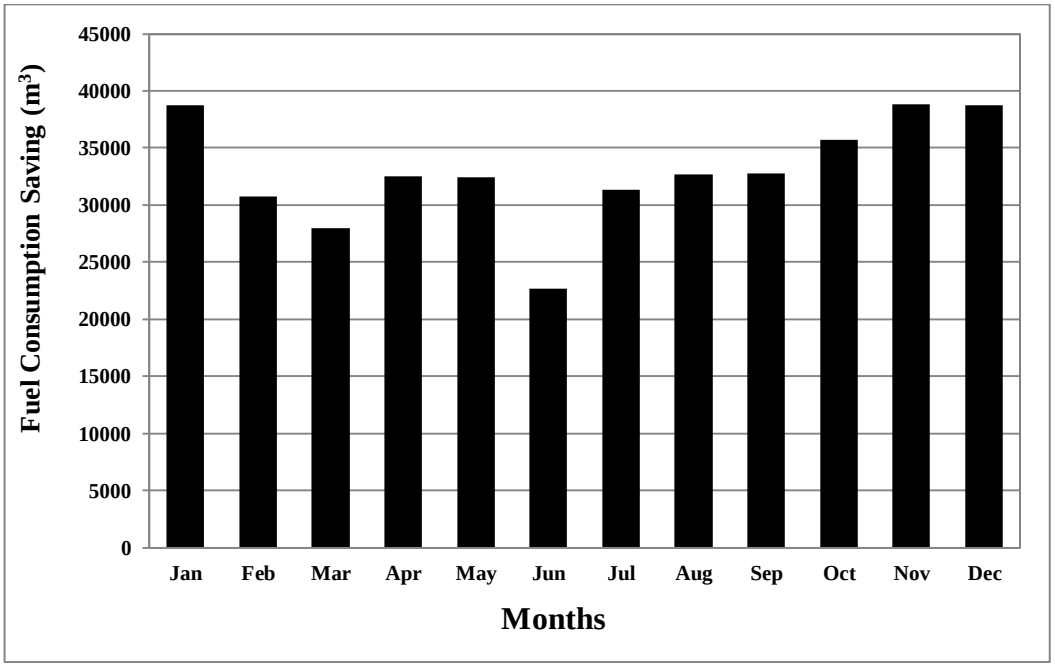

FIGURE 6.40 − Fuel consumption reduction in the CAES system by the evacuated tube solar collector system

According to the figure, in three months of the year; namely, January, November and December, providences around 39,000 m^3/month natural gas are possible while in June, as the worst month of the year, only 22,000 m^3 natural gas is saved. It should be noted that for providing this statistics, the auxiliary heater efficiency of 50% has been taken into account.

On the other hand, for simulating the power productive CGS, as one of the main components of the proposed configuration, CGS inlet natural gas temperature, which is a functional of ambient temperature, and the CGS inlet and outlet natural gas pressures are the primary essential information. Figure 6.41 shows the monthly averaged inlet natural gas temperature along with the ambient temperature to see the difference of natural gas temperature and environment temperature.

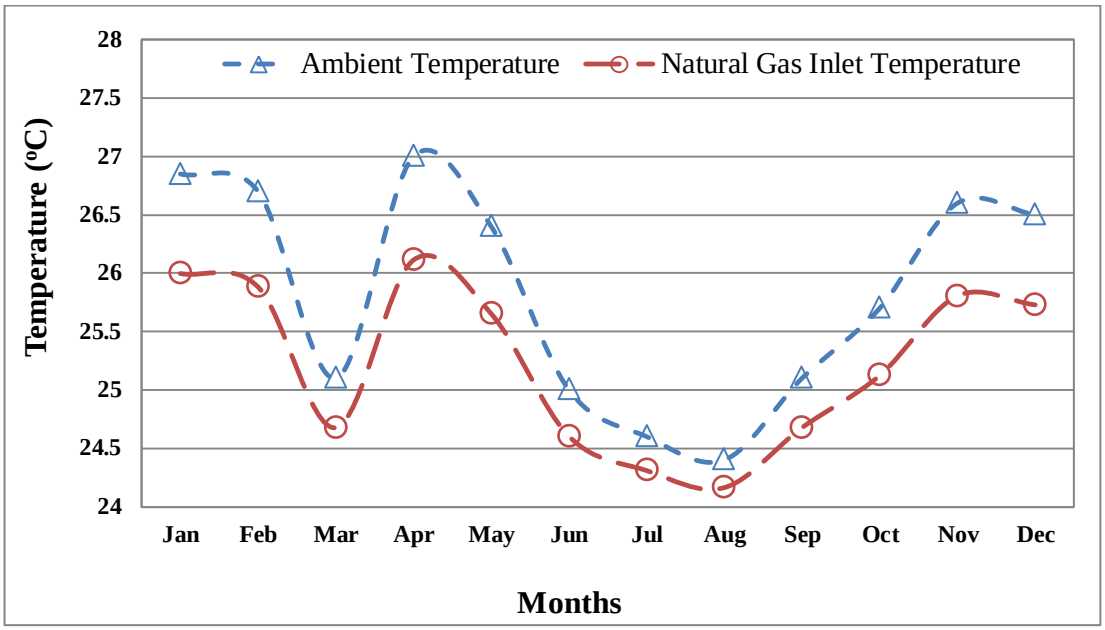

FIGURE 6.41 − The inlet natural gas versus ambient temperatures in the CGS

According to the figure, natural gas temperature is always below the ambient temperature and the difference is higher for higher ambient temperatures so that as the ambient temperature decreases toward to 24 ^{o}C, the natural gas stream temperature also approaches this value. It is reminded that natural gas temperature is a functional of ambient temperature as transmission pipeline is buried underground at the depth of 1.5 m.

Figure 6.42 gives information about the pressure variation of natural gas at the station inlet and outlet. Note that, as there is no real information about this parameter and on the other hand, these parameter are very essential for simulating the CGS and pay attention to the fact that the inlet and outlet pressures of different CGSs in a specific country are usually in the same range, the data related to Sao Bras Do Suacui station in Minas Gerais is used for the understudy station (Gasmig, 2015).

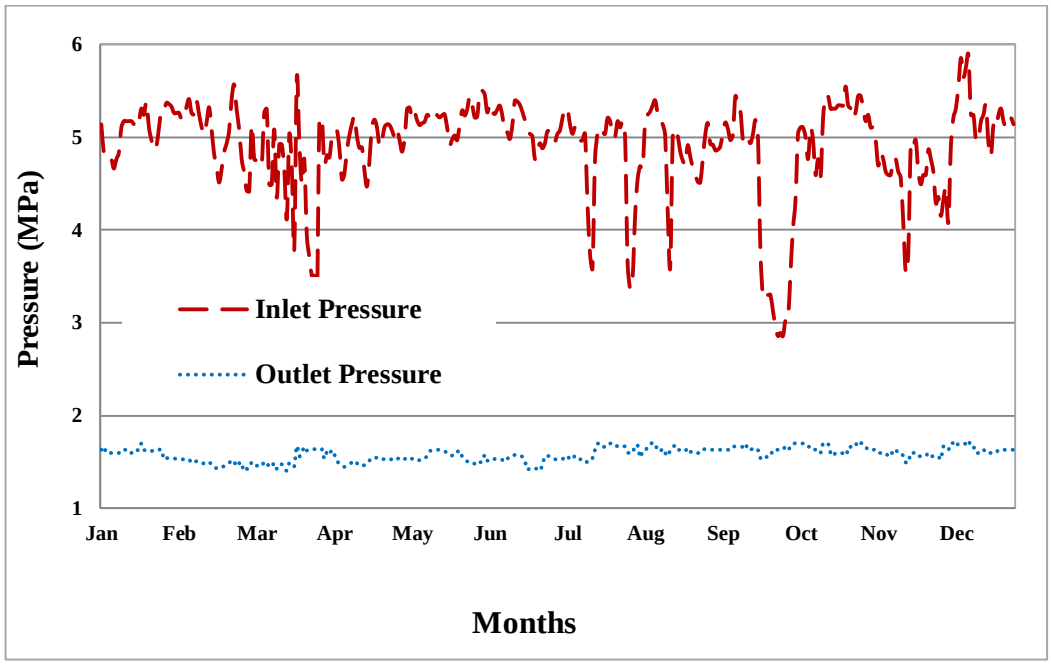

FIGURE 6.42 − The inlet and outlet natural gas pressures in the CGS

As can be seen, the inlet pressure is about 5 MPa and the outlet pressure fluctuates around 1.7 MPa.

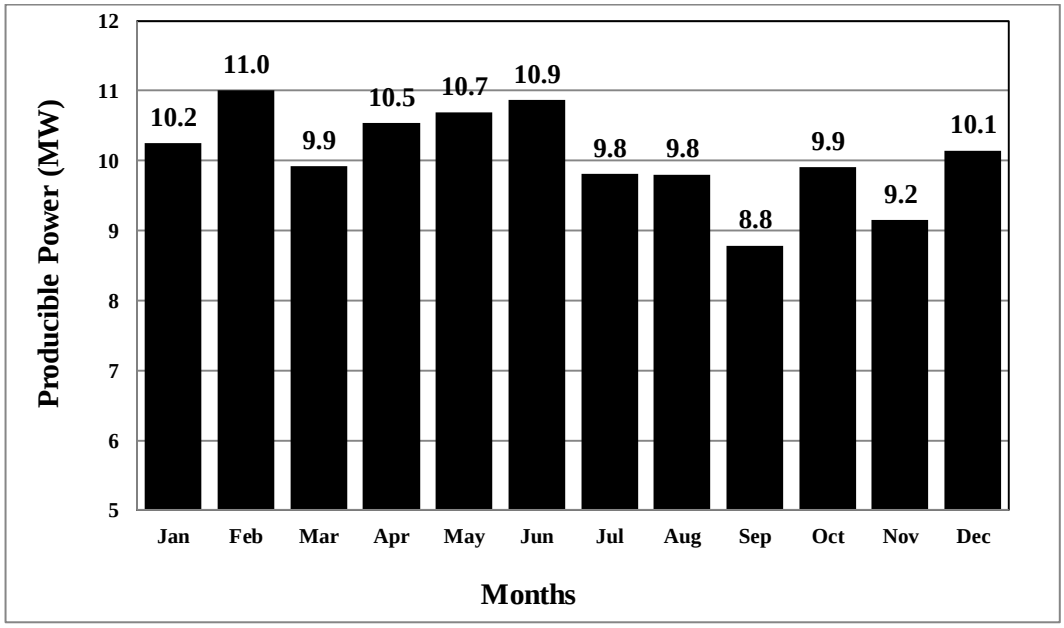

FIGURE 6.43 − Monthly averaged producible power at the CGS station

Figure 6.43 shows the monthly averaged producible power from the natural gas stream in this station in case of employing a turbo-generator pack with an overall conversion efficiency of almost 80% (expander isentropic efficiency of 85% and generator efficiency of 95%). According to the figure, the maximum power at the CGS could be produced in

February which is almost 11 MW and the least value of power which is approximately 8.8 MW is produced in September.

Figure 6.44 compares the amount of total monthly fuel consumption at the CGS when the proposed solar heating system is and is not employed along with the line heaters. Also, this figure shows the total fuel consumption reduction percentage in each month.

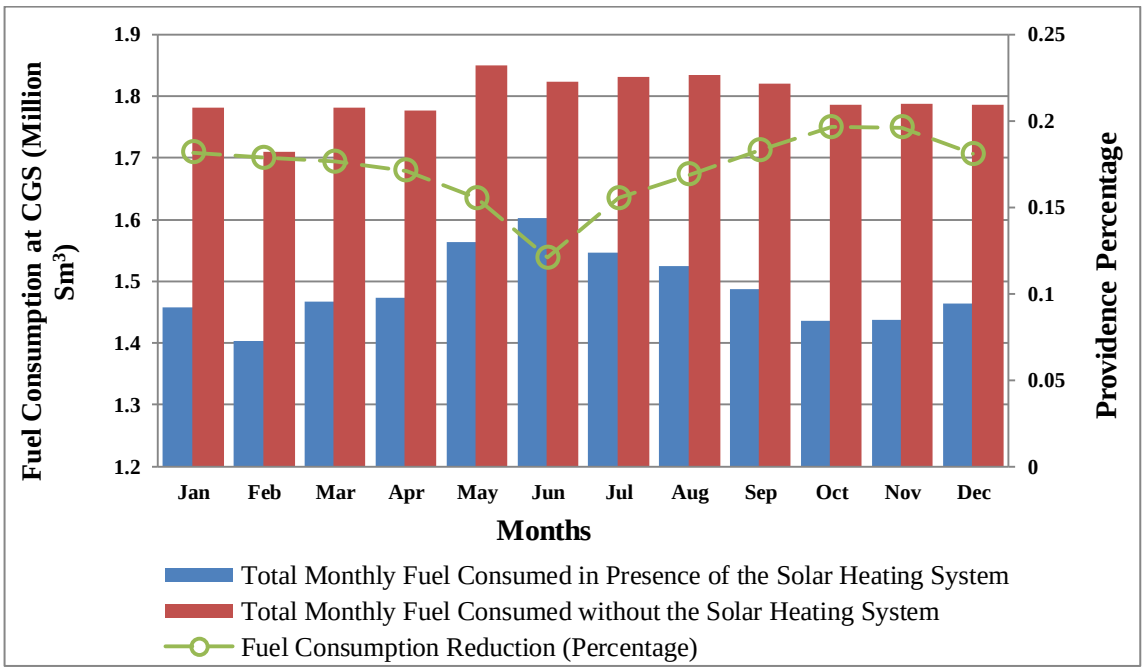

FIGURE 6.44 − The total monthly fuel consumed by the line heaters in the CGS when the proposed solar system is/is not utilized

As the figure shows, in the system without a solar heating system, the maximum amount of fuel is consumed in May while in the system equipped with the solar heating unit the maximum fuel is consumed in June. This can clearly show how much the sky unclearness affects the solar systems performance in June. The minimum amount of fuel, however, in both cases, is consumed in February when the ambient temperature stays at its maximum level and consequently, the evacuated tube collectors can collect higher values of solar irradiation for heating purposes. On the other hand, reconsidering the figure, one could observe the fuel consumption providence occurred at the CGS due to the use of the solar system with the peak value of 19% in October and a low point of only 12% in February. It is noteworthy here that the solar heating system employed in the CGS includes 5200 evacuated tube collectors sloped at 12^{o} toward north with the characteristics detailed in table 5.7.

As it was explained before, the number of collector modules is so selected that the natural gas temperature at the solar heat exchanger outlet equals to 85 ^{o}C and also does not exceed this value over the whole year. Naturally, in most days (the days with clear sky), the maximum temperature is achievable at noon as the maximum solar irradiation is available at this time. Note that although by increasing the number of collectors more solar energy could be harvested and supplied to the system in daily hours (except midday), exceeding the natural gas temperature from the desired temperature before the line heaters equals to unnecessary increase in initial investment of the solar heating system that can affect the proposal justification economically.

Figure 6.45 shows the maximum obtainable natural gas temperature at the heat exchanger outlet for various numbers of solar collector modules along with the total annual proportional fuel consumption reduction in the CGS. As can be seen, the maximum temperature of 85 ^{o}C is obtainable when 5200 collector modules are hired by which 17.2% fuel saving is possible during a whole year. Obviously, as the size of solar heating system increases, both the maximum expectable temperature of outlet natural gas from the solar heat exchanger and the capital cost of solar system increase. Also, as the figure shows, the fuel saving proportion rate reduces as the number of collectors exceeds 5200 because higher portions of collected solar heat are wasted at midday hours.

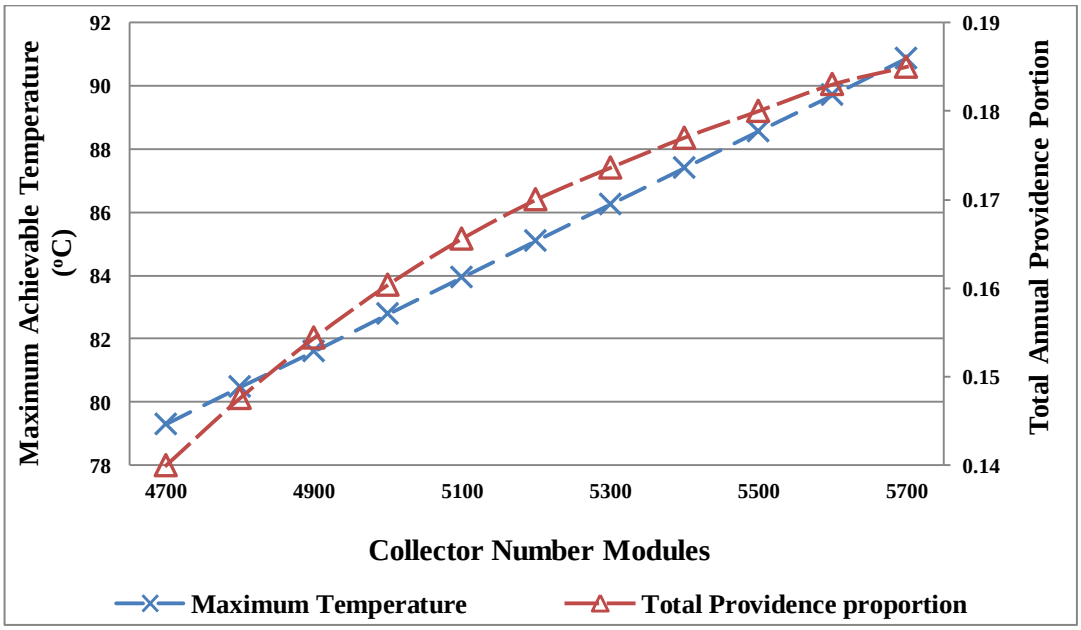

FIGURE 6.45 − The maximum achievable temperature for outlet natural gas from the solar heat exchanger and total annual fuel consumption reduction proportion by various numbers of collector modules

Finally, figure 6.46 shows the amount of total monthly revenue in the CGS over the year resulted from employed solar heating system. According to the figure, the most saving is occurred in October and November with almost 95,000 USD while the least fuel consumption reduction is carried out in June by less than 60,000 USD. The total annual benefit in the CGS is equal to well over 1,000,000 USD.

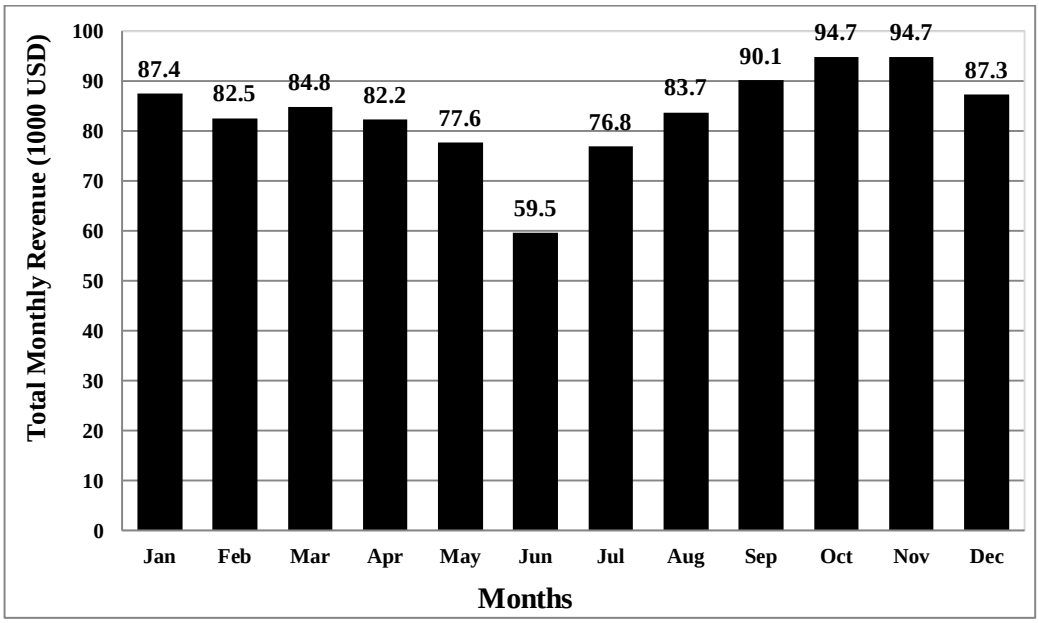

FIGURE 6.46 − The total monthly benefit expectable in the CGS by the proposed solar system

Figure 6.47 shows the values of total daily exergy and energy provided for both of the CGS station and the CAES system by the solar heating units comprising 7000 evacuated tube solar collectors. According to the figure and confirming the results obtained in exergy analysis of simple flat plate collectors in the first configuration assessment, there is a big difference between the exergy value received from the sun by the collector modules and that they could enter the system as the beneficial exergy of heating process. This actually means that exergy efficiency of the solar thermal collector modules in the system should be too low.

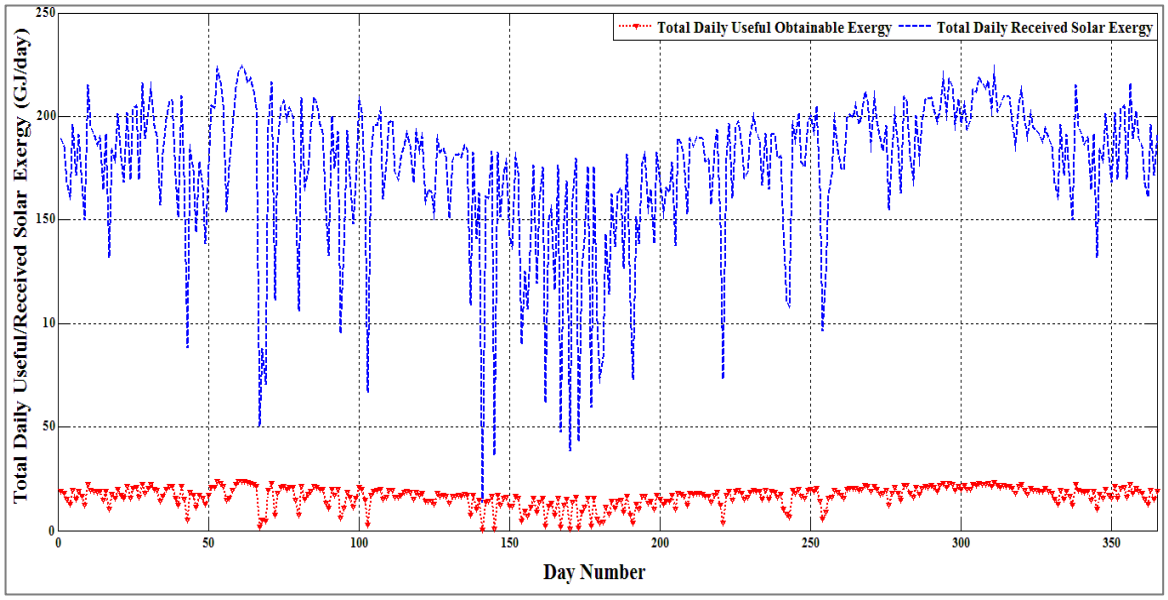

FIGURE 6.47 − Total daily exergy and energy provided by the solar heating units in the power plant

Figure 6.48 compares the values of total daily exergy and energy efficiencies of the solar heating systems in the power plant. Obviously, the energy efficiency of the solar systems could rise up to even 60% in a few days while it does not fall below 42% except a single day by 38% energy efficiency. On the other hand, the exergy efficiency of the system could only come up to 11%, though it is much better than those reported for flat plate collectors which itself could show the effects of utilizing evacuated tube collectors instead of simple flat plate collectors in the system.

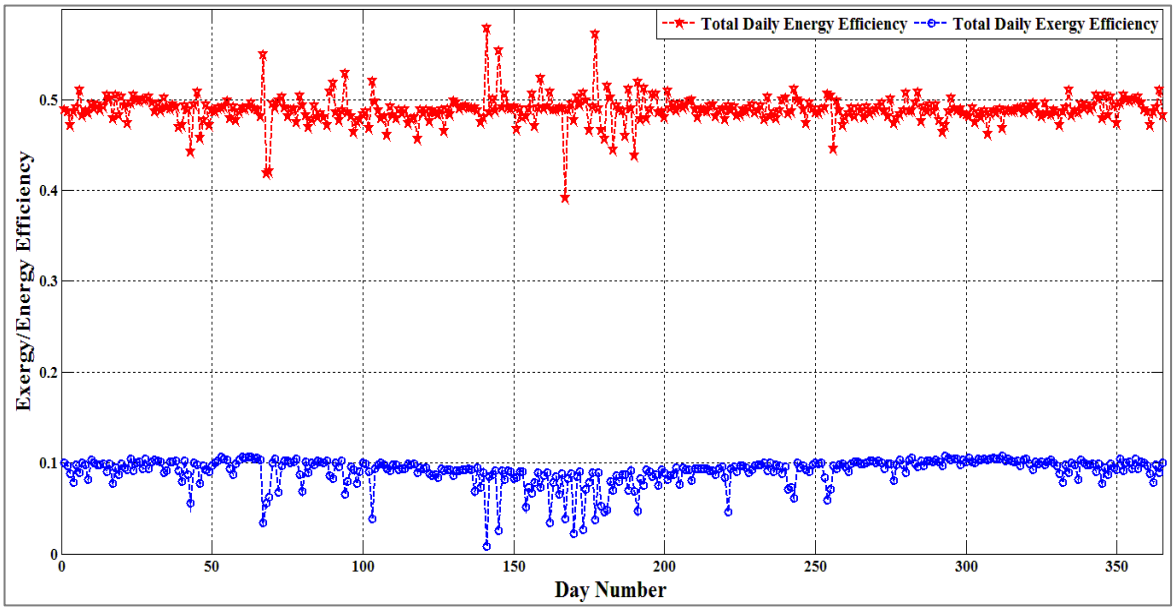

FIGURE 6.48 − The total daily exergy and energy efficiency values of the solar systems in the power plant

Figure 6.49 gives information about the total daily exergy and energy efficiencies of the CGS station, including the solar heating unit, the line heaters and the turbo expanders, for an entire year.

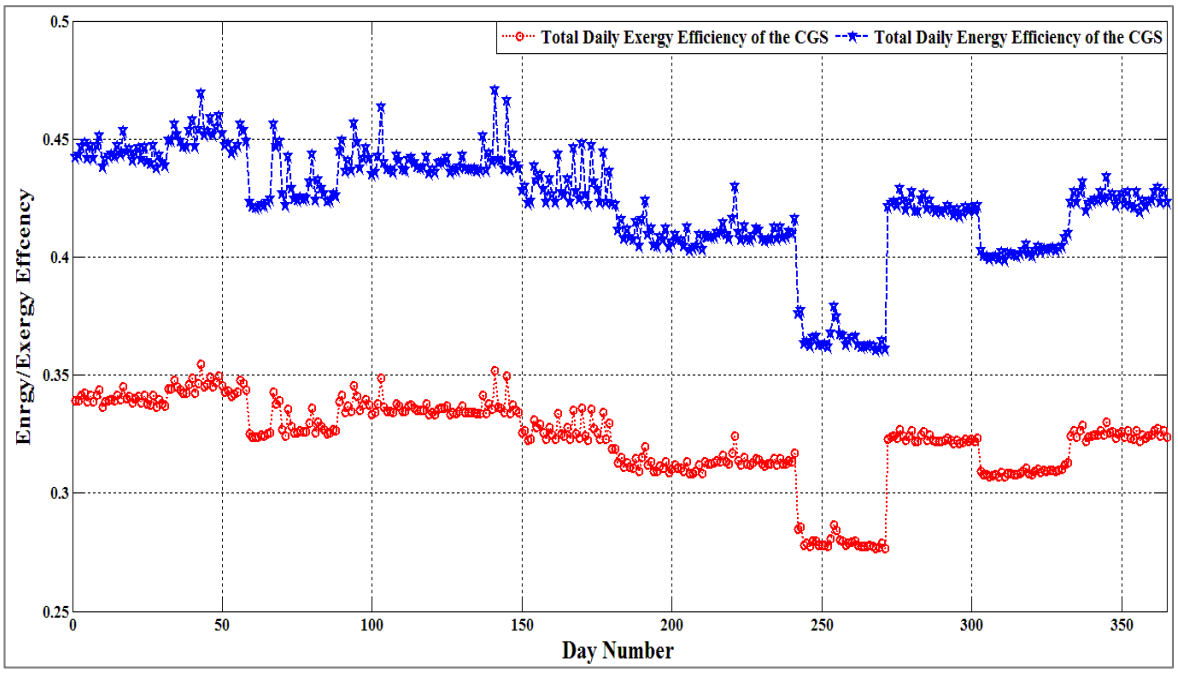

FIGURE 6.49 − The total daily exergy and energy efficiency values of the CGS station

Evidently, in the CGS also, the level of exergy efficiency is much lower than energy efficiency. This is mainly because, huge amount of exergy is wasted through the line heater exhaust due to the low thermal efficiency of the line heater. According to the figure, exergyefficiency mostly fluctuayes around 32-35% while energy efficiency varies between 40-45%. However, it should be noted that as the freely available natural gas exergy is harvested in a CGS, even with this level of exergy and energy efficiencies, it is worth considering this kind of stations as adequate stabilizers for renewable energy source power plants or even as individual power production stations.

Figure 6.50 shows the total daily exergy and energy efficiencies of the CAES system in this power plant including the compression unit, expansion part and the solar heating system during the sample operational year considered.

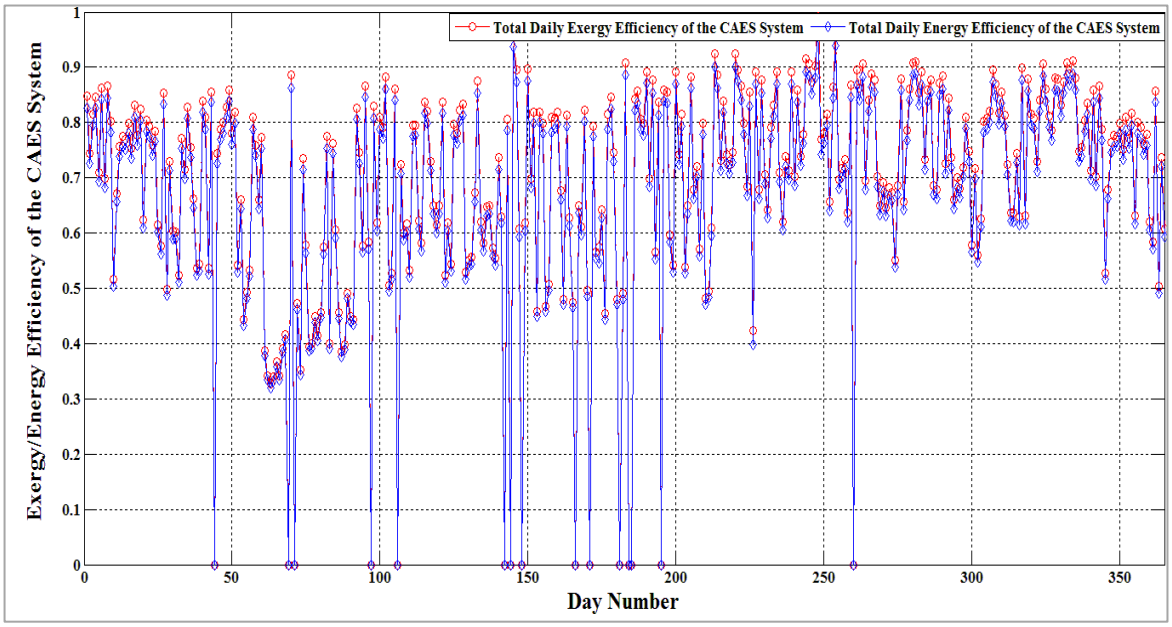

FIGURE 6.50 − The total daily exergy and energy efficiency values of the CAES system in the power plant

According to the figure, both of the energy and exergy of the CAES system in this configuration are much better than the CAES efficiencies in the first proposed configuration for the PV plant. As the main reasons of this enhancement in the CAES system two main factors could be addressed. First, removing the air heater from the CAES system which caused a considerable amount of energy and exergy in the previous configuration by itslef and employing evacuated solar collectors and second, extending the 4-hour period of nightly power production by the CAES system to 6 hours which minimizes the energy waste of the CAES system as much as possible. The other noticible oint is that the exergy and efficiency values are really close in the CAES system and the reason is that the only difference in the formulas used for calculating these two items is about the net energy or exergy values entered the CAES control volume by the collector moduels that are slightly different.

Figure 6.51 also shows the overall daily exergy and energy efficiencies of the whole power plant with all its assessories system. This figure also proves the great enhancement occured in the power plant efficiencies relative to the previous configuration. Here, both the exergetic and energetic efficiencies fluctuate around 20-25% whilein previous configuration the total daily exergy and energyefficiencies of the power plant were always around 14-17%.

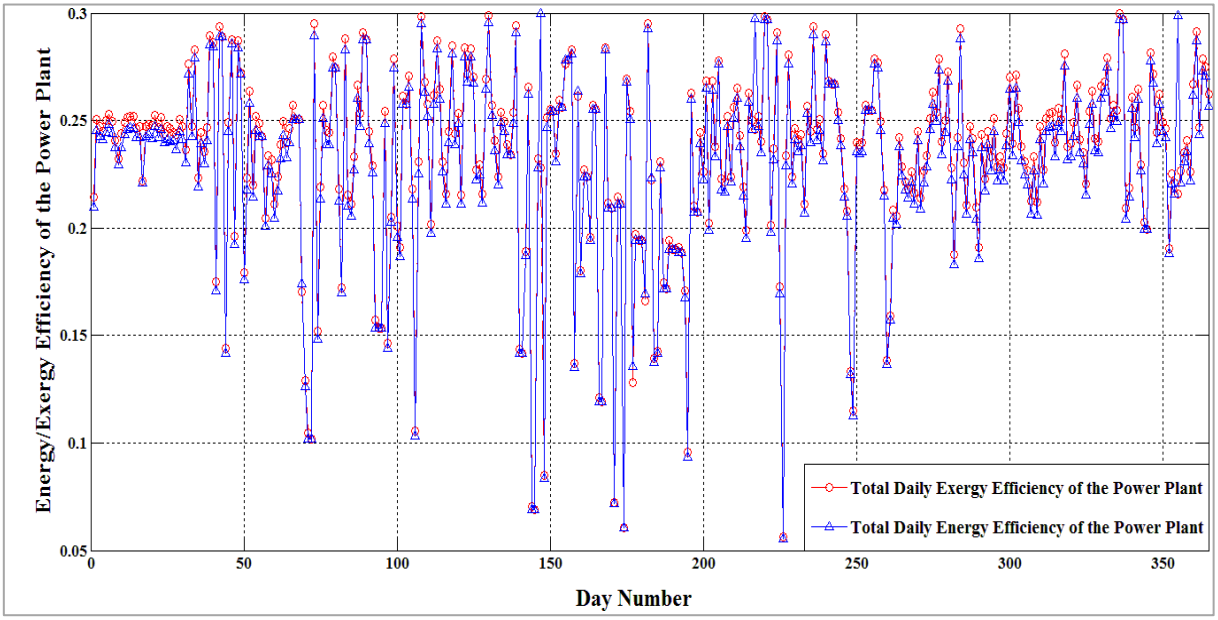

FIGURE 6.51 − The total daily exergy and energy efficiency values of the whole power plant

In the end, to assess the overall annual effect of the CAES system on the PV plant and the CGS power production station performance, figure 6.52 presents a detailed report of the whole system performance including the total annual stored energy by the CAES system, the total annual electricity shortage compensated by the CAES system, the total annual peak consumption power produced by the CAES system and CGS power generation station, the total amount of electricity shortage remained in the system for which the power plant is fined financially, annual power that is wasted as the CAES capacity is limited and the total power that is produced by the CGS station in other hours of the day (from 24 to 6 am).

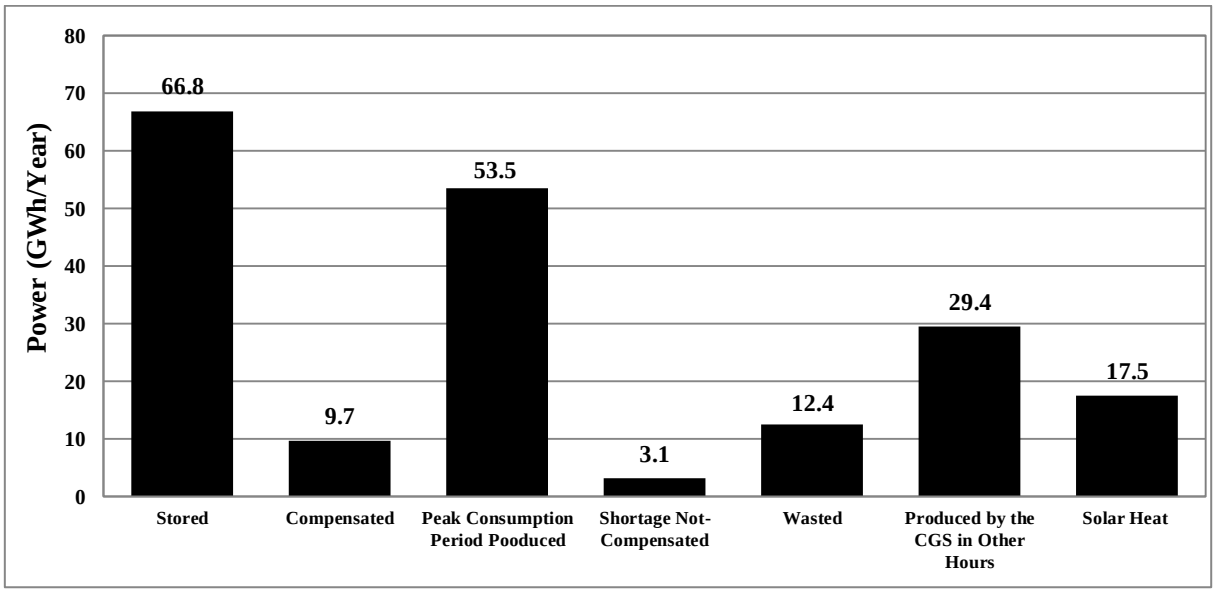

FIGURE 6.52 − Total annual performance of the whole system

As can be seen, the CAES capacity and the power sales strategy have been so precisely defined that not only the vendible power stands at its maximum level, but also the non-recoverable power slumps remain at minimum possible level. It is worth mentioning that the total annual power that is directly sold to the grid from the PV farm is 214 GWh.

And eventually, considering the results of economic analysis carried out on the first and second power production configuration studied, one could compare the financial aspects of these two projects. In this regards, figure 6.53 compares the IRR values of these systems.

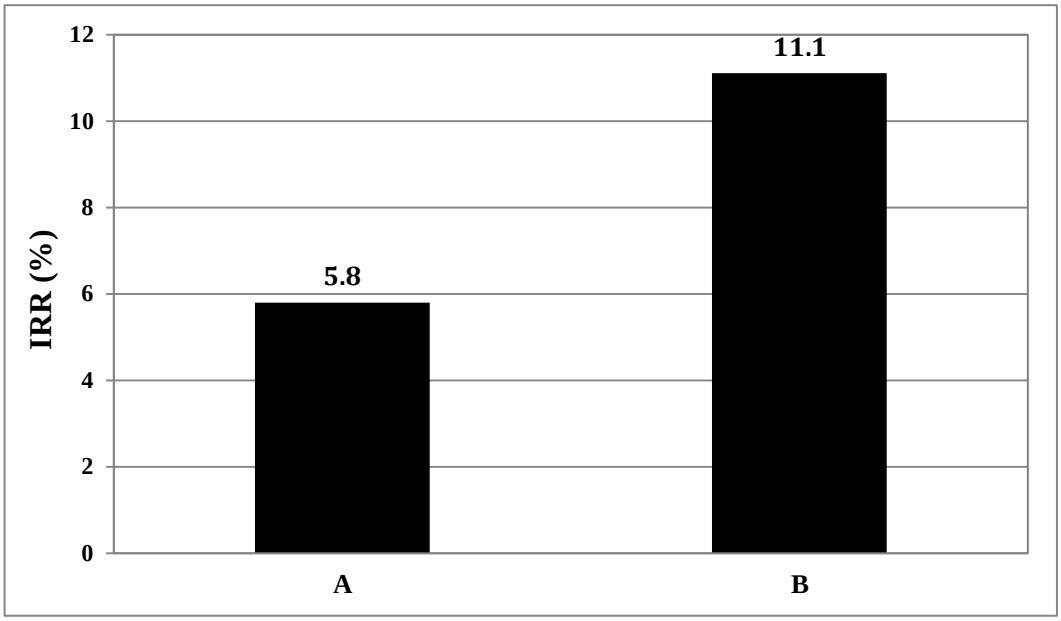

FIGURE 6.53 − IRR of previous/current systems

As the chart shows, the IRR corresponding with the new proposed system is much better and its value has increased from 0.058 in the previous system to 0.111 in the new system. It bears mentioning that the IRR presented is related to the 8^{th} year of operation of the power plants, the O&M costs in both systems have been considered to be equal to 3.5% of the total capital costs and fuel (natural gas) price has been considered 0.28 USD/Sm^3.

7. Conclusions

The main problems of renewable energy power plants is that the source of energy is inherently intermittent. Therefore, instantaneous variations of electricity demand in the grid could not be accurately responded. For overcoming this problem, firstly, unpredictable and steep ramps in the electricity demand of grid, and secondly, the ramps in the intensity of the corresponding energy source should be taken into account. Therefore, accurate forecast would eliminate these problems entirely. As accurate prediction of these two parameters is not achievable practically; the best solution seems to be employing an energy storage system and reclaiming the stored energy by the time of demand. Various energy storage systems have already been proposed in the literature. Normally, traditional renewable energy source power plants use conventional batteries for this objective. However, a battery is not the best candidate for large scale applications due to the too big size of the battery required and some technical problems such as self-discharging. Among other storage systems, the CAES system has been found to be the best system for such applications. Many studies have already been done on the CAES technology, however, simulating the transient performance of a CAES system in a renewable energy source power plant has been remained as a big challenge for the experts yet.

On the other hand, Brazil is among countries with the highest amount of receivable solar irradiation. In spite of this great solar energy potential, not many grid connected PV farm has been installed in Brazil by now, though a few more PV plants are supposed to be run in small capacities shortly. The largest in operation PV plant in Brazil has an installed capacity of 3 MWp and made up of 19,424 panels in the city of Tuberão (Tractebelenergia, 2014). A bigger plant is also going to be installed with a capacity of 8.5 MWp in Luziania (Eco, 2014). Also, all in operation solar power plants in this country are equipped with traditional storage systems i.e. batteries. Therefore, in this work, in the first place, constructing a large scale grid connected PV plant with 100 MWp capacity and accompanying with a CAES system in the most appropriate location in Brazil was proposed. The proposed system performance was simulated and analyzed exergy-energetically under real transient operational conditions over a whole year. Next, as thermo-economic issues, the most efficient power sales strategy for the plant was found and the CAES system sizing for this power plant was carried out. In order to have a comprehensive economic assessment, the

NPV method was used to calculate the payback period of the plant and all possible losses and uncertainties for such a power plant were taken into account. The results illustrated how a CAES system can increase the efficiency and reliability of a PV plant provided that the power sales strategy and the CAES system components sizes are chosen properly. The results of the simulation conducted on this configuration showed that the exergy and energy efficiencies of the power plant could only rise up to 21% and 19%, respectively. These values even could fall down to 13% and 12%, respectively. Therefore, comparing the efficiency of the proposed configuration with the conventional power plants (vapor power plants, gas turbine plants, combined cycle plants and etc with efficiencies in range of 25% to 45%), one finds the obtained efficiency from the proposed system lower than the conventional power plants. However, the great advantage of the investigated system is that the energy source in a PV farm is the free and endless solar energy, while the conventional power plants burn huge amount of fossil fuels every day and it causes their operational costs much more. This makes the investigated power plant superior to the conventional power plants. Also, comparing the proposed system with other renewable energy source power plants like PV farms, concentrating solar power plants and wind farms while using batteries or other energy storage systems, one would find the proposed configuration much more preferable due to the many advantages of the CAES system relative to the other energy storage systems. The payback period of this plant, even with all the conservative considerations taken into account through the economic analysis, was finally calculated to be less than 9 years.

In the meantime, as the second proposed configuration in this work, in order for enhancing the stability of the power produced by the PV farm, decreasing the the effects of solar irradiation fluctuations and increasing the power plant total annual revenue, the previous power plant was proponed to be accompanied with a power productive CGS station. The CAES system sizing and power sales strategy selection procedures were carried out for this confugration again and the optimized power plant was also analyzed energy-exergetically comprehensively. With this proposal, it was proved that how much connecting another power supply source, like a CGS station, could increase the reliability of the power plant performance. It was also demonstrated that not only the size of the CAES system in this system is much smaller than what required in the previous configuration, but also the level of direct vendible power to the grid could increase significantly. According to the results of the simulation accomplished on this power plant, the exergy and energy efficiencies of the power

plant may go respectively up to 30% and 29%, which show geart enhancement in the system performance. Finally, an IRR analysis was carried out to assess the effects of this improvement on the economical performance of such a power plant, resulting to much better economic outcomes of the new proposed system. According to the results, the IRR of the power plant increases from 5.8% to 11.1% over this improvement.

In the end, considering the results presented in this work, firstly, constructing PV plants equipped with CAES systems and secondly, parallelizing them with CGS power productive stations in the countries with high solar energy potential is highly recommended.

8. Further Works

This study could be expanded in many aspects as it involves various technologies such as PV technology, CAES systems, solar thermal systems and CGS stations.

About the PV technology part of the project, based on the results derived from the simulation carried out on both of the proposed configurations in this thesis, it could be understood that the performance of such a power plant could be improved significantly if PV cells with higher energy conversion efficiencies are produced. The results revealed that significant amount of exergy is destructed in PV cells. Therefore, the first possible work in this area is focusing on solar energy harvesting aspect of the project by introducing novel solar cell types with higher efficiencies. Also, considering the effects of the recently emerged phenomenon El Nino on the level of total annual solar irradiation receivable in the target location can be a part of a future work in this area.

In simulating the CAES system, this work considered the compressors to work based on isentropic procedures which may be somehow far from the real operational process of the compressors. Therefore, simulating the compressors while working based on real procedures could be another possible future work in this area. The same simulation for the expander set could also be done as the turbines have also been considerd to work based on isentropic processes. In fact, the compressors and turbines must operate based on polytropic procedures for which the physical properties of the employed devices could have significant impact on their performance. Another assumption taken in the CAES system of this dissertation is about the overal effectivness of the heat exchangers which has been considered to be constant and eqaul to 0.9. Although this assumption is totally reasonable, the heat exchangers could be simulated individually in an exclusive work. For this objective, the heat exchangers should be designed and sized based on the maximum and minimum heat transfer rate required in the system. The working fluid mass flow rate and all of the the heat exchangers physical characteristics must be specified in this study.

Also, in simulating the solar thermal systems of the project, it was disclosed that the solar collector efficiencies are not satisfactory enough and significant improvement in thermal energy preparation of project could be achieved by more efficient collector types. Therefore, in addition to the studies proposed to be conducted on introducing more efficient

solar collectors, efforts for selecting the best solar collector types in both the CAES system and the CGS station could be beneficial. As middle range temperatures (85 ^{o}C and 140 ^{o}C) are required uniformly and constantly, concentrating collectors may be good choices for this objective as well.

About the auxiliary power productive station employed to stailize the poweroutput of the PV plant, which has been proposed to bea CGS station in this thesis, firstly, feasibility of employing other power producers than turbo-expanders, such as expansion engines or combined heat and power (CHP) and etc., may be interesting studies. Also, proposing and modelling other similar systems suitable for this objective can be further adequate future works in this area.

Finally, the same studies on various energy storage systems in different renewable energy source power plants which could determine the the most efficient power production system among all, maybe a deserving work. In this respects, various external power productive stations as the accompaniment unit of the power plant may also be considered.

REFERENCES

Arabkoohsar A, Farzaneh-Gord M, Deymi-Dashtebayaz M, Machado L, Koury R N N, Energy and exergy analysis of natural gas pressure reduction points equipped with solar heat and controllable heaters, Renewable energy, 2014, 72, pp: 258-270.

Arnold M S, 'Surface production operations: design of gas-handling systems and facilities, 2nd edn, 2; 1999, Burlington, MA, Elsevier.

Al-Hasan A Y, Ghoneim A A, Abdullah A H, Optimizing electrical load pattern in Kuwait using grid connected photovoltaic systems, Energy Conversion and Management, 2004, 45, pp: 483-94.

Andersen A N, Lund H, New CHP partnerships offering balancing of fluctuating renewable electricity productions. J Cleaner Prod, 2007, 15(3), pp: 288–93.

Bal M L, Satya S, Naik S N, Solar dryer with thermal storage systems for drying agricultural food products: A review, Renewable and Sustainable Energy Reviews, 2009, 14, pp: 2298–314.

Barker L, Neber M, Lee H, Design of a low-profile two-axis solar tracker, Solar Energy, 2013, 97, pp: 569-576.

Bisio G, Thermodynamic Analysis of the Use of Pressure Exergy of Natural Gas, Energy, 20 (2), 1995, pp: 161-167.

Blarke M, Lund H, Large-scale heat pumps in sustainable energy systems: system and project perspectives, Therm Sci, 2007, 11 (3), pp: 141–52.

Benz N, Gut M, Rub W, Solar process heat in breweries and dairies, Proceedings of EuroSun 98, Portoroz, Slovenia on CD-ROM, 1998.

Benz N, Gut M, Beikircher T, Solar process heat with non-concentrating collectors for food industry, Proceedings of ISES Solar World Congress on CD ROM, Jerusalem, Israel, 1999.

Botterud A, Chapter 11–Forecasting Renewable Energy for Grid Operations, Renewable Energy Integration, 2014, pp: 137-147.

Breeze P, Chapter 10 - Power System Energy Storage Technologies, Power Generation Technologies (Second Edition), 2014, pp: 195-221.

Bullough J C, Koller M, Nowi A, Zunft S, Advanced adiabatic compressed-air energy-storage for the integration of wind energy, In: Proceedings of the European wind energy conference, London, UK, 2004.

Cavallo A, Controllable and affordable utility-scale electricity from intermittent wind resources and compressed air energy storage (CAES), Energy, 2007, 32(2), pp:120–7.

Chin C S, Babu A, McBride W, Design, modeling and testing of a standalone single axis active solar tracker using MATLAB/Simulink, Renewable Energy, 2011, 36(11), pp: 3075-3090.

Chenni R, Makhlouf M, Karabacho T, Bouzid A, A detailed modeling method for photovoltaic cells, Energy, 2007, 32, pp: 1724-30.

COSERN: http://www.cosern.com.br/

CPC: http://www.cpc.noaa.gov/products/JAWF_Monitoring/Brazil/index.shtml.

Cunow E, Giesler B, The megawatt solar roof at the new Munich Trade Fair Centre—an advanced and successful new concept for PV plants in the megawatt range. Solar Energy Materials & Solar Cells, 2001, 67, pp: 459–67.

Denholm P, Improving the technical, environmental and social performance of wind energy systems using biomass-based energy storage, Renew Energy, 2006, 31(9), pp: 1355–70.

Denholm P, Kulcinski G L, Life cycle energy requirements and greenhouse gas emissions from large scale energy storage systems. Energy Convers Manage, 2004, 45(13), 2153–72.

Deshmukh M K, Deshmukh S S, Modeling of hybrid renewable energy systems, Renewable and Sustainable Energy Reviews, 2008, 12, pp: 235-49.

Diagne M, David M, Boland J, Schmutz N, Lauret P, Post-processing of solar irradiance forecasts from WRF model at Reunion Island, Solar Energy, 2014, 105, pp: 99-108.

Dresser-Rand: FCC power recovery expanders, available at: http://www.dresserrand.com/turbo/eq/ expand.asp

Duffie J. A, Beckman W.A. Solar Engineering of Thermal Processes. Second Ed, New York, Willy, 1991.

Dufo-López R, Lujano-Rojas J M, Bernal-Agustín J L, Comparison of different lead–acid battery lifetime prediction models for use in simulation of stand-alone photovoltaic systems, Applied Energy, 2014, 115, pp: 242-253.

El-Shatter T F, Eskandar M N, El-Hagry M T, Hybrid PV/fuel cell system design and simulation. Renewable Energy, 2002, 27, pp: 479–85.

El-Shatter T F, Eskander M N, El-Hagry M T, Energy flow and management of a hybrid wind/PV/fuel cell generation system, Energy Conversion and Management, 2006, 47, pp: 1264-80.

Eriksen P B, Economic and environmental dispatch of power/CHP production systems, Electr Power Sys Res, 2001, 57(1), pp: 33–39.

Espcinc: http://www.espcinc.com/

European Commission, Proposal for a directive of the European Parliament and of the Council on the promotion of the use of energy from renewable sources, Brussels, 2008.

European Commission, Directive of the European Parliament and of the Council on the promotion of cogeneration based on a useful heat demand in the internal energy market, Brussels, 2002.

Farzaneh-Gord M, Arabkoohsar A, Rezaei M, Deymi-Dashtebayaz M, Feasibility of Employing Solar Energy in Natural Gas Pressure Drop Stations, J. of the Energy Institute, 2011, 84, pp: 191-196.

Farzaneh-Gord M, Arabkoohsar A, Deymi-Dashtebayaz M, Khoshnevis A B, New method for applying solar energy in greenhouses to reduce fuel consumption, Int J Agric & Biol Eng, 2014, 6(4), pp:64-75.

Farzaneh-Gord M, Arabkoohsar A, Deymi-Dashtebayaz M, Farzaneh-Kord V, Feasibility of Accompanying Uncontrolled Linear Heater with Solar System in Natural Gas Pressure Drop Stations, Energy, 2012, 41, pp: 420-428.

Farzaneh-Gord M, Niazmand A, Deymi-Dashtebayaz M, Rahbari H R, Thermodynamic analysis of natural gas reciprocating compressors based on real and ideal gas models, International Journal of Refrigeration, In Press, Accepted Manuscript, Available online November 2014.

Farzaneh-Gord, M., Magrebi J., Exergy of Natural Gas Flow in Iran's Natural Gas Fields, International Journal of Exergy, Vol 6, No. 1, pp: 131-142, 2009.

Farzaneh-Gord M., Manzari M., Maghrebi M., Hashemi S., Eftekhari H. and Farokhi A., 2007. Using pressure exergy of natural gas in Bandar-Abbas refinery gas pressure drop station, The 2nd ICMSAO, March 24-27, 2007, Abu Dhabi, UAE.

Farzaneh-Gord M, Hashemi S, Sadi M, 2007, Energy destruction in Iran's natural gas pipe line network, Energy Exploration and Exploitation 25, pp: 393-406

Fthenakis V, Frischknecht R, Raugei M, Kim H C, Alsema E, Held M, Wild-Scholten M, Methodology guidelines on life cycle assessment of photovoltaic electricity, 2nd edition, 2011.

Gadhamshetty V, Gude V G, Nirmalakhandan N, Thermal energy storage system for energy conservation and water desalination in power plants, Energy, 2014, 66, pp: 938-949.

Ghali K, Ghaddar N, Alsaidi A, Experimental and Theoretical Study of an Optimized Integrated Solar Desalination and Air Conditioning Unit, International Journal of Green Energy, 2011, 8(1), pp: 81-99.

Giramonti A J, Lessard R D, Blecher W A, Smith E B, Conceptual design of compressed air energy storage electric power systems, Appl Energy, 1978, 4(4), pp: 231–49.

Glendenning I, Long-term prospects for compressed air storage, Appl Energy, 1976, 2(1), pp: 39–56.

Gow J A, Manning C D, Development of a model for photovoltaic arrays suitable for use in simulation studies of solar energy conversion systems, In: Proc, Sixth IEEE international conference on power electronics and variable speed drives, 1996, 1, pp: 69-74.

Grazzini G, Milazzo A, Thermodynamic analysis of CAES/TES systems for renewable energy plants, Renewable Energy, 2008, 33, 1998–2006.

Greeff L, Visser J. A, Ptasinski K. J, Janssen F. J. J. G, Using turbine expanders to recover exothermic reaction heat-flow sheet development for typical chemical processes, Energy, 2004, 29, 2045–2060.

Green M A, Photovoltaics: technology overview, Energy Policy, 2000, 28, pp: 989-998.

Griffin P, Ballard I, Barnham K, Nelson J, Zachariou A, Epler J, Hill G, Button C, Pate M,

The application of quantum well solar cells to thermophotovoltaics, Solar Energy Materials and Solar Cells, 1998, 50(1), pp: 213-219.

Hinderink P, Kerkhof F. P. J. M, Lie A. B. K, Swan J. de A, Vander K. H. J., Exergy analysis with a flow sheeting simulator, Part 1: Theory; calculating exergies of material streams, Chem. Eng. Sci., 51, (20), 4693–4700.

http://www.tractebelenergia.com.br/wps/portal/internet

http://www.espcinc.com/

http: //www.eco-inov.com.br/blog/

Incropera F P, Dewitt D P, Fundamentals of heat and mass transfer, 5th Ed, New York: John Wiley, 2002.

International Energy Agency and Organization for Economic Co-operation and Development, IEA renewables information. <http://www.sourceOECD.org/database/17266580/renewables>.

Ito M, Kato K, Sugihara H, Kichimi T, Kichimi J, Kurokawa K, A preliminary study on potential for very large scale photovoltaic power generation (VLSPV) system in the Gobi desert from economic and environmental viewpoints, Solar Energy Materials & Solar Cells, 2003, 75, pp: 507–17.

John P B, David G I, A probabilistic method for calculating the usefulness of a store with finite energy capacity for smoothing electricity generation from wind and solar power, Journal of Power Sources, 2006, 162, pp: 943-8.

Kalogirou S, Solar Energy Engineering: Process and Systems, 1st edition, 2009, ISBN: 978-0-12-374501-9.

Kalogirou S, Solar thermal collectors and applications, Progress in Energy and Combustion Science, 30, 2004, pp: 231–295.

Ke J C, Wang Y H, Chen K L, Huang C J, Effect of open-circuit voltage in organic solar cells based on various electron donor materials by inserting molybdenum trioxide anode buffer layer, Solar Energy Materials and Solar Cells, 2015, 133, pp: 248-254.

Ken A, Maurice S, Surface Production Operations (2nd Edition) Volume 2 - Design of Gas-Handling Systems and Facilities, 1999, Elsevier.

Khadidjaa B, Drisa K, Boubekerb A, Noureddinec S, Optimization of a Solar Tracker System for Photovoltaic Power Plants in Saharian region, Example of Ouargla, Energy Procedia, 2014, 50, pp: 610–618.

King D L, Dudley J K, Boyson W E, PVSIMC: a simulation program for photovoltaic cells, modules, and arrays. In: Proc, Twenty Fifth IEEE Photovoltaic Specialists Conference, 1996, 1, pp: 1295-7.

Kivaisi RT, Installation and use of a 3 kWp PV plant at Umbuji village in Zanzibar, Renewable Energy, 2000, 19, pp: 457-72.

Kondoh J, Ishii I, Yamaguchi H, Murata A, Otani K, Sakuta K, Electrical energy storage systems for energy networks, Energy Convers Manage, 2000, 41(17), pp: 1863–74.

Kousksou T, Bruel P, Jamil A, El-Rhafiki T, Zeraouli Y, Energy storage: Applications and challenges, Solar Energy Materials and Solar Cells, Part A, 2014, 120, pp: 59-80.

Lacchini C, Carlos J, Santos V. Dos, Photovoltaic energy generation in Brazil–Cost analysis using coal-fired power plants as comparison, Renewable Energy, Volume 52, April 2013, Pages 183-189

Li W, Simplified steady-state modeling for variable speed compressor, Applied Thermal Engineering, 2013, 50(1), pp: 318-326.

Liu C P, Chang M W, Chuang C L, Effect of rapid thermal oxidation on structure and photo-electronic properties of silicon oxide in monocrystalline silicon solar cell, Current Applied Physics, 2014, 14(5), pp: 653-658.

Liu S, Niu X, Shan W, Lu W, Zheng J, Yunfeng Li, Duan H, Quan W, Han W, Wronski C R, Yang D, Improvement of conversion efficiency of multicrystalline silicon solar cells by incorporating reactive ion etching texturing, Solar Energy Materials and Solar Cells, 2014, 127, pp: 21-26.

Linden V S, Bulk energy storage potential in the USA, current developments and future prospects, Energy, 2006, 31(15), pp: 3446–57.

Maclay J D, Brouwer J, Samuelsen S G, Dynamic analyses of regenerative fuel cell power for potential use in renewable residential applications. International Journal of Hydrogen Energy, 2006, 31, pp: 994-1009.

Manor A, Katz E A, Open-circuit voltage of organic photovoltaics: Implications of the generalized Einstein relation for disordered semiconductors, Solar Energy Materials and Solar Cells, 2012, 97, pp: 132-138.

Mathiesen B V, Lund H, Comparative analyses of seven technologies to facilitate the integration of fluctuating renewable energy sources, IET Renew Power Generation, 2009, 3(2), pp: 190–204.

Mathiesen B V, Lund H, Norgaard P, Integrated transport and renewable energy systems, Utilities Policy, 2008, 16(2), pp: 107–16.

Meibom P, Kiviluoma J, Barth R, Brand H, Weber C, Larsen H V, Value of electric heat boilers and heat pumps for wind power integration, Wind Energy, 2007, 10(4), pp: 321–37.

Mendez L, Naravarte L, Maninach A G, Izquierdo P, Carrasco L M, Eyras R, Centralized stand-alone PV system in micro grid in Morocco. In: Proc. 3rd world conference on photovoltaic energy conversion, Osaka, Japan, 2003, 3, pp: 2326-8.

Midilli A, Dincer I, Rosen M A, The Role and Future Benefits of Green Energy, International Journal of Green Energy, 2007, 4(1), pp: 65-87.

Müller A, Bründlinger R, Arz O, Miller W, Schulz J, Lauss G, PV-off-grid Hybrid Systems and MPPT Charge Controllers, a State of the Art Analyses, Energy Procedia, 2014, 57, pp: 1421-1430.

Muneer T, Asif M, Kubie J, Generation and transmission prospects for solar electricity: UK and global markets, Energy Conversion and Management, 2003, 44, pp: 35–52.

Muneer T, Maubleu S, Asif M, Prospects of solar water heating for textile industry in Pakistan, Renewable and Sustainable Energy Reviews, 2006, 10, pp: 1–23.

Münster M, Use of waste for heat, electricity and transport – challenges when performing energy system analysis, In: Proceedings from the fourth Dubrovnik conference on sustainable development of energy, water and environment systems, Dubrovnik, Croatia, 2007.

Muthusivagami R M, Velraj R, Sethumadhavan R, Solar cookers with and without thermal storage-A review, Renewable and Sustainable Energy Reviews, 2010, 14, pp: 691–701.

Najafi-mod M.H., Alizadeh A., Mohamadian A., Mousavi J., Investigation of relationship between air and soil temperature at different depths and estimation of the freezing depth (Case

study: Khorasan Razavi), Journal of water and soil of Ferdowsi University of Mashhad, Vol. 22, No. 2, 2008.

Najjar Y S H, Zaamout M S, Performance analysis of compressed air energy storage (CAES) plant for dry regions, Energy Convers Manage, 1998, 39(15), pp: 1503–11.

Nelson D B, Nehrir N H, Wang C, Unit sizing and cost analysis of standalone hybrid wind/PV/fuel cell power generation systems. Renewable Energy, 2006, 31, pp: 1641–56.

Norton B, Solar process heat: distillation, drying, agricultural and industrial uses, Proceedings of ISES Solar World Congress, Jerusalem, Israel on CD-ROM, Jerusalem, Israel, 1999.

Ozdemir S, Altin N, Sefa I, Single stage three level grid interactive MPPT inverter for PV systems, Energy Conversion and Management, 2014, 80, pp: 561-572.

Pavković D, Hoić M, Deur J, Petrić J, Energy storage systems sizing study for a high-altitude wind Energy application, Energy, 2014, 76, pp: 91-103.

Pathak M.J.M., Sanders P.G., Pearce J.M., Optimizing limited solar roof access by exergy analysis of solar thermal, photovoltaic, and hybrid photovoltaic thermal systems, Applied Energy, Volume 120, 1 May 2014, Pages 115-124.

Poghosyan V, Hassan M I, Techno-economic assessment of substituting natural gas based heater with thermal energy storage system in parabolic trough concentrated solar power plant, Renewable Energy, 2015, 75, pp: 152-164.

Poponi D, Analysis of diffusion paths for photovoltaic technology based on experience curves, Solar Energy, 2003, 74, pp: 331-40.

Porto M P, Machado L, Koury R N N, An alternative solution based on compressed and liquefied air storage systems for reducing power output variability in PV farms, 22nd International Congress of Mechanical Engineering, Ribeirão Preto, SP, Brazil, 2013.

PowerSouth: http://www.powersouth.com/mcintosh_power_plant/compressed_air_energy

Pozivil J., 2004. Use of expansion turbine in natural gas pressure reduction stations. J. Acta Montanistica Slovaca 9, 258-260

Raju M, Khaitan S K, Modeling and simulation of compressed air storage in caverns: A case study of the Huntorf plant, Applied Energy, 2012, 89(1), pp: 474-481.

Reference Module in Chemistry: Secondary Batteries-Lead Acid Systems, Flooded Batteries,

Reference Module in Chemistry, Molecular Sciences and Chemical Engineering, from Encyclopedia of Electrochemical Power Sources, 2014, pp: 677-692.

Rehman S, Bader M A, Al-Moallem S A, Cost of solar energy generated using PV panels, Renewable and Sustainable Energy Reviews, 2007, 11, pp: 1843–57.

Riordan M, Hoddeson L, Crystal Fire. Norton, New York, 1997.

Rodrigues E M G, Godina R, Santos S F, Bizuayehu A W, Contreras J, Catalão J P S, Energy storage systems supporting increased penetration of renewable in islanded systems, Energy, 2014, 75, pp: 265-280.

Russell M C, Grid-tied PV system modeling: how and why. In: Proc. IEEE first world conference on photovoltaic energy conversion, 1994, 1, pp: 1040-3.

Safaei H, Keith D W, Hugo R J, Compressed air energy storage (CAES) with compressors distributed at heat loads to enable waste heat utilization, Appl. Energy, 2013, 103, pp: 165 179.

Salgi G, Lund H, System behavior of compressed-air energy-storage in Denmark with a high penetration of renewable energy sources, Appl Energy, 2008, 85(4), pp: 182–9.

Shahid S M, Elhadidy M A, Economic analysis of hybrid photovoltaic-diesel-battery power systems for residential loads in hot regions-A step, Renewable and Sustainable Energy Reviews, 2008, 12(2), pp: 488-503.

Sharma A, Chen R C, Lan N Vu, Solar-energy drying systems: A review, Renewable and Sustainable Energy Reviews, 2009, 13, pp: 1185–210.

Sharma A, Chiu H H, Ahrens F W, Ahluwalia R K, Ragsdell K M, Design of optimum compressed air energy-storage systems, Energy, 1979,4(2), pp: 201–16.

Stachel J, Einstein's Miraculous Year, Princeton University Press, New York, 1998.

Swider D J, Compressed air energy storage in an electricity system with significant wind power generation, IEEE Trans Energy Convers, 2007, 22(1), pp: 95–102.

Thanaraka P, Sae-Eirb K, Economic analysis of CO2 emission reduction from large scale photovoltaic power plant in Thailand, Energy Procedia, 2012, 14, pp: 837–842.

Thirugnanasambandam M, Iniyan S, Ranko G, A review of solar thermal technologies, Renewable and Sustainable Energy Reviews, 2010, 14, pp: 312–322.

Tonsolar: http://www.e-tonsolar.com/upload/Datasheet-ETS6-3BB-Diagona_2015.pdf

Transsen: http://www.transsen.com.br/en/produtos

Unterrieder C, Zhang C, Lunglmayr M, Priewasser R, Marsili S, Huemer M, Battery state-of-charge estimation using approximate least squares, Journal of Power Sources, 2015, 278, pp: 274-286.

Wark K, Richards J D E, Thermodynamics, 6th edition, Tom Casson, 1999.

Wies R W, Johnson R A, Agrawal A N, Chubb T J, Simulink model for economic analysis and environmental impacts on a PV with diesel-battery system for remote villages. IEEE Transactions on Power Systems, 2005, 20, pp: 692-700.

Zekai S, Solar Energy Fundamentals and Modelling Techniques, 3rd Ed., London: Springer 180, 2008.

Zervas P L, Sarimveis H, Palyvos J A, Markatos N C G, Model-based optimal control of a hybrid power generation system consisting of photovoltaic arrays and fuel cells, Journal of Power Sources, 2008, 18, pp: 327-38.

Zhang X, Cuevas A, Demaurex B, Wolf S, Sputtered Hydrogenated Amorphous Silicon for Silicon Heterojunction Solar Cell Fabrication, Energy Procedia, 2014, 55, pp: 865-872.